Synthesis, Spectroscopic Properties and Cytotoxicity of Boron- Dipyrromethene Fluorescent Dyes

Submitted in fulfilment of the requirements

of the degree of

Master of Technology: Chemistry

in the Faculty of Applied Science at

Durban University of Technology

Nirvashini Bipath

Month and Year in which the dissertation/thesis is submitted

Supervisor: Prof. R. M. Gengan . . . . . Date: 27 August 2014

Joint Supervisor: Prof.A. A. Chuturgoon . . . . . Date: 27 August 2014

Declaration

I, Nirvashini Bipath, hereby declare that this dissertation entitled "Synthesis, spectroscopic properties and cytotoxicity of boron- dipyrromethene fluorescent dyes'', submitted to the Durban University of Technology, in fulfilment of the requirements for the award of the Degree of Master of Technology, Organic Chemistry, in the Faculty of Applied Sciences, is the result of my own work and that all sources used or quoted have been indicated and acknowledged by means of complete references.

Signed: …… Nirvashini Bipath

Date: ……..

Signed: …… Professor. R.M Gengan (Supervisor)

Date: ……

Signed: …… Professor A. A. Chuturgoon (Joint Supervisor)

Date: ……

Department of Chemistry

Durban University of Technology

June 2014

Acknowledgement

I am highly indebted to Professor R.M. Gengan, Professor A. A. Chuturgoon and colleague Anand Krishnan for their persistent guidance and encouragement throughout the duration of this study. It was their knowledge that had inspired the new routes for this project.

The ongoing support from my colleagues at the nanotechnology laboratory during this project inspired and was a great motivation to me. Most of all I would like to thank my parents and brother for constantly being of support and believing in my abilities.

Mainly I thank GOD for watching over me and giving me strength, health and courage during my difficult times. The journey with I embarked on was not easy but with the Almighty's strength I came out victorious.

Abstract

In this study, we report the synthesis of three quinolone bearing imidazole derivatives **2**, **3** and **4** and two quinolone bearing BODIPY dyes **5** and **7**.

In the synthesis of **2**, **3** and **4**, the first step was the preparation of the starting compound 2-chloro-3-formyl quinoline (**1**); the Vilsmeier-Haack cyclisation protocol was used. Compound **1** was used with the appropriate diamine, together with $POCl_3$ to produce **2**, **3** and **4**. These compounds were characterized by IR, ^{1}H-NMR and ^{13}C-NMR.

In the synthesis of **5**, compound **1** was used whilst **6** was used for the synthesis of **7**. This was via. a one-pot synthesis using conventional reflux apparatus and Schlenk technique. These compounds were characterized by IR, ^{1}H-NMR and ^{13}C-NMR. Four other BODIPY dyes were also synthesized but their purification by column chromatography were unsuccessful. However a HPLC method was developed using **2** as a model; the best eluting solvent was 65 % methanol.

After synthesis, **2, 3, 4, 5** and **7** were used for spectroscopic studies by UV-visible and fluorescence spectroscopy. In the UV-visible studies, **2, 3 and 4** were dissolved, separately, in five solvent viz. ethanol, methanol, dichloromethane, chloroform and acetonitrile. The UV profile of each compound was obtained and the maximum absorbance was then used for fluorescence studies.

In the fluorescence studies, all the compounds displayed a fluorescence nature when excited with the various wavelengths. The fluorescence properties, namely Stoke shift, quantum yield, life time, molar absorptivity and brightness, were investigated to establish the properties of each compound in all five solvent systems. The Stoke shift was evident in all compounds and the quantum yields were below one which indicates no other electron transfer mechanisms occurring. The results displayed a favorable response and this further lead to analysis of the synthesized compounds for it potential application as a chemosensor. Eight metal ions were used to investigate this property. All eight metal ions, when reacted

with the synthesized compounds, as ligands, showed chemosensor properties, viz. photon induced electron transfer, inter-molecular charge transfer and fluorescence resonance electron transfer, as a quenching and enhancement of emission and excitation peaks were observed.

The compounds were further investigated for its potential for its use as a photovoltaic cells. The energies of the compounds were obtained from the analyses of the reflectance and transmission spectra. It was found that the synthesized compounds displayed properties which were positive for its use as a photovoltaic cell.

Biological analyses using molecular docking analyses and MTT assays were conducted to determine the use of these as an anti-cancer drug. Compounds **2** and **3** formed hydrogen bonds with GLU 25 and LEU 27, respectively with MDM2-p53 proteins. Following the molecular docking studies, the MTT assay was performed on all five synthesized compounds. The BODIPYs with the quinoline moieties demonstrated a reduction in the rate of A549 cell proliferation when compared to the imidazole and benzimidazoles; this was observed for compounds **5** and **7.** Further, a comparison between imidazoles clearly shows that compounds **3** and **4** also decreased cell proliferation. In contrast compound **2** exhibited an increased rate of cell proliferation. The optical density of the control cell, is much higher that the plates for concentration 31.25 µg/ mL to 500 µg/ mL. However **2** cannot be discarded; this compound clearly shows that it possesses anti-hyperglycaemic properties and further studies are recommended.

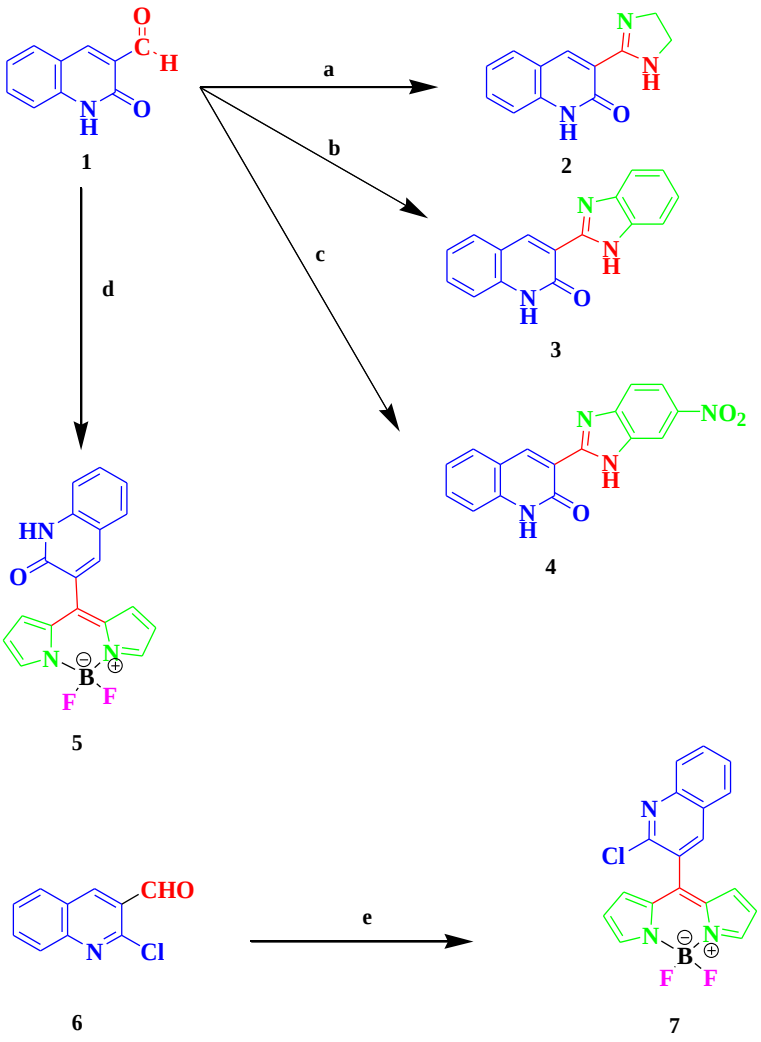

a. $POCl_3$ in ethanol, ethylene diamine, 100-120°C, 5 hours

b. $POCl_3$ in ethanol, 1,2-diamino benzene, 100-120°C, 5 hours

c. $POCl_3$ in ethanol, *p*-nitro (1,2-diamino) benzene, 100-120°C, 5 hours

d. (i) DCM, TFA, 1hour (ii) DDQ, DCM, 30 min (iii) TEA,BF_3.OEt_2, 2 hours

e. (i) DCM, TFA, 1hour (ii) DDQ,DCM, 30 min (iii) TEA,BF_3.OEt_2, 2 hours

Title	Page Numbers

List of Figures:

List of Schemes:

Tables

List of Appendices

General Remark

Numbers are used to represent chemical structures, in each chapter, and the Tables and Figures are numbered accordingly. All Figures found in each chapter are followed by a discussion and includes interpretation of NMR and IR spectra. The following abbreviation is found in the text:

Abs	-	Absorbance
$BF_3.OEt_2$	-	Boron trifluoride diethyl etherate
BODIPY	-	Boron dipyrromethene
$CHCl_3$	-	Chloroform
DCM	-	Dichloromethane
DMF	-	Dimethylformamide
DDQ	-	2,3-Dichloro-5,6-dicyano-1,4-benzoquinone
DMSO	-	Dimethyl sulfoxide
EA	-	Ethyl acetate
EDTA	-	Ethylenediaminetetraacetic acid
EtOH	-	Ethanol
MeOH	-	Methanol
MTT	-	3-(4,5-dimethylthiazol-2-yl)-2,5-diphenyltetrazolium bromide
NMR	-	Nuclear Magnetic Resonance Spectroscopy
OD	-	Optical density
PCl_3	-	Phosphorous trichloride
PE	-	Petroleum ether
$POCl_3$	-	Phosphoryl chloride
TEA	-	Triethylamine
TLC	-	Thin layer chromatography
TFA	-	Trifluoroacetic acid
TMS	-	Tetramethylsilane
g	-	Grams
mL	-	Milli litres

mmol	-	Milli molar
µM	-	Micro molar
nm	-	Nanometers
Hrs	-	Hour
Min	-	Minutes
UV	-	Ultra-violet
UV/Vis	-	Ultra-Violet/ Visible radiation

The solvents used for syntheses were of analytical and reagent grade. Reagents were purchased from Sigma Aldrich, Merck and Capital Labs. DCM was dried before use.

Thin layer Chromatography (TLC) was performed using a glass capillary tube and silica gel plates (silica gel material on an aluminium plate) with particle size 8.0-12.0 µm and pore diameter of 60 Å. Petroleum ether, ethyl acetate, chloroform and methanol were used as solvents used for the development of the TLC plate. A dark chamber with a UV lamp, equipped with the functions to observe short and long UV-wavelengths was used for the determination of the compounds' spectroscopic nature by locating a spot formed by the compound on the TLC plate. An iodide chamber was also set up as an alternative and for confirmation of the compounds.

The purification of crude products were performed by using column chromatography with activated silica gel as the packing material.

Chapter One: Introduction

Quinoline and quinoline-bearing derivatives are heterocyclic compounds containing one or more nitrogen atoms. Numerous simple and complex molecules have been extracted from natural sources and can be synthesised in high purity[1]. These molecules have displayed excellent antimalaria[2], anti-flammatory[3], bactericidal[4], fungicidial[5] and anti-cancer[6] properties.

Imidazole and its derivative have also played a vital role in chemistry research. These compounds are aromatic heterocycles which consists of two nitrogen groups on a carbon ring which create a five-membered structure. Imidazole compounds display similar properties to that of quinoline compounds such as antimalarial[7], anti-flammatory[8, 9], antifungal[10], bactericidal[11] and anti-aging agents[12], anticoagulants[13], antiviral[14], anti-tubercular[15], anti-diabetic[16] and anti-cancer[17, 18] properties. Due to these important biological properties displayed by quinoline and imidazoles, we focused on this class of organic molecules.

In this research study, we wanted to synthesise novel quinoline-imidazole and BODIPY derivatives and assess their electronic and biological potentials via fluorescence, molecular modelling and anti-cancer principles.

The objectives of this study were to:

a) Synthesize quinoline derivatives, bearing an imidazole moiety, via. a simple reaction which is cost effective.
b) Synthesize a BODIPY core containing a quinoline moiety
c) Purify the compounds by means of chromatographic techniques and characterise the compounds by spectroscopic techniques.

d) Characterise the target compounds' intrinsic properties by fluorescence spectroscopy and apply these properties for chemosensors.

e) Investigate the potential of selected compounds for solar application.

f) Evaluate the anti-cancer properties of the synthesized compounds by computational molecular modelling and determine the biological activity in lung cancer line A529.

In **Chapter two**, we discuss relevant literature pertaining to the research themes presented in this study such as:

- Synthesis of organic molecules and the importance of quinolines
- Alkaloids and its contributions to man-kind by its applications
- Quinoline derivative and its occurrences
- Imidazoles, BODIPYs and its application
- Cancer and its historical overview
- Molecular docking and its application
- Biological MTT testing and its applications to solar cells
- Topics such as supramolecular chemistry and its historical overview
- Chemical dyes and its historical establishment
- Fluorescence phenomena and its applications

In **Chapter three**, the experimental procedures are highlighted for the synthesis of the quinolines, quinolones and BODIPY dyes with a quinoline moiety. The procedures used to prepare standard solutions with a range of solvent systems were used in spectroscopic analyses. The test procedure for the investigation of the compounds to act as a photovoltaic cells is also

included. This is followed by the protocols used for molecular docking studies for scanning of anti-cancer properties including the procedure for cytotoxicity analyses and the preparation of the MTT assay.

In **Chapter four**, the results obtained from the synthesis and spectroscopic analyses are discussed. This chapter outlines:

- The synthesis mechanisms used
- The characterisation of the synthesized compounds
- The analysis of the UV/Visible spectroscopy data
- Results from the fluorescence studies
- The potential for quinoline derivatives to be used as a chemosensor
- The anti-cancer result from the molecular docking studies
- The cytotoxicity test results using cancer cell lines A529
- Results from photovoltaic cell studies.

Reference

1. Quinolines and Isoquinolines. *Quinolines and Isoquinolines,* [WWW] Available from: <http://www.chtf.stuba.sk/~szolcsanyi/education/files/Chemia%20heterocyklickych%20zlucenin/Prednaska%201/Odporucane%20studijne%20materialy/(Izo)chinol%EDn-synt%E9za.pdf> [Accessed on: 21 December 2013]
2. Foley, M.; Tilley, L. (1998). 'Quinoline Anti-malarials: Mechanisms of Action and Resistance and Prospects for New Agents.' *Pharmacology & Therapeutics,* Volume 79, Issue 1, pp. 55-87
3. Ratheesh, M.; Sindhu, G.; Helen, A.; (2013). 'Anti-Inflammatory Effect Of Quinoline Alkaloid Skimmianine Isolated From *Ruta graveolens L.*' *Inflammation Research,* Volume 62, Issue 4, pp. 367-376
4. Vudumula, U.; Adhikari, M. D.; Ojha, B.; Goswami, S.; Das, G. and Ramesh, A. (2012) 'Tuning The Bactericidal Repertoire And Potency Of Quinoline-Based Amphiphiles For Enhanced Killing Of Pathogenic Bacteria.' *RSC Advances,* Volume 2, Issues 9, pp. 3864-3871
5. Dreikorn, B. A.; Jourdan, G. P.; Davis, L. N.; Suhr, R.G. ; Hall, H. R.; and Arnold, R. W. (1991) 'Synthesis and Fungicidal Activity of 4-Phenethylaminoquinoline and its Analogues and Derivatives.' *Synthesis and Chemistry of Agrochemicals II,* Lilly Research Laboratories, Eli Lilly and Company, P.O. Box 708, Greenfield, IN 46140. Pp. 553–565
6. Karthik, S.; Saha, B.; Ghosh, S. K. and Pradeep Singh, N. D. (2013) 'Photoresponsive quinoline tethered fluorescent carbon dots for regulated anticancer drug delivery.' *Chemical Communications,* Volume49, Issue 89, pp. 10471-10473

7. Pfaller M.A. and Krogstad D.J. (1983) ‘Oxygen enhances the antimalarial activity of the imidazoles.’ *The American Journal of Tropical Medicine and Hygiene,* Volume 32, Issue 4, pp. 660-665
8. Silva , V. G.; Silva, R. O.; Damasceno, S. R. B .; Carvalho, N. S.; Prudêncio, R. S.; Aragão, K. S.; Guimarães, M. A.; Campos, S. A.; Véras, L. M. C.; Godejohann, M.; Leite, J. R. S. A.;. Barbosa, A. L. R. and Medeiros, J. R. (2013) ‘Anti-inflammatory and Antinociceptive Activity of Epiisopiloturine, an Imidazole Alkaloid Isolated from *Pilocarpus microphyllus*.’ *Journal of Natural Products*, Volume 76, Issue 6 , pp. 1071–1077
9. Steel, H.C, Tintinger, G.R, Anderson, R. (2008) ‘Comparison of the Anti-Inflammatory Activities of Imidazole Antimycotics In Relation To Molecular Structure.’ *Chemical Biology and Drug Design*, Volume 72, Issue 3, pp. 225-228
10. Sud, I. J and Feingold, D.S. (1982) ‘Action of Antifungal Imidazoles on Staphylococcus Aureus.’ *Antimicrobial Agents And Chemotherapy*, Volume 22, Issue 3, pp. 470-474
11. Khan, A.; Sarkar, S.; Sarkar, D. (2008) ‘Bactericidal Activity of 2-Nitroimidazole Against The Active Replicating Stage Of Mycobacterium Bovis BCG And Mycobacterium Tuberculosis With Intracellular Efficacy In THP-1 Macrophages.’ *International Journal of Antimicrobial Agents*, Volume 32, Issue 1, pp. 40–45
12. Babizhayev, M .A. (2006) ‘Biological Activities Of The Natural Imidazole-Containing Peptidomimetics N-Acetylcarnosine, Carcinine And L-Carnosine In Ophthalmic And Skin Care Products.’ *Life Sciences*, Volume 78, pp. 2343 – 2357
13. Lee, J. J.; Bruley, D. F.; Kang, K. A. (2008) ‘Manipulation of the Affinity Between Protein and Metal Ions by Imidazole and PH for Metal Affinity Purification of Protein c

from Cohn Fraction IV-1.' *Advances In Experimental Medicine And Biology*, Volume 614, pp. 93-100

14. Sharma, D.; Narasimhanb, B.; Kumara, P.; Judgea, V.; Naranga, R.; De Clercqc, E. and Balzarinic, J. (2009) 'Synthesis, Antimicrobial and Antiviral Evaluation of Substituted Imidazole Derivatives.' *European Journal of Medicinal Chemistry*, Volume 44, Issue 6, pp. 2347–2353
15. Pandey J.; Tiwari V. K.; Verma, S.S.; Chaturvedi, V.; Bhatnagar, S.; Sinha, S.; Gaikwad, A. N.; Tripathi, R. P. (2009) 'Synthesis And Antitubercular Screening Of Imidazole Derivatives.' *European Journal of Medicinal Chemistry*, Volume 44, Issue 8, pp. 3350–3355
16. Crane, L.; Anastassiadou, M.; El Hage, S.; Stigliani, J. L.; Baziard-Mouysset, G.; Payard, M.; Leger, J.M.; Bizot-Espiard, J.G.; Ktorza. A.; Caignard, D. H. and Renard, P. (2006) 'Design and Synthesis Of Novel Imidazoline Derivatives With Potent Antihyperglycemic Activity In A Rat Model Of Type 2 Diabetes.' *Bioorganic and Medical Chemistry*, Volume 14, Issue 22, pp. 7419-7433.
17. Baviskar, A. T.; Madaan, C.; Preet, R.; Mohapatra, P.; Jain, V.; Agarwal, A.; Guchhait, S. K.; Kundu, C. N.; Banerjee, U. C.; Bharatam, P. V. (2011) 'N-Fused Imidazoles As Novel Anticancer Agents That Inhibit Catalytic Activity Of Topoisomerase Iiα And Induce Apoptosis In G1/S Phase.' *Journal of Medicinal Chemistry*, Volume 54, Issue 14, pp. 5013–5030
18. Krężel, I. (1998) 'New derivatives of imidazole as potential anticancer agents.' *Il Farmaco,*Volume 53, Issue 5, pp. 342–345

Chapter Two: Literature Survey

2.1 Alkaloids

Alkaloids are a group of naturally occurring chemical compounds which contain nitrogen atoms[1]. They are produced by a large variety of organisms, including bacteria, fungi, plants, and animals. Alkaloids demonstrate pronounced physiological effects when consumed or administered[2], as exemplified by recreational drugs such as an anesthetic **(1)** as stimulant cocaine **(2)**, caffeine **(3)**, nicotine **(4)**, an analgesic morphine **(5)**, and an antimalarial drug quinine **(6)**.

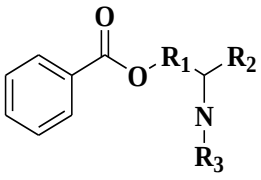

1

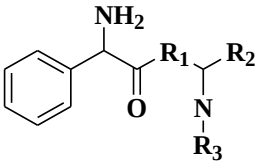

2

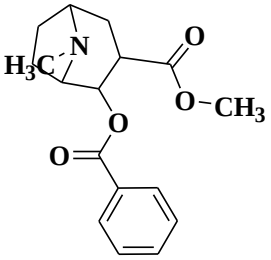

3

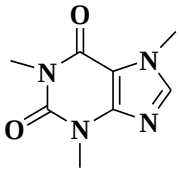

4

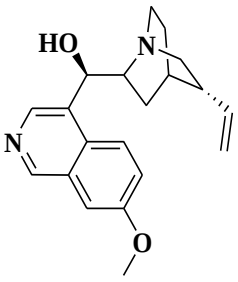

5

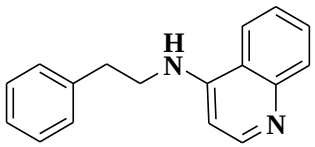

6

Alkaloids can be characterized by four factors viz, by their plant origin, its existence as a basic salt form, as an ammonia like compound and by their name also to mimic the natural one. Due to the diversity of alkaloids, no uniform classification is available. However, they can be divided into ornithine-derived alkaloids which are sub-divided into tropane and pyrrolizidine. Lysine-derived alkaloids also exist, such as phenylalanine-, tyrosine- and dihydroxyphenylalanine-

derived alkaloids, Tryptophan-derived alkaloids, miscellaneous alkaloids such as indolizidine, imidazole, purine, reduced pyridine, terpenoid and steroidal alkaloids also exist. Miscellaneous alkaloids have been explored for possible drug design and can be applied in various fields which will be discussed in detail later.

2.1.1 Historical Overview of Alkaloids

Alkaloids were used by man since the early ages as hallucinogenic plants[3]. The first pure alkaloid was isolated and reported by a scientist F.W.A. Sertürner in 1806[4]. He also produced a number of other salts and demonstrated their physiological effects. The resultant compound was relatively pure. In the period 1820-1840, a number of alkaloids were recorded but it was not until the proper organic chemistry techniques were implemented that structural elucidation of alkaloids were reported. Historically, the classification of alkaloids were done by using the alkaloids in it as a natural source but, this was unsuccessful because there was limited knowledge of the structure. They have been placed logically in the following nine chemical-structural categories, namelyacridines, amides, amines, benzylisoquinolines, canthinones, imidazoles, indolquinazolines, furoquinolines, and quinazolines[6a] and today there are over 3000 different types of alkaloids[6b] and can be classified as either biosynthetic, chemical, pharmacological and taxonomic .

2.1.2. Quinolines Alkaloid

Quinoline alkaloids are a class of organic compounds of the aromatic heterocyclic series characterized by a double-ring structure composed of a benzene and a pyridine ring fused at two adjacent carbon atoms. The benzene ring contains six carbon atoms, while the pyridine ring contains five carbon atoms and a nitrogen atom. The compound has a molecular formula of

C_9H_7N. Quinolines are used extensively in medicine and are found to be useful as antimalaria[7], anti-flammatory[8], bactericidal[9], fungicidial[10] and anti-cancer[11] drugs.

2.1.2.1 Occurrence and Progress of Quinolines

Alkaloid quinolines were first discovered in 1834 by Friedlieb, Ferdinand Runge. It was extracted from coal tar[12] and named "Leukol"[13]. The compound has since found application in medicine and research and is still ongoing. The successful application of quinoline derivatives are documented and reported by chemists[14]. In 1991, derivative **6** synthesis was reported[10] and its characteristics resembled that of an antifungal agent. This compound was synthesized to evaluate the foliar fungicides as it demonstrated a high level of fungicidal activity, especially against downy mildew of grape.

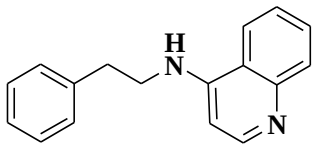

6

A few years later, scientist synthesized derivatives **7-9** to investigate the anti-malarial properties[7]. The malaria parasite was reported to be destructive to itself upon high concentrations of **7**. It interfered with the polymerization of heme and/or the detoxification of the reactive oxygen species, effectively killing the parasite with its own metabolic waste as the parasite degrades hemoglobin to heme. Derivatives **26** and **27** displayed some effectiveness in the destruction of the malarial parasite, as well.

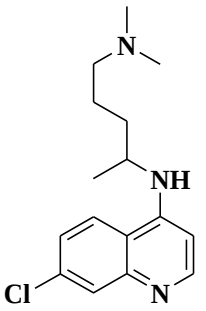

7

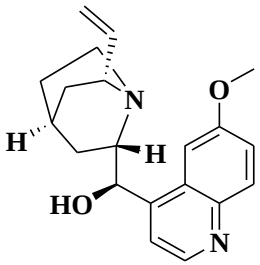

8

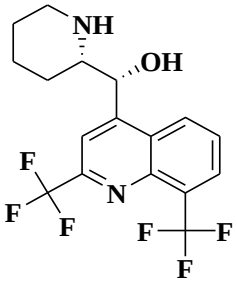

9

Following many discoveries of quinoline derivatives, it was later reported[9] that N-methyl-8-dodecoxy quinolinium iodide amphiphile **10** displayed bacterial inhibiting action**.** This amphiphile contained a fluorescent head group and varying hydrophobic chain length.

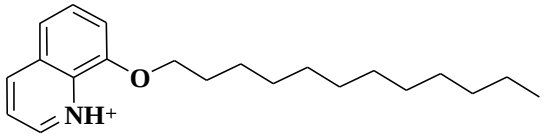

10

In the same year, it was reported[8] that quinoline derivatives have exhibited anti-inflammatory properties whilst other scientists reported a derivative which demonstrated anti-cancer properties[11]. Extracted quinoline alkaloid skimmianine **11** from *Rutagraveolens L*. was used to evaluate the effect on carrageenan-induced acute inflammation[8]. Its multi-targeted mechanism of action was used to conclude its potential therapeutic efficacy. The report[11] explored fluorescent carbon nanoparticles with 7-methoxy quinoline **12** to investigate the ability to phototrigger the regulated delivery of anticancer drugs. **12** was use for the phototriggering because of weak fluorescence and ability for one photon and two photon excitations.

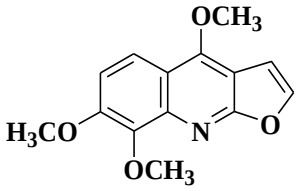

11

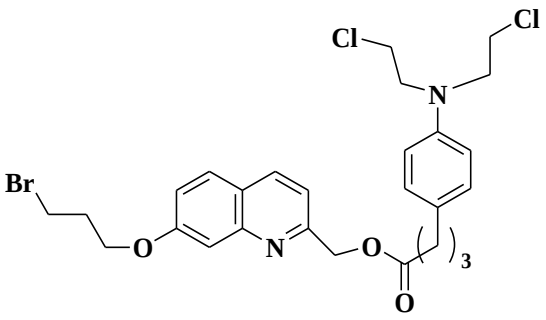

12

2.1.3 Imidazoles

Imidazoles exists in two equivalent tautomeric forms due to the two nitrogen groups present in the 5-membered cyclic structure[13]. Its pharmaceutical applications[14] such as antimalarial[15], anti-flammatory[16, 17], antifungal[18], bactericidal[19], anti-aging agents[20], anticoagulants[21], antiviral[22], anti-tubercular[23], anti-diabetic[24] and anti-cancer[25, 26] are well documented.

2.1.3.1. Occurrence and Progress of Imidazoles

Imidazole was first reported in 1858 in low yields[27]. It is used in the chemical industry as an intermediate in the production of pharmaceuticals, pesticides, dye intermediates, auxiliaries for textile dyeing and finishing, photographic chemicals and corrosion inhibitors[28]. In 1982, it was reported[19] that imidazole antifungal agents are active against gram-positive bacteria, *Staphylococcus aureus*, by interfering with their ergosterol synthesis. Miconazole **(13)** and ketoconazole **(14)** are two imidazoles which were tested to demonstrate antifungal properties.

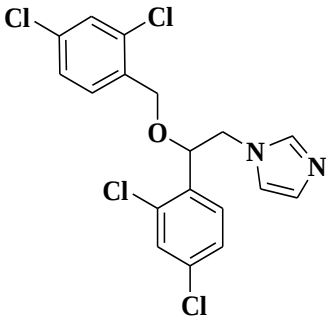

13

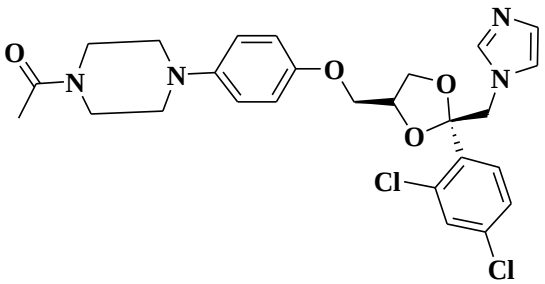

14

Also reported[16] was **14** which demonstrated an antimalarial activity. It was found that at high oxygen levels it caused oxidative stress against the parasite Plasmodium falciparum.

In 2006, it was concluded that peptidomimetics N-acetyl-L-carnosine **(15)**, L-carnosine **(16)** and carcinine **(17)** were anti-ageing agents because they showed good antioxidant protective effects[21].

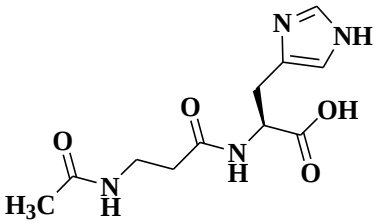

15

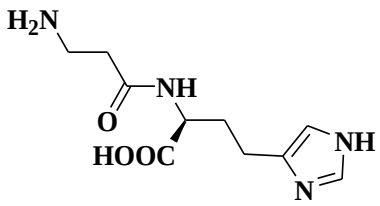

16

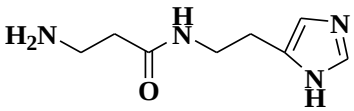

17

It was reported that the imidazole methyl group derivatives of **18** demonstrated anti-hyperglycemic activity *in vivo* in type-2 diabetic rats[26].

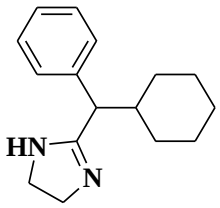

18

In 2008 two reports reported two more properties of interest viz: antibacterial and anticoagulant respectively. First, it was showed that 2-nitroimidazoles **19** and **20** were highly active against Mycobacterium Bovis BCG and Mycobacterium tuberculosis[20]. This was followed by the report of imidazole for the use as purification of Protein C in blood plasma[22].

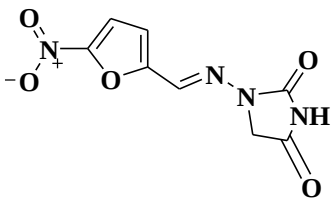

19

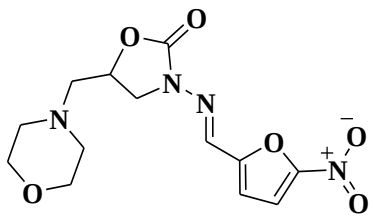

20

Derivatives **21** to **24** displayed antimicrobial activity and **24** displayed antiviral properties on gram positive and fungal species[23]. This was done by Structure- activity relationship (SAR) studies which indicated the presence of an electron withdrawing groups which was necessary for the antimicrobial activity of the synthesized compounds. Whilst antiviral screening of was done by placing against a panel of viral strains.

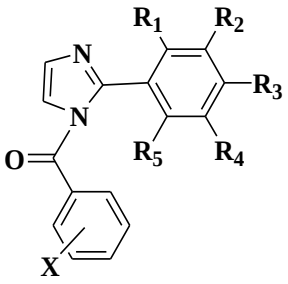

R_1= Cl
R_2= H
R_3= H
R_4= H
R_5= H
X =4-NO_2

21

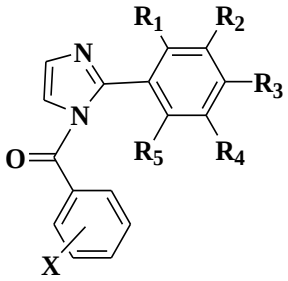

R_1= COOH
R_2= H
R_3= H
R_4= H
R_5= H
X =4-NO_2

22

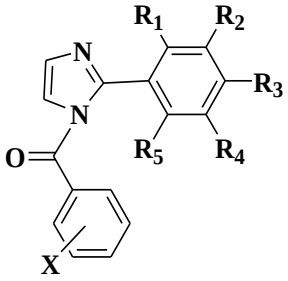

R_1= H
R_2= H
R_3= Cl
R_4= H
R_5= H
X =2-Br

23

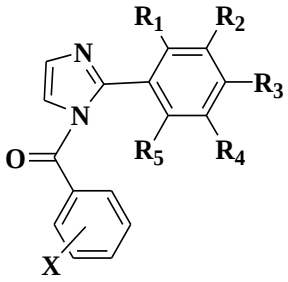

R_1= H
R_2= H
R_3= NO_2
R_4= H
R_5= H
X = 2-Br

24

It was later reported[24] that the synthesis of imidazole derivative **25** showed antitubercular properties against *Mycobacterium tuberculosis*.

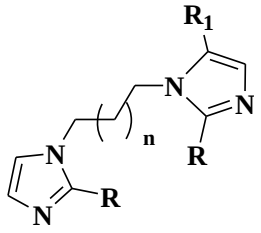

25

The synthesis of bicyclic novel N-fused aminoimidazoles[26] and the anti-cancer properties of imidazoles[27] were reported in 1998. The report[26] used the data to conclude that the amidinohydrazine derivative, N-(4,5-dihydro-1H-imidazol-yl)-N-(2-hydroxyethyl) hydrazine hydroiodide **(26)** showed minimal anticancer activity at the time. In 2011[27], N-fused

aminoimidazoles (**27-31**) as potent DNA non-intercalating topoisomerase IIβ catalytic inhibitors and anticancer activity in kidney and breast cancer cell lines was reported.

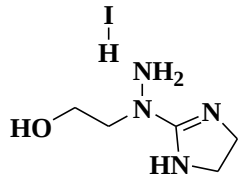

26

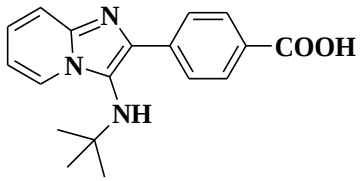

27

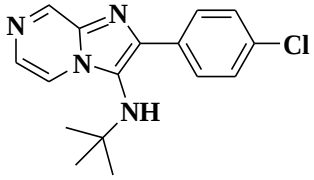

28

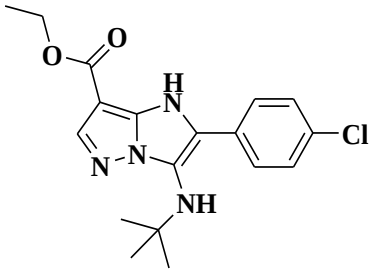

29

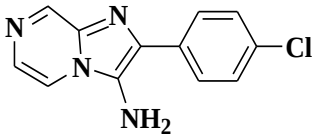

30

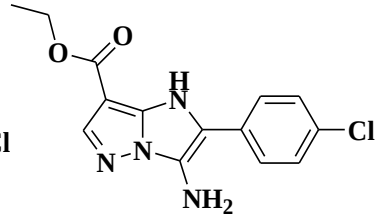

31

Most recently, the anti-inflammatory agent of imidazole derivative[17] **32** was extracted from *Pilocarpusmicrophyllus* leaves.

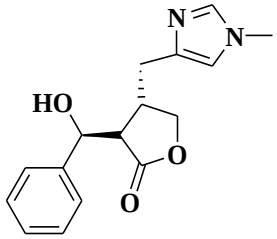

32

2.2 BODIPY

BODIPY fluorophores are aromatic compounds which have gained tremendous interest since their discovery. The two fused pyrrole ring structure linked with a four coordination boron atom and methene are characteristic features which can be observed for the identification of a

BODIPY core **33**. These complexes have an excellent thermal and photo-stability and have found applications in a number of imaging processes such as: - optical engineering[29], analytical chemistry[30], biological *in vivo* imaging[31] insensing applications[32], and in material science[33]. The small Stokes shift, higher quantum yield, high solubility and molar co-efficient makes BODIPY complexes most versatile in comparison to other fluorescence compounds[34].

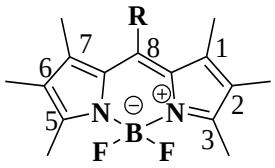

33

The first BODIPY[35] was reported in 1968. Since then, research on BODIPY has advanced with much interest as a result of the properties of the BODIPY core **33**. The synthesis and characterization of **34** and **35** by condensation in a one-pot synthesis[36]. They found use as a porphyrin accessory pigment in light-harvesting arrays.

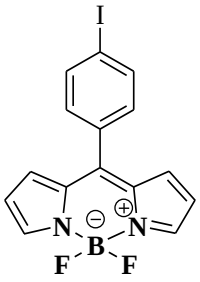

34

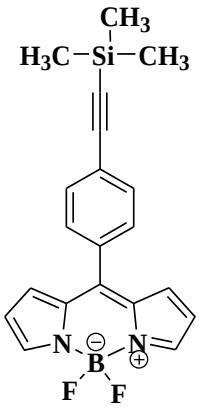

35

Investigation of the molecular switching properties of the BODIPY **36,** in various solvents[37] was reported. Spectroscopic data revealed that at steady-state, high quantum yields and high molar co-efficient were obtained for all the solvents used. This demonstrating that **37** was suitable for use in the NIR region as a multifunctional molecular system as a dual-mode chemical switch[38]. It was also reported the synthesis of an IR emitting complex **37** could be used as a chemosensor. A number of derivatives were used.

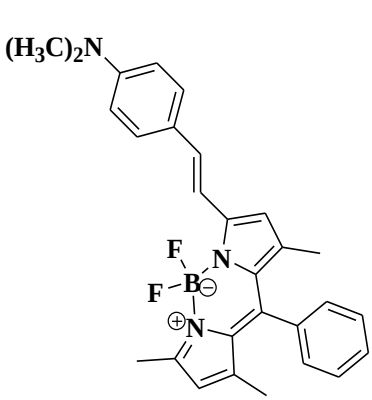

36

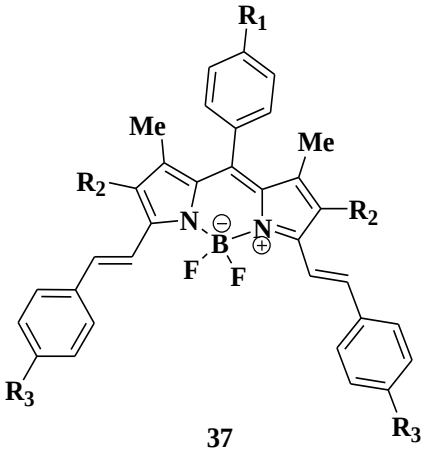

37

The synthesis of **38** demonstrated that it been used as a colourmetric and fluorescent chemodosimeter for the analysis of fluoride ions[39].

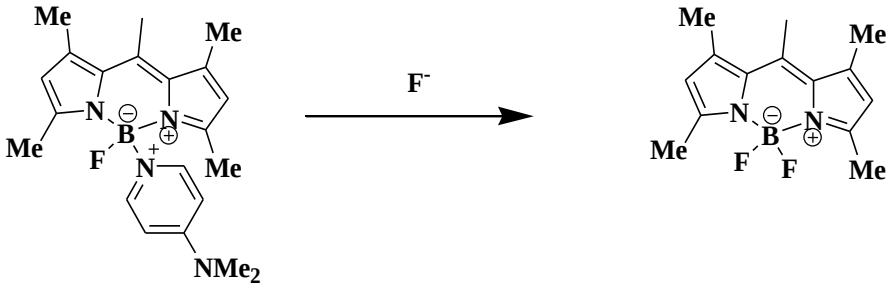

38

non-fluorescent

39

fluorescent

Following this was a report which demonstrated a convenient synthesis of a water soluble BODIPY nitrilotriacetic acid (NTA) derivative[40] . By incorporating the NTA to the BODIPY core, two water soluble BODIPY dyes **40** and **41** were produced.

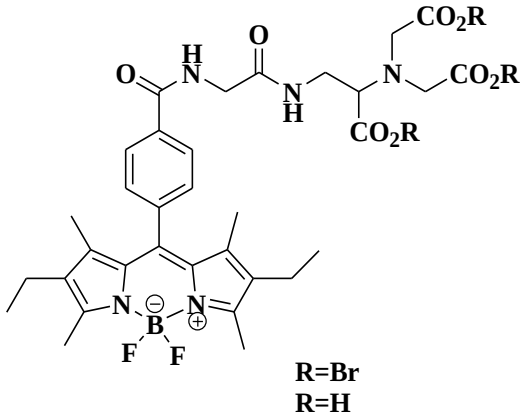

40

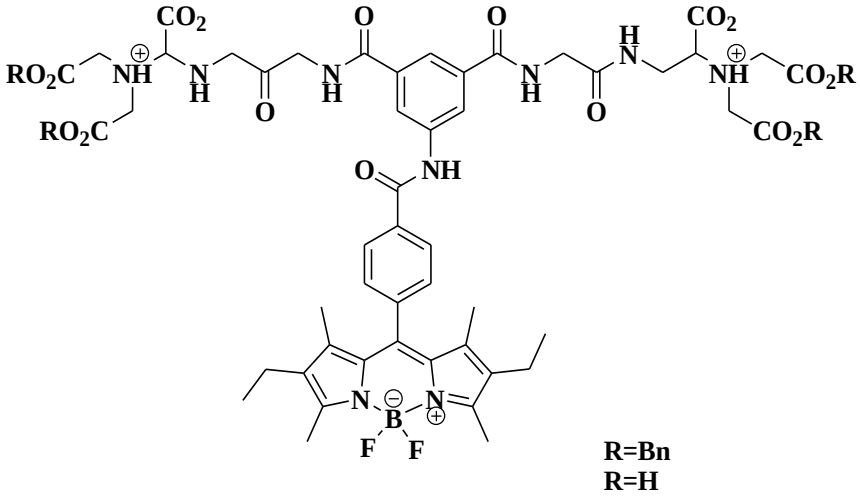

41

BODIPY core of the covalent link meso-furyl boron-dipyrromethene ferrocene[41] conjugates was reported and discussed in 1987. It was found that all four compounds displayed charge transfer properties by electrochemical analyses. These four compounds are **42** to **45**.

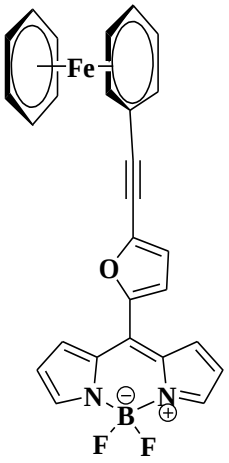

42

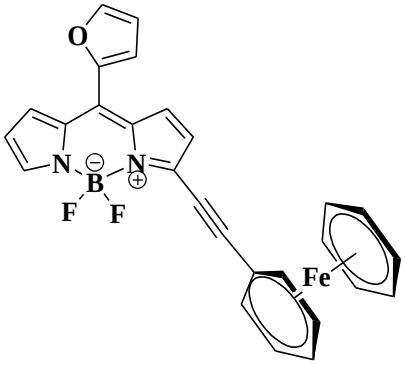

43

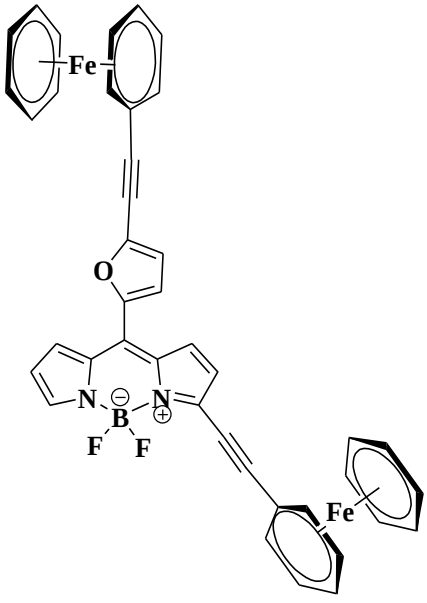

44

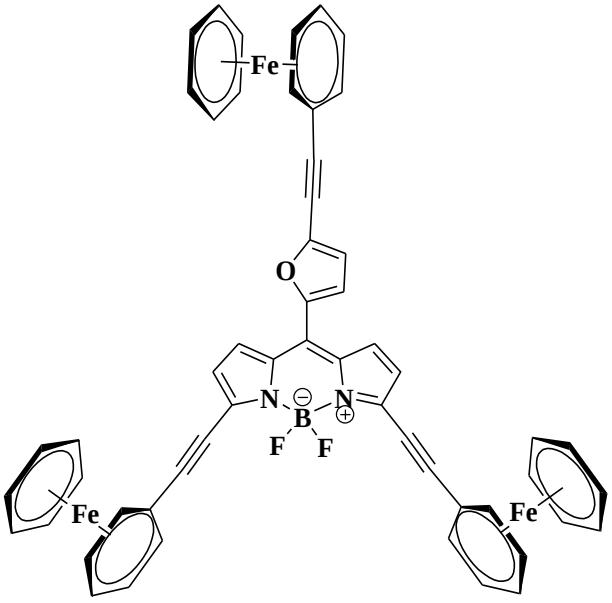

45

In order to determine properties of the BODIPY core, the spectroscopic properties of novel BODIPY dyes were investigated in two separate reports[42, 43]. In the report produced in 2010, a usage of BODIPY dye were report characterized[42]. The Stoke shift and quantum yields were determined in different solvents. Compound **46** was used as a standard in the investigations.

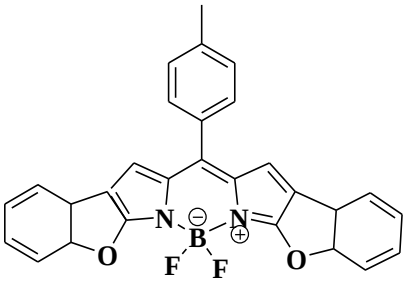

46

The synthesis of the BODIPY core with 1, 7- disubstituted derivatives, **47** and **48** was reported[43]**.** The spectroscopic properties were also investigated, and it was established that the spectral properties vary with the substituted groups but high quantum yields were obtained for all derivatives.

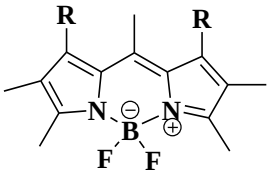

47

a. R=Ph
b. R= 2-thienyl
c. R= Ph═ CH2
d. R=PhCH═C

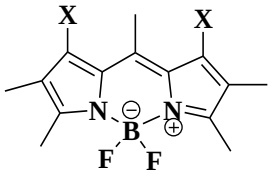

48

a. X= Cl
b. X= Br
c. X= H

From the biological perspective, BODIPYs have found application as fluorescence probes and chemosensors for bio-imaging. Me_4-BODIPY-8 derivatives can be used as fluorescence probes in membranes[44]. This was accomplished by quenching of the BODIPY due to iodide in cholesterol enriched phosphatidylcholine (major component in membranes) in bilayer vesicles. The evaluation was performed by spectral characterization by vitue of the disappearance of emission peaks. Earlier reported[45], in 2008, that cellular membranes i.e. plasma membranes, containing differing compositions of cholesterol and sphingolipids could be determined by BODIPY fluorophores, on a BODIPY core **49**.

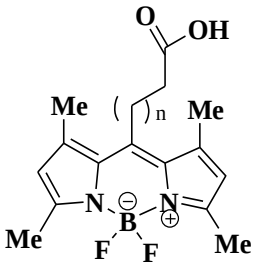

a. n = 1
b. n = 3
c. n = 5
d. n = 7

49

As research progressed, fluorescent bithiazole-based ΔF508-CFTR corrector was incorporated in a BODIPY core[46]. The ΔF508-CFTR is a defect in the cellular processing of cystic fibrosis. The bithiazole-based ΔF508-CFTR BODIPY conjugate **50** was used to demonstrate this mutation in mice.

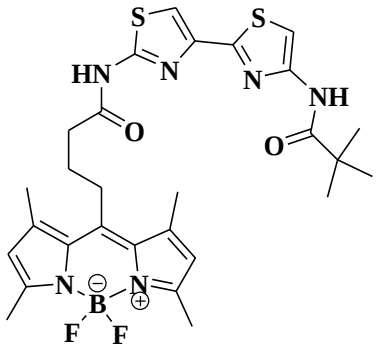

50

Following is a synthesized BODIPY-cyclooctyne derivative **51** and used it for proteomic studies[47].

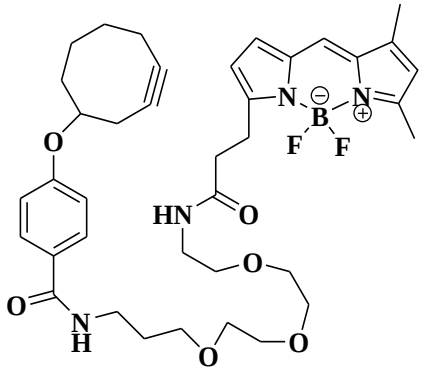

51

2.3 Supramolecular Chemistry

Supramolecular chemistry is a study of the weaker and reversible non-covalent bonds between molecules i.e. intermolecular forces. Emphasis is placed on molecular chemical systems and focus is not merely based on the molecular level of a molecule. These chemical systems are made up of a discrete number of assembled molecular subunits or components[48,49] . This pivotal point which is examined in supramolecular chemistry refers to the weaker and reversible non-covalent interaction between molecules, compared to traditional chemistry which focuses on covalent bonding[50]. Supramolecular chemistry demonstrates a number of important concepts

such as molecular self-assembly, molecular recognition and complexation, template-directed synthesis, mechanically-interlocked molecular architectures, dynamic covalent chemistry, biomimetic, molecular machinery and imprinting[51]. All of these concepts are possible due to forces which include electrostatic effects, hydrogen bonding, hydrophobic forces, metal co-ordination, pi-pi interactions and van der Waals forces[52]. The study of non-covalent interactions is critical for the understanding of many biological processes[53].

2.3.1 Historical Overview of Supramolecular Chemistry

The importance of supramolecular chemistry was established by Donald J. Cram, Jean-Marie Lehn, and Charles J. Pedersen in the year 1987. Their work in this area were only recognized after these chemists were awarded the Nobel Prize in Chemistry. The development of selective "host-guest" complexes, in which a host molecule recognizes and selectively binds to a certain guest, was cited as an important contribution[54].

Intermolecular forces were discovered by a physical chemist Johannes Diderik van der Waals hence the given interaction was named ‘’van der Waals forces’’[55]. Hermann Emil Fischer used this concept in his research in supramolecular chemistry and was awarded the Nobel Prize. In 1890, he suggested that the enzyme-substrate interactions take the form of a "lock and key", which became the basis for molecular recognition and host-guest chemistry[56]. Non-covalent bonds, such as the hydrogen bond was conceptualized in 1920 by Latimer and Rodebush[57].

These principles were further used to enhance the knowledge of protein structures and other biological processes. A historical event occurred when these principles were used by scientists to conclude that the double helical structure of deoxyribonucleic acid consisted of two separate

strands of nucleotides connected through hydrogen bonds. The use of non-covalent bonds is essential for DNA replication. After this breakthrough, chemists explored this concept and applied it to synthetic systems. In the 1960s, researchers were active in synthesizing shape-selective receptors and ion-selective receptors. In the 1980s, research in this area progressed at a rapid pace and concepts such as mechanically-interlocked molecular architectures had emerged. In the 1990s, researchers developed molecular machinery and highly complex self-assembled structures and sensors and methods of electronic and biological interfacing. It was during this point that electrochemical and photochemical themes became integrated into supramolecular systems. Nanotechnology was also a strong influence on this subject, with building blocks such as fullerenes, nanoparticles and dendrimers becoming widely used in synthetic systems.

2.4 Chemical Dyes

Dyes are complex unsaturated aromatic compounds exhibiting characteristics such as intense colour and characteristic solubility[58]. They consist of different types of colouring particles which differ in chemical composition, the coloring may be temporary or permanent[59]. There are two classes of dyes viz natural dyes and synthetic dyes.

The natural dyes occur in roots, berries, bark, leaves, wood, fungi, and lichens[60] whilst synthetic dyes are made by humans. Well known plant-based dyes are woad, indigo, saffron, madder, tyrian purple, kermes, cochineal, and logwood. Woad and indigo dyes **(52)** are blue dyes that can be extracted in small concentrations from the Indigofera tinctoria plant. Woad may be used to prevent cancer as it is high in Glucobrassicinn[61]. Saffron can be used as golden yellow dye **(53)** which can been obtained from the flower of Crocus sativus, commonly known as the saffron crocus[62]. Saffron contains more than 150 volatile and aroma-yielding compounds and is

known for its medicinal history. Several research studies have inferred that saffron may have possible anti-carcinogenic, anti-mutagenic, immunomodulating, and antioxidant-like properties[63,64]. Madder roots, also known as Rubiatinctorium belong to the plant family Rubiaceae[65]. Alizarin **(54)**, commonly known as Mordant Red 11 and Turkey Red, are red dyes that are obtained from madder[66]. This is used for dyeing textile fabrics. Tyrian purple **(55)** is a dye which is secreted by a sea snail known as Murex and is used in the textile industry[67]. Kermes is deep red in colour and is produced from a scale insect, Kermes vermilio. Aluminum and calcium salts of carminic acid are responsible for the crimson colour in Carmine dyes [68]. Haematoxylin **(56)** is a natural dye obtained from Logwood. It is oxidized to form haematein compounds which produce strongly coloured complexes with certain metal ions. It is used for staining cell nuclei in histological studies[69].

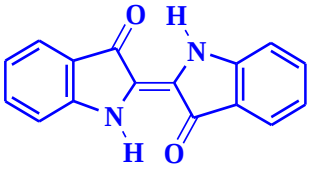

52

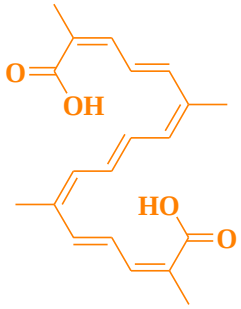

53

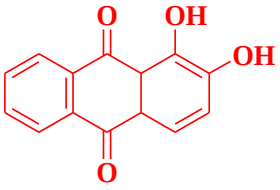

54

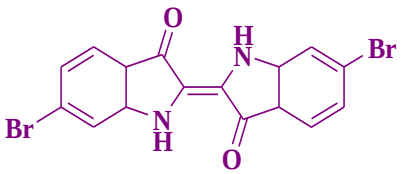

55

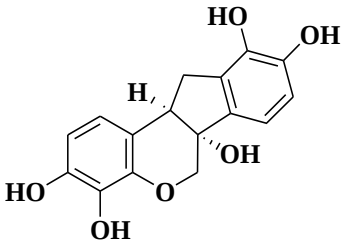

56

Synthetic dyes are classified as acidic, basic, direct or substantive, mordant, vat, reactive, disperse and azoic. These are usually formulated in industry and in research facilities[70]. Dyes can

be used as therapeutic agents and test reagents in medicine and in scientific research. Some of these dyes are called as Nitroso, Indophenol, Nitro, Azine, Azo, Oxazine, Azoic, Thiazine, Stilbene, Sulfur, Carotenoid, Lactone, Diphenylmethane, Aminoketone, Triarylmethane, Hydroxyketone, Xanthene, Anthraquinone, Acridine, Indigoid , Quinoline, Phthalocyanine, Methine , Natural organic coloring Matters, Thiazole, Oxidation bases, Indamine and Inorganic colorants[71].

2.4.1 Historical Overview of Dyes

In 1856, William Henry Perkin synthesized the first synthetic dye known as 'Mauve', an aniline based dye obtained from tar coal. He discovered this when he was working for a cure for Malaria [72,73]. This success led him to discover the synthetic versions of alizarin and indigo which were derived from plants. Although evidence suggests that dyeing methods were used in fabrics, found in Egyptian tombs[73] around 4,000 years ago, it was the 1800's which witnessed the development of dyes. The historical outcomes of dyeing indicated that natural dyes were highly unstable owing to their complex nature and that there were numerous attempts of extracting it in ancient times. Following the late 1850's, numerous chemists attempted in making dyes but it was only in 1860s that a manufacturing plant in the United States of America produced the first aniline, nitrobenzene, picric acid dyes as well as other ranges of dyes. After the 1860s, research in dyeing began to expand into specific industries.

2.5 Phenomenon of fluorescence

2.5.1 Photochemistry

Photochemistry can be defined as the branch of chemistry whereby molecules absorb light (radiant energy) to bring about chemical changes in chemical reactions[74]. Light can be described

as electromagnetic radiation which requires a source of energy. The electromagnetic spectrum exhibits the distribution of electromagnetic radiation according to their various frequencies. **Figure 2.1** is a model of the electromagnetic spectrum. When a substance absorbs electromagnetic radiation, it undergoes a photochemical reaction. Each molecule in the chemical system absorbs a photon.

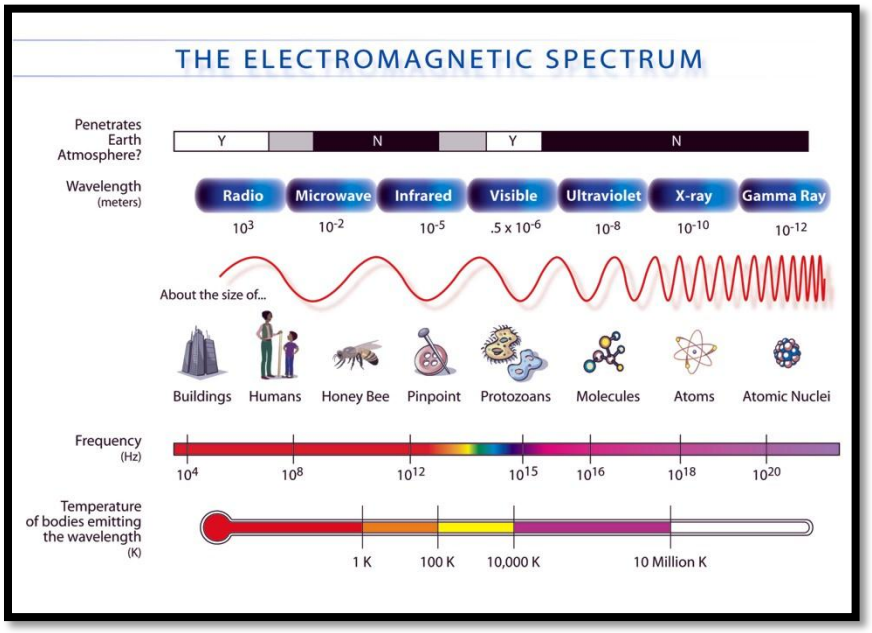

Figure 2.1: Electromagnetic Spectrum Indicating the different Wavelengths and Frequencies[75]

In this study, the wavelength regions concerned for the characterizations of the organic compounds are the IR, UV-Visible and X-Ray region. As one goes across the spectrum from left to right (**Figure 2.1)**, the frequency of electromagnetic radiation increases. Each frequency has a different interaction on a molecule. For example,

- Radiowaves: collective oscillation of charge carriers in bulk material.
- Microwaves: molecular rotation

- Near infrared radiation: molecular vibration
- Visible radiation: molecular electron excitation
- Ultraviolet radiation: excitation of molecular and atomic valence electrons
- X-radiation: excitation and ejection of core atomic electrons using the Compton scattering (for low atomic numbers) and is used in fluorescence spectroscopy.
- Gamma radiation- energetic ejection of core electrons in heavy elements that also used the Compton scattering (for all atomic numbers), excitation of atomic nuclei, including dissociation of nuclei.

2.5.2 Fluorescence and Fluorescence Spectroscopy

Fluorescence is a phenomenon which is observed when a molecule absorbs electromagnetic radiation and emits it. Generally, the light emitted from the molecule is of lower frequency. This is a form of luminescence. Fluorescence can be elucidated in a systematic mechanism with the use of the Jablonski diagram (**Figure 2.2**). The Jablonski Diagram can be used to describe basic principles of molecular photophysics.

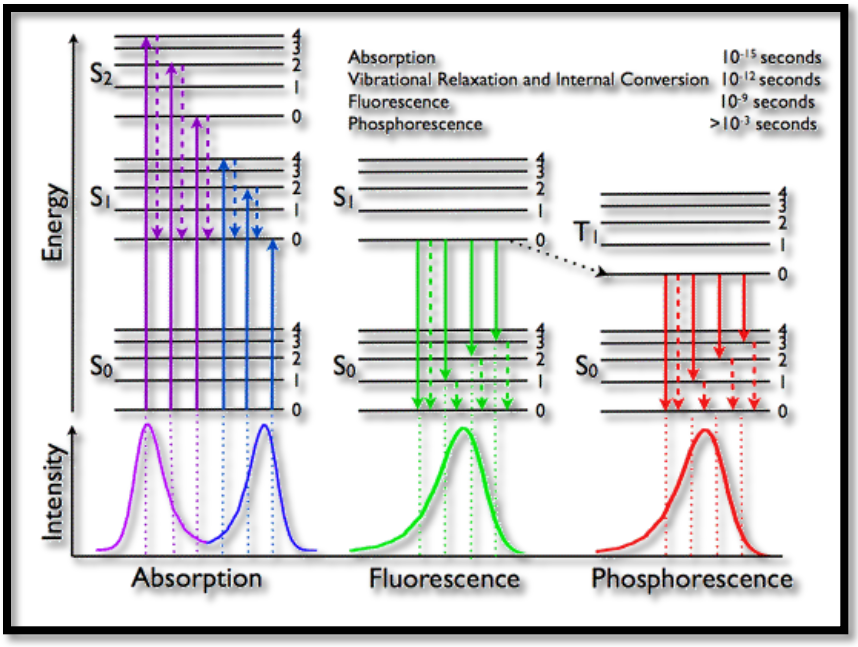

Figure 2.2: Jablonski Diagram demonstrating various electronic states in a molecule[76]

In **Figure 2.2**, the electronic states of the molecule and the transitions which may occur are demonstrated within the molecule's orbital. The electronic states on the vertical axis demonstrate the energy and the horizontal axis represents the spin multiplicity. The S_0 state is the singlet state with anti-parallel (anti-bonding) spin. It is diamagnetic. The S_1 state is the higher singlet state. All transitions between the electronic states allow the same spin multiplicity. Fluorescence compounds are referred to as fluorophores.

The first state is molecular excitation. This process occurs when the electrons in the molecule from the S_0 state is excited by electromagnetic radiation. The electron in the molecule absorbs the radiation as a photon which then results in the excitation to singlet state S_1'. The second stage is where the excited state exists for an infinite amount of time and it is during this time, the fluorophore undergoes conformational transition and interacts with the molecular environment. Here the energy is dissipated from S_1' to yield S_1, a more relaxed singlet state and fluorescence is

created. Thereafter, the third stage commences and the photon returns back to the S_0 singlet ground state, emitting energy in the form of radiation. The energy emitted from the third stage is lower (higher wavelength) than the energy absorbed by the molecule. In fluorescence there are a number of factors which may be employed to characterize the molecular fluorescence nature of a compound as represented in **Table 1.**

Table 1: Characteristic Properties of Fluorescence

Aspect	**Measurement Nature**
Quantum Yield	Ratio of the number of fluorescent photons vs. the number of photons initially excited
Stoke shift	Difference between the wavelength or energy of the fluorescent photon and the excited photon
Lifetime	The amount of time the photons remain in the excited state
Molar absorptivity / extinction coefficient	Measures how strong the chemical species can absorb light at a particular wavelength
Brightness	Quantifies how bright a compound fluoresces

2.5.3 Quantum Yield

The quantum yield of a compound can be defined as the ratio of fluorescent photons emitting radiation to the number of photons initially excited[77]. The symbolic representation of

fluorescence quantum yield is given by ϕ. The quantum yield of a compound can be determined experimentally with the use of a predetermined fluorophore quantum yield (standard) and the same parameters of the standard can be implemented to the chemical species to be determined. Calculation of the quantum yield can be performed by two approaches, namely the comparative method (equation 1) and the single-point method (equation 2)[78]. Single point method is more efficient than the comparative method; however, the accuracy can be questioned. The quantum yield should ideally be less than 1.00 unless PET mechanism occurs.

Equation 1.

$$\Phi = \Phi_R \left(\frac{m}{m_R}\right)\left(\frac{n^2}{n_R^2}\right)$$

Where Φ is the quantum yield, subscript R refers to the reference standard, m is the gradient of the curve of intensity of the referenced standard vs. absorbance of the chemical species and n denotes the solvent refractive index.

Equation 2.

$$\Phi = \Phi_R \left(\frac{I}{I_R}\right)\left(\frac{OD_R}{OD}\right)\left(\frac{n^2}{n_R^2}\right)$$

Φ is the quantum yield, subscript R refers to the reference standard, I is the integrated fluorescence intensity, OD is the optical density (absorbance) and n denotes the solvent refractive index.

2.5.4 Stoke Shift

Stoke shift can be defined as the spectral position for the wavelength maximum of the absorption (λ_{ex}) and luminescence (λ_{em}) peaks arising from the same electronic transition[79]. The explanation for the shift in wavelength relates to the lifetime in which the photon interacts with the S_1 singlet excited state thus resulting in a longer wavelength than the excited wavelength. One can experimentally obtain and perform a calculation directly from the absorption and fluorescence spectra. Equation 3 can be used to calculate the shift of a fluorophore.

Equation 3:

$$Stroke\ Shift = \lambda_{em} - \lambda_{ex}$$

Whereby em denotes the emission spectra wavelength maxima and the ex-denotes the excitation wavelength maxima.

2.5.5 Lifetime

The lifetime of a compound is a measure of the average time the fluorophore remains in the excited state prior to returning down to ground state[80]. This is dependent on the fluorophore nature. The characteristic time constant of this decay (the fluorescence lifetime), is in the range of a few picoseconds (10-12 s) to several nanoseconds (10-9 s) Lifetimes can be measured by two routes, one being Lifetime Time Correlated Single Photon Counting (TCSPC) and other being phase shift ø and modulation m. This lifetime can be used to calculate the homogeneous nature of the excited photon within the environment.

Equation 4:

$$I\ (t) = \alpha\ e^{\frac{-t}{\tau}}$$

Whereby α is the intensity at time 0, t is the time after absorption and τ is the lifetime (a fraction of the molecules in the excited state which has a decrease factor of 1/e).

2.5.6 Molar Absorptivity/ Extinction Coefficient

The molar absorptivity (ε)[81] of a chemical species can be used to quantify how strong the chemical species can absorb electromagnetic radiation (light). For the determination for this molar absorptivity, Beer-Lamberts Law is employed as in equation 5, which relates the absorption of light to the properties of the material through which the light is traveling. The law also demonstrates the relationship between absorbance and concentration of a chromophore[82].

Equation 5:

$$A = \varepsilon B c$$

Where by A is the absorbance of the chemical species, B denotes the path length of the cuvette used in sample analysis and c denotes the concentration of the chemical species.

2.5.7 Fluorescence Brightness

The brightness of the fluorophore can be determined by the product of the quantum yield and the molar absorptivity. This determination can be used to discuss the efficiency of the fluorophore. Following equation 5, the brightness of a fluorophore can be calculated with equation 6.

Equation 6:

$$Brightness = \Phi x \varepsilon$$

2.5.8 Application of Fluorescence

The application of fluorescence into fluorescence spectroscopy has become an exceedingly advantageous technique of the 21st century. Over the decades, this technique has found to be

incredibly beneficial in research fields such as biochemistry, medicine and chemistry especially when analyzing organic compounds[83]. Due to its high sensitivity and selectivity to biochemical environments, the technique is used extensively in the medical field for drug design and drug tracing[37] and outputs can be attained with high resolution[84]. This technique is a versatile imaging tool and can be utilized as a chemosensor. Chemosensors are fluorophores (receptors) which have incorporated binding sites to communicate via a mechanism. This mechanism involves the transfer of signals of the fluorophore in a specific environment for binding. These signal moieties may be observed through UV/Vis Spectroscopy, Voltammetry or Fluorescence spectroscopy.

2.5.8.1 Chemosensors

As mentioned, chemosensors are fluorophores which are used to communicate via signals when involved in an interaction with an analyte. There has been a great deal of research surrounding chemosensor and their ability to detect anions and cations. This research conducted involves the Cu^{2+} sensor of the Zinpyr Family Based Fluorescein[85]. A new Zn^{2+} Chemosensor on the Functionalized 8-hydroxylquinoline was designed[86]. For this, the sub-division of fluorescence spectroscopy measurements are based on the Stokes shift and intensity. Chemosensors consist of a receptor and a reporter. A guest binds with the receptor and a signal is then observed by the reporter. This process involved in fluorescent sensor makes chemosensors one of the most powerful tools for monitoring metal ion *in vivo* system[86]. This is due to its simplicity and high sensitivity designed for imaging[87]. This tool is important as it plays an important role in biology as nutritional microelements and as ligands to proteins. Chemosensors undergo three different mechanisms, namely photo-induced electron transfer (PET), intermolecular charge transfer (ICT) and fluorescence resonance energy transfer (FRET). These mechanisms could be used to give an

explanation of the nature of the fluorescence profile of a chemosensor. The concept of fluorescence 'switch on or off' is also based on these three mechanisms.

2.5.8.1.1 Photo-induced Electron Transfer

In the PET mechanism, the chemosensor utilizes the atom spaces to connect to a fluorescent group of a receptor and these comprises of high-energy non-bonding electron pairs[87]. Once the fluorescent group is connected to the receptor, there is a transfer of an electron to the excited fluorescent group which then results in a quench of the fluorescence signal. However, in the presence of a metal ion, a coordinated electron pair would prevent the electron transfer and consequently the fluorescence would be turned on[88, 89]. The bis(2-picolyl)amine based was studied as a PET sensor for transition metal ions, which had demonstrated the fluorescent on-off switches[90]. In addition to this study, the optical signal of the receptor in the presence of zinc metal ions, had demonstrated the fluorescent switch as in **Figure 2.3** and **Figure 2.4**.

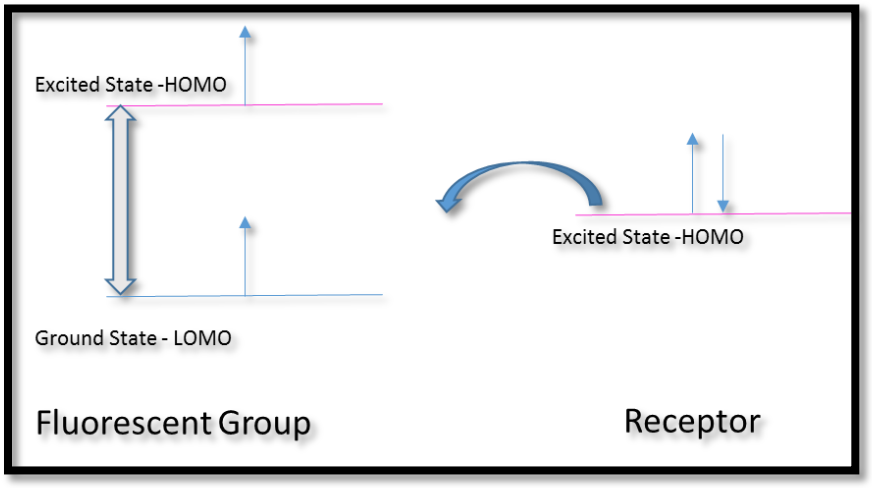

Figure 2.3: Photon-Electron Transfer Mechanism

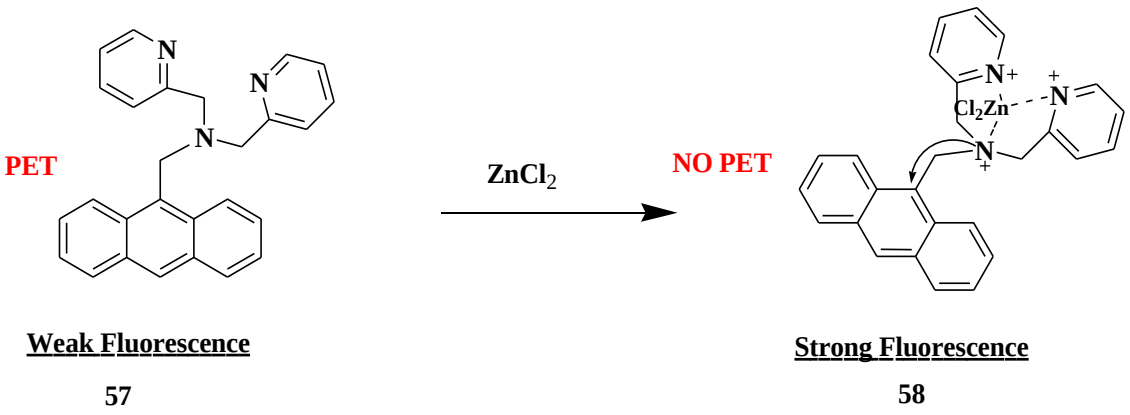

Figure 2.4: Photon-induced Electron Transfer Mechanism[43]

2.5.8.1.2 Intermolecular Charge Transfer

An ICT (Intermolecular Charge Transfer) system is a ratiometric system and in comparison to PET mechanism, as there are no spacers. Receptors which contain an amino group usually form a new conjugation system with the p-electron. This results are electron rich and electron poor terminals which in turn leads to ICT from the electron donor within the fluorophore which is then binds to the metal ion. When this occurs, the cation reduces the electro donator capacity of the receptor and a blue emission shift is observed. Similarly, the receptor is an electron acceptor; the coordination of the cation will result in a red shift. This further strengthens the pull – push effect[91]. This can be demonstrated on **Figure 2.5**.

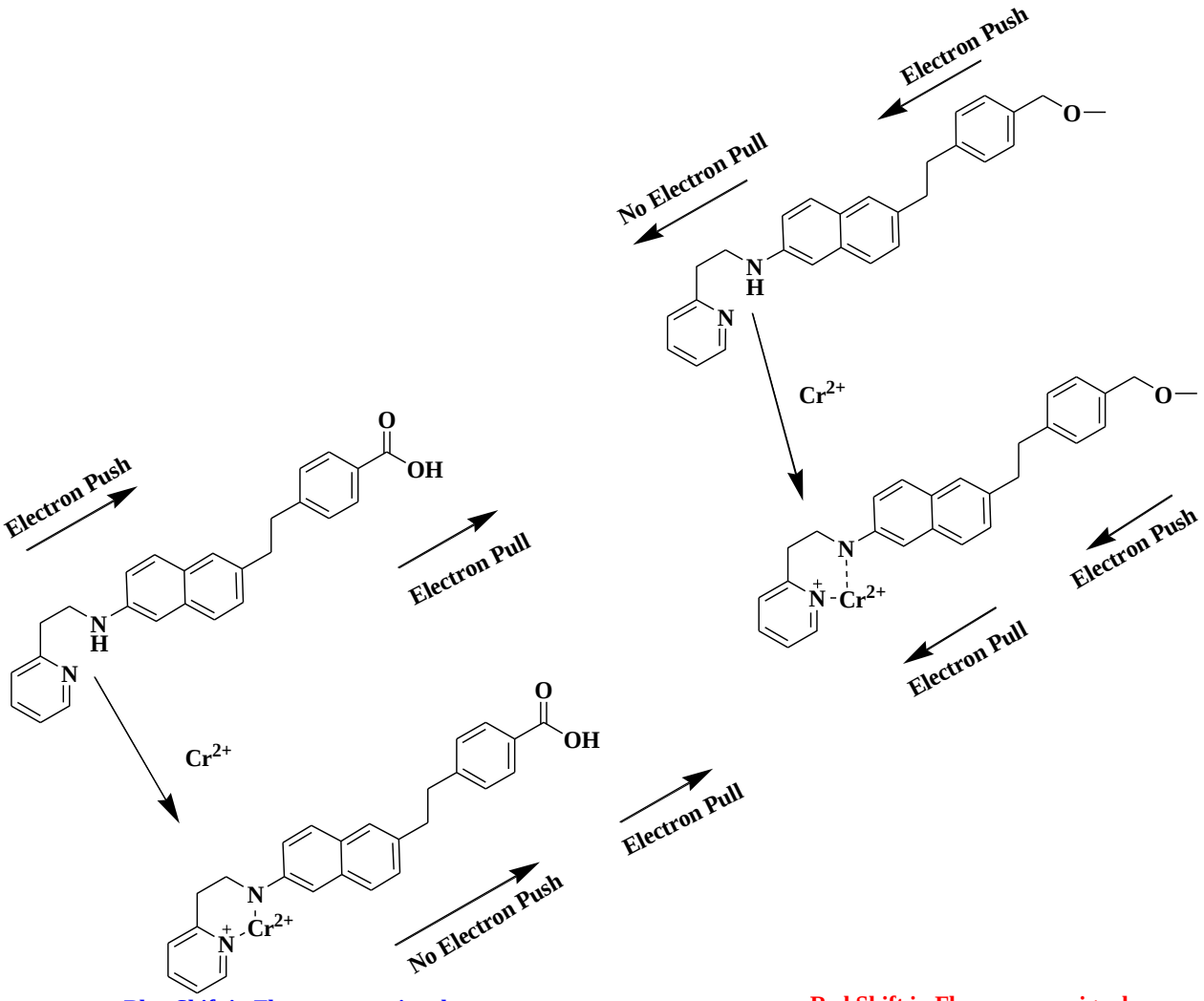

59 60

Figure *2.5: ICT Mechanism*

2.5.8.1.3 Fluorescence Resonance Energy Transfer (FRET)

Fluorescent resonance energy transfer (FRET) is a powerful technique which is used for study of the conformational distribution and dynamics of biological molecules[92]. It can be described as a distance dependent, non-radiative transfer of excitation energy from an excited donor fluorophore, to a suitable proximal ground state acceptor fluorophore. It is one of few tools available for measuring nanometer scale distances and the changes in distances, both *in vitro* and *in vivo*[93]. These FRET- based sensors usually contain two fluorophores which are connected by a

covalent bond and contains spaces within the molecule. In order to observe it, three conditions need to be met[94]. These are:-

a) The donor should have sufficient lifetime for transfer of energy to occur.
b) The donor and acceptor molecules must be in close proximity to one another (typically 10-100 Å) – distance of 10nm.
c) The excitation spectra of the acceptor must overlap the fluorescence emission spectrum of the donor (as in **Figure 2.6**).

Quenching can be explained in two contexts i.e. contact quenching and collision quenching. Contact quenching occurs when a complexed molecule consisting of a fluorophore and a quenching molecule is in direct contact prior to excitation. Here the energy is directly transferred to the contact molecule. Collision quenching can be explained as a reaction between the fluorophore and the quenching molecule in solution. There is an immediate transfer of energy to the contact molecule.

The mechanism of the two approximately parallel fluorophores undergoes overlapping. When energy is transferred, the phenomenon observed is the quenching of the donor fluorescence with a reduced lifetime, and an increase in the fluorescence emission is visible. This phenomena was reported and can be used to describe the process of FRET in his research publication[94]. Directly from his publication, **Figure 2.7** displays the chemosensor design.

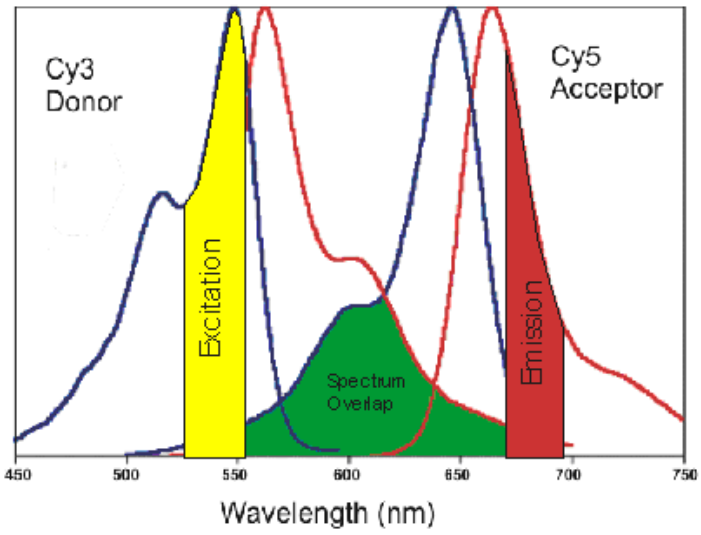

Figure 2.6: Fluorescence Resonance Electron Transfer Spectra exhibiting Overlap[94]

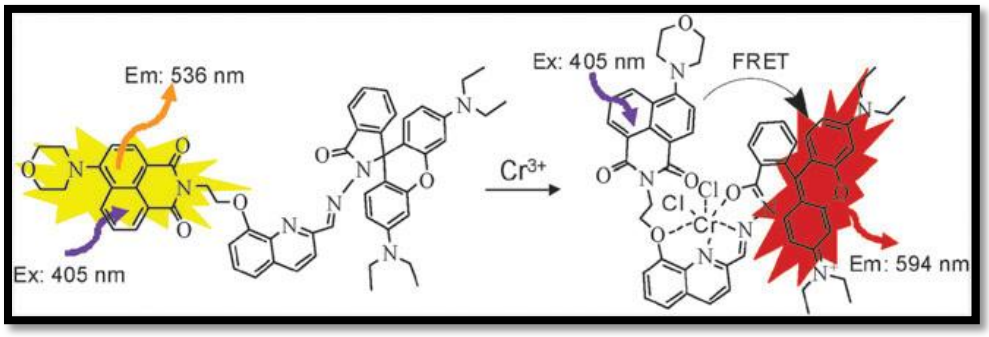

Figure 2.7: FRET Chemosensor designed by Zhou (2008) et al[94]

Chemosensors are used in a vast array of applications, such as biomedicine, bio-processing, environmental applications and food safety. A highly sensitive chemosensor for Cr^{3+} which demonstrated the use of rhodamine B with a ferrocene substituent (FD7) as a fluorescent probe[95]. This was used for monitoring Cr^{3+} in living cells. **Figure 2.8** is an example of chemosensor as a bio-chemosensor.

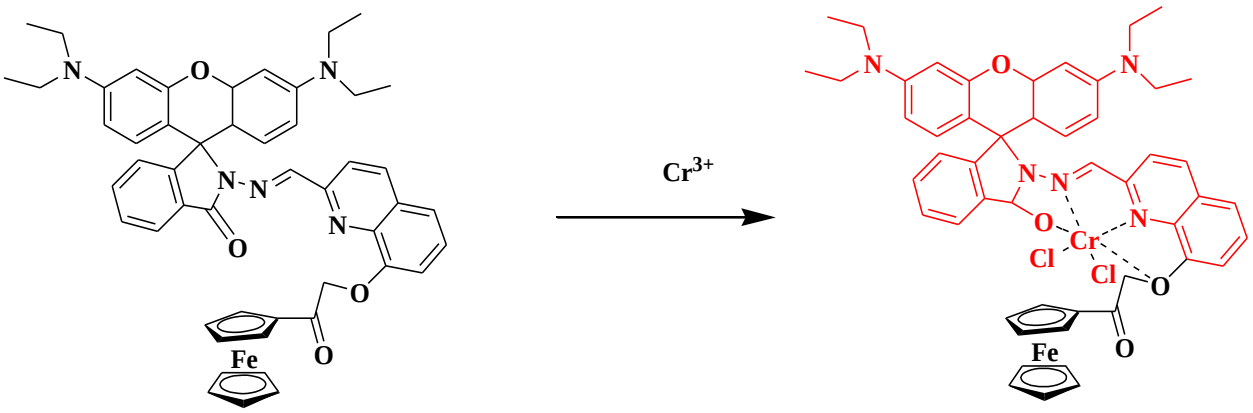

Figure 2.8: Highly sensitive chemosensor for Cr^{3+} - rhodamine B with a ferrocene substituent (FD7) [96]

It was first reported that chemosensors found application in aqueous solutions[96]. After much improvements to the design of a new Zn^{2+} chemosensor based on 8-hydroxyquinoline the experiment was performed in aqueous solution of metal ion. The outcome suggested the 8-hydroxylquinoline serve as a 'Switch-on' chemosensor due to its high selectivity to Zn^{2+} in comparison to other metal ions (**Figure 2.9**). Coumarin based fluorescent probes with a high selectivity for Cu^{2+} was designed and synthesized[97]. In human neuroblastoma, SH-SY5Y cells were treated with (E)-3-(2,5-dimethyloxybenzylideneamino)-7-hydrox-2H-chromen-2-one. These are among a few of many research applications.

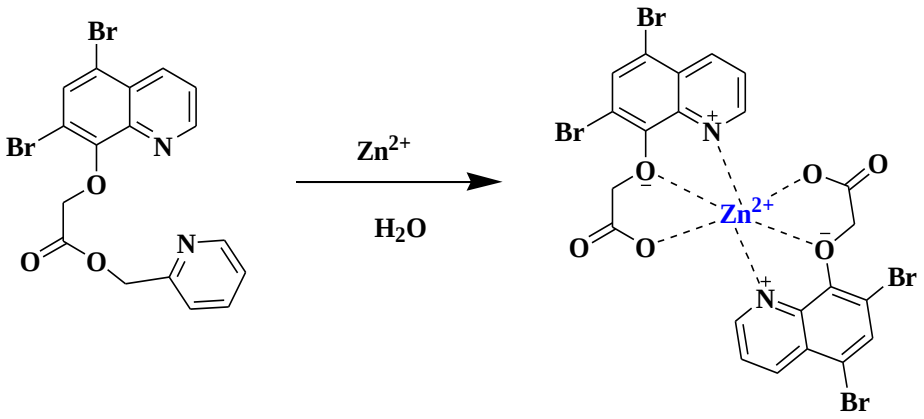

61 **62**

Figure 2.9: A new Zn^{2+} chemosensor based on 8-hydroxyquinoline

2.6 Photovoltaic Cells

Photovoltaic cells (solar cells) are the direct conversion of electromagnetic radiation into electricity at the atomic level[98]. Some materials show a property called photoelectric effect that causes them to absorb photons of light and release electrons. To determine whether a compound poses the ability to act as a photovoltaic cell, measurements can be conducted using cell efficiency and this can be done by reflectance spectroscopy.

Reflectance spectroscopy is the study of light as a function of wavelength that has been reflected or scattered from a solid, liquid, or gas[99]. The primary mechanisms of reflectance spectroscopy are absorption and scattering, both of which vary with wavelength to produce the reflectance spectrum that is recorded[100]. The standard spectroscopic measurements are displayed as transmittance percentages. This can be obtained using equation 7[101] and by using the absorbance results obtained from analyses.

Equation 7:

$$Absorbance = \log(\frac{1}{T})$$

T is the transmittance. Equation 8 is the conversion of transmittance to percentage.

Equation 8:

$$T = \frac{\%T}{100}$$

2.7 Cancer Lines

Cancer is a disease which is caused when cell growth becomes irregular and genes are directly damaged. It also combines with existing genetic faults within cells to cause cancerous mutations[102]. Cancer is medically identified as malignant neoplasia[103]. This is generally caused by a number of factors such as tobacco use, dietary factors, infections, exposure to radiation, lack of physical activity, obesity, and environmental pollutants[104]. There are a many types of cancer which an individual may suffer from and can it spread to the entire human body which may be fatal. However, many forms of chemotherapy[105] and research are presently been undertaken to establish a possible cure for this disease. For the objective of the project, A529 lung cancer cell lines were focused on. Lung cancer is known as carcinomas that is derived from epithelial cells[106] in the lungs. There are two main types of lung cancer:- small-cell lung carcinoma (SCLC) and non-small-cell lung carcinoma (NSCLC) [107].

2.8 Molecular Modeling Docking Studies

Molecular computational modeling docking is a technique which is used to predict the preferred orientation of one ligand to a protein when bound to each other to form a stable complex. This preferred orientation obtained is then used to predict the strength of the binding affinity between two molecules used for the two methods namely scoring functions and matching[108]. Proteins are

obtained from a protein bank and are bound with the novel ligand to form a theoretical interaction between the two.

The p53-MDM2 relationship is tumor suppressor gene found in the human body. p53 is also known as protein 53 and is a tumor suppressor in the human body[109]. This interaction between MDM2 and p53 is closely controlled by a complex array of post-translational modifications, which in turn dictates the stability and activity of p53 and MDM2[110].It plays a critical role in repairing of DNA, differentiation, senescence, apoptosis and cell-cycle arrest[111]. However, in human cancer, it is evident that the p53 tumor suppressor is inactive and is mutated to form p53-MDM2. MDM2 is the human murine double minute 2 oncoprotein[112]. Inhibitors of the p53-MDM2 binding interaction are expected to restore the activity of p53 back to normal and to act as an anti-cancer agent[113].

2.9 Cytotoxicity

The cytotoxicity can be defined as the ability of a substance to be toxic to a specific nature of cells[114]. The cytotoxicity and cell viability can be measured be methods such as Colony Formation, Crystal Violet method, MTT and WST method, Tritium-labeled Thymidine Uptake Method[115]. These methods form the basis of a number of *in vitro* assays of a cell population's responses. From all these techniques, the MTT assay is much more superior as it is easy to use, highly reproducible, and safe and can be used for cell viability or cytotoxicity[116].

MTT assay is dependent on colour change. MTT (3-(4,5-dimethylthiazol-2-yl)-2,5-diphenyltetrazolium bromide) is reduced to form purple formazan in living cells. The Scheme 1 below demonstrates the reaction undergone when the reduction of the 3-(4,5-dimethylthiazol-2-

yl)-2,5-diphenyltetrazolium bromide occurs. The extent of the reduction reaction is measured by the use of a UV-Vis spectrophotometer at a wavelength range 550-600 nm[117].

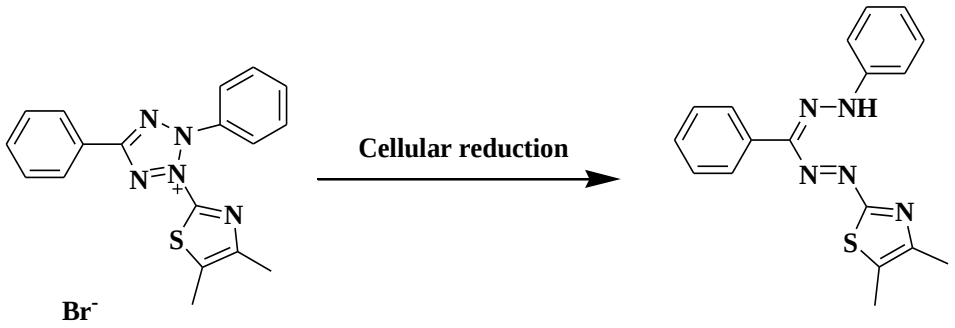

63 **64**

Scheme 1: Cellular reduction of yellow MTT to purple formazan

References

1. *Alkaloids*, [WWW], Available from: <http://www.reboundhealth.com/cms/images/pdf/alkaloids%20id%2013982%20id%2014425.pdf> [Accessed on 24 November 2013]
2. The Vault of Erowid, (1995), *Golden Guide: Hallucinogenic Plants*, [WWW], Available From: <https://www.erowid.org/library/books_online/golden_guide/g11-20.shtml> [Accessed on 22 April 2013]
3. National Institute on Drug Abuse, (2009), *DrugFacts: Hallucinogens - LSD, Peyote, Psilocybin, and PCP*, [WWW], Available from <http://www.drugabuse.gov/publications/drugfacts/hallucinogens-lsd-peyote-psilocybin-pcp > [Accessed on 22 April 2013]
4. Schmitz, R. (1985), 'Friedrich Wilhelm Sertürner and the Discovery of Morphine,' *American Institute of the History of Pharmacy*, Vol. 27, No. 2, pp. 61 - 74
5. Brownstein, M. J. (1993), A Brief History Of Opiates, Opioid Peptides, And Opioid Receptors, *Proceedings of the National Academy of Science of the United States of the America*, Vol. 90, Issue. 12, pp. 5391-5393
6. a) Duoc, N. (2012) *Classification Of Alkaloids*. [WWW] Available from: <http://www.epharmacognosy.com/2012/07/classification-of-alkaloids.html> [Accessed on 26 August 2014]

   b) Encyclopædia Britannica (1994) *Alkaloid*. [WWW] Available From: http://global.britannica.com/EBchecked/topic/15672/alkaloid [Accessed on: 24 November 2013]

7. Foley, M.; Tilley, L. (1998). 'Quinoline Anti-malarials: Mechanisms of Action and Resistance and Prospects for New Agents.' *Pharmacology & Therapeutics,* Volume 79, Issue 1, pp. 55-87
8. Ratheesh, M.; Sindhu, G.; Helen, A.; (2013). 'Anti-Inflammatory Effect Of Quinoline Alkaloid Skimmianine Isolated From *Ruta graveolens L.*' *Inflammation Research,* Volume 62, Issue 4, pp. 367-376
9. Vudumula, U.; Adhikari, M. D.; Ojha, B.;Goswami, S.; Das, G. and Ramesh, A. (2012) 'Tuning The Bactericidal Repertoire And Potency Of Quinoline-Based Amphiphiles For Enhanced Killing Of Pathogenic Bacteria.' *RSC Advances,* Volume 2, Issues 9, pp. 3864-3871
10. Dreikorn, B. A.; Jourdan, G. P.; Davis, L. N.; Suhr, R.G. ; Hall, H. R.; and Arnold, R. W. (1991) 'Synthesis and Fungicidal Activity of 4-Phenethylaminoquinoline and its Analogues and Derivatives.' *Synthesis and Chemistry of Agrochemicals II,* Lilly Research Laboratories, Eli Lilly and Company, P.O. Box 708, Greenfield, IN 46140. pp. 553–565
11. Karthik, S.; Saha, B.; Ghosh, S. K. and Pradeep Singh, N. D. (2013) 'Photoresponsive Quinoline Tethered Fluorescent Carbon Dots For Regulated Anticancer Drug Delivery.' *Chemical Communications,* Volume 49, Issue 89, pp. 10471-10473
12. Wikipedia (2013) Q*uinolines*. [WWW] Available From: <http://en.wikipedia.org/wiki/Quinoline> [Accessed on: 24 November 2013]
13. Gumos, J. (1977). 'Quinolines Part 1.' *Introduction.* John Wiley and Son Inc. pp. 2-3

14. The American Heritage® Medical Dictionary, (2004), Imidazole, [WWW], <http://medical-dictionary.thefreedictionary.com/imidazole> [Accessed on 10 February 2014]
15. Tai, H. and Yuan, B. (1978), On The Inhibitory Potency Of Imidazole And Its Derivatives On Thromboxane Synthetase, *Biochemical and Biophysical Research Communications*, Vol.80, Issue 1, pp. 236–242
16. Pfaller M.A. and Krogstad D.J.(1983) 'Oxygen enhances the antimalarial activity of the imidazoles.' *The American Journal of Tropical Medicine and Hygiene*, Volume 32, Issue 4, pp. 660-665
17. Silva , V. G.; Silva, R. O.; Damasceno, S. R. B .; Carvalho, N. S.; Prudêncio, R. S.; Aragão, K. S.; Guimarães, M. A.; Campos, S. A.; Véras, L. M. C.; Godejohann, M.; Leite, J. R. S. A.;. Barbosa, A. L. R. and Medeiros, J. R. (2013) 'Anti-inflammatory and Antinociceptive Activity of Epiisopiloturine, an Imidazole Alkaloid Isolated from *Pilocarpus microphyllus*.' *Journal of Natural Products*, Volume 76, Issue 6 , pp. 1071–1077
18. Steel, H.C, Tintinger, G.R, Anderson, R. (2008) 'Comparison Of The Anti-Inflammatory Activities Of Imidazole Antimycotics In Relation To Molecular Structure.' *Chemical Biology and Drug Design*, Volume 72, Issue 3, pp. 225-228
19. Sud, I. J and Feingold, D.S. (1982) 'Action Of Antifungal Imidazoles On Staphylococcus Aureus.' *Antimicrobial Agents And Chemotherapy*, Volume 22, Issue 3, pp. 470-474
20. Khan, A.; Sarkar, S.; Sarkar, D. (2008) 'Bactericidal Activity Of 2-Nitroimidazole Against The Active Replicating Stage Of Mycobacterium Bovis BCG And

Mycobacterium Tuberculosis With Intracellular Efficacy In THP-1 Macrophages.' *International Journal of Antimicrobial Agents*, Volume 32, Issue 1, pp. 40–45

21. Babizhayev, M .A. (2006) 'Biological Activities Of The Natural Imidazole-Containing Peptidomimetics N-Acetylcarnosine, Carcinine And L-Carnosine In Ophthalmic And Skin Care Products.' *Life Sciences*, Volume 78, pp. 2343 – 2357
22. Lee, J. J.; Bruley, D. F.; Kang, K. A. (2008) 'Manipulation of the Affinity Between Protein and Metal Ions by Imidazole and pH for Metal Affinity Purification of Protein C from Cohn Fraction IV-1.' *Advances In Experimental Medicine And Biology*, Volume 614, pp. 93-100
23. Sharma, D.; Narasimhanb, B.; Kumara, P.; Judgea, V.; Naranga, R.; De Clercqc, E. and Balzarinic, J. (2009) 'Synthesis, Antimicrobial And Antiviral Evaluation Of Substituted Imidazole Derivatives.' *European Journal of Medicinal Chemistry*, Volume 44, Issue 6, pp. 2347–2353
24. Pandey J.; Tiwari V. K.; Verma, S.S.; Chaturvedi, V.; Bhatnagar, S.; Sinha, S.; Gaikwad, A. N.; Tripathi, R. P. (2009) 'Synthesis And Antitubercular Screening Of Imidazole Derivatives.' *European Journal of Medicinal Chemistry*, Volume 44, Issue 8, pp. 3350–3355
25. Crane, L.; Anastassiadou, M.; El Hage, S.; Stigliani, J. L.; Baziard-Mouysset, G.; Payard, M.; Leger, J.M.; Bizot-Espiard, J.G.; Ktorza. A.; Caignard, D. H. and Renard, P. (2006) 'Design And Synthesis Of Novel Imidazoline Derivatives With Potent Antihyperglycemic Activity In A Rat Model Of Type 2 Diabetes.' *Bioorganic and Medical Chemistry*, Volume 14, Issue 22, pp. 7419-7433.

26. Baviskar, A. T.; Madaan, C.; Preet, R.; Mohapatra, P.; Jain, V.; Agarwal, A.; Guchhait, S. K.; Kundu, C. N.; Banerjee, U. C.; Bharatam, P. V. (2011) 'N-Fused Imidazoles As Novel Anticancer Agents That Inhibit Catalytic Activity Of Topoisomerase Iiα And Induce Apoptosis In G1/S Phase.' *Journal of Medicinal Chemistry*, Volume 54, Issue 14, pp. 5013–5030
27. Krężel, I. (1998) 'New Derivatives Of Imidazole As Potential Anticancer Agents.' *Il Farmaco*,Volume 53, Issue 5, pp. 342–345
28. Chawla, A.; Sharma, A. and Sharma. A. K. (2012), Review: A Convenient Approach For The Synthesis Of Imidazole Derivatives Using Microwaves, *Der Pharma Chemica*, Vol. 4, Issue. 1, pp. 116-140
29. Life Technologies, *BODIPY Dye Series—Section 1.4*, [WWW] Available from: http://www.lifetechnologies.com/za/en/home/references/molecular-probes-the-handbook/fluorophores-and-their-amine-reactive-derivatives/bodipy-dye-series.html [Accessed on 12 May 2012]
30. Economopoulos, S. P.; Chochos, C. L.; Ioannidou, H. A.; Neophytou, M.; Charilaou, C.; Zissimou, G. A.; Frost, J. M.; Sachetan, T.; Shahid, M.; Nelson, J.; Heeney, M.; Bradley, D. D. C.; Itskos, G.; Koutentis, P. A. and Choulis, S. A. (2013). Novel BODIPY-Based Conjugated Polymers Donors For Organic Photovoltaic Applications, *RSC Advances*, Vol. 3, Issue, 26, pp. 10221-10229
31. Qi, H.; Teesdale, J. J.; Pupillo, R. C.; Joel Rosenthal, J. and Bard, A. J.; (2013). Synthesis, Electrochemistry, and Electrogenerated Chemiluminescence of Two BODIPY-Appended Bipyridine Homologues. *Journal of American Chemical Society*, Vol. 135, Issue 36, pp. 13558–13566

32. Vázquez-Romero, A.; Kielland, N.; Arévalo, M.J.; Preciado, S.; Mellanby, R. J.; Feng, Y.;Lavilla, R. and Vendrell, R. (2013) Multicomponent Reactions for de Novo Synthesis of BODIPY Probes: In Vivo Imaging of Phagocytic Macrophages. *Journal of American Chemical* Society, Vol.135 Issue 43, pp. 16018–16021
33. Cao, X.; Lin, W.; Yu, W. and Wang. J., (2011), Ratiometric Sensing of Fluoride Anions Based on a BODIPY-Coumarin Platform, *Organic letters,* Vol. 13, Issue. 22, pp. 6098–6101
34. http://www.inchem.org/documents/sids/sids/288324.pdf [Accessed on 10 February 2014]
35. Trieds, A. and Kreuzer, F.H, (1968). Difluorboryl-Komplexe von Di- und Tripyrrylmethenen, *Justus Liebigs Annalen der Chemie*, Vol. 718, Issue. 1., pp. 208-223
36. Wagner, R. and Lindsey, J. S. (1996). Boron-Diyrromethene Dye For Incorporation In Synthetic Multi-Pigment Light-Harvesting Array. *Pure and Applied Chemistry*, vol. 68, pp. 1373-1380.
37. Rurack, K.; Kollmannsberger, M. and Daub, J. (2001). Molecular Switching In The Near Infrared (NIR) With The Functionalized Boron-Pyrromethene Dye. *Angewandte Chemie*, Vol 40, Issue 2, p. 385-387
38. Dost, S.; Atilgan, s. and Akkaya, E. U. (2006). Distyryl-Boradiazaindacenes: Facile Synthesis Of Novel Near IR Emitting Fluorophore. *Tetrahedron*, Vol. 62, pp. 8484-8488
39. Rao, M. R.; Mobin, S. M.; Ravikanth, M. (2009). Boron-Dipyrromethene Based Specific Chemodosimeter For Fluoride Ion. Tetrahedron, Vol.66, pp.1728-1734
40. Brellier, M.; Dportail, G. and Baati, R. (2009). Convenient Synthesis Of Water-Soluble Nitrilotriacetic Acid (NTA) BODIPY Dyes. *Tetrahedron*, Vol. 51, pp. 1269-1272

41. Khan, T. K.; Pissurlenkar, R. R. S.; Shaikh, M. S. and Ravikanth, M. (2011). Synthesis and Studies Of Covalently Linked Meso-Furyl Boron—Dipyrromethene- Ferrocene Conjugates. Journal of Organometallic Chemistry. Vol. 697, pp. 65-73
42. Leen, V.; Qin, W.; Yang, W.; Cui, J.; Xu, C.; Tang, X.; Liu, W.; Robeyns, K.; Van Meervelt, L.; Beljonne, D.; Lazzaroni, R.; Tonnele, C.; Boens, N. and Dehaen, W. (2010). Synthesis, Spectroscopy, Crystal Structure Determination And Quantum Chemical Calculations Of BODIPY Dyes With Increasing Conformational Restriction And Concomitant Red-Shifted Visible Absorption And Fluorescence Spectra. *An Asian Journal*, Vol.5, Issues 9, pp. 2016-2036
43. Leen, V.; Miscora, D.; Yin, S.; Filarowski, A.; Ngongo, J. M.; Van der Auweraer, M.; Boens, N. and Dehaen, W. (2011). 1,7-Disubstituted boron dipyrromethene (BODIPY) Dyes: Synthesis and Spectroscopic Properties. *The Journals or Organic Chemistry*, Vol. 76, Issue 20, pp. 8168-8176
44. Boldyrev, I.A.; Zhai, X.; Momsen, M.M.; Brockman, H.L.; Brown, R.E. and Molotkovsky, J.G. (2007). New BODIPY Lipid Probes For Fluorescence Studies Of Membranes. *Journal of Lipid Research,* Vol. 48, Issues 7, pp. 1518-1532
45. Marks, L. D.; Bittman, R. and Pagano, R. E. (2008). Use Of BODIPY- Labeled Sphingolipid And Cholesterol Analogs To Examine Membrane Microdomain In Cells. *Histochemistry and Cell Biology*, Vol.130, pp. 819-832
46. Davison, H. R.; Taylor, S.; Drake, C.; Phuan, P.; Derichs, N.; Yao, C.; Jones, E. F.; Sutcliffe, J.; Verkman, A. S. and Kurth, M. J. (2011). Functional Fluorescently Labeled Bithiazole ΔF508-CFTR Corrector Imaged in Whole Body Slices in Mice. *Bioconjugate Chemistry*, Vol. 22, Issue. 12, pp. 2593-2599

47. Beatty, K. E.; Szychowski, J.; Fisk, J.D. and Tirrell, D.A. (2011). A BODIPY-Cyclooctyne for Protein Imaging in Live Cells. *ChemBioChem*, Vol.12, Issue. 14, pp. 2137-2139

48. Yamaguchi, N. (1999) *Chapter 1*. [WWW] Available at <http://scholar.lib.vt.edu/theses/available/etd-082099-101928/unrestricted/ch1.pdf>[Accessed 24 November 2013]

49. Lan. Y. *Supramolecular Chemistry: General Principles, Selected Examples and Applications*. [PDF] Powell Group. Available from <http://ak-powell.chemie.uni-karlsruhe.de/teaching/Supramolecular%20Chemistry.pdf >. [Accessed on 23 November 2013]

50. Lehna, J. M. 'From Supramolecular Chemistry Towards Constitutional Dynamic Chemistry And Adaptive Chemistry', *Chem. Soc. Rev*., 2007, Vol. 36, pp. 151-160,

51. Dighe, N. S; Pattan,S. R.; Musmade, D.S.; Dengale, S. S.; Kalkotwar, R. S.; Gaware, V. M. and Hole, M. B. (2010) Supramolecular chemistry: An overview. Research Journal of Pharmaceutical, Biological and Chemical Sciences, Vol. 1, Issue 2, pp. 291-301

52. Friedrich-Schiller-Universität Jena. *Supramolecular Chemistry*. [WWW] Schubert group. Available from <http://www.schubert-group.de/index.php?option=com_jresearch&view=researcharea&task=show&id=4&Itemid=84 >[Accessed on 28 April 2013]

53. Chandran,K. C. (2013). *'Potentization'- A Phenomenon Belonging to the Domain Of Supra-molecular Chemistry*. [WWW]. Available from <http://dialecticalhomeopathy.com/2013/07/30/supra-molecular/ > [Accessed on 25 August 2013]

54. Nobelprize.org. (2013) Donald J. Cram, Jean-Marie Lehn, and Charles J. Pedersen in the year 1987. [WWW]. Available from <http://www.nobelprize.org/nobel_prizes/chemistry/laureates/1987/ > [Accessed on 25 August 2013]
55. Princeton. *Van der Waals force*.[WWW]. Available from :< https://www.princeton.edu/~achaney/tmve/wiki100k/docs/Van_der_Waals_force.html >[Accessed on 25 August 2013]
56. Hanes, R. and Borich, D. (2009) 'Beacon Sciences: Commercialisation from biothreat detection to beauty enhancement'. *Journal of Commercial Biotechnology*. Vol. 15, Issues 4,pp. 347–359
57. Latimer, W. M. and Rodebush, W. H., (1920). Polarity And Ionization From The Standpoint Of The Lewis Theory Of Valence, *Journal of the American Chemical Society*, Vol. 42, pP. 1419-1433
58. Health Dictionary (2005), *Dyes*, Available from :<http://www.healthdictionary.info/Dyes.htm>. [Accessed on 25 August 2013]
59. American Cancer Society (2011), *Hair Dyes*. [WWW]. Available from: <http://www.cancer.org/cancer/cancercauses/othercarcinogens/intheworkplace/hair-dyes.> [Accessed on 25 August 2013]
60. BBC News, Health 2006, *War paint plant 'tackles cancer'*, Available from: < http://news.bbc.co.uk/2/hi/4783831.stm >. [Accessed on 13 August 2006].
61. Wikipedia 2013, Available from:< http://en.wikipedia.org/wiki/Trade_and_use_of_saffron>, [Accessed on 11 October 2103]

62. Amina,B. Hosseinzadehb, H.2012. 'Evaluation Of Aqueous And Ethanolic Extracts Of Saffron, Crocus Sativus L., And Its Constituents, Safranal And Crocin In Allodynia And Hyperalgesia Induced By Chronic Constriction Injury Model Of Neuropathic Pain In Rats', *Fitoterapia*, Vol.83, no. 5, pp. 888–895
63. Ferrence,C.S. & Bendersky, G. 2004. 'Therapy with Saffron and the Goddess at Thera', *Perspectives in Biology and Medicine*, Vol 47, no. 2, pp. 199-226
64. Wild Colours, *Dyeing with Madder roots*, Available from:<http://www.wildcolours.co.uk/html/madder_dye.html >.[Accessed on 09 August 2013*]*
65. Wikipedia, *Alizarin*. Available from: < http://en.wikipedia.org/wiki/Alizarin>. [Accessed on 02 October 2013]
66. Cooksey, C. J. 2001. 'Tyrian Purple: 6,6'-Dibromoindigo and Related Compounds', *Molecules*,vol.6, pp. 736-769
67. Kirby, J.; Spring, M. and Higgitt, C. (2007), *The Technology of Eighteenth- and Nineteenth-Century Red Lake Pigments*. Available from: <http://www.nationalgallery.org.uk/upload/rtf/kirby_spring_higgitt2007.rtf >. [Accessed on 21 October 2013].
68. Myers,R. Ph.D. *The Basic Chemistry of Hematoxylin*. Available from: <http://www.leicabiosystems.com/pathologyleaders/the-basic-chemistry-of-hematoxylin/>. [Accessed on 05 May 2011].
69. Druding, S. C. (2003) *Dye History from 2600 BC to the 20th Century*, [WWW] Welcome to Crystal Palace Yarns, Available from <www.straw.com/sign/dyehist.html>[Accessed on 28 April 2013]

70. ColorantsHistory.Org (2003) *Colorants Industry History*, [WWW] Available From: < http://www.colorantshistory.org/ >. [Accessed on 30 November2013]

71. Kiernan, J. A., (2001). Classification and Naming Of Dyes, Stains and Fluorochromes, *Biotechnic & Histochemistry*, Vol.76, Issues. 5 & 6, pp. 266 – 277

72. Encyclopædia Britannica, *History of dyes*, [WWW] Available from: <http://www.britannica.com/EBchecked/topic/174980/dye/277817/History-of-dyes>. [Accessed on 30 November 2013]

73. Merriam- Webster (2013), *Photochemistry*, [WWW] Available from: <http://www.merriam-webster.com/dictionary/photochemistry> [Accessed on 28 October 2013]

74. Chambers, L. (2010), *Electromagnetic Spectrum Diagram*, [WWW] Available from: <http://mynasadata.larc.nasa.gov/science-processes/electromagnetic-diagram/> [Accessed on 23 April 2013]

75. Visserand, A.J.W.G. and Rolinski, O. J. (2010) *Basic Photophysics*, [WWW] Available from: <http://www.photobiology.info/Visser-Rolinski.html> [Accessed on 23 April 2013]

76. Jobin Yvon Ltd. *A Guide to Recording Fluorescence Quantum Yields*, [WWW], Available from: <http://www.chem.ufl.edu/~kschanze/manuals/quantumyieldguide.pdf> [Accessed on 23 April 2013]

77. Allen, M. W. (2010) *Measurement of Fluorescence Quantum Yields*, [WWW], Thermo Fisher Scientific, Available from: <http://www.thermoscientific.fr/eThermo/CMA/PDFs/Product/productPDF_58470.PDF> [Accessed on 23 April 2013]

78. Quantum yield equation

79. Nic, M.; Jirat, J.; Kosata, B. (2006), *Stokes shift*, [WWW], IUPAC, Available from:<http://goldbook.iupac.org/S06031.html> [Accessed on 23 April 2013]

80. Life Technologies, (2010), *Fluorescence Fundamentals*, [WWW], Thermo Fisher Scientific Inc., Available from:< http://www.lifetechnologies.com/za/en/home/references/molecular-probes-the-handbook/introduction-to-fluorescence-techniques.html> [Accessed on 23 April 2013]

81. Leica Microsystems (2002), *FLIM - The Method*, [WWW] Available from: <http://www.leica-microsystems.com/products/confocal-microscopes/confocal-methods/flim/> [Accessed on 23 April 2013]

82. University of Delaware, (2007), Beer Lambert's Law and Spectrophotometry, [WWW], Available from: <http://research.ce.udel.edu/~imhoff/cieg337/file_downloads/Spectrophotometry_handouts.pdf> [Accessed on 27 April 2013]

83. Albani, J.R. (2007) 'Principles and Applications of Fluorescence Spectroscopy', Wiley-Blackwell, ISBN: 978-1-4051-3891-8

84. Minkin, V. I.; Dubonosov, A. D.; Bren, V. A. and Tsukanovb, A. V. (2008), Chemosensors With Crown Ether-Based Receptors, *ARTIVOC*, Vol. 2008, Issue. 4, pp. 90-102

85. Palacios, M.A; Nishiyabu, R.; Marquez, M. and Anzenbacher, P. Jr. (2007), Supramolecular Chemistry Approach to the Design of a High-Resolution Sensor Array for Multi-anion Detection in Water, *Journal of the American Chemical Society*, Vol. 129, Issue. 24, pp. 7538–7544

86. Woodroofe, C.C. Masalha, R. Barnes, K. Frederickson, C.J. & Lippard. S. J. (2004). 'Membrane-Permeable and –Impermeable Sensor of the Zinpyr Family and Their Application to Imagining of Hippocampal Zinc In Vivo'. *Chemistry & Biology*, Vol. 11, pp. 1659-1666
87. Wang, R. M.; Huang, S. B.; Zhao, N.; Chen, Z. N. (2010). 'The New Zn^{2+} Chemosensor based on Functionalized 8-Hydroxylquinoline.' *Inorganic Chemistry Communication*, Volume. 13, pp. 1432-1434
88. Zhou, Y.; You, X.; Fang, Y.; Li, J.; Liu, K. and Yao, C. (2010), A Thiophen-Thiooxorhodamine Conjugate Fluorescent Probe For Detecting Mercury In Aqueous Media And Living Cells, *Organic & Biomolecular Chemistry*, Vol. 8, Issue. 21, pp. 4819-4822
89. Wu. J.; Liu, W.; Ge, J.; Zhang, H. and Wang, P. (2011), New Sensing Mechanisms For Design Of Fluorescent Chemosensors Emerging In Recent Years, *Chemical Society Reviews*, Vol. 40, Issue. 7, pp. 3483-3495
90. Sarker, M. Banthia, S. & Samantha, A. (2006). 'A Highly Selective 'off-on' Fluorescence Chemosensor for Cr (III).' *Tetrahedron Letter*. Vol 45, pp. 7575 – 7578
91. Ha, T. (2001). 'Single-Molecule Fluorescence Resonance Energy Transfer.' *Methods*, Vol. 25, Issue 1, pp. 78–86
92. Ha, T. Enderle, Th. Ogletreet,D. F. Chemla, D. S. Selvin, P.R & Weiss. S. (1996).' Probing The Interaction Between Two Single Molecules: Fluorescence Resonance Energy Transfer Between A Single Donor And A Single Acceptor,' *Proc. Natl. Acad. Sci. USA*, Vol. 93, pp. 6264-6268

93. Heid, P. *(2005). An Introduction to Fluorescence Resonance Energy Transfer (FRET) Technology and its Application in Bioscience.*[WWW] Available From: <http://www.biotek.com/resources/articles/fluorescence-resonance-energy-transfer.html> [Accessed on 28 October 2013].

94. Zhou, Z.; Yu, M.; Yang, H.; Huang, K.; Li, F.; Yi, T. & Huang C. (2008). FRET-Based Sensor For Imaging Chromium(III) In Living Cells, *Chemical Communications*, Issue.29, pp. 3387-389

95. Huang, K. Yang, H. Zhou, Z. Yu, M. Li, F. Gao, X. Yi, T and Huang, C. (2008) 'Multisignal Chemosensor for Cr^{3+} and Its Application in Bioimaging,' *Org. Lett.*, Vol.10, No.12 pp 2557–2560

96. Czanick. A. W. (1994) 'Chemical Communication in Water Using Fluorescent Chemosensors,' *Acc. Chem. Res*. Vol. 24, pp. 302 – 308

97. Beltran, O.G. Mena, G. Friedrich, L. C. Ferreira, J. C. N. Vargas, V. Quina, F. H. Nuneaz. M. T. Cassel, B. K. (2012), 'Design And Synthesis Of New Coumarin-Based 'Turn-On' Fluoresecent Probe Selective For Cu^{2+},' *Tetrahedron Letters.* Vol. 53, pp. 5280 – 5283

98. Gil Knier (2011), *How do Photovoltaics Work?*, [WWW], Available from: <http://science.nasa.gov/science-news/science-at-nasa/2002/solarcells/> [Accessed on 24 November 2013]

99. Clark, R.N., *Reflectance Spectra*, in Rock Physics and Phase Relations - A Handbook of Physical Constants, T.J. Ahrens, Editor. 1995, American Geophysical Union. pp. 178-188

100. University of Western Australia, *Introduction to Diffuse Reflectance Spectroscopy (DRS)* [WWW], Available from: <http://obel.ee.uwa.edu.au/skin/introduction-to-diffuse-reflectance-spectroscopy > [Accessed on 10 February 2014]

101. Gratton, E. and Fantini, S., *Reflectance and Transmittance Spectroscopy*, [WWW], Available from:<http://ase.tufts.edu/biomedical/research/fantini/publications/NIRS_experimental/4_Comp_Series_Photochem_Photobiol_4_211_2004.pdf> [Accessed on 10 February 2014]

102. National Cancer Institute, *Types of Cancer*, [WWW], Available from: <http://www.cancer.gov/cancertopics > [Accessed on 12 February 2014]

103. The University of Utah Eccles Health Sciences Library, (2013), *Malignant Neoplasms*, [WWW], Available from :< http://library.med.utah.edu/WebPath/NEOHTML/NEOPL107.html. > [Accessed on 12 February 2014]

104. Daneai, G.; Hoorn, S. V.; Lopez, A. L. and Ezznati, M., (2005), Causes of Cancer In The World: Comparative Risk Assessment Of Nine Behavioural And Environmental Risk Factors, *The Lancet*, Vol. 366, Issue. 9499, pp. 1784–1793

105. Ciardiello, F. and Tortora. G., (2001), A Novel Approach in the Treatment of Cancer: Targeting the Epidermal Growth Factor Receptor, *Clinical Cancer Research*, Vol. 7, pp. 2958-2970

106. The Addario Lung Cancer Medical Institute,(2009), *Catalyzing & Accelerating Lung Cancer Research*, [WWW], <http://www.alcmi.net/about_lung_cancer > [Accessed on 12 February 2014]

107. American Cancer Society, (2013), *Types of Lung Cancer*, [WWW], Available From: <http://www.cancer.org/cancer/lungcancer-non-smallcell/detailedguide/non-small-cell-lung-cancer-what-is-non-small-cell-lung-cancer > [Accessed on 12 February 2014]

108. Dania Alarcon-Vargas. D and Ronai. Z. (2001). p53–MDM2—The Affair That Never ends. *Carcinogenesis*. Volume 23, Issue 4, pp. 541-547

109. Hwang. B. J.; Ford, J. M.; Hanawalt, P. C. and Chu, G. (1999), Expression Of The p48 Xeroderma Pigmentosum Gene Is p53-Dependent And Is Involved In Global Genomic Repair, *PNAS*, Vol. 96, Issue. 2, pp. 424–428

110. Shoichet, B. K.; McGovern, S. L.; Wei, B. and Irwin. J. J.,(2002), Lead Discovery Using Molecular Docking, Current Opinion in Chemical Biology, Vol. 6, Issue. 4, pp. 439-446

111. Zhuang, C.; Miao, Z.; Zhu, L.; Dong, G.; Guo, Z.; Wang, S.; Zhang, Y.; Wu, Y.; Yao, J.; Sheng, C. and Zhang, W., (2012), Discovery, Synthesis, And Biological Evaluation Of Orally Active Pyrrolidone Derivatives As Novel Inhibitors Of p53-MDM2 Protein-Protein Interaction, *American Chemical Society*, Vol.55, Issue. 22, pp. 9630-9642

112. Wikipedia, (2014), *MDM2*, [WWW], Available From: <http://en.wikipedia.org/wiki/Mdm2> [Accessed on 12 February 2014]

113. Miyazaki, M.; Naito, H.; Sugimoto, Y.; Yoshida, K.; Kawato, H.; Okayama, T.; Shimizu, H.; Miyazaki, M.; Kitagawa, M.; Seki, T.; Fukutake, S.; Shiose, Y.; Aonuma, M. and Soga, T., (2013), Synthesis And Evaluation Of Novel Orally Active p53-MDM2 Interaction Inhibitors, *Bioorganic and Medicinal Chemistry*, Vol. 21, Issue. 14, pp. 4319-4331

114. MedicineNet.com, (1996), *Definition of Cytotoxic*, [WWW], Available from: <http://www.medterms.com/script/main/art.asp?articlekey=19883> [Accessed on 12 February 2014]

115. Dojindo Molecular Technologies, Inc, (2013), Measuring Cell Viability / Cytotoxicity, [WWW], Available from: <www.dojindo.com/Protocol/Cell_Proliferation_Protocol_Colorimetric.pdf > [Accessed on 28 October 2013]

116. Mosmann, T., (1983), Rapid Colorimetric Assay For Cellular Growth And Survival: Application To Proliferation And Cytotoxicity Assays, *Journal of Immunological Methods*, Vol. 65, Issues. 1–2, pp. 55–63

117. Skehan, P.; Storeng, R.; Scudiero, D.; Monks, A.; McMahon, J.; Vistica, D.; Warren, J. T.; Bokesch, H.; Kenney, S. and Boyd, M. R., (1990), New Colorimetric Cytotoxicity Assay for Anticancer-Drug Screening, *Journal of the National Cancer Institute*, Vol. 83, Issue. 13, pp. 1107-1112

Chapter Three: Experimental

3.1. Instrumental Parameters and Reagents

^{1}H-NMR spectra (400 MHz), ^{13}C-NMR spectra (400 MHz) and ^{19}F-NMR spectra (600 MHz) were recorded using $CDCl_3$ as a solvent. For all NMR spectra was obtained using Burker instrument with tetramethylsilane (TMS) as an internal standard. Chemical shifts are quoted in parts per million (ppm). IR spectra were recorded on a Varian Scimitar 1000 FT-IR using an ATR attachment and the absorption wavelengths were expressed in reciprocal centimeters (cm^{-1}). The Shamadizu spectrophotometer was used to analyze test samples in the UV/Visible region. A Varian Cary Fluorescence spectrophotometer was used for the determination of fluorescence properties. A Shimadzu HPLC system coupled to a UV Detector and RF-10AXL Fluorescence detector was used. The HPLC column contained packing material C18 particles diameter of 5 microns (dimension of 250 x 4.6 mm). Reverse-phase solvent composition (MeOH and water) was used.

All reagents used were of Reagent Grade quality and purchased from Merck, Fluke and Sigma Aldrich. Silica gel, of particle size 40-63 µm, was obtained from Sigma Aldrich. Lung cancer cells (A529) were purchased from Highveld Biologicals (Johannesburg, SA). Cell culture reagents were purchased from Whitehead Scientific (Johannesburg, SA).

3.2. Synthesis and Spectroscopic Data of Organic Compounds

3.2.1. Synthesis of 2-chloro-3-formylquinoline (6)

N-phenylacetamide (0.6758 g; 5 mmol) and dry DMF (1.16 mL; 15 mmol) were transferred into a round bottom flask and placed in an ice-water bath to maintain the temperature between 0-5 °C. The mixture was stirred and $POCl_3$ (5.59 mL, 60 mmol) was added drop-wise. After the

addition of $POCl_3$, the reaction vessel was transferred to a heating mantle. The mixture was stirred at 80-90^{0}C for 16 hours. It was then poured into a beaker of crushed ice and stirred using a glass rod for periodic intervals of 5-15 minutes until a precipitate formed. This precipitate was filtered under vacuum, dried and rinsed with deionized water and dried again. The product was dissolved in ethyl acetate and then made into a slurry using silica gel. The slurry was then transferred in a glass column and the organic mixture was separated with 1% ethyl acetate in petroleum ether, using column chromatography.

3.2.2. Synthesis of 2-oxo-3-formylquinoline (1)

2-Chloro-3-formylquinoline (4.700 g; 25 mmol) was placed in a round bottom flask containing 50% acetic acid (150 mL). The mixture was refluxed for 5 hours. The mixture was cooled with ice until the solid was filtered and recrystallized with methanol. The yield was 95%.

3.2.3. Synthesis of 3-(4,5-Dihydro-1H-imidazol-2-yl)-1H-quinolin-2-one (2)

Equimolar ratio of Synthesis of 2-chloro-3-formylquinoline **(6**) (4.300 g; 2.5 mmol) and 1,2-diaminoethane (0.1670 mL; 2.5 mmol) were placed in a 100 mL round bottom flask containing ethanol. Phosporous oxychloride (0.22 mL) was added and the mixture was refluxed at 100^{0}C-120^{0}C for 5 hours. The progress of the reaction was monitored by TLC. The mixture was poured into a beaker containing ice and the precipitate was filtered. The product was separated from the crude mixture by column chromatography with a solvent mixture of 1% methanol in chloroform. The yield was 89.3 % (mass 0.7475 g).

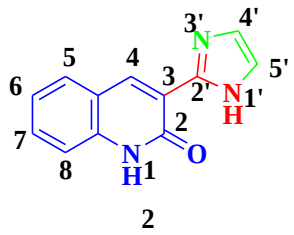

Spectroscopic Information of **2**:

IR: 2925 (Ar-H, sharp), 2856 (Ar-H, sharp), 1662 (C=O stretch, sharp), 1617 (C=C, sharp), 1576 (C=N, sharp)

δ_H: 12.5 (s, 1H, NH-1), 9.21(s, 1H, NH-1´), 8.61 (s, 1H, H-4), 8.16 (d, 1H, H-5´), 7.98 (d, 1H, H-4´), 7.86 (d, 1H, H-8), 7.65 (t, J= 7.16 Hz,1H, H-6), 7.45 (d, 1H, H-5), 7.32 (t, J= 7.52 Hz, 1H, H-7)

δ_C: 161.29 (C=O bond), 152.16 (C=N bond), 142.24, 141.27, 139.55, 132.07, 129.52, 123.14, 122.39, 118.77, 115.77, 113.24

3.2.3. Synthesis of 3-(1H-benzoimidazol-2-yl)-1H-quinolin-2-one (3)

Equimolar ratio of **6** (0.4353 g; 2.5 mmol) and 1,2 diaminobenzene (0.3128 g; 2.5 mmol) were placed in a 100 mL round bottom flask containing ethanol. Phosphrous oxychloride (0.22 mL) was added and the mixture was refluxed at 100^0C-120^0C for 5 hours. The progress of the reaction was monitored by TLC. The mixture was poured into a beaker containing ice and the precipitate was filtered. The product was separated from the crude mixture by column chromatography with an eluting solvent mixture of 50 % EA: PE. The yield was 73.2 %.

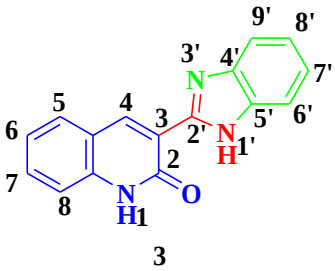

Spectroscopic Information of **3**:

IR: 3338 (N-H, sharp), 2923 (Aromatic, sharp), 1658(C=O Stretch, sharp), 1619 (C=N, sharp)

δ_H: 12.64 (s, 1H, NH-1), 12.44 (s, 1H, NH-1´), 9.10 (s, 1H, H-4), 7.95 (d, 1H, H-9´), 7.72 (d, 1H, H-8), 7.66 (d, 1H, H-6´), 7. 63 (d, 1H, H-4), 7.59 (t, J= 1.16 Hz, 1H, H-7´), 7.43 (d, 1H, H-5), 7.29 (t, J= 7.24Hz, 1H, H-6, H-7 interchangeable), δ 7.20 (t, J= 3.12 Hz, H-6, H-7 interchangeable)

δ_C: 161.30, 148.24, 143.27, 139.55, 139.20, 134.90, 132.07, 129.54, 123.14, 122.77, 122.39, 120.50, 119.64, 118.77, 115.76, 113.24.

3.2.4 Synthesis of 3-(6-nitro-1H-benzoimidazol-2-yl)-1H-quinolin-2-one (4)

Equimolar ratio of **6** (0.4693 g; 2.5 mmol) and 4-nitro-1,2-diaminobenzene (0.3992 g; 2.5 mmol) were placed in a 100 mL round bottom flask containing ethanol. Phosporous oxychloride (0.22 mL) was added and the mixture was refluxed at 100^0C-120^0C for 5 hours. The progress of the reaction was monitored by TLC. The mixture was poured into a beaker containing ice and the precipitate was filtered. The product was separated from the crude mixture by column chromatography with an eluting solvent mixture of 50 % EA: PE. The yield was 66.9 %.

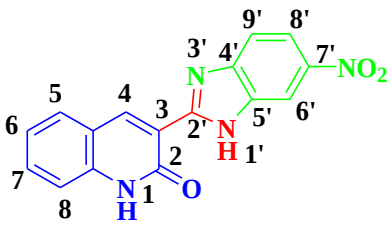

4

Spectroscopic Information of **4**:

IR: 3432 (N-H, sharp), 2923(Aromatic, sharp), 1640 (C=O Stretching, sharp), 1517 & 1304 (Nitro, sharp), 1616 and 1573 (Quinoline, sharp)

δ_H: 13.3 (s, 1H, NH-1), 12.4 (s, 1H, NH-1´), 9.38 (s, 1H, H-6´), 8.67 (d, 1H, H-4), 8.53 (d, 1H, H-6´) 8.02 (d, 1H, H-8'), 7.91 (d, 1H, H-8), 7.83 (d, 1H, H-9'), δ 7.68 (dd, J= 4.64 Hz, 2H, H-5 interchangeable), 7.47 (t, J= 5.44 Hz, 1H, H-7), 7.34 (t, J= 5.00 Hz, 2H, H-6).

δ_C: 161.08, 153.42, 147.80, 143.45, 142.40, 141.25, 139.60, 134.29, 132.93, 132.79, , 123.33, 123.29, 118.83, , 115.89, 115.89, 114.70,

3.2.5. Synthesis of 4,4-difluoro-4-bora-3a,4a-diaza-s-indacene quinoline derivatives (6), (1), (81), (83) and (85)

General reaction protocol for the synthesis of BODIPY dyes

An accurate mass (1 mmol) of the selected compound (**6**, **1**, **81**, **83**, **85) (presented in Table. 2)** and pyrrole (0.139 mL, 2 mmol) where place in a double sprouted round bottom flask in a 1:2 molar ratio with 75 mL DCM under inert atmosphere. One drop of TFA was added. The reaction was mechanically stirred for one hour. The progress of the reaction was monitored by TLC. Then DDQ (1mmol) in 1 mL of DCM was added to the reaction mixture. This reaction mixture was

stirred for an additional 30 minutes. This was then followed by the addition of 2 mL of TEA and 2mL of $BF_3.OEt_2$. The mixture was stirred for 2 hours.

Table 2: Substrates and quantities used for the preparation of 4,4-difluoro-4-bora-3a,4a-diaza-s-indacene-quinoline derivatives

Compounds Used	Quantity used (mmol)	Volume or Mass used
6	1	0.1915 g
1	1	0.1730 g
81	2	0.270 mL
83	2	0.828 mL
85	1	0.1522 g
87	1	0.1452 g

Spectroscopic Information:

Compound 5

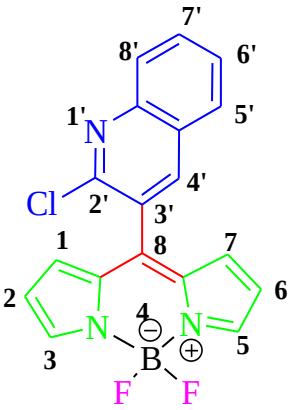

IR: 3478 (N-H, board), 2923 (Ar-H, sharp), 1617 (C=C, board), 1542 (C-N, sharp), 1215 (C=N, sharp), 1617, 749 (C-Cl, sharp)

δ_H: 8.23 (s, 1H, H-4), 8.14 (d, 1H, H-5, H-3, interchangeable), 7.98(s), 7.89 (tt, J= 2.00 Hz, 2H, H-2 & H-6, interchangeable), 7.69 (tt, J= 7.68 Hz, 2H, H-7'& H-6' interchangeable), 7.24(s), 6.74 (d, 1H, H-8), 6.53(d, 1H, H-1)

δ_C: 147.09, 147.07, 144.62, 139.72, 139.10, 134.49, 131.08, 129.82, 127.67, 127.20, 126.88, 125.39, 124.72, 118.28

δ_F: approx. -135 (m) and -137(m)

Compound 7

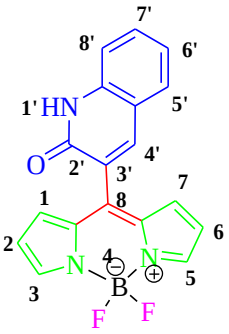

IR: 3493 (N-H, board), 2922 (Ar-H, sharp), 1617 (C=O, board), 1215 (C=N, sharp)

δ_H: 11.70 (s, N-H, H-1), 7.98 (d, 1H, H-8'), 7.62 (q, J= 7.16 Hz, interchangeable), 7.32 (q, J= 8.16 Hz, interchangeable), 7.03 (d, 1H, H-8'), 6.51 (d, 1H, H-1)

δ_C: 161.55, 144.89, 143.00, 138.93, 135.39, 132.50, 130.79, 128.61, 125.92, 123.53, 118.81, 116.03

δ_F: approx. -143.22 (m) and -147.39 (m).

Attempted synthesis of BODIPY dyes:

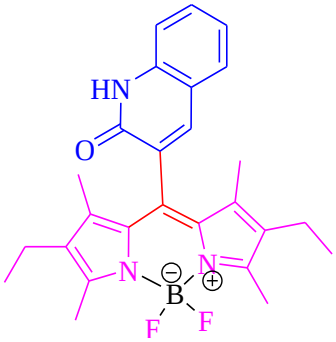

Fraction 5-6: 2973, 880 (Aromatic, sharp), 2895 (Alkyl C-H Stretching, board)

Fraction 7: 2977, 881 (Aromatic, sharp), 2882 (Alkyl C-H Stretching, board)

Fraction 8: 2977, 881 (Aromatic, sharp), 2882 (Alkyl C-H), 1326 (N-H Stretching, board)

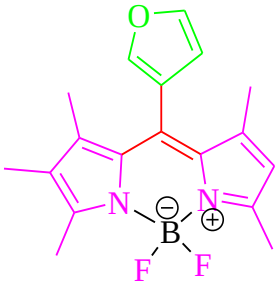

Fraction 1: 2977, 881 (Aromatic, sharp), 1319, 1085 (C-N, sharp), 1085-1045(C-O, sharp)

Fraction 8: 2921, 1574, 884 (Aromatic, sharp), 1269, 1077 (C-N, sharp), 1077 (C-O, sharp)

Fraction 13-14: 2921, 1617, 885 (Aromatic, sharp), 1273, 1179 (C-N, sharp), 1074 (C-O, sharp)

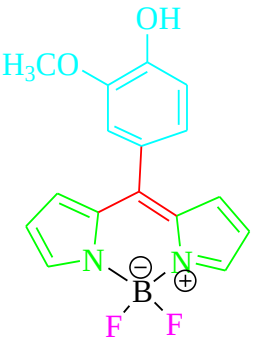

Fraction 3: Approx. 2900, 1661, 621 (Aromatic, sharp), 1316 (C-N, sharp), 3400 (O-H, board)

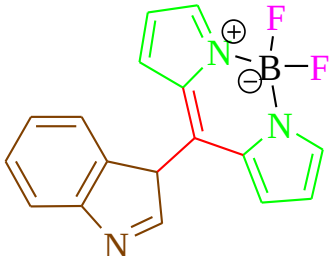

Fraction 9: 2921, 1661 (Aromatic, sharp), 1316 (C-N, sharp)

3.3.3 General Procedure used for Spectroscopic Analyses

3.3.3.1. Preparation of Stock Solutions for UV/Visible Analysis

An accurate mass of the compound (presented in **Table 3**) was weighed and quantitatively transferred into 50 mL volumetric flasks. The solution were made up to the mark with each of the solvents EtOH, MeOH, $CHCl_3$, CH_2Cl_2 and ACN, separately. All 25 solutions were then homogenized. The UV cuvette was rinsed (3x) with the respective solvent and the samples were analyzed on the instrument. The concentration of each solution was calculated as 30 µM.

Table 3: Masses Weighed of Synthesized Compounds

	Mass (g)	**Molecular Mass (g/mol)**
2	3.19E-4	212
3	4.21E-4	281
4	4.59E-4	306
5	5.23E-4	355
7	5.30E-4	353

3.3.3.2. Fluorescence Spectroscopy

3.3.3.2.1 Fluorescence Determination

For the determinations of the fluorescent behaviour of the compounds**,** 0.3 µM solutions were prepared from the 30 µM solutions by dilutions (equation 9). In each case, 0.5 mL of the 30 µM solutions were quantitatively transferred using a graduated pipette into 50 mL volumetric flasks. The solutions were made up to mark using the appropriate solvent. The BODIPY dyes required a further dilution of ten times more to obtain a good spectra. The solutions were analyzed on the Varian Cary fluorescence spectrophotometer.

Equation 9

$$C_{initial}V_{initial} = C_{final}V_{final}$$

C represents the concentration and, V represents the volume and of both the initial and final respectively.

3.3.3.2.2. Quantum Yield

For the quantum yield of the synthesized compounds, five standard solution were prepared in each solvent systems used. The 30 µM solutions were used to prepare a 10 µM solution and a 1.0 µM solution by serial dilution. The 10 µM solution was prepared by using a graduated pipette and volumes of 33 mL were transferred into 100 mL volumetric flasks and the solutions were made up to mark with the various solvents. The five solutions of each synthesized compound were diluted by serial dilution to 1.0 µM and each solution was made up to mark 10 mL volumetric flask. This was used to prepare a further five additional solutions of concentrations 0, 0.2, 0.4, 0.6, 0.8 and 1.0 µM using equation 9 (**Figure 3.1**). Volumes of 2.0, 4.0, 6.0 and 8.0 mL were pipetted respectively into 10 mL volumetric flasks. The solutions were then made up with

the solvents used for the analyses. The resulting solutions were homogenized and fluorescence studies were performed. The BODIPY dye required a further 10 times dilution to obtain a spectra.

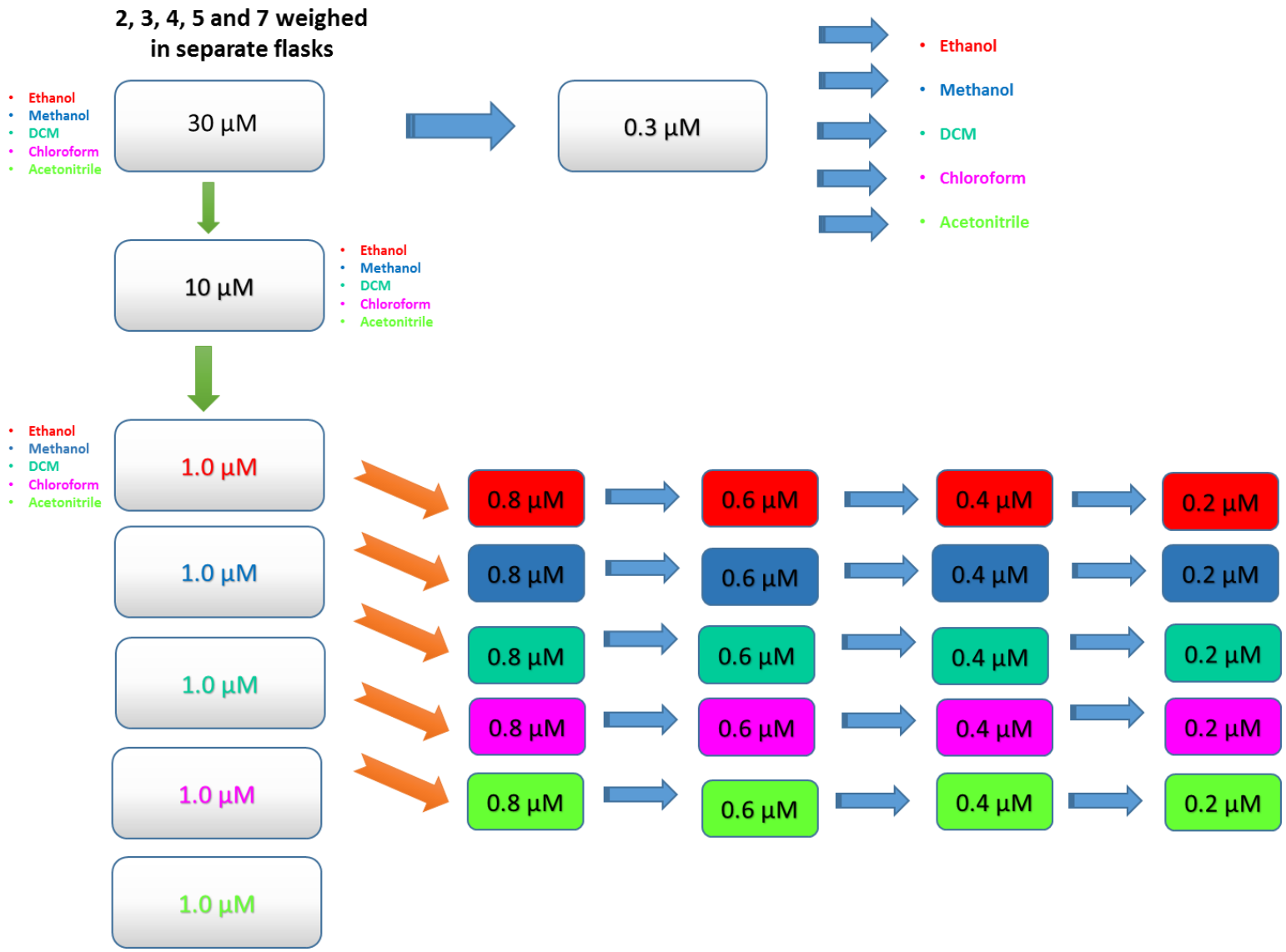

Figure 3.4: Schematic Representation Showing Preparation of Solution

In order to perform the calculation for the quantum yield, a standard of known quantum yield was used. Fluorescein was selected as the standard. It was diluted to 30 µM. Further serial dilution was done to yield concentrations of 0, 0.2, 0.4, 0.6, 0.8 and 1.0 µM. 0.0005 g was massed out on an analytical balance and was quantitatively transferred into a 50 mL volumetric flask. Using 0.1M NaOH, which was previously prepared, the standard was dissolved and made up to the mark.

Sodium hydroxide was prepared by weighing 4.00 g, using an analytical balance. It was transferred into a 1000 mL volumetric flask. Deionized water was used to dissolve the NaOH pellets, and the solution was made up to the mark.

3.3.4. Binding Metals

The preparation of the compounds in the HEPES buffer was done by weighing 1.1665 g of HEPES powder and transferring it into three 100 mL volumetric flasks using 9 parts of deionized water (90 mL). The compounds were massed out separately (**Table 3**) and the masses were multiplied by a factor of two since 200 mL volumetric flasks were actually used to accommodate for the volumes of sample required. The compounds were dissolved using 20 mL of ACN. This was then transferred quantitatively into the buffer solution to made up to mark (v/v = 1:9). The solutions' pH values ranged from 12 pH units to 7.2 pH units.

For the preparation of 200 µM solutions of metal ions for binding studies, the following metal salts were used and masses can be found on **Table 4**. These metal ions were individually transferred quantitatively into separate 100 mL volumetric flasks. The metal salts were dissolved with deionized water and made up to mark.

Table 4: Mass of Metal salts weighed

Metal Salt Used	Molecular Mass (g/mol)	Mass Weighed (g)
$Zn(NO_3)_2$	297.49	0.00595
$CoCl_2.6H_2O$	237.93	0.00476
$Cd(NO_3)_2.4H_2O$	236.42	0.00473
$Ni(NO_3)_2.6H_2O$	290.79	0.00582
$Pb(NO_3)_2$	331.20	0.00663
$Fe(NO_3)_2$	241.86	0.00484
$Cu(NO_3)_2.3H_2O$	241.60	0.00483
$Hg_2(NO_3)_2.2H_2O$	324.60	0.00649

For the fluorescence studies, 1.5 mL of compound in HEPES buffer, and each metal salt solution was taken in an equi-volume and placed into a vial. The resulting metal complex mixtures were analyzed and the data obtained. This procedure was repeated for all five compounds. Each of the 8 metals ion and all 40 complex mixtures were analyzed.

3.5 General Procedure for Photovoltaic cells

The solutions prepared in 3.3.3.1 were used for this study. The spectrophotometer was set on reflectance mode and the same procedure was used for samples analyzed by UV/Vis spectroscopy.

3.5. The Protocol used for Molecular Docking Studies

3.5.1. Preparation of Protein Structure

The crystal structure of human MDM2 (PDB ID: 3VZV) was retrieved from the Protein Data Bank. After selection of the protein structure, the protein preparation wizard of Schrodinger suite was used to prepare protein structure. All the water molecules were removed from the protein structure, metals were treated, and hydrogen atoms were added. All atom force field (OPLS-2005) charges and atom types were also assigned. The protein structure energy was minimized.

3.5.2. Preparation of Ligand and Docking Studies

The structures of chemical compounds were not available in pubchem database. Chemsketch was used to draw the compound structure, and all ligands prepared for molecular docking studies used ligprep version 2.3. The ligand structure energy was minimized and partial atomic charges were computed using the OPLS-2005 force field by using Schrödinger suite.

3.6 General Procedure for Cytotoxicity

3.6.1 Maintenance of A529 cells in culture

A529 cells were cultured (37^oC, 5% CO_2) to 90% confluency in $25cm^3$ flasks in complete culture media (CCM) [Eagle's minimum essential medium, 10% foetal calf serum, 1% L-Glutamine and

1% penstrepfungizone]. The culture medium is by far the most important single factor in culturing cells[5a, b]. The extracellular medium must meet the essential requirements (nutritional, hormonal and stromal factors) for survival and growth.

3.6.2 Trypsinisation

In order to sub-culture plate cells for the various experimental assays, the process of trypsinisation was used to detach cells once 90% confluency was reached. The process of trypsinisation involved the critical step of rinsing the cells with 3mL aliquots of warm 0.1M PBS and incubating the cells with 1mL of trypsin-EDTA (Lonza) for 1 minute.

The cells were monitored using an inverted light microscope (Olympus IXSI; 20x magnification) and once they were rounded, rypsin was discarded and CCM was added to the flask of cells. The flask was agitated to detach the cell suspension and enumerated by dye exclusion using a haemocytometer. Trypan blue (0.4%) was utilised in a dye exclusion procedure for cell counting. The principle of dye exclusion using trypan blue is based on compromised cell membranes. In dead/damaged cells the dye is readily allowed entry into the cells and are stained blue. Viable cells remain unstained.

3.6.3 Cell Proliferation and Metabolic Activity Assay

A529 cells (15,000/well) were incubated for 24h, using a range of concentrations of each compound in triplicate, in a microtitre plate together with an untreated control (cells incubated with CCM only). Each experiment was conducted twice on separate occasions in order to confirm the consistency. The cells were then incubated ($37^{o}C$, 5% CO_2) with the MTT substrate (5 mg/ml in PBS) for 4h. Thereafter all supernatants were aspirated and DMSO (100 µl/well)

was added to the wells. Finally the optical density was measured at 570 nm and a reference was measured at a wavelength of 690 nm with an ELISA plate reader (Bio-Tek µQuant).

The net MTT-dependent absorbance (optical density (OD)) of each sample were calculated by subtracting the average absorbance of the blank from the average absorbance of each sample. The data was represented as mean OD ± standard deviation.

Percentage cell viability can be calculated by the following equation:

Equation 10:

$$\% \text{ Cell viability} = \frac{\text{mean absorbance of treated cells}}{\text{mean absorbance of control cells}} \times 100$$

Table 5: The Data Obtained for MTT Assay Studies for Compound **2**

Concentration ug/ml						
	0	31.25	62.5	125	250	500
OD1	0.41	0.505	0.783	0.793	0.907	0.676
OD2	0.426	0.561	0.698	0.432	0.748	0.599
OD3	0.389	0.558	0.644	0.579	0.616	0.671
Mean	0.4083	0.5413	0.7083	0.6013	0.757	0.6487
Std. deviation	0.01856	0.0315	0.07007	0.1815	0.1457	0.04309

Table 6: The Data Obtained for MTT Assay Studies for Compound **3**

	Concentration (µg/mL)					
	0	31.25	62.5	125	250	500
OD1	1.599	1.076	1.125	1.083	1.042	1.104
OD2	1.216	1.117	1.104	1.045	1.053	1.18
OD3	1.64	1.2	1.076	0.98	0.99	1.142
Mean	1.485	1.131	1.102	1.036	1.028	1.142
Std. deviation	0.2339	0.06317	0.02458	0.05209	0.3365	0.038

Table 7: The Data Obtained for MTT Assay Studies for Compound **3**

	Concentration (µg/mL)					
	0	31.25	62.5	125	250	500
OD1	1.631	1.17	1.198	1.211	1.174	1.272
OD2	1.826	1.154	1.178	1.126	1.372	1.292
OD3	1.266	1.198	1.234	1.241	1.466	1.227
Mean	1.574	1.174	1.203	1.193	1.337	1.264
Std. deviation	0.2843	0.02227	0.02838	0.05965	0.1461	0.03329

Table 8: The Data Obtained for MTT Assay Studies for Compound **5**

	Concentration (µg/mL)					
	0	31.25	62.5	125	250	500
OD1	1.754	1.228	1.197	1.215	1.304	1.01
OD2	1.747	1.181	1.052	1.174	1.092	0.966
OD3	1.856	1.181	1.052	1.149	1.079	0.943
Mean	1.786	1.197	1.1	1.179	1.158	0.973
Std. deviation	0.06101	0.02714	0.03332	0.1263	0.1263	0.03404

Table 9: The Data Obtained for MTT Assay Studies for Compound **7**

	Concentration (µg/mL)					
	0	31.25	62.5	125	250	500
OD1	1.838	1.184	1.128	1.202	1.061	0.996
OD2	1.856	1.171	1.15	1.156	1.071	1.008
OD3	1.91	1.172	1.205	1.152	1.154	1.016
Mean	1.868	1.176	1.161	1.17	1.095	1.007
Std. deviation	0.03747	0.007234	0.03966	0.02778	0.05105	0.01007

Chapter 4: Results and discussion

Synthesis, Purification and Characterization of Imidazole Bearing Quinoline Derivatives

In this study, three imidazole bearing quinoline derivatives were synthesized from an oxo-formyl quinolone derivative which was prepared from a chloro-formyl quinoline derivative. The synthesis, purification and characterization are discussed.

The 2-chloro-3-formyl-quinoline **(6)** was synthesized from acetanilide **(72)** by the Vilsmeier-Haack reaction by the procedure reported in the literature[1-3]. Briefly, DMF was cooled, phosphoryl chloride ($POCl_3$) added drop-wise and the mixture was heated to 80-90°C for 16 hours. After work-up, the precipitate was filtered, air dried and the crude mixture separated by column chromatography to produce **6** in 95% yield. The reaction outline is presented in **Scheme 2**. **Scheme 3** shows the formation of the electrophile when DMF reacts with $POCl_3$. **Scheme 4** shows the reaction of **72** with the electrophile.

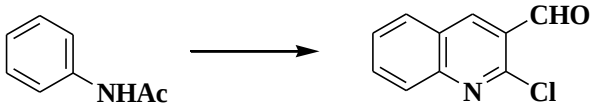

72 6

Scheme 2: Synthesis of 2-chloro-3-formyl-quinoline

(i) $POCl_3$/DMF, 80-90°C, 16 hours

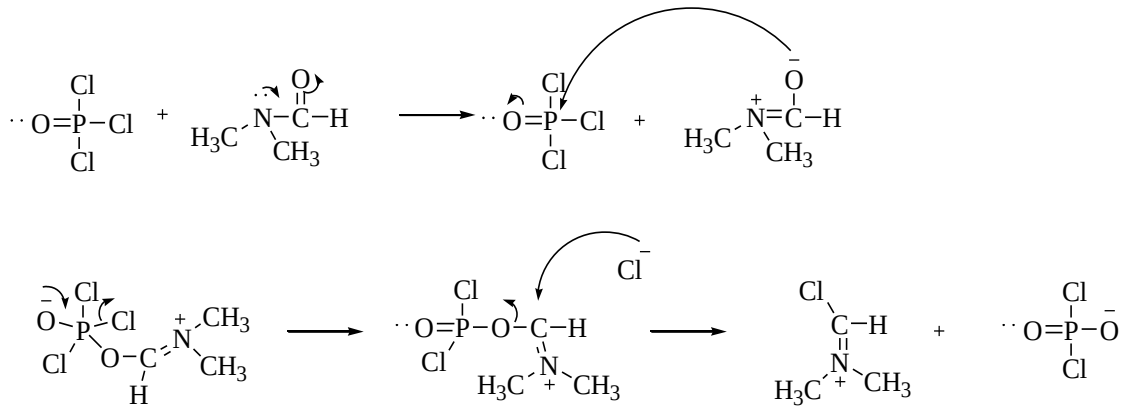

Electrophile Formation

Scheme 3: The mechanism illustrating the formation of an electrophile

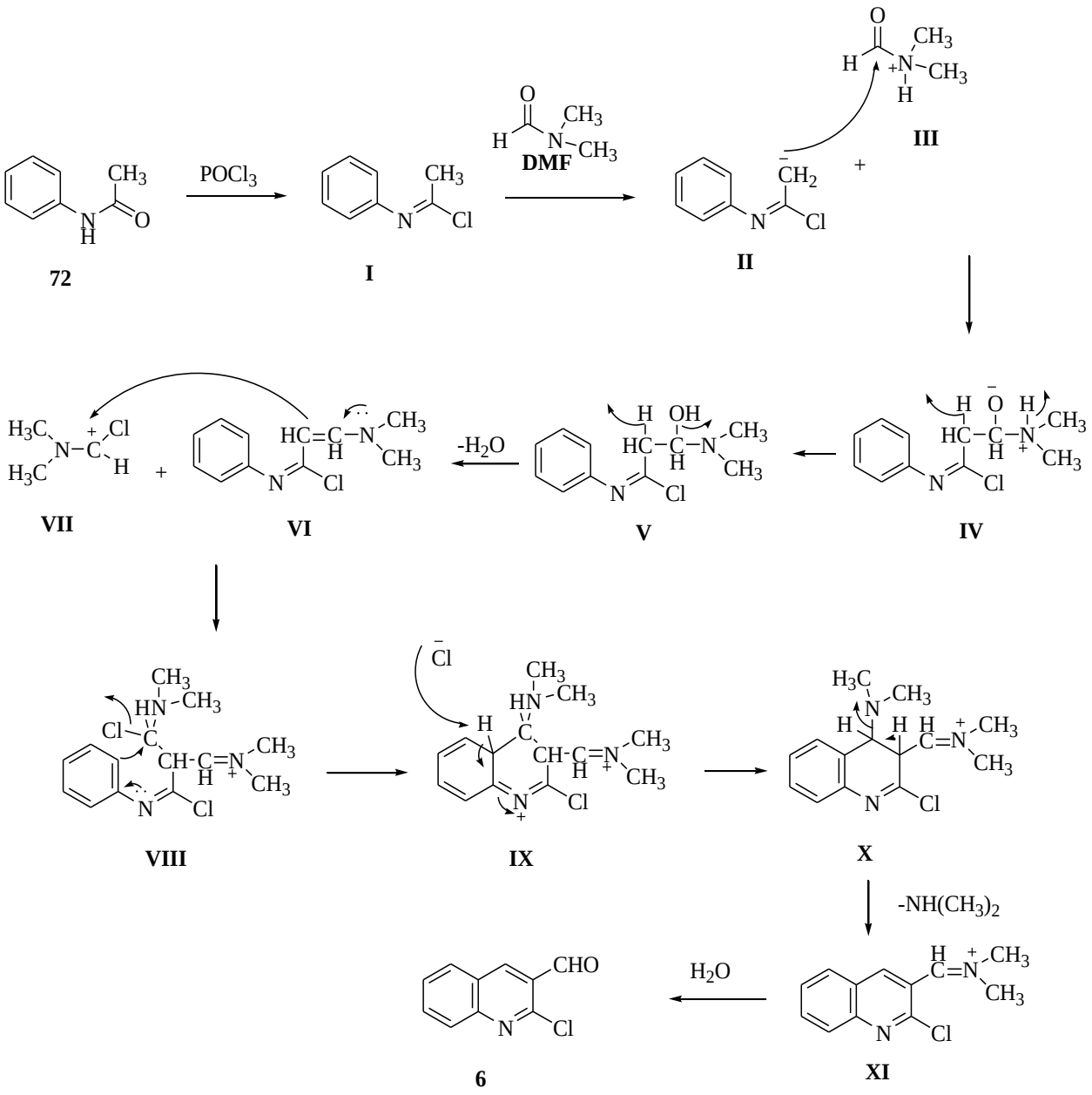

Scheme 4: Mechanism for the reaction of 72 with the electrophile to form 6

The above mechanism starts by chlorination of N-anilide **(72)** to form a chloro amine product **(I).** The chloro amine product reacts with DMF and produces a kinetically controlled intermediate **(II)**. The enolate then attacks the aldehyde group, followed by condensation. This reaction is following a Knoevenagel condensation which resulted in the formation of enamine product **(VI).** In the enamine product **(VI)** the lone pairs from the nitrogen atom move toward the carbon

bonded to the double bond, causing a high electron density. Therefore, the enamine acts as a nucleophile which attacks the electrophile to produce an imine intermediate product **(VIII).** The latter undergo intramolecular cyclisation and aromaticity to produce a chloro-imine quinoline **(XI).** The imine quinoline is then hydrolyzed by water to produce the target 2-chloro-3-formyl quinoline compound **(6).**

2-Oxo-formyl-quinoline **(1)** was synthesized from **6** in the presence of acetic acid. **Scheme 5** shows this reaction[3]. This reaction is well known and the reaction protocol is well established in our research laboratory.

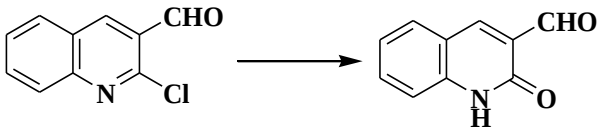

6 **1**

Scheme 5: Synthesis of 2-oxo-3-formyl-quinoline

(i) AcOH, heat, 5 hours

The next step in the research plan was to synthesize three selected imidazoles which contained a quinoline moiety. Compound **2** was synthesized from **1** and ethylene diamine (**73**). Briefly, equimolar quantities of **1** and **73** were refluxed in an ethanolic solution of $POCl_3$ for 5 hours (**Scheme 6**)[4]. The progress of the reaction was monitored by TLC. The crude product was purified by column chromatography using a solvent system comprising 50 % EA: PE. The yield obtained was 89.3%.

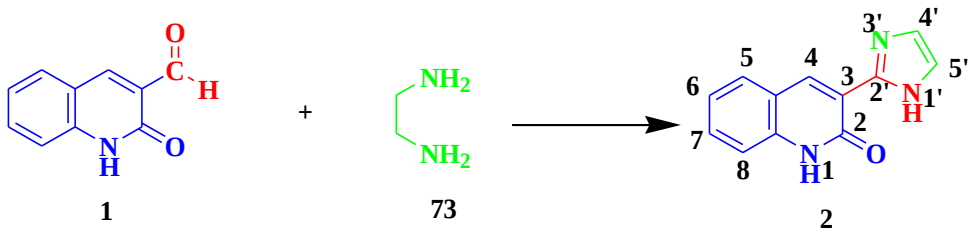

Scheme 6: Synthesis of 3-(4,5-Dihydro-1H-imidazol-2-yl)-1H-quinolin-2-one

(i)$POCl_3$/EtOH, 100-120°C, 5 hours

Compound **2** was analyzed by IR, ^{1}H-NMR, expanded ^{1}H-NMR and ^{13}C- NMR; the spectra are presented in **Appendix 1- 4 (Page 141-144),** respectively. The IR spectrum shows absorptions at 2925 2856, 1662, 1617 and 1576 cm^{-1} is assigned to Ar-H, Ar-H, C=O and C=N, respectively. The quinoline core[5] absorbs at 1620-1570 cm^{-1}. In the ^{1}H-NMR spectrum, three signals are observed in the aromatic region at δ 6-8 ppm[6]. Also signals at δ 12.5 (s, 1H), 9.21 (s, 1H) 7.68 (s, 1H) are assigned to N-H (position 1), N-H (position 1') and C-H (position 4), respectively. In the ^{13}C-NMR spectrum, the chemical shift at δ 160.44 ppm is assigned to C=O whist the seven aromatic carbon absorbed at δ 115.40 -152.17 ppm.

This is an *in situ* two step reaction involving condensation followed by intramolecular aromatic cyclisation. To our knowledge there is documented literature on this mechanism and hence the following mechanism, presented in **Scheme 7**, is proposed:

In the first step, **1** behaves a nucleophile and attacks the phosphorous of $POCl_3$ to form an unstable intermediate **I** which is subsequently attacked by **2** at the carbonyl carbon to generate an intermediate **II**. The hydrogen on the positively charged nitrogen is removed and bonds to an oxygen to form an unstable intermediate **IV**. This contains a phosphorous-bearing bulky group which subsequently leaves thereby creating an intermediate imine (**V**). This mechanism is

followed by an intramolecular electrophilic and nucleophilic step and a series of subsequent hydrogen rearrangement as illustrated by intermediates **VI-IX** to form **2**

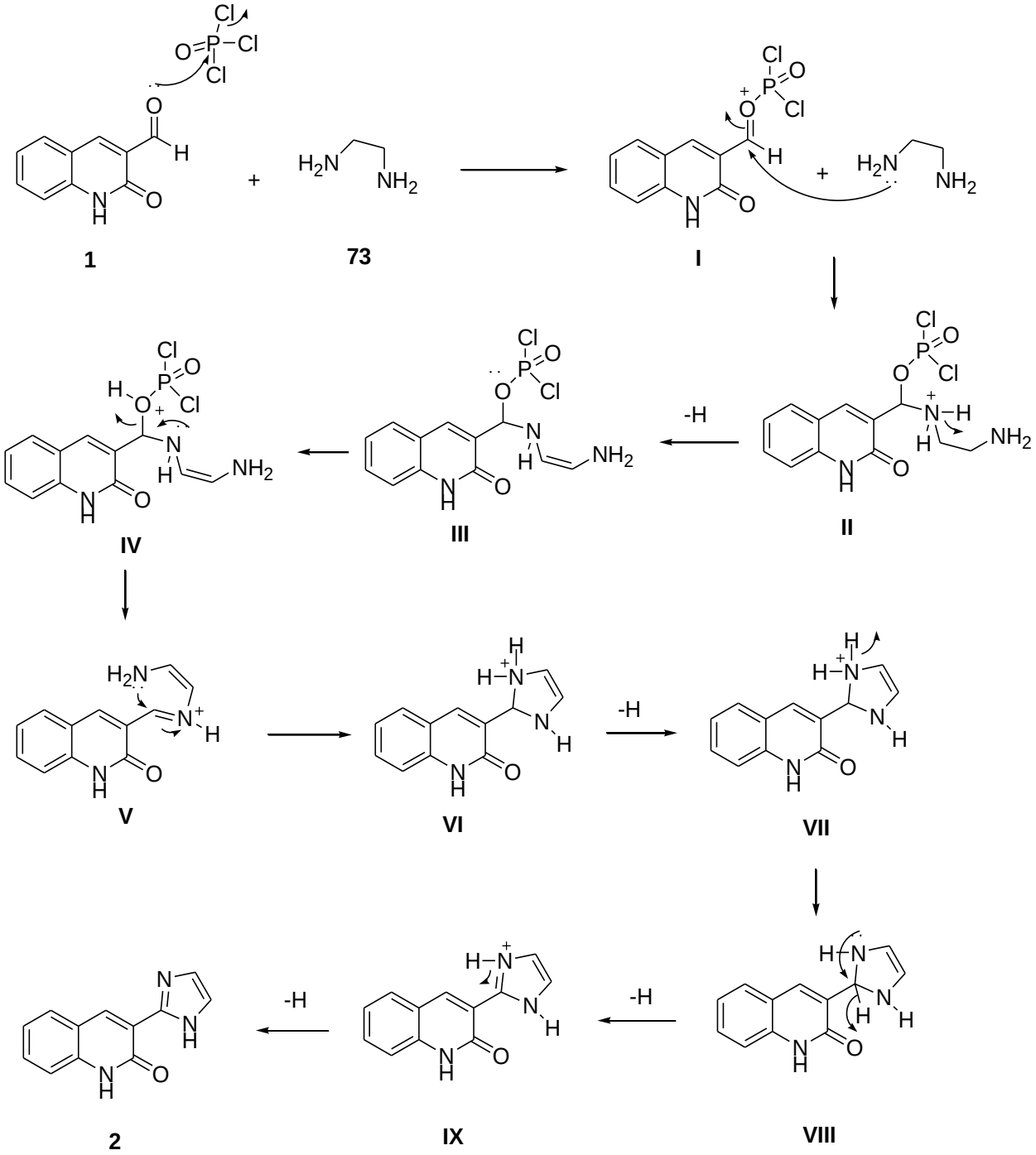

Scheme 7: Proposed Reaction Mechanism for the Synthesis of 2

To determine the bond lengths and bond angles, the Chemdraw ultra software was used. The data, presented in Table 20 (**Appendix 5, Pages 145 -147**), was used to express the molecular geometry of the molecule and understand the approximate location for bonding and transfer properties[7]. The molecule is slightly rigid in nature which is due to the nitrogen-linked double bond; most of the other bonds were close to 120° which is optimal for trigonal planar shape in accordance to VSEPR Theory [8]. The ORTEP representation of **2** is presented in **Figure 4.1**. This compound **2** was used for a multi-disciplinary study which follows in this chapter. Applications such as fluorescence, chemosensor and anti-cancer potential are reported.

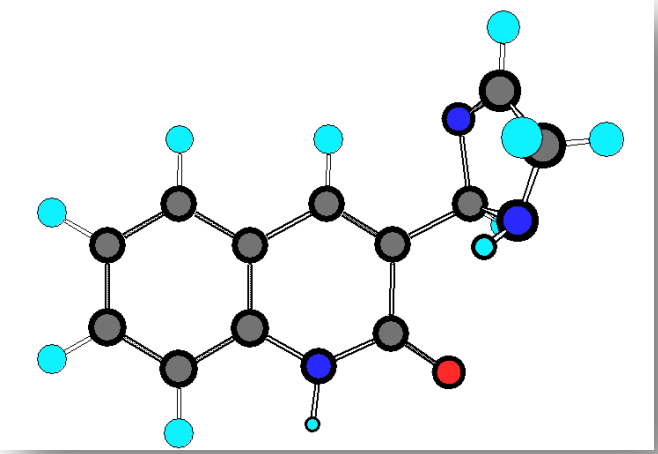

Figure 4.1: ORTEP of 3-(4,5-Dihydro-1H-imidazol-2-yl)-1H-quinolin-2-one

Having developed an experimental protocol for the synthesis of **2**, two more derivatives were synthesized i.e. **3** and **4** from appropriate diamine derivatives. In selecting the appropriate amine as substrates for these reactions, the effect of an aromatic moiety and electron-withdrawing group was investigated in the fluorescence, sensor and anti-cancer studies; discussed later in this chapter. **Scheme 8** outlines the synthesis of **3** from **1** and **74.** The yield of **3** was 73.2%.

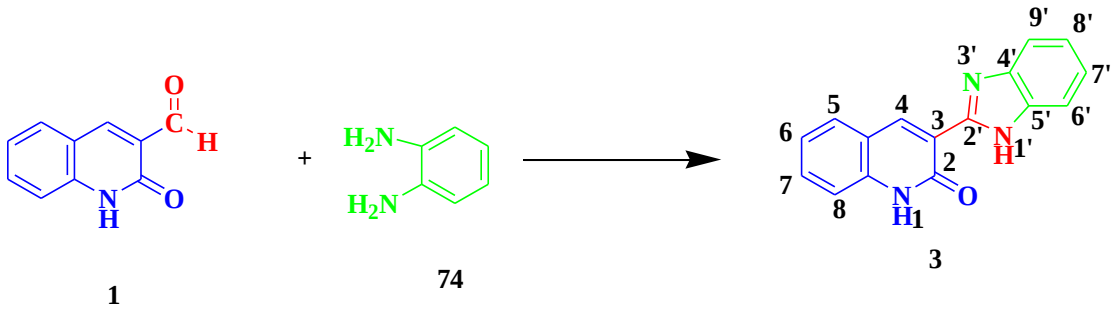

Scheme 8: Synthesis of 3-(-1H-Benzoimidazol-2-yl)-1H-quinolin-2-one

(i)$POCl_3$/EtOH, 100-120°C, 5 hours

The IR, ^{1}H-NMR, expanded ^{1}H-NMR and ^{13}C-NMR spectra of **3** are presented in **Appendix 6-9 (pages 148 -150),** respectively. The IR spectrum shows absorptions at 3338, 2923, 1658 and 1619 cm^{-1} and is assigned to N-H, Aromatic, C=O and C=N, respectively. The quinoline core absorbs at 1620- 1571 cm^{-1}. In the ^{1}H-NMR spectrum, nine signals were observed in the aromatic region at δ 6-8 ppm. Also signals at 12.64 (s, 1H), 12.44 (s, 1H) and 7.64 (s, 1H) were assigned to N-H (position 1), N-H (position 9) and C-H (position 4), respectively. In the ^{13}C-NMR spectrum, the chemical shift at δ 161.30 was assigned to C=O whist the aromatic carbons absorb at δ 153.23-148.23 ppm.

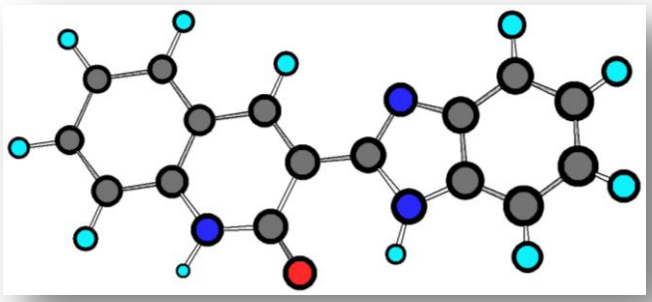

Figure 4.2: ORTEP of 3-(1H-Benzoimidazol-2-yl)-1H-quinolin-2-one

The ORTEP presentation of **3** is presented in **Figure 4.2**. The bond geometry that the molecular is almost planar with bond angles close to 120° (**Appendix 10, Table 21, Page 151-152).**

Scheme 9 outlines the synthesis of **4** from **1** and **75.** The yield of the orange-red solid **4** was 66.9%.

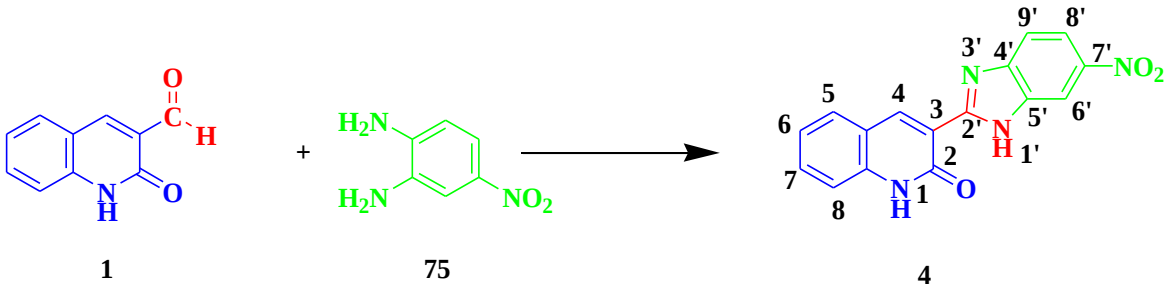

1 75 4

Scheme 9: Synthesis of 3-(6-Nitro-1H-benzoimidazol-2-yl)-1H-quinolin-2-one

(i) POCl3/EtOH, 100-120°C, 5 hours

The IR, ^{1}H-NMR, ^{1}H-NMR (expanded) and ^{13}C-NMR spectra of **4** are presented in **Appendix 11 15 (pages 153 - 157),** respectively. The IR spectrum shows absorptions at 3432, 2923 and 1640 cm^{-1} assigned to N-H, Ar-H and C=O, respectively. The nitro group absorbed at 1517 and 1304 cm^{-1}.

The quinoline core absorbs at 1616-1573 cm^{-1}. In the ^{1}H-NMR spectrum, proton signals are observed in the aromatic region at δ 6-8 ppm. Also signals at 13.3 (s, 1H), 12.4 (s, 1H) and 8.67 (s, 1H) are assigned to N-H (position 1), N-H (position 9) and C-H (position 4), respectively. In the ^{13}C- NMR spectrum, the chemical shift at δ 161.30 ppm is assigned to C=O whilst the aromatic carbons absorbed δ 153.42 -110.16 ppm.

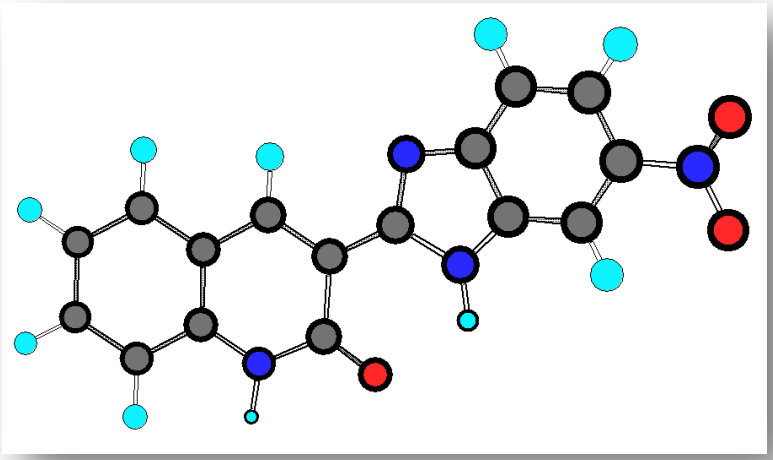

Figure 4.3: ORTEP of 3-(6-Nitro-1H-Benzoimidazol-2-yl)-1H-quinolin-2-one

Compound **4** (**Figure 4.3**) was also found to be trigonal planar in geometry. The data is presented in **Appendix 16 (Table 22, pages 158-159).**

Synthesis, Purification and Characterization of BODIPY dyes

In this study two novel BODIPY dyes were synthesized, purified and characterized. Also an attempted purification of three BODIPY dyes is presented. A HPLC method is also reported to separate one of the BODIPY dyes from a crude mixture.

The synthesis of BODIPY dyes required inert-nitrogen conditions [8] hence the Schlenk set-up [9] was used (**Figure 4.4)**.

Figure 4.4: Schlenk Setup for inert reaction conditions

The synthesis of the BODIPY dye **7** from the starting compound **6** was achieved by a series of 3 steps. In the first step (**Scheme 10.1**), **77** was synthesized[10] by using a 2:1 molar ratio of **6** and **76** in DCM. This reaction was catalyzed with a single drop of TFA. Small aliquots of the reaction

mixture was removed and neutralized in order to monitor the progress of the reaction by TLC. This procedure was repeated until the completion of the first step of the reaction was accomplished; this reaction took one hour.

In the second step, DDQ was added as an oxidant for the dehydrogenation process (**Scheme 10.2**). The reaction was mechanically stirred for a period of 30 minutes and TLC analysis showed all the substrates were converted to the new product **78,** formed *in situ.*

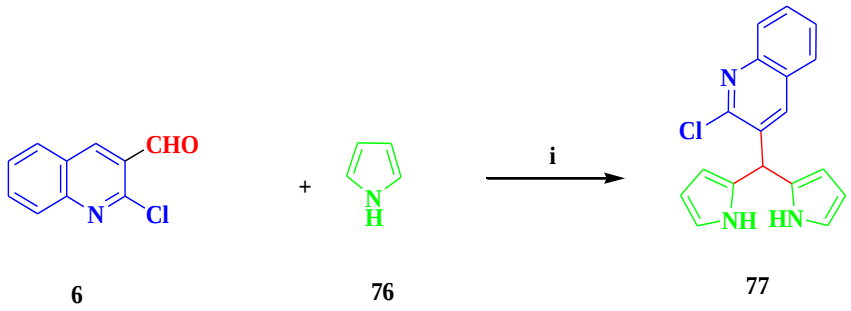

6 **76** **77**

Scheme 10.1: Synthesis of 3-[Bis-(1H-pyrrol-2-yl)-methyl]-2-chloro-quinoline

(i)Dichloromethane, one drop TFA, 1 hour

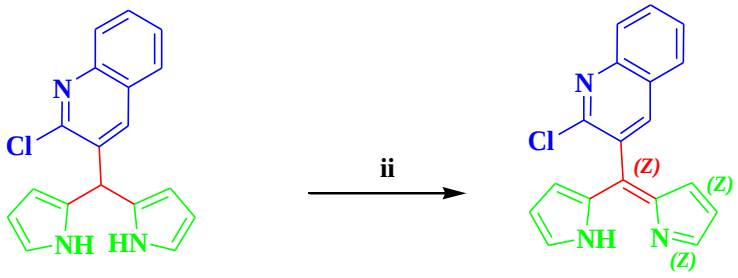

77 **78**

Scheme 10.2: Synthesis of 2-chloro-3-[(1H-pyrrol-2-yl)-pyrrol-2-ylidene-methyl]-quinoline

(ii)DDQ, DCM, 30 minutes

In the final step of the reaction (**Scheme 10.3**), TEA and $BF_3.OEt_2$ were added and the mixture was mechanically stirred for 2 hours. The progress of the reaction was monitored by TLC; 2 hours of reflux produced the final product **7** in a crude mixture. This was for cyclization process to occur between the N-5 pyrrole and the N-11 amine to form the BODIPY core to form an electrostatic bond. The final mixture is presented in **Figure 4.5**

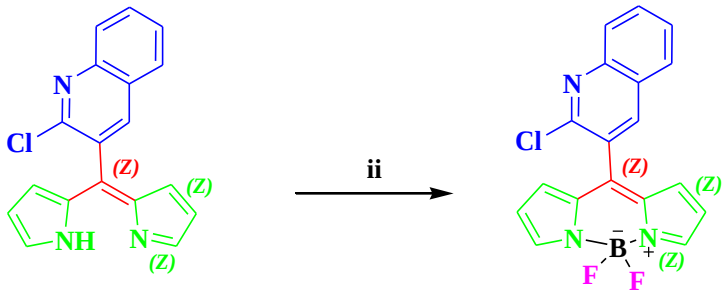

78 **7**

Scheme 10.3: Synthesis of 4,4-difluoro-4-bora-3a,4a-diaza-s-indacene-2-chloro-quinoline

(iii)TEA, $BF_3.OEt_2$, 2 hours

The crude reaction mixture was neutralized with deionized water and DCM. The organic layer was separated, dried in anhydrous sodium sulphate and evaporated *in vacuo*. The crude product was purified by column chromatography with an eluting solvent system composed of hexane: DCM in a 1:4 ratio (v/v). Red crystals, 82% yield, were collected.

Compound **7** was analyzed by IR, ^{1}H-NMR, ^{13}C-NMR and ^{19}F-NMR. The IR, ^{1}H-NMR, expanded ^{1}H-NMR, ^{13}C-NMR and ^{19}F-NMR are presented in **Appendix 17-21 (pages 160 - 164),** respectively. ^{13}C- NMR shows chemical shifts at 150- 125 ppm thereby confirming the presence of an aromatic group. The ^{19}F-NMR shows two signals at δ 140 -150 ppm.

Figure 4.5: Black reaction mixture

The Chemdraw ultra software was used to determine the bond lengths and bond angles of **7**. The data is presented in **Appendix 22 (pages 165 - 167)**. VSEPR theory suggests that **7** is planar in nature (**Figure 4.6**).

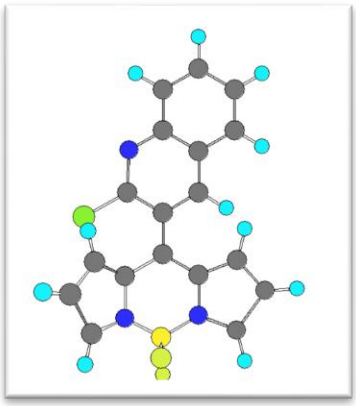

Figure 4.6: ORTEP Diagram of 4,4-difluoro-4-bora-3a,4a-diaza-s-indacene-2-chloro-quinoline

Having designed and conducted a successful method for the synthesis of **7**, this new protocol was used to synthesis five novel BODIPY dyes i.e. **5**, **82**, **84, 86** and **88**.

Hence, **79** was synthesized by using a 2:1 molar ratio of **1** and **76** in the presences of TFA and inert conditions. The reaction mixture was stirred mechanically and TLC was used to monitor the progress of the reaction. **Scheme 11.1** presents the outline of the reaction. In the next step, DDQ was added to produce **80** (**Scheme 11.2**).

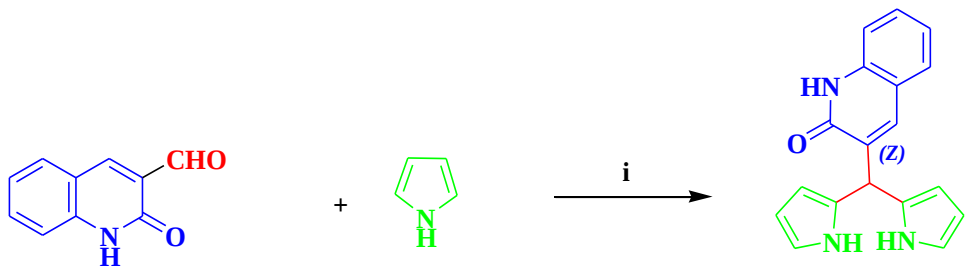

1 **76** **79**

Scheme 11.1: Synthesis of 3-[Bis-(1H-pyrrol-2-yl)-methyl]-1H-quinolin-2-one

(i) Dichloromethane, one drop TFA, 1 hour

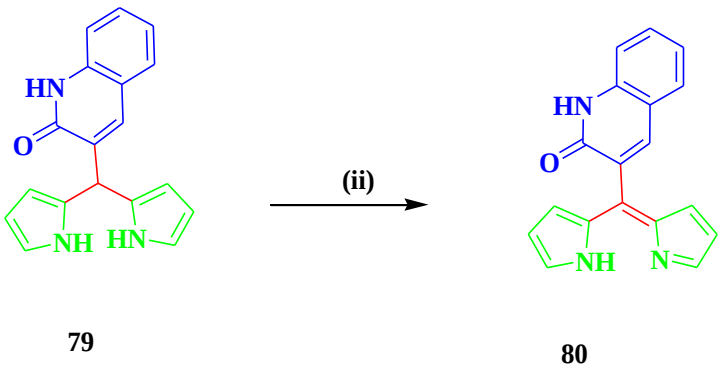

79 **80**

Scheme 11.2: Synthesis of 3-[(1H-pyrrol-2-yl)-pyrrol-2-yliene-methyl]-1H-quinolin-2-one

(ii) DDQ, DCM, 30 minutes

Finally, TEA and BF_3. OEt_2 was added and the mixture was refluxed (**Scheme 11.3**) to give a crude mixture containing **5**.

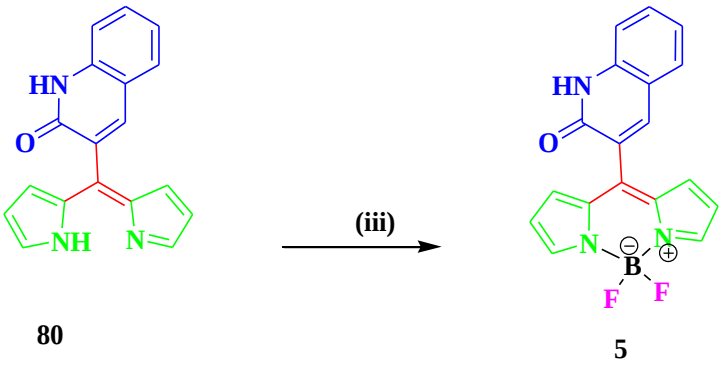

80 **5**

Scheme 11.3: Synthesis of 4,4-difluoro-4-bora-3a,4a-diaza-s-indacene-quinolin-2-one

(iii) TEA, BF_3.OEt_2, 2 hours

The purification was achieved by column chromatography with chloroform as the eluting solvent. **Figure 4.7** shows the fractions collected from the glass column**.** The red eighth fraction was left to air-dry to produce dark-red crystals [11a,b,] . Compound **5** was analyzed by IR, ^{1}H-NMR, ^{13}C- NMR and ^{19}F-NMR. All the characterization analysis confirmed the product as **5**, however the yield was low (<40 %). The IR, ^{1}H-NMR, expanded ^{1}H-NMR ^{13}C-NMR, ^{19}F-NMR and expanded ^{19}F-NMR are presented in **Appendix 23- 28 (pages 168 - 172),** respectively.

Figure 4.7: Fractions obtained from glass column chromatography for 4,4-difluoro-4-bora-3a,4a-diaza-s-indacene -quinolin-2-one

Chemdraw ultra software was used to determine the bond lengths and bond angles. The data is presented in **Appendix 29 (Table 24, pages 173- 175)**. **Figure 4.8** shows the ORTEP projection.

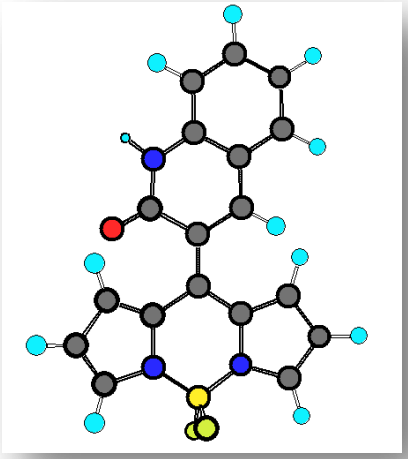

Figure 4.8: ORTEP Diagram of 4,4-difluoro-4-bora-3a,4a-diaza-s-indacene-quinolin-2-one

To synthesize the third BODIPY dye **82** we used **1** and **81** (Scheme 12) in a 1:2 molar ratio and followed the reaction protocol outlined in the synthesis of **5** and **7**. Purification of the crude mixture was conducted by column chromatography. The fluorescent red color solution was collected in fraction 5-8 (**Figure 4.9**), air dried and the red solid was characterized by IR and ^{1}H-NMR (**Appendix 30-36 (page 176 - 179)).** Analysis of the data indicated that **82** remained unpurified. The IR spectrum indicated that fluorine was present due to the bands in the ranges 1000-1360 cm^{-1}. Also two strong absorption bands were observed just over the frequency around 1000 cm^{-1}. The ^{1}H-NMR spectrum displayed contaminant signals which hindered the characterization, however the aromatic protons appears at δ 6-8 ppm. Literature[12] indicates that the purification step may encounter difficulties due to the possibly of hydrolysis of the BODIPY dye in the silica gel column. It must be noted that small- scale reactions were used in the synthesis of BODIPY dyes and therefore it is recommended that the reaction be repeated on a larger scale so that sufficient crude mixture is available for purification and subsequent characterization.

Figure 4.9: Fractions 7-8 collected from the glass column for purification of 82

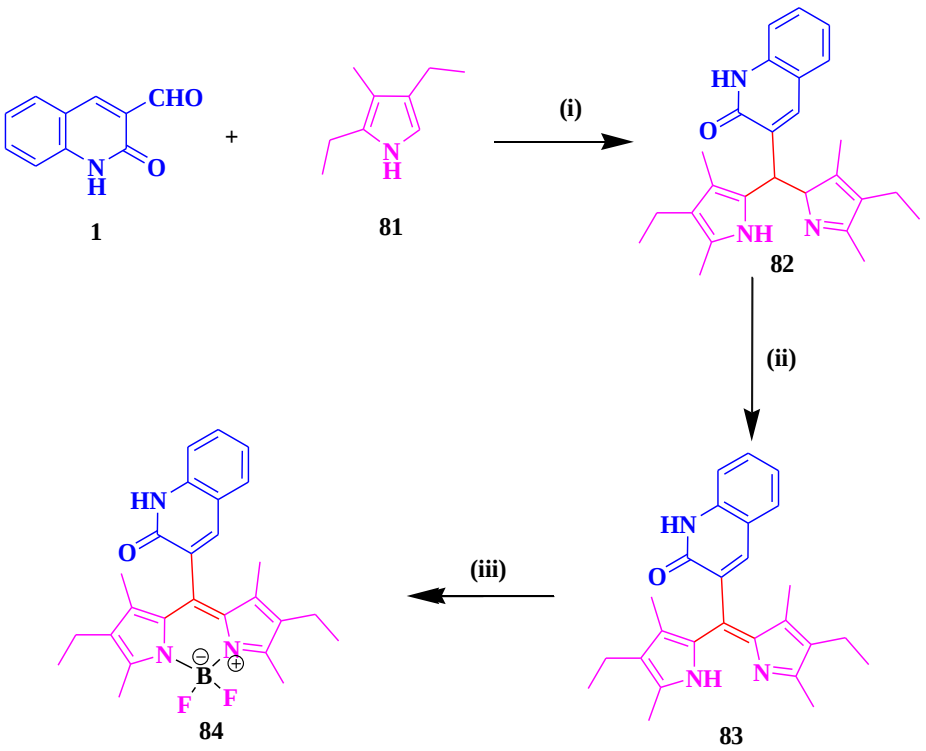

Scheme 12. Synthesis of 82 from 1 and 3-(2,6-diethyl-1,3,5,7-tetramethyl-4H-3a,4a-diaza-s-indacene)-1H-quinolin-2-one (81)

In the synthesis of BODIPY dyes **86, 88** and **88**, presented in **Schemes 13, 14** and **15**, respectively, similar purification problems existed. Although the red fluorescent solution was collected (**Figure 4.9**), air dried and analyzed, contaminants were still present. The IR and NMR spectra are presented in **Appendix 37- 44 (pages 180 - 183).**

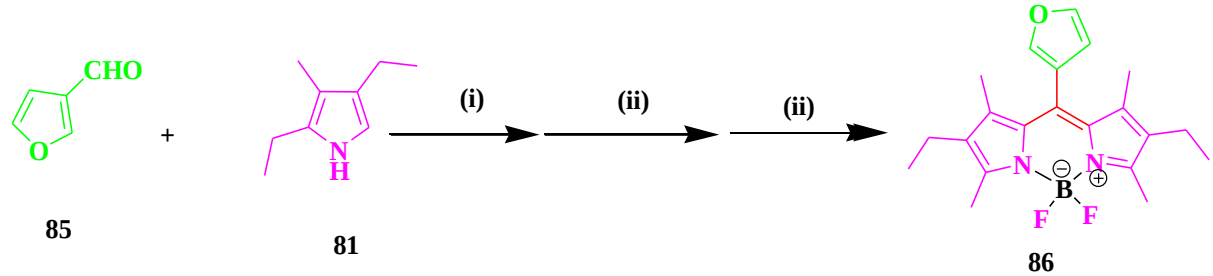

Scheme 13. Synthesis of 3-(2,6-diethyl-8-furan-3-yl-1,3,5,7-tetramethyl-4H-3a,4a-diaza-s-

indacene)-1H-quinolin-2-one

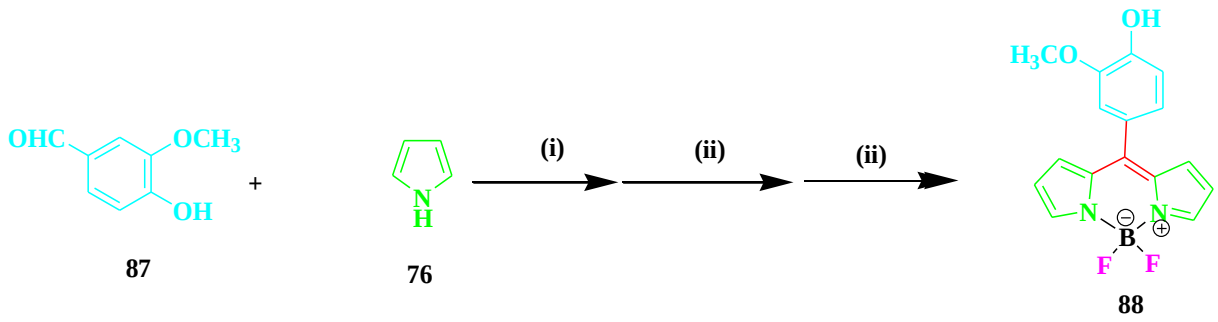

Scheme 14. Synthesis of 8-(4-Hydroxy-3-methoxy-phenyl)-4H-3a,4a-diaza-s-indacene

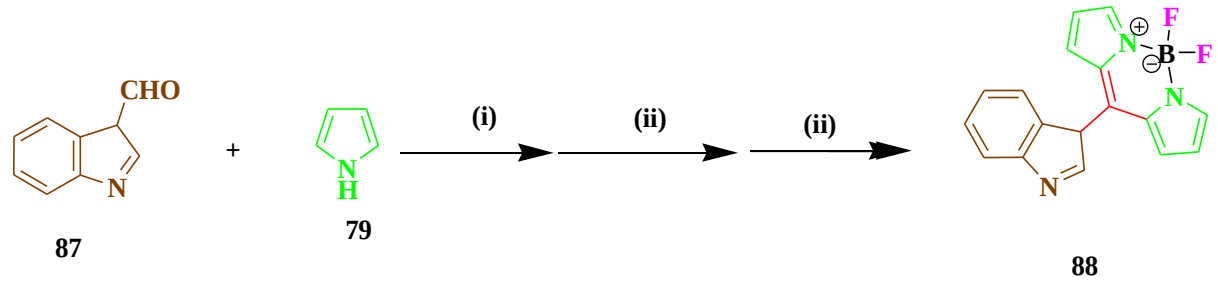

Scheme 15. Synthesis of 8-(3H-Indol-3-yl)-4H-3a,4a-diaza-s-indacene

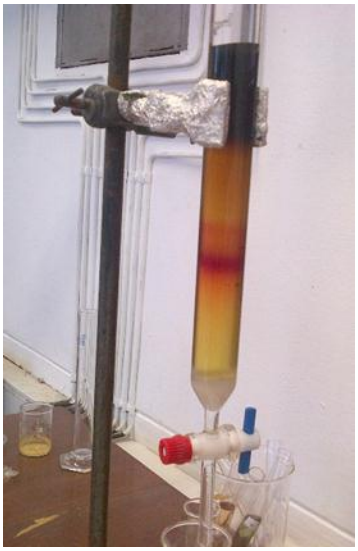

Figure 4.10. Column Chromatography showing the colored BODIPY dyes present

Further investigations on purification of these compounds is recommended.

In summary, three novel quinoline-imidazole and two BODIPY dyes were synthesized and characterized. Four novel BODIPY dyes were also synthesized however separation problems were encountered: a recommendation is made that the reaction be scaled-up and other combination of solvents be investigated for purification.

In order to find a suitable method of separation, a high precision analytical technique viz. High pressure liquid chromatography (HPLC) was investigated. Compound **5** was chosen as a model example since it was in high purity and a crude mixture was available. A Shimadzu HPLC system linked to a UV detector coupled to a RF-10AXL Fluorescence detector was used. A HPLC column containing the packing material of 5 microns C18, column dimension 250 x 4.6 mm and reverse-phase solvents were used. The analyses were performed in eluting solvents: 100% MeOH, 80% MeOH in water and 65% MeOH in water. **Figure 4.11- 4.13** shows the effect of the mobile phase in separating the crude mixture. Initially, three peaks were observed (**Figure 4.11**). However the second peak showed evidence of co-elution. As the ratio of MeOH to water decreased to 80% (**Figure 4.12**) it was clearly evident that the second peak was separated into an addition peak with a retention time 3.4 minutes. Since a separation was observed, the mobile phase composition was reduced to 65% MeOH in water and this yielded a clear separation of the third peak. A pure sample **5** (**Figure 4.14)** was run with the same mobile phase composition and a retention time of 6.37 minutes was recorded. On comparing the chromatograph, it is deduced that the broad peak 6.58 minutes could be identified to be **5.** In conclusion, HPLC can be used to identify and preparative HPLC is recommended for future investigating the separation and purification of BODIPY dyes.

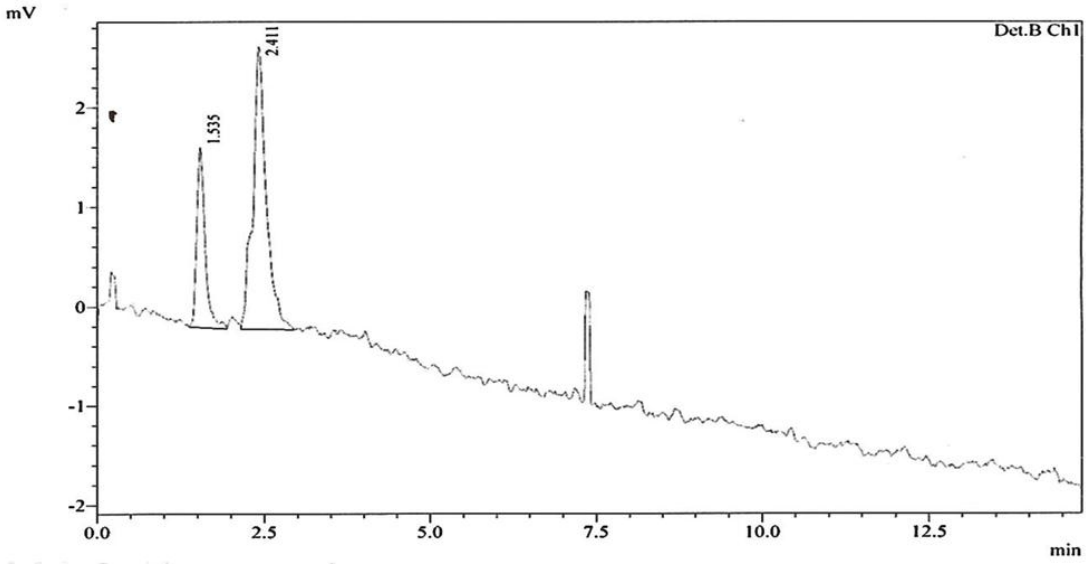

Figure 4.11: Separation of the crude mixture with 100% methanol

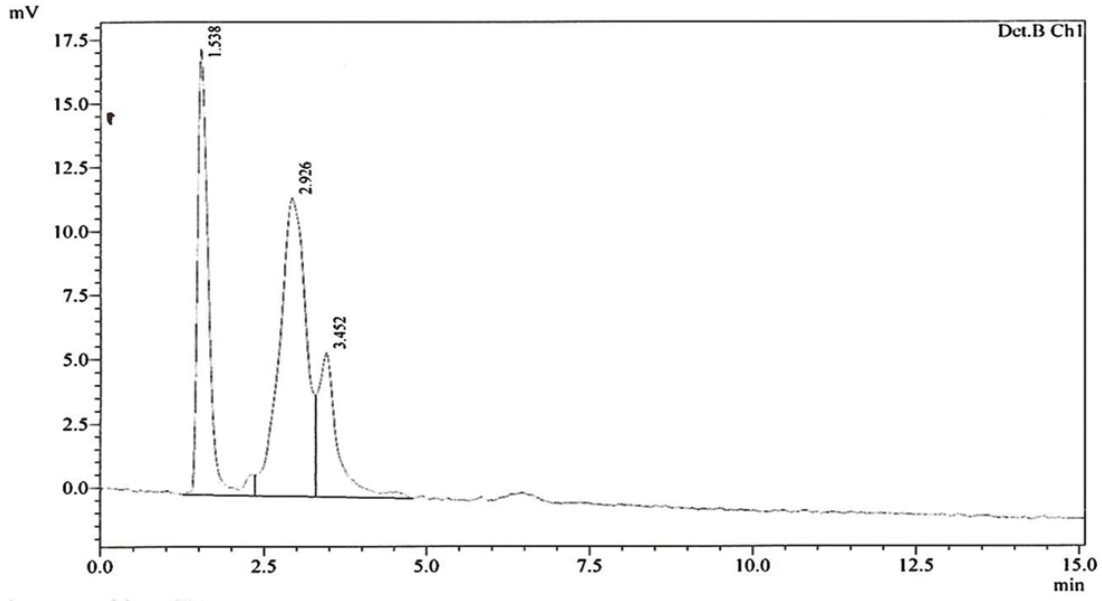

Figure 4.12: The chromatogram showing separation of the crude mixture with an aqueous 80 % methanol mixture

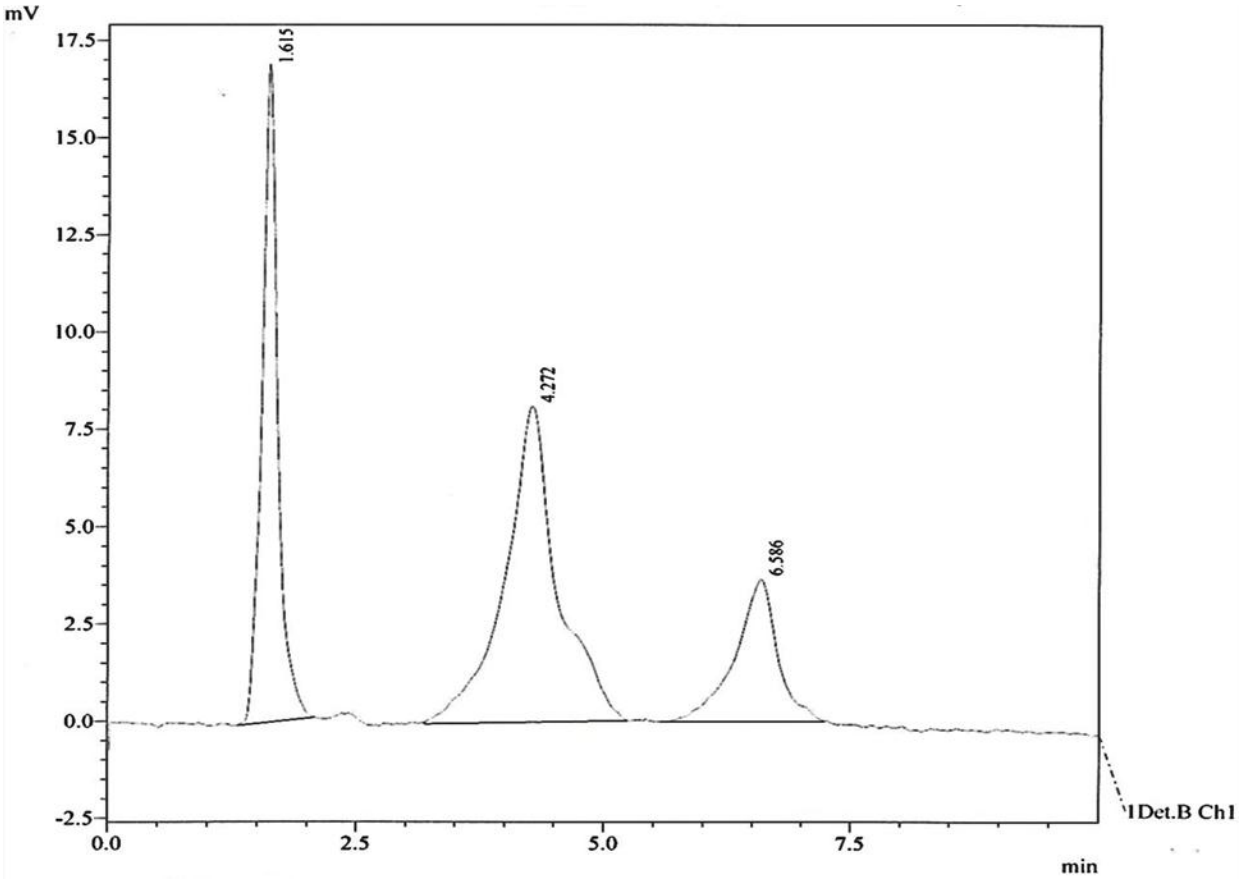

Figure 4.13: The chromatogram showing separation of the crude mixture with an aqueous 65% methanol mixture

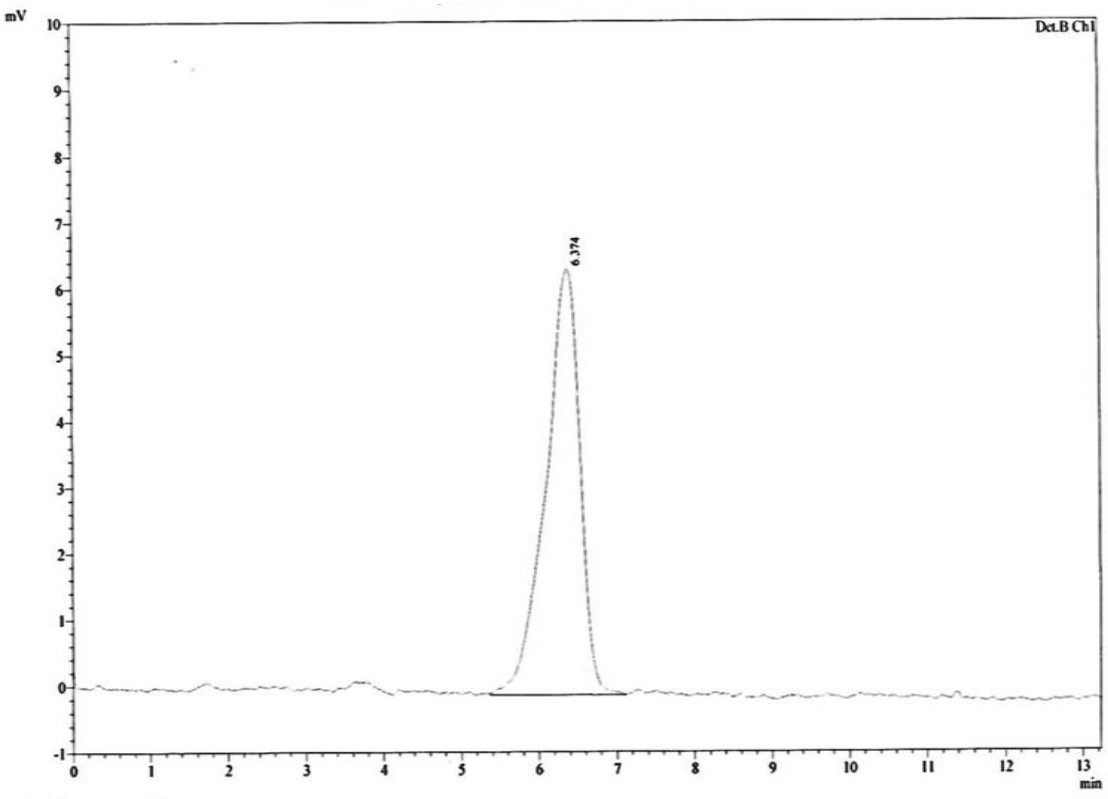

Figure 4.14: The chromatogram of BODIPY 5 in an aqueous 65% methanol mixture

Spectroscopic Evaluation of Quinoline Bearing Imidazole and BODIPY Dye Derivatives

In this study, three imidazole bearing quinoline derivatives and two BODIPY dyes were investigated for their properties via UV-visible and fluorescence spectroscopic techniques.

UV-Visible Spectroscopy

The optical analyses of **2**, **3**, **4**, **5** and **7** were recorded in five solvents viz. ethanol, methanol, dichloromethane, chloroform and acetonitrile. Briefly, each compound was weighed accurately and dissolved in each of the solvents mentioned; this gave a total of 25 solution. The UV-Vis measurements and the wavelength of maximum absorption (λ_{max}) were recorded[18] in the range 300-700 nm (**Table 10**).

Table 10: The wavelength of maximum absorption obtained from UV-visible Spectra in Different Solvents

Compounds	EtOH	MeOH	DCM	$CHCl_3$	ACN
2	313	329	300	315	312
3	330	330	330	330	330
4	378	377	279	378	378
7	508	507	511	512	505
5	507	507	511	513	504

Typical analysis of the 5 compounds in acetonitrile as solvent: the UV profile of compound **2** (**Appendix 46 (pages 185))** exhibited three strong absorption bands at wavelength region 278-279 nm, 311 -312 nm and 380 nm; λ_{max} at 312 nm gave the strongest absorption. The three regions of absorption shows the interaction[13a] between the electronic states that occurs within the

molecule. This demonstrates the possible spin allowed transitions and spin forbidden transitions[13b].

The UV profile of compounds **3** (**Appendix 47 (page 186))** and **4** (**Appendix 48 (pages 187))** shows a single strong absorption band at 330 nm and 378 nm, respectively.

The UV profile of compounds **5** and **7** shows a single absorption band at 505 nm and 504 nm, respectively.

All compounds displayed different behavior when dissolved in each solvent. Compound **2** shows three strong peaks which were evident in all solvents (**Appendix 46 (pages 185))** However the third absorption band was not completely visible in ethanol. It was evident that there was a red shift in the λ_{max}. The shift in λ_{max} for the solvents is presented in **Table 10** (**page 110**). Compound **2** displays intermolecular charge transfer (ICT) in solution which could be occurring between the quinoline and the imidazole ring system during electronic excitation. Compounds **3** and **4** shows an analogous wavelength shift across the various solvent polarities but with slight shift of 1 nm. Compounds **5** and **7** shows a shift in λ_{max} of 3-4 nm in different solvents. The difference in wavelength could be due to the dielectric function of the solvents as a contributing factor[14].

Fluorescence Spectroscopy

The fluorescent behavior of compounds **2**, **3**, **4**, **5** and **7** were studied by recording their profile in five solvents viz. ethanol, methanol, dichloromethane, chloroform and acetonitrile with a single excitation at specific wavelength range obtained from their UV-visible profile **(Appendix 51-55, pages 190-194)**. The λ_{max} in each of the solvents is presented in **Table 11**.

Table 11: The wavelength of maximum absorption obtained from fluorescence spectroscopy in different solvents

Compounds	EtOH	MeOH	DCM	$CHCl_3$	ACN
2	384	382	403	406	406
3	430	428	430	430	407
4	456	462	451	433	471
7	521	523	527	527	506
5	524	525	526	527	518

A single emission band was observed for compound **3** with two humps on either side of the maxima fluorescence band; this indicates that there was an intermolecular interaction lifetime [15] with the excitation singlet state. Compound **4** shows minimal fluorescent behavior judging from the intensity units. The spectra (**Appendix 53 (page 192)**) clearly indicates the excitation bands as well as the low emission band.

For compounds **7** (**Appendix 54 (page 193)**) and **5** (**Appendix 55 (page 194)**), the solutions were diluted by 100 times dilution factor because they exhibited highly intense fluorescence band. Some of the bands in fluorescence spectra illustrates the excitation bands along with the emission bands. In comparison to the UV-Vis spectra (**Appendix 46-50 (pages 185 -189**) the bands for each remain almost the same as $CHCl_3$ and methanol and follows the same order and DCM is the smallest band observed.

The fluorescence spectra of compound **2** (**Appendix 51 (page 190)**), dissolved in ACN, shows a high fluorescence band which was approximately three times higher than in the other solvents. Compound **3** (**Appendix 52 (page 191)**) in ethanol exhibits the higher emission band which was followed by methanol and this is the reverse sequence obtained for UV-Vis studies apart from

$CHCl_3$ and CH_2Cl_2. Compound **4** (**Appendix 53 (page 192)**) shows a higher fluorescence profile in ACN and ethanol.

The UV-visible and fluorescence spectra of **7** shows identical absorption in $CHCl_3$ and methanol and follows the same order; DCM is the smallest band observed. The fluorescent emission bands shows that ethanol has the highest emission bands and can be correlated to the UV-vis spectra. However, the remainder of the solvents behave in quite contradictory manner.

This shift in λ_{max} between the UV-Vis Spectra and fluorescence spectra can be quantified by the Stokes shift. **Table 12** shows the results obtained for λ_{max} from UV-visible and fluorescence Spectroscopy in Different Solvents.

Table 12: The wavelength of maximum absorption obtained from UV-visible and fluorescence spectroscopy in different solvents.

	EtOH		MeOH		DCM		$CHCl_3$		ACN	
Compounds	**λ_{max} UV**	**λ_{max} Fluorescence**	**λ_{max} UV**	**λ_{max} Fluorescence**	**λ_{max} UV**	**λ_{max} Fluorescence**	**λ_{max} UV**	**λ_{max} Fluorescence**	**λ_{max} UV**	**λ_{max} Fluorescence**
2	313	384	329	382	300	403	315	406	312	406
3	330	430	330	428	330	430	330	430	330	407
4	378	456	377	462	279	451	378	433	378	471
7	508	521	507	523	511	527	512	527	505	506
5	507	524	507	525	511	526	513	527	504	518

The Stokes shift, shift in wavelength of a fluorophore from the initial excitation wavelength [16], was calculated by using the equation:

Equation 3:

$$Stoke\ Shift = \lambda_{em} - \lambda_{ex}$$

Where λ_{em} denotes the emission spectra wavelength maxima and λ_{ex} denotes the excitation

The Stoke shift data is presented in **Table 13**. It was observed that there was a gradual red shift in wavelength of the emission bands. This indicated a large Stoke Shift between the excitation wavelength and the emission wavelength. The non-polar solvents demonstrated a larger red shift in compounds **2, 3, 4** and polar solvents displayed a larger shift in compounds **7** and **5**. This further indicated that the photons did change conformation or interaction with the molecular excited singlet state before returning to ground state when the orbital energy levels changed in the solvents (**Figure 4.15**). **Table 13** illustrates the extent of the red shift using as indicated by

the calculated Stoke shift. This shift in wavelengths illustrates the utility of the compounds as fluorescent probes. The comparison of the Stokes shift is presented in **Appendix 56-80 (page 195 - 219)**. In order to correlate the data of the UV-Vis spectra with the fluorescence spectra, the intensity of the compound was reduced to match that of the UV-Vis spectra of the compounds. The reduction factor, used for each compound, can be found on **Table 14**.

Table 13: The Stoke Shift calculated for five compounds in different solvents

Compounds	EtOH (nm)	MeOH (nm)	DCM (nm)	CHCl3 (nm)	ACN (nm)
2	71	53	103	91	94
3	100	98	100	100	77
4	78	85	172	55	93
7	13	16	16	15	2
5	17	18	15	14	14

Table 14: Reduction Factor of Fluorescence Intensity for Stokes Shift

Compounds	EtOH	MeOH	DCM	Chloroform	ACN
2	-	-	-	-	-
3	5000	3000	500	1500	250
4	10	-	10	-	50
7	600	600	250	700	350
3.15	1500	1500	1500	1500	1000

The fluorescence quantum yield of the five quinoline moieties derivatives, in the solvents, was determined by using Fluorescein[17] as a reference. The excitation wavelength, obtained from UV-

visible spectra, was used to determine the efficiency behavior of the quinoline derivatives[18]. The reference standard was also excited using the same wavelengths as the test compounds, at the different concentrations for each compound in the various solvents employed. The quantum yield measurements were then performed by recording the absorption and fluorescent spectra of the compounds and fluorescein standard. This was done in a range of concentrations i.e. 0; 0.2, 0.4, 0.6, 0.8 and 1.0 µM. This was further used to plot the intensity of each compound against the absorbance obtained (see **Appendix 81-85 (pages 220 - 229)**). Similarly, the same approach was used for the fluorescein reference standard **Appendix 86 (page 230)**. The gradients were determined by utilizing the Microsoft Excel equation function to obtain the equation of a straight line. The gradient was then placed into equation 1 and with the reference values of the refractive index[19-23] for the five solvent used (see **Appendix 87 (page 232))**, this made it possible to calculated the quantum yield for each compound.

Equation 1:

$$\Phi = \Phi_R \left(\frac{m}{m_R}\right)\left(\frac{n^2}{n_R^2}\right)$$

Where Φ is the quantum yield and subscript R imply reference standard, m is the gradient of the curve of intensity of referenced standard vs. absorbance of the chemical species. N denotes the solvent refractive index. The quantum yield of fluorescein was referenced to be 0.79 [24a,b].

When the quantum yield analyses were performed for compounds **2, 3, 4, 5** and **7**, it was noted that at a high linear dynamic range of 1.0 µM, there was curvature observed at a point on the graph (see **Appendix 81 (page 220) – Appendix 85 (page 228)**). A plot against the wavelengths at which maxima intensity for emissions vs. maxima absorbance was constructed. The quantum yield of all compounds gave a value of less than 1. This indicates that there was no photo-

induced or radiation-induced chain present to trigger transformation[25] but a quantum state was formed. Each compound did confirm some decay of the excitation photons in the pathway in the quantum states. From the data presented in **Table 15**, it is clear that no single solvent significantly influenced the compounds nature to enhance decay and thus promotes fluorescence within the compounds. However, it can be deduced that methanol and ACN are the two solvents that have the highest decay in comparison to the other solvents. Compound **7** demonstrated a high quantum yield and close to the optimal factor of 1 in chloroform. This confirm the reasoning behind the high intensity obtained by the compound in the fluorescence spectra. Dielectric function of each solvent can be used to discuss the permittivity of the solvents that would influence the properties of the molecules when radiated with light source from the instruments[26].

Table 15: Quantum Yield of the imidazole-quinoline and BODIPY dyes in various solvent

Quantum Yield of Compounds					
Compounds	EtOH	MeOH	DCM	Chloroform	Acetonitrile
2	0.044	0.103	0.043	0.043	0.073
3	0.531	0.346	0.147	0.279	0.184
4	0.011	0.031	0.012	0.013	0.232
7	0.476	0.510	0.269	0.725	0.232
5	0.099	0.061	0.073	0.093	0.031

The lifetime of photons was measured with the use of the Varian Cary Fluorescence spectrophotometer by Lifetime Time Correlated Single Photon Counting (TCSPC). The data presented in **Table 16** was obtained directly from the instrument; this represents the average behavior of the photon when it is excited within its quantum state. Since all the compounds

demonstrated a fluorescent nature, this data can be used to discuss the fluorescent decay of the compounds[27]. This fluorescence decay implies that all the excited molecules exist in a homogenous environment.

Table 16: Lifetime Data of the imidazole-quinoline and BODIPY dyes in Various Solvents

Lifetime($\boldsymbol{\tau}$)-ms	EtOH	MeOH	DCM	Chloroform	ACN
2	90.49	100.59	90.49	90.49	90.49
3	102.80	102.80	102.80	102.80	102.80
4	102.82	102.80	102.80	102.80	102.80
7	90.49	90.49	100.59	90.49	90.49
5	90.49	100.59	90.49	90.49	90.49

The molar absorptivity was calculated to quantify how strong the chemical species can absorb electromagnetic radiation (light) [28]. The Beer-Lamberts law[29] *equation 5* was used:

Equation:5

$$A = \varepsilon B c$$

The symbol A denotes the absorbance units of the chemical species, B the path length of the cuvette used for the analyses of the compounds and c is the concentration used in order to obtain the absorbance spectra from the UV/Vis spectrophotometer. Absorbance's were obtained from the spectra in **Appendix 46-50 (pages 185 - 189)** and used in equation 5 for each compound in each solvent. **Table 17** illustrates the calculated molar extinction coefficient at the characteristic wavelengths. The reason for examining just these wavelengths is due to the fact that these wavelengths were used for fluorescence studies and will be used later in the calculation for the brightness of the fluorophores.

Table 17: Molar Extinction of the imidazole-quinoline and BODIPY dyes Compounds

Compounds	EtOH	MeOH	CH_2Cl	$CHCl_3$	ACN
2	7.87E+03	1.10E+04	1.19E+04	7.87E+03	4.01E+04
3	8.07E+03	8.73E+03	1.05E+04	1.16E+04	1.37E+04
4	2.18E+04	2.01E+04	3.46E+04	3.87E+03	1.52E+04
5	6.23E+03	1.33E+03	1.63E+03	1.03E+03	3.57E+03
7	2.17E+04	2.66E+04	1.78E+04	2.42E+04	2.40E+04

Table 17 shows that all the compounds absorbs electromagnetic radiation strongly. This was deduced from the data obtained since all are above 1000 units. Hence, this explains the appearance of a UV-Vis spectra.

The molar extinction coefficient was used to calculate the brightness of the fluorophore. By using the quantum yields, obtained from **Table 15,** and inserting the data in equation 6, the brightness was calculated, and presented in **Table 18**.

Equation 6:

$$Brightness = \Phi \, x \, \varepsilon$$

Table 18: Calculated Brightness of the imidazole-quinoline and BODIPY dyes compounds

	Ethanol	Methanol	DCM	Chloroform	Acetonitrile
2	3.46E+02	1.14E+03	5.13E+02	3.38E+02	**4**3E+03
3	4.28E+03	3.02E+03	1.55E+03	3.23E+03	**2**1E+03
4	2.40E+02	6.22E+02	4.15E+02	5.03E+01	3.52E+03
5	47E+03	6.80E+02	4.39E+02	7.49E+02	8.27E+02
7	2.15E+03	1.62E+03	1.30E+03	2.25E+03	7.45E+02

These results indicate that the compounds are brightly coloured when radiated with electromagnetic radiation.

Compounds were analyzed using the Shimadzu UV-Vis spectrophotometer for their photovoltaic property. A comparative analysis was performed on the sample solutions as an indication whether the reflectance type fell into the two categories, namely specular[30] and diffused reflectance[31]. All analyses were conducted in the visible range of 300-700 nm since the solar spectrum encountered on earth is in the UV-visible region. In order to achieve a suitable comparison of the spectra, the UV/Vis spectra was multiplied by a 100 times to achieve a suitable scale. From the spectra **Appendix 88 -112 (pages 232-256),** it is evident that the specular reflectance obtained was a mirror image of the absorbance spectra. This also indicated that there was no scattering of light and hence maximum absorbance by the compounds were obtained.

The reflectivity of the compounds where analyzed for its potential to be a solar photovoltaic cell. In order to achieve this, the structure of the synthesized compounds are required to be of focus to determine if the structural composition could be an n-type, p-type or p-n junction cells[1]. p-type is a pure crystal structure with no doping and n-type are doped and said to have holes in the

structure. In n-type semiconductor type, there are a lone pair of electrons that can diffuse into the crystal lattice, as it is not part of the bonding. This mobile electrons are allowed to move through the compound (material) to conduct electricity. For this study p-n junction cells semiconductors is of focus. From this, p-n junction cell can convert light energy into electricity[32]. This is possible by a process called ionization[33]. Ionization process occurs when the atoms are radiated with light energy and a negative electron is ejected from the atom and leaving behind a positive hole to develop a positive and negative terminal which is much like a battery. The movement will dissipate energy and thus, to return back to the hole to cancel the potential. This creates a current to flow through the material in a single direction and electricity can be captured.

All the compounds all are assumed to be n-type crystal lattices[31]. Photovoltaic cells undergo two main processes to undergo photovoltaic conversion[32]. The first is the absorbance of light in the useful spectral range and secondly is the reflected incident beam that can be reabsorbed by the surrounding indentation of the compound surface. Reflected light is usually overcome with the use of a film as reflected light cannot be used for photovoltaic conversion. Lost in reflectivity can be used to calculate the energy efficiency as a solar cell.

Individual solvents where initially run, through the instrument, to outline the influence that solvents have on the compound. This was then followed by the analyses of the sample solutions to obtain the reflectance in percentage; an assumption was that it would have a direct affiliation of the compound itself. These reflectance spectra is presented in **Appendix 113- 117 (pages 257 - 261).** The spectra resemble the UV-Vis Spectra in **Appendix 46-50 (pages 185 - 189).**

The transmittance in percentage was obtained with the use of equation 7 and 8. The transmission spectra can be viewed in **Appendix 118-122 (pages 262 - 266)** for all the compounds. The

compounds in different solvents displayed different transmittance from each other and also resembled the behaviour of the reflectance spectra in **Appendix 113- 117 (pages 257 - 261).**

Since the maximum amount of light was absorbed by the synthesized compound, we used equation 10 to calculate the energy gaps, shown in the transmittance spectra.

Equation 10

$$E = \frac{h.c}{\lambda}$$

Table 19: Energy Gaps at λ_{max} of the imidazole-quinoline and BODIPY dyes

	EtOH		MeOH		DCM		$CHCl_3$		ACN	
	λ_{max}	E (ev)	λ_{max}	E (ev)	λ_{max}	E (ev)	λ_{max}	E (ev)	λ_{max}	E (ev)
2	313	6.35E-19	329	6.05E-19	300	6.63E-19	315	6.31E-19	312	6.05E-28
3	330	6.03E-19	330	6.03E-19	330	6.03E-19	330	6.03E-19	330	6.03E-28
4	378	5.26E-19	377	5.28E-19	279	7.13E-19	378	5.26E-19	378	5.28E-28
7	508	3.92E-19	507	3.92E-19	511	3.89E-19	512	3.88E-19	505	3.92E-28
5	507	3.92E-19	507	3.92E-19	511	3.89E-19	513	3.88E-19	504	3.92E-28

The energy was converted to joules by multiplying the energy in ev by 1.602 x 10^{-19}. From the data obtained, it was evident that at a low concentration of 30 µM the energy involved in the excitation of electrons at the particular wavelengths was relatively low. This is the maximum for solar irradiance. Since we used very small quantities our assumption is that if the concentration is increased higher, a larger amount of energy will be produced. Energy efficiencies can be used to observe the potential as a photovoltaic cell; further research is recommended to accomplish this objective.

The binding properties[34] between the imidazole-quinoline derivatives i.e **2**, **3** and **4** and metal ions were investigated. Eight metal ions were selected for the binding studies; these were Zn^{2+}, Co^{2+}, Cd^{2+},Ni^{2+}, Pb^{2+}, Fe^{2+}, Cu^{2+} and Hg^{2+}. The eight solutions of concentration 200 µM were prepared whilst the synthesized compounds were made up to 30µM in HEPES buffer solution. HEPES was used to maintain the pH since carbon dioxide in the atmosphere[35] can change the pH. Each metal solution was placed in a vial with equi-volume of the compound and mixed thoroughly. Upon completion of instantaneous shake of the vial the resulting solutions were analyzed with the fluorescence spectrophotometer and a response was obtained. The binding properties are presented in **Appendix 128, 138, 148 (pages 272, 282 and 292),** respectively. Compounds **2, 3** and **4** dimerises to accomplish the coordination to form a complex with the six bonding sites for charge transfer with the metal ions. This was confirmed with Gibbs free for its affinity and was found to be 24.726 $KJ.mol^{-1}$ (**Appendix 158 (page 302)**). The orbital of the metal ions split into eg and $T_2ġ$ by following the crystal field theory for binding[36] (electron transfer to occur between the ligand and metal ions). This gives rise to charge transfer which entails the movement of electrons from the ligand to the metal ion orbitals or vice versa. The electrons undergoes electronic transition into the excited states and followed by the return to the ground state and hence emitting radiation in the form of light. The wavelength of which the radiation light was emitted was measured by fluorescence spectroscopy. All orbitals of metal ions are degenerate but can undergo a change in energy with the nature of the ligands and thus influencing the complex[37]. What was also observed was that there was two emission peaks observed as compared to the compounds placed in ACN. This phenomena is a result of electrons remaining longer in the excited states and thus longer lifetime should be observed. **Figure 4.15** and **4.16** displays a graphical representation of **2** in the buffer solution and in the presence of the

metal ions. These results indicate that **2** could be used for determining metals in water. Another observation is that metal ions of the same period showed a slow decrease in intensity with an increasing number of electrons presence in the d energy levels as exemplified by Fe^{2+}, Co^{2+}, Ni^{2+}, Cu^{2+} and Zn^{2+}. Although Zn^{2+}, Cd^{2+} and Hg^{2+} are of the same group on the Periodic Table with a d^{10} configuration, no specific behavior was observed apart from the enhancement of the excitation signal. In the case of Pb^{2+} metal ions, an enhancement of 100 times was observed. This suggests that **2** has potential application for removal of Pb^{2+} in waste water treatments. The first excitation band showed slight difference from the compound bands and the second band displayed the same quenching of bands as compared to the other seven metal cations (**Appendix 128 (page 272)**).

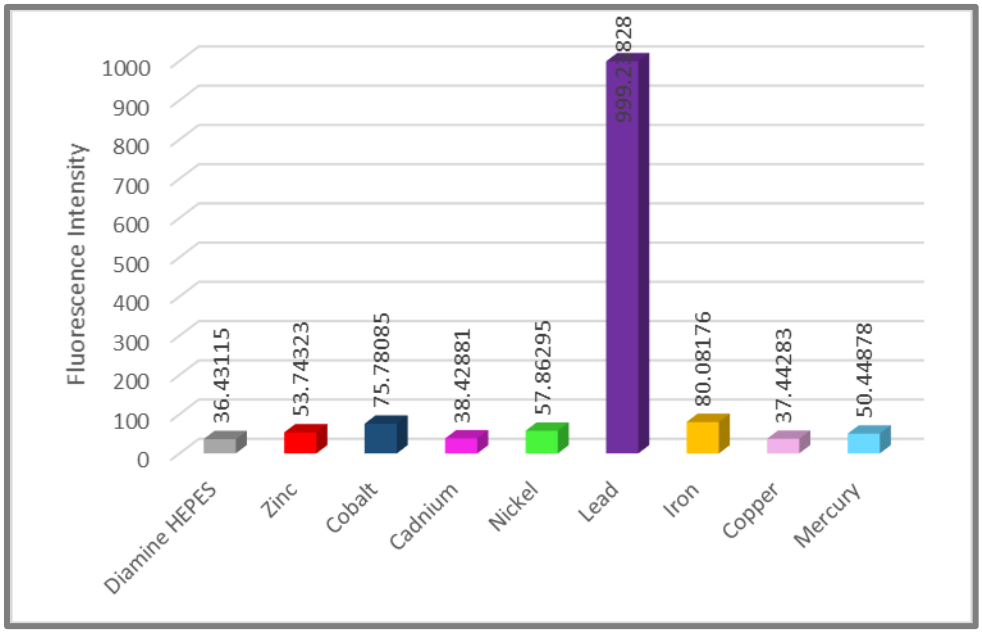

Figure 4.15: Fluorescence response of 2 in various metal ions in CH_3CN-HEPES buffer solution

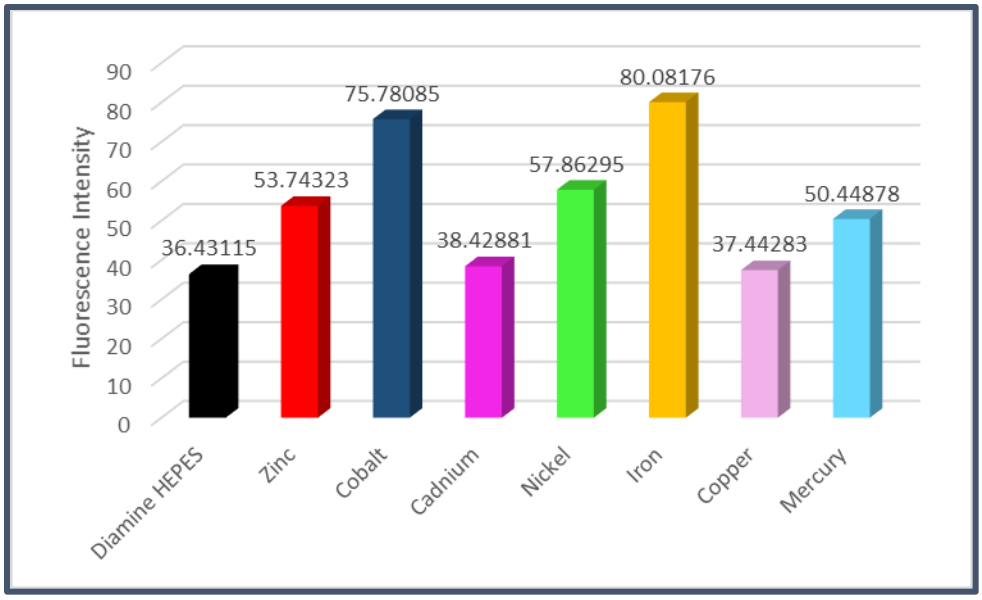

Figure 4.16: Fluorescence response with an exclusion of lead ion.

Compound **3** demonstrated good binding profile with the metal ions. The excitation and emission bands were observed (**Appendix 138 (page 282)** and the binding profile is presented in **Figure 4.17**. On comparing the spectra (**Appendix 139, (page 283)),** it was observed that pure **3** displayed the excitation band but when in HEPES buffer two bands were displayed. These were two bands are the excitation and the emission bands. Also, this compound's nature altered the spectral properties by adjusting the pH and forms a complex with HEPES; fluorescence is affected by pH and as there is a difference from being in the pure compound. Cobalt ions exhibited a similar profile as that of the zinc metal complex since the metals have atomic numbers next to each other. All the other complexes enhanced the excitation signal but quenched the emission band as a result of Photon Electron Transfer [38].

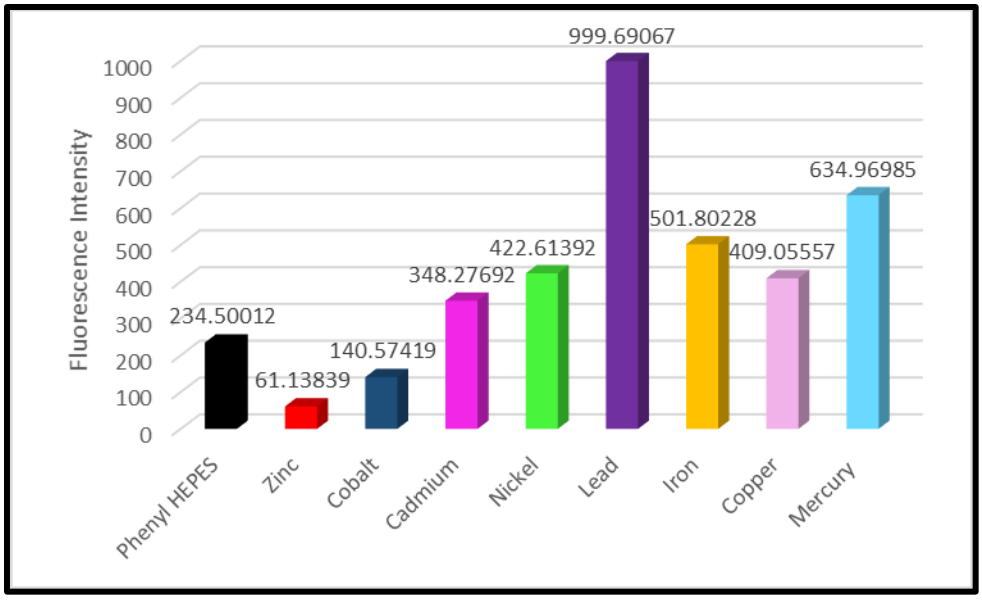

Figure 4.17: Fluorescence response of 3 in various metal ions in CH_3CN-HEPES buffer solution

Compound **4** demonstrated little or no emission band (**Appendix 148 (pages 292))** but evidence was shown that the excitation band signal was enhanced for all the metals. This indicates a good potential of its use for determining metal ions by the emission bands. **Figure 4.18** shows that Pb^{2+}, Fe^{2+}, Cu^{2+} and Hg^{2+} metal complexes gives a large enhancement of the signal in the excitation band beyond maximum intensity. The measurement range was limited to 1000 intensity which resulted in the complexes band to be cut off. However, it is evident that the bands would extend much higher than 1000 absorbance units.

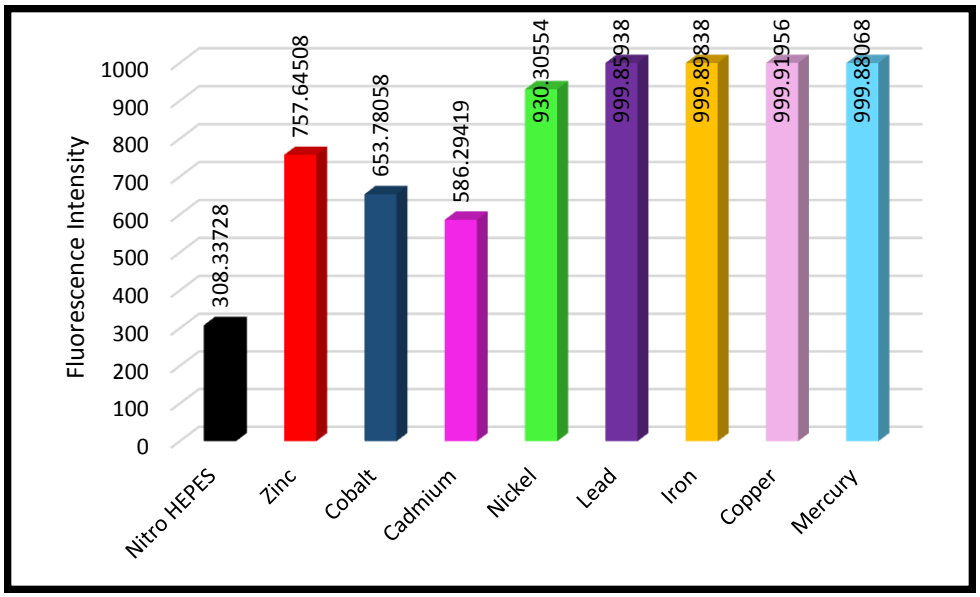

Figure 4.18: Fluorescence response of 4 in various metal ions

The possible mechanism for the formation of coordination complexes between the organic compound, as the ligand, and metal ion can be explained with Crystal Field Theory. However, the signal observed can also be explained with PET. It utilizes the atom spaces to connect a fluorescent group to a receptor and these comprises of high-energy non-bonding electron pairs. Once the fluorescent group is connected to the receptor, there is a transfer of an electron to the excited fluorescent group and results in a quench of the fluorescence signal. However, in the presence of a metal ion, coordination of electron pairs would prevent the electron transfer within the structure and consequently the fluorescence with be turned on more strongly. From the results obtained, it is evident that for the quinoline compounds were both a quench and enhancement in the fluorescent signal as compared to the original spectra to the spectra obtained of the compounds in HEPES. It is evident that regardless of the higher concentration used, the signal quenched as a result of the pH change of the compounds' environment. This quenching can be explained with fluorescent resonance energy transfer (FRET) by cancelling or overlapping of the two peaks. It can be regarded as distance dependent non-radiative transfer of

excitation energy from an excited donor fluorophore to a suitable proximal ground state acceptor fluorophore. At pH 12, the binding with receptor moiety can be observed as a results of the fluorescence increase by means of a photo induced electron transfer (PET) switching mechanism.

The spectra in **Appendix 129 (pages 273)** demonstrates two emission bands undergoes a red shift. The double emission bands demonstrate the electronic transition between two different excited states. The pure compound showed an intensity reading which was enhanced 100 times to show the comparison to the compound in HEPES, as when the compound was dissolved. When the pH was decrease to 7.2 the intensity of the compound decreased. This also showed the effect of solvent and pH on the nature of the compounds. Compound **3** in **Appendix 139 (pages 283)** showed one excitation band, but the excitation band in HEPES buffer displayed two band. The two photons are the excitation and the emission bands. Also, this compound's nature was altered as the spectral properties are adjusted by the change in pH units and forms complex with HEPES. When pure **4** (10 times enhanced signal by calculation), in ACN, was compared to the compound made up in HEPES buffer, it was clear that the emission band disappeared due to the quenching of the band (**Appendix 149 (pages 293)).** By adjusting the nature of the pure compound it was observed that the excitation signal was also enhanced by adjusting the pH to 7.2 units.

Molecular Docking Studies

The binding mode of **2** within the active site of the human MDM2 protein was analyzed. One hydrogen bond interaction was formed between **2** and human MDM2 protein. The hydrogen atom of **2** interacted with back bone of polar residue of Glu25 (**Figure 4.19a)**. The bond length between 2 and the active site of the human MDM2 protein was 1.90 Å. The glide score of -3.350 Kcal/mol and glide energy of -18.051 Kcal/mol was noted. Furthermore the following residues were mainly involved in hydrophobic interaction: LEU57, ILE61, PHE91, VAL93, ILE99 and TYR100 (**Figure 4.19b**). The raw data can be found in **Appendix 159 (page 302).**

The binding mode of **3** within the active site of the human MDM2 protein was analyzed. One hydrogen bond interaction was formed between **3** and MDM2. The hydrogen atom of **3** was interacted with the back bone of hydrophobic residue of Leu27 (**Figure 4.20a)**. The bond length between **3** and the active site of the human MDM2 protein was 1.57 Å. The glide score of -5.843 Kcal/mol and glide energy of -41.338Kcal/mol was noted. Furthermore, the following residues were mainly involved in hydrophobic interaction VAL28, LEU54, PHE955, TYR104, VAL108, and VAL109 (**Figure 4.20b**). The raw data can be found in **Appendix 159 (page 302).**

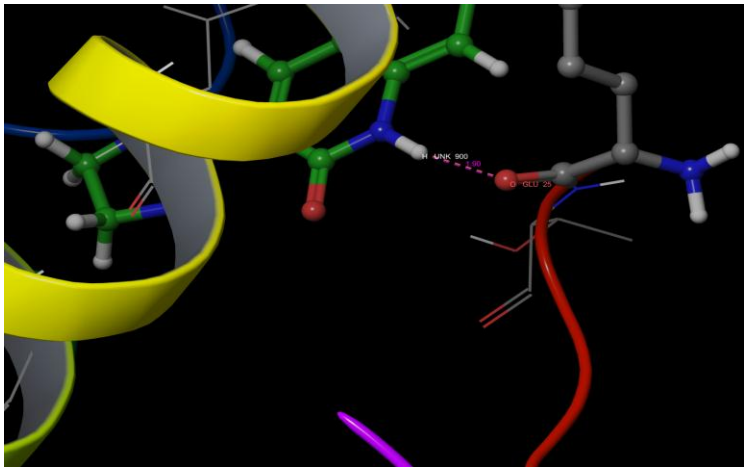

(a) Hydrogen bond formation and bond length of docking 2 to human MDM2

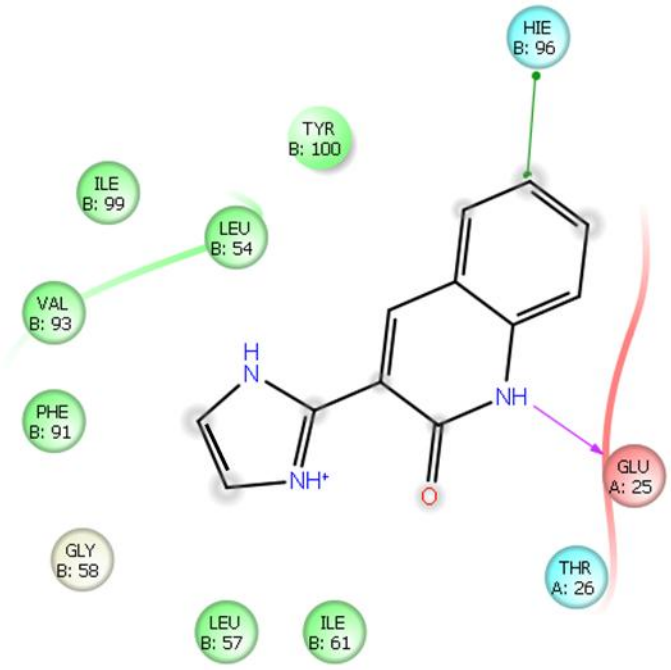

(b) Residues of hydrogen bond and hydrophobic interactions

Figure 4.19: Docking Results of 2 with Human MDM2

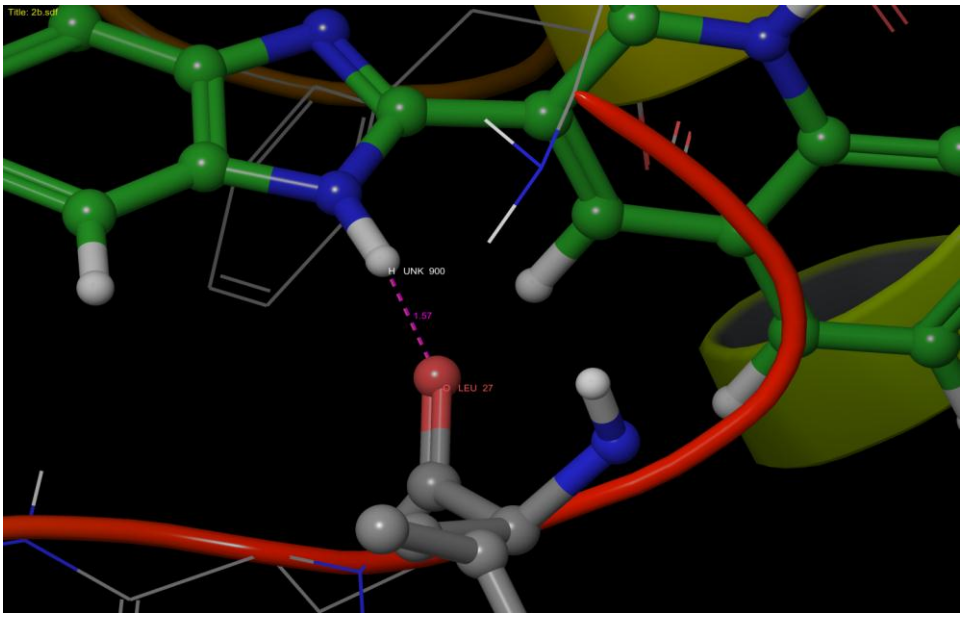

(a) Hydrogen bond formation and bond length of docking 3 to human MDM2

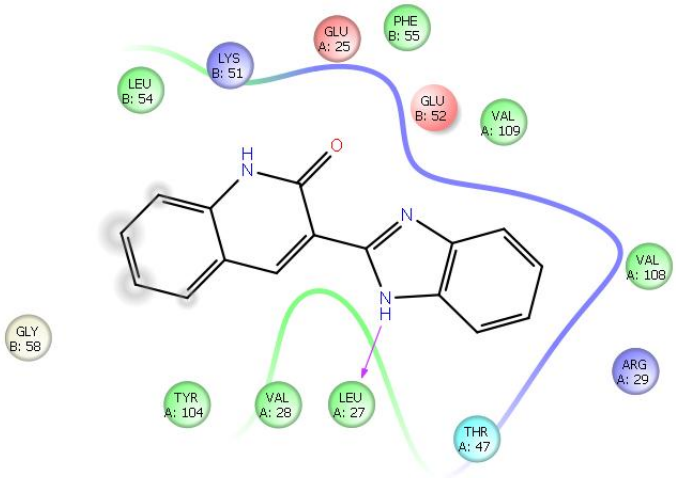

(b) Residues of Hydrogen Bond And Hydrophobic Interactions

Figure 4.20: Docking Results of 3 with Human MDM2

Cytotoxicity Studies Using A549 Lung Cancer Cells

The molecular docking studies did not display significant activity but the [3-(4,5-dimethylthiazol-2-yl)-2,5-diphenyl tetrazolium bromide] (MTT) assay was still performed for all the synthesized compounds. The effect of the newly synthesized compounds in A549 cells were measured using the MTT dye reduction assay[39]. This assay measures cell proliferation/metabolic activity *in vitro*. This technique was particularly useful for cells that were metabolically active based on their redox potential and capacity of dehydrogenase enzymes to convert yellow water-soluble salt into a purple water-insoluble formazan product. The insoluble crystals were then dissolved in dimethyl sulfoxide (DMSO) and the absorbance was analyzed on a spectrophotometer. The amount of formazan produced was directly proportional to cell number thus allowing for the determination of cell viability and proliferation.

A549 lung cancer cells were used for these investigations and cells were cultured to confluency and then treated with the synthesized compounds. The effect of the newly synthesized compounds in A549 cell was measured using MTT assay. The results from the MTT assays showed that compounds **3, 4** and **5** demonstrated a reduction in cell viability (**Figure 4.21**).

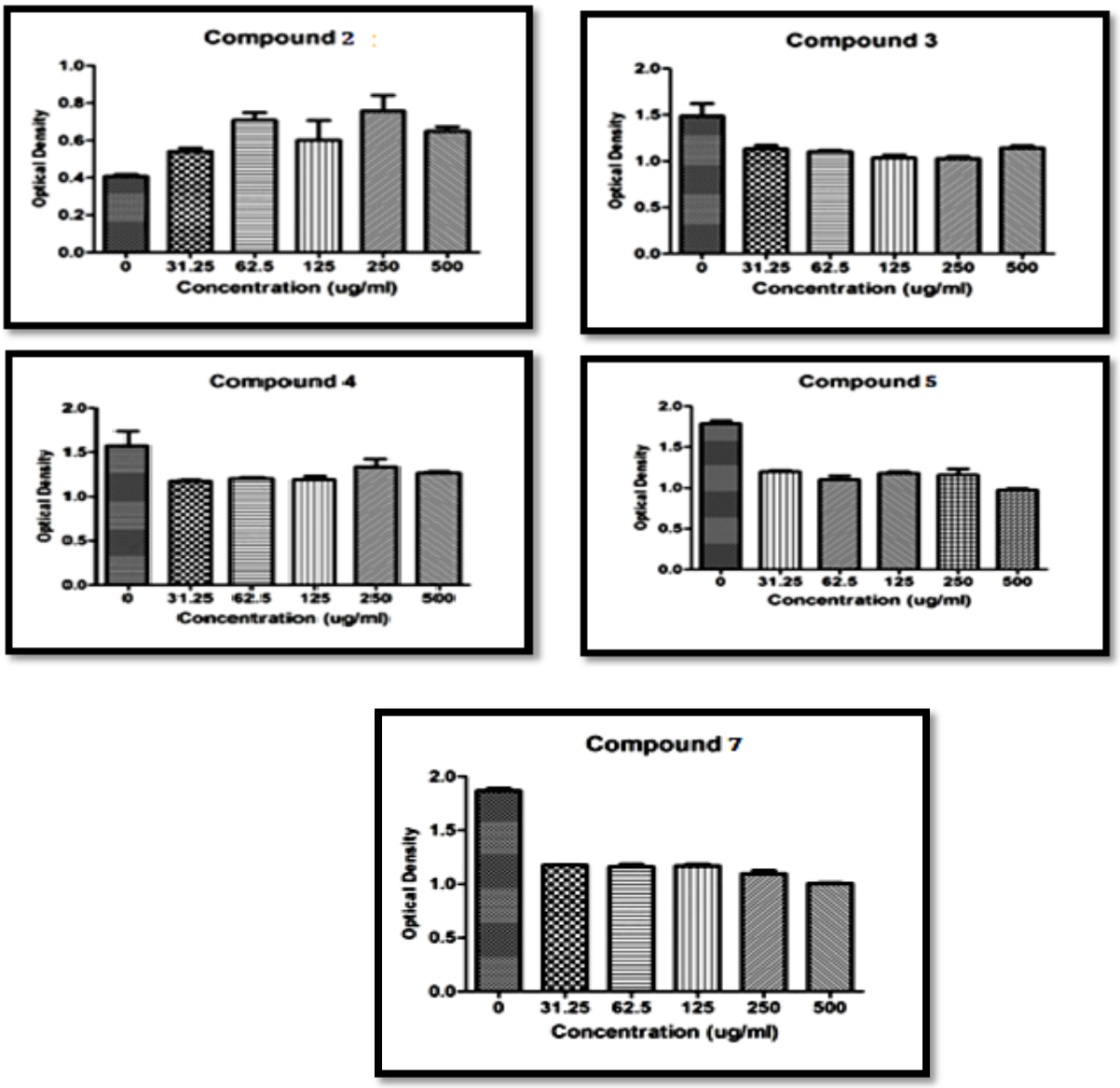

Figure 4.21: Cell Viability of compounds 2, 3, 4, 5 and 7

The BODIPYs with the quinoline moieties demonstrated a reduction in the rate of A549 cell proliferation when compared to the imidazole and benzimidazoles. This can be seen for compounds **5** and **7.** The special feature about these compounds is that they possess both a quinoline moeity and two fluorine atoms. Quinolines generally have anti-proliferative properties

however this is enhanced due to the fluorine. In a possible mechanism, the fluorine atom could bind to DNA to form adducts which would prevent proliferation.

Further, a comparison between imidazoles clearly shows that compounds **3** and **4** also decreased cell proliferation. In contrast compound **2** exhibited an increased rate of cell proliferation. The optical density of the control cell, is much higher that the plates for concentration 31.25 µg/ mL to 500 µg/ mL. However **2** cannot be discarded; this compound clearly shows that it possesses anti-hyperglycaemic properties. It can be useful in type 2 diabetes – so it may have use in human endocrine diseases. Also, the incubation times were short (<24 hrs); all these observations are acute. If left longer (>60 hours) there may be a completely different profile of toxicity**.** This can be used to indicate the reduction in the rate of the cell proliferation[43] of the cancer cells thus making these synthesized compounds toxic to this cancer lines and can be used as anti-cancer agents.

Finally, it is suggested that all these compounds need to be tested for apoptosis inducing ability in order to determine a mechanism on cellular activity.

References

1. Tóth, J.; Blaskó, G.; Dancsó, A.; Tõke, L. and Nyerges, M. (2006), Synthesis Of New Quinoline Derivatives, *Synthetic Communication*, Vol. 36, Issue. 23 pp. 3581-3589
2. Meth-Cohn, O. and Narine, B. (1987), Versatile New Synthesis Of Quinolines, Thicnopyridines And Related Fused Pyridines, *Tetrahedron,* Vol. 19, pp. 2045-2048
3. Srivastava, A. and Singh, R. M., (2005), Vilsmeier- Haack Regent: A Facile Synthesis of 2-Chloro-3-Formylquinoline From N-Arylacetamide And Transformation Into Different Functionalities, *Indian Journal of Chemistry,* Vol. 44B, pp. 1868-1875
4. Malathi, M. (2009), *Synthesis of Application Based Novel Quinoline Heterocycles.*, Published thesis (PhD), Department of Chemistry, Bharathiar University- India
5. William, K. L., (2003), *Macroscale and Microscale Organic Experiments,* 4th ed., Houghton Mififlin Company, New York, pp. 194-215,
6. Michigan State University, (2013), *Proton Chemical Shift Ranges*, [HTML], Available From: <http://www.cem.msu.edu/~reusch/OrgPage/nmr.htm> [Accessed 24 November 2013]
7. Gillespie, R. J., (1996), Improving Our Understanding Of Molecular Geometry And The VSEPR Model Through The Ligand Close-Packing Model And The Analysis Of Electron Density Distributions. Coordination Chemistry Reviews, Vol. 197, pp. 51-69
8. Jameson, L. P. and Dzyuba, S. V., (2013), Expeditious, Mechanochemical Synthesis of BODIPY dyes, *Beilstein Journal of Organic Chemistry*, Vol. 9, pp. 786-790
9. Millar, S. (2013), *Tips And Tricks For The Lab: Air- Sensitive Techniques*, [WWW], Chemistry View, Available from:

<http://www.chemistryviews.org/details/education/3728881/Tips_and_Tricks_for_Lab_Air-Sensitive_Techniques_1.html> [Accessed on: 10 February 2014]

10. Lui, K. M.; Tsai, M. S.; Jan, M. S.; Chau, C. M. and Wang, W. J., (2011), Convenient One-Pot Synthesis Procedure For The 4,4-Demethoxy-Boradiaza-S-Indacene Dyes And Their Application To Cell Labelling, *Tetrahedron*, Vol.67, pp. 7919-7922
11. **a)** Arroyo, I. J.; Hu, R.; Merino, G.; Tang, B .Z. and Pena-Caberera, E., (2009). The Smallest And One Of The Brightest. Efficient Preparation and Optical Properties of the Parent Borondipyrromethane System., *Journal of Organic Chemistry*, Vol. 74, pp. 5719-5722. **b)** Leen, V.; Miscoria, D.; Yin, S.; Filarowski, A.; Ngongo, J.N.; Van Der Auweraer. M.; Boens, N. And Dehaen, W. (2011). 1.7-Disubstituted Boron Dipyrromethene (BODIPY) Dyes: Synthesis And Spectroscopic Properties, *Journal of Organic Chemistry*, Vol. 76, pp. 8168-8176.
12. Zhu, S.; Zhang, J.; Vegesna, G.; Luo, F.; Green, S. A. and Liu. H., (2011), Highly Water-Soluble Neutral BODIPY Dyes with Controllable Fluorescence Quantum Yields, Organic Letters, Vol. 13, Issue. 3, pp. 438–441
13. a) Matsen, F. A., (1950), Molecular Orbital Theory and Spectra of Monosubstituted Benzenes. I. The Resonance Effect[1], *Journal of American Chemical Society*, Vol. 72, Issue. 11, pp. 5243–5248. b) Nic, M.; Jirat, J. and Kosata, B., (2014), *Laporte rule*. [WWW], IUPAC, Available from: < http://goldbook.iupac.org/L03454.html> [Accessed on: 02 April 2014]
14. Olmon, R.L.; Slovick, B.; Johnson, T. W.; Shelton, D.; Oh, S.; Boreman, G.D. and Raschke, M. B., (2012), Optical Dielectric Function Of Gold, *Physical Review B* 86, 235147. doi: http://dx.doi.org/10.1103/PhysRevB.86.235147

15. Penzkofer, A. and Blau, W., (1982), Theoretical Analysis Of S_1 -State Lifetime Measurements Of Dyes With Picosecond Laser Pulses, Optical and Quantum Electronics, Vol. 15, pp. 325-347
16. Nic, M.; Jirat, J. and Kosata, B., (2006), Stokes shift, [WWW], IUPAC, Available from: < http://goldbook.iupac.org/S06031.html> [Accessed on 23 April 2013]
17. Brouwer. A. M., (2011), Standards For Photoluminescence Quantum Yield Measurements In Solution (IUPAC Technical Report), *International Union of Pure and Applied Chemistry*, Vol. 83, No. 12, pp. 2213–2228
18. Allen, M. W., (2010), *Measurement of Fluorescence Quantum Yields*, [WWW], Thermo Fisher Scientific, Available from: <http://www.thermoscientific.fr/eThermo/CMA/PDFs/Product/productPDF_58470.PDF> [Accessed on 23 April 2013]
19. Wohlfarth, C. (2008), *Refractive Indices of Pure Liquids and Binary Liquid Mixtures (Supplement to III/38)*, Landolt-Börnstein - Group III Condensed Matter, Vol. 47, pp. 108-115
20. Merck Millipore, (2012), *Methanol*, [WWW], Available from: <http://www.merckmillipore.com/africa/chemicals/methanol/MDA_CHEM-106012/p_q_yb.s1Lm_cAAAEWpuEfVhTl> [Accessed on 15 June 2012]
21. Merck Millipore, (2012), *Dichloromethane*, [WWW], Available from: < http://www.merckmillipore.com/africa/chemicals/dichloromethane/MDA_CHEM-106049/p_Tfqb.s1L2y4AAAEW8.EfVhTl?WFSimpleSearch_NameOrID=dichloromethane&BackButtonText=search+results> [Accessed on 15 June 2012]

22. Merck Millipore, (2012), Chloroform, [WWW], Available from: < http://www.merckmillipore.com/africa/chemicals/chloroform/MDA_CHEM-102431/p_Tfqb.s1L2y4AAAEW8.EfVhTl?WFSimpleSearch_NameOrID=chloroform&BackButtonText=search+results > [Accessed on 15 June 2012]
23. Merck Millipore, (2012), Acetonitrile, [WWW], Available from: < http://www.merckmillipore.com/africa/chemicals/acetonitrile/MDA_CHEM-100003/p_W.Sb.s1LthUAAAEWtOEfVhTl?WFSimpleSearch_NameOrID=acetonitrile&BackButtonText=search+results > [Accessed on 15 June 2012]
24. a) Lakowicz, R. J. (1999), *Principles of Fluorescence Spectroscopy*, 2nd Ed., Kluwer Academic/Plenum Publishers, New York, London, Moscow, Dordrecht. b) Yang, Z.; Wang, M.; Yong, A. M.; Wong, S. Y.; Zhang, X.; Tan, H.; Chang, A. Y.; Li, X and Wang, J., (2011), Intrinsically Fluorescent Carbon Dots With Tunable Emission Derived From Hydrothermal Treating Glucose In The Presence Of Monopotassium Phosphate, *Chemical Communications*, Vol. 47, Issue. 42 pp. 11615-11617
25. Serpone, N. and Salinaro, A., (1999), Terminology, Relative Photonic Efficiencies And Quantum Yields In Heterogeneous Photocatalysis. Part I: Suggested Protocol. *International Union Of Pure And Applied Chemistry*, Vol. 71, Issue. 2, pp. 303–320
26. Grady, N.K., (2004), *Influence Of Dielectric Function Properties On The Optical Response Of Plasmon Reasonant Metallic Nanoparticles*. Published thesis (MSc), Rice University.
27. Kumar. S. (2006), Spectroscopy of Organic Compounds, [WWW], Guru Nanak Dev University, Available from:

<www.uobabylon.edu.iq/eprints/publication_11_8282_250.pdf> [Accessed on 24 May 2013]

28. Beer lamberts law
29. U.S. DEPARTMENT OF COMMENCE, NATIONAL BUREAU OF STANDARDS (1987) *NBS Measurement Services: Spectral Reflectance, July 1987*. U.S. Government Printing Office: Washington. pp. 1.
30. U.S. DEPARTMENT OF COMMENCE, NATIONAL BUREAU OF STANDARDS (1976) *Development of an NBS Reference Spectrophotometer For Diffused Transmittance and Reflectance, October 1976*. U.S. Government Printing Office: Washington. pp. 1
31. Chua, L.; Zaumseil, J.; Chang, J.; Ou, E. W. C.; Ho, P. K. H.; Sirringhaus, H. and Friend, R. H., (2005), General Observation Of N-Type Field-Effect Behaviour In Organic Semiconductors, *Letters to Nature*, Vol. 434, pp. 194-199
32. Rauschenbach, H.S. (1976), Solar cell array design handbook - The Principles and Technology of Photovoltaic Energy Conversion. National Aeronautics and Space Administration.
33. Tams, C. and Enjalbert, N., *The Use of UV/Vis/NIR Spectroscopy in the Development of Photovoltaic Cells*, [WWW], Perkin Elmer, Available From: < http://www.perkinelmer.com/PL/CMSResources/Images/44-74323APP_UseofUVVisNIRinDevelopmentPV.pdf.> [Accessed on: 23 May 2013]
34. Wang, R. N.; Huang, S. B.; Zhao, N. and Chen, Z. N. (2010). A New Cu^{2+} Chemosensor Based On Functional 8-Hydroxylquinoline. *Inorganic Chemistry Communications*, Vol.13, pp. 1432-1434

35. Life Technologies, (2013), *HEPES*, [WWW], Available from: <http://www.lifetechnologies.com/za/en/home/life-science/cell-culture/mammalian-cell-culture/reagents/hepes.html> [Accessed on: 12 September 2013]
36. Cotton, F .A.; Wilkinson, G. and Gaus, P. L., (1995), Basic Inorganic Chemistry, Chapter 23: Introduction To The Transition Elements: Ligand Field Theory, 3rd edn. Maidenhead: John Wiley & Son. pp. 504-509
37. J.J. Borrás-Almenara, J. J.; Coronadoa, E.; Clemente-Juanb, J. M.; Palic, A. V. and Tsukerblatc. B. S., (2001), Magnetic Exchange between Orbitally Degenerate Metal Ions: The Problem of Magnetic Anisotropy, *Journal of Solid State Chemistry*, Vol.159, Issue 2, pp. 268–280
38. a. Sarker, M. Banthia, S. & Samantha, A. (2006). 'A Highly Selective 'off-on' Fluorescence Chemosensor for Cr (III).' *Tetrahedron Letter*. Vol 45, pp. 7575 – 7578. b. Banthia, S. & Samantha, A. (2006). 'A New Strategy for Ratiometric Florescence Detection of Transition Metals Ions.' *The Journal of Physical Chemistry B*. Vol. 110, pp. 6437 – 6440
39. Mosmann, T., (1983), Rapid Colorimetric Assay For Cellular Growth And Survival: Application To Proliferation And Cytotoxicity Assays, *Journal of Immunological Methods*, Vol. 65, Issues. 1–2, pp. 55–63

Chapter 5: Conclusion and Recommendations

The aim of the project was to synthesize novel imidazole and BODIPY dyes containing a quinoline moiety and to investigate their spectroscopic properties and biological activities.

Synthesis, purification and characterization of imidazole bearing quinoline derivatives

Five quinoline derivatives were successfully synthesized and characterized using IR, ^{1}H-NMR, ^{13}C-NMR and ^{19}F-NMR spectroscopic techniques. In addition, four BODIPY dyes were synthesized, however, difficulties were encountered in the purification step and hence it is recommended that a high precision analytical instrument be used for the separation of these compounds. HPLC was used for the separation of BODIPY dyes from the reaction mixture.

Spectroscopic evaluation of quinoline bearing imidazole and BODIPY dye derivatives

UV-Visible Spectroscopy

The optical analyses of **2**, **3**, **4**, **5** and **7** were recorded in five solvents viz. ethanol, methanol, dichloromethane, chloroform and acetonitrile. All the synthesized derivative exhibited a UV-visible profile and these wavelengths were used for fluorescence analyses.

Fluorescence Spectroscopy

The fluorescent behaviour of **2**, **3**, **4**, **5** and **7** were studied by recording their profile in five solvents viz. ethanol, methanol, dichloromethane, chloroform and acetonitrile with a single excitation at specific wavelength range obtained from their UV-visible profile. It was observed that non-polar solvents gave a more stable fluorescent profile compared to a polar solvent.

Fluorescent properties studied were Stoke shift, quantum yield, life time, molar absorptivity and brightness. For all the derivatives synthesized a Stoke shift was observed for all the solvents

studies. The quantum yields for the compounds displayed a linear behavior at low concentrations and all displayed a quantum yield of below 1 which indicated that there was no PET observed to trigger transformation but quantum states were formed. The life time of the compounds was also determined with the use of Varian Cary Fluorescence spectrophotometer and this displayed the fluorescent decay of each compound in its solvent system. The molar absorptivity was calculated to quantify how strong the chemical species can absorb electromagnetic radiation and this was further used to calculate of the brightness of the fluorophore. The results indicate that the compounds are brightly coloured when radiated with electromagnetic radiation.

After the fluorescent studies were conducted, the compounds were further investigated for its potential as a photovoltaic cell. All of the synthesized compounds demonstrated a positive result for its ability to be a photovoltaic cell. The energies of the compounds were obtained from the analyses of the reflectance and transmission spectra. This is a starting point for further research as one could explore properties of quantum efficiency and energies associated with solar cells.

The binding properties between the imidazole-quinoline derivatives i.e **2**, **3** and **4** and metal ions were investigated. Eight metal ions were selected for the binding studies; these were Zn^{2+}, Co^{2+}, Cd^{2+},Ni^{2+}, Pb^{2+}, Fe^{2+}, Cu^{2+} and Hg^{2+}. Compounds **2, 3** and **4** dimerise to accomplish the coordination to form a complex with the six bonding sites for charge transfer with the metal ions. This was confirmed with Gibbs free energy for its affinity and was found to be 24.726 $KJ.mol^{-1}$. The orbital of the metal ions split into eg and $T_2ġ$ by following the crystal field theory for binding (electron transfer to occur between the ligand and metal ions).

Molecular docking studies

The binding mode of **2** and **3** within the active site of the human MDM2 protein was analyzed. A single hydrogen bond interaction was observed for **2** and **3** and was correlated to the back bone of a polar residue Glu25 and hydrophobic residue Leu27, respectively.

Cytotoxicity studies using A549 lung cancer cells

Although the molecular docking studies did not display significant activity MTT assays were still performed for all the synthesized compounds. A549 lung cancer cells were used for these investigations. The BODIPYs with the quinoline moieties demonstrated a reduction in the rate of A549 cell proliferation when compared to the imidazole and benzimidazoles. A further comparison between imidazoles clearly showed that compounds **3** and **4** also decreased cell proliferation; compound **2** exhibited an increased rate of cell proliferation.

In conclusion, the aims and objectives of this study were achieved. However, a number of difficulties were encountered in the separation of the target compounds by column chromatography. All synthesized compounds exhibited a potential for fluorescence application and further research is required to determine this potential. The biological investigation revealed that **3, 4, 5** and **7** could be a pathway to future drug design for anti-cancer drug. Whilst **2** can be investigated as a hyper-glymercic drug.

Appendix 1: IR Spectra of 3-(4,5-Dihydro-1H-imidazol-2-yl)-1H-quinolin-2-one

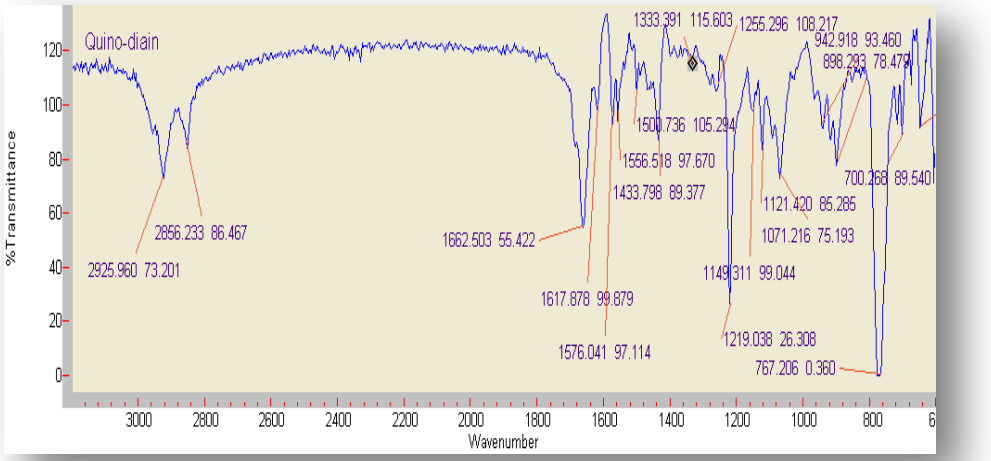

Appendix 2: H-NMR of 3-(4,5-Dihydro-1H-imidazol-2-yl)-1H-quinolin-2-one

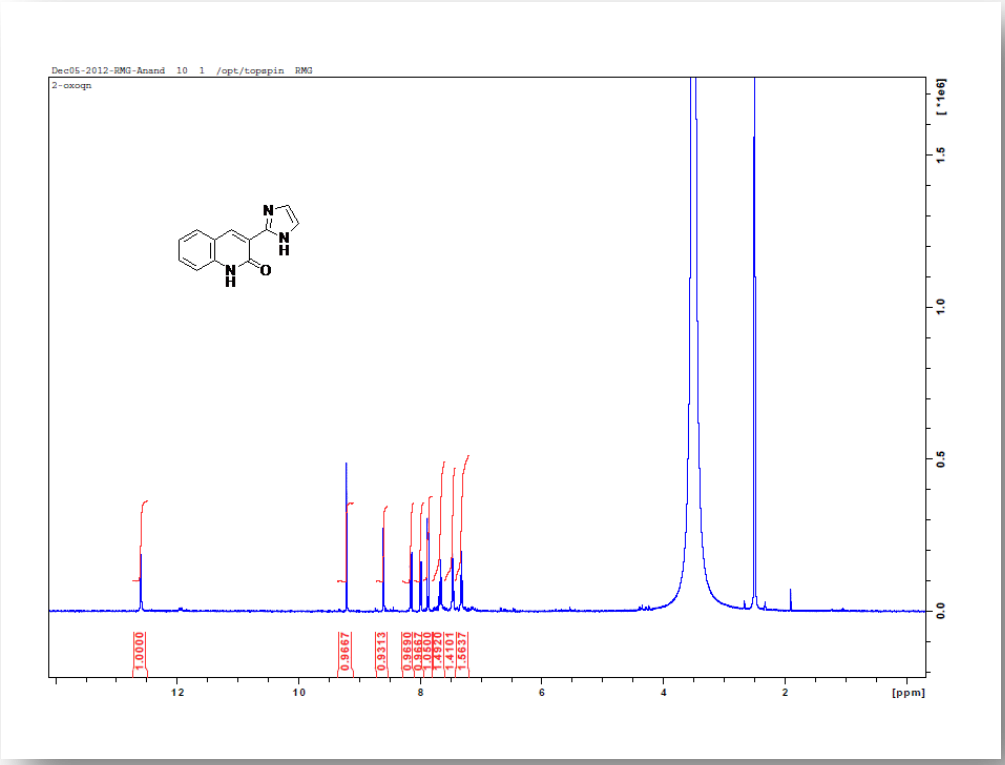

Appendix 3: Expanded Spectra of 3-(4,5-Dihydro-1H-imidazol-2-yl)-1H-quinolin-2-one

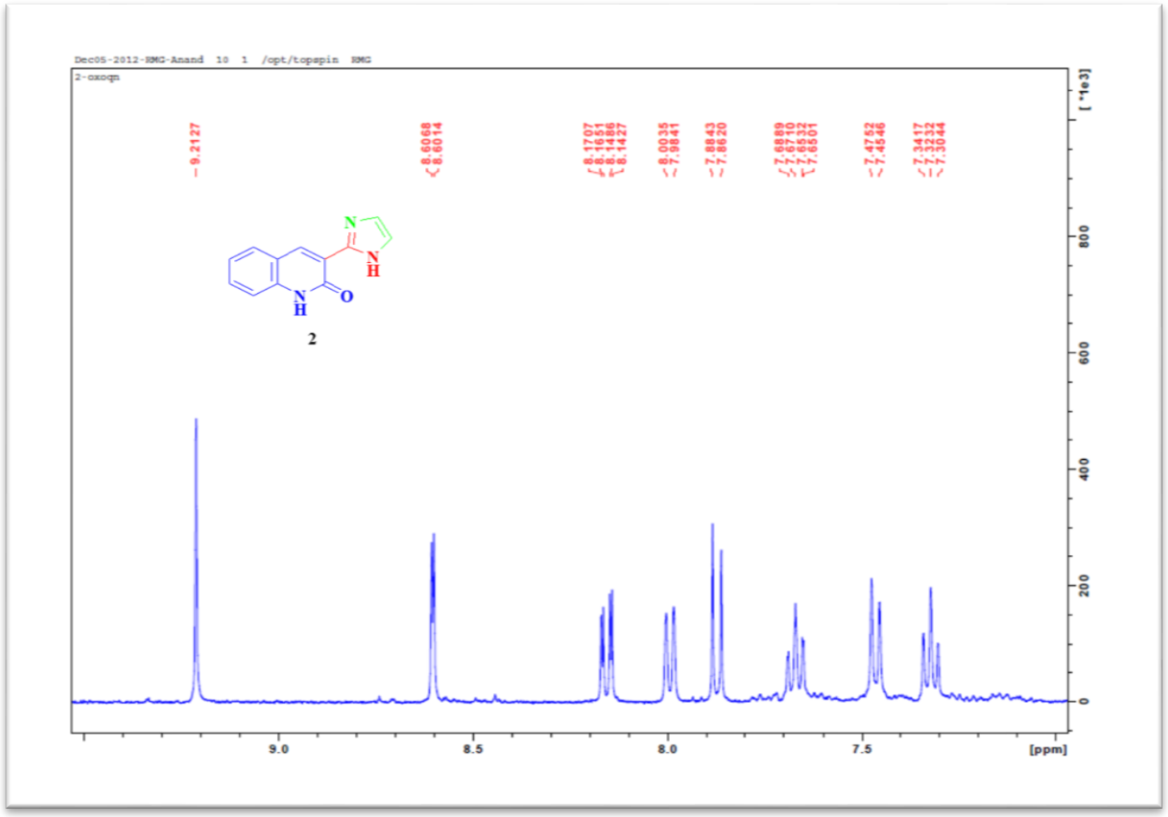

Appendix 4: C-NMR of 3-(4,5-Dihydro-1H-imidazol-2-yl)-1H-quinolin-2-one

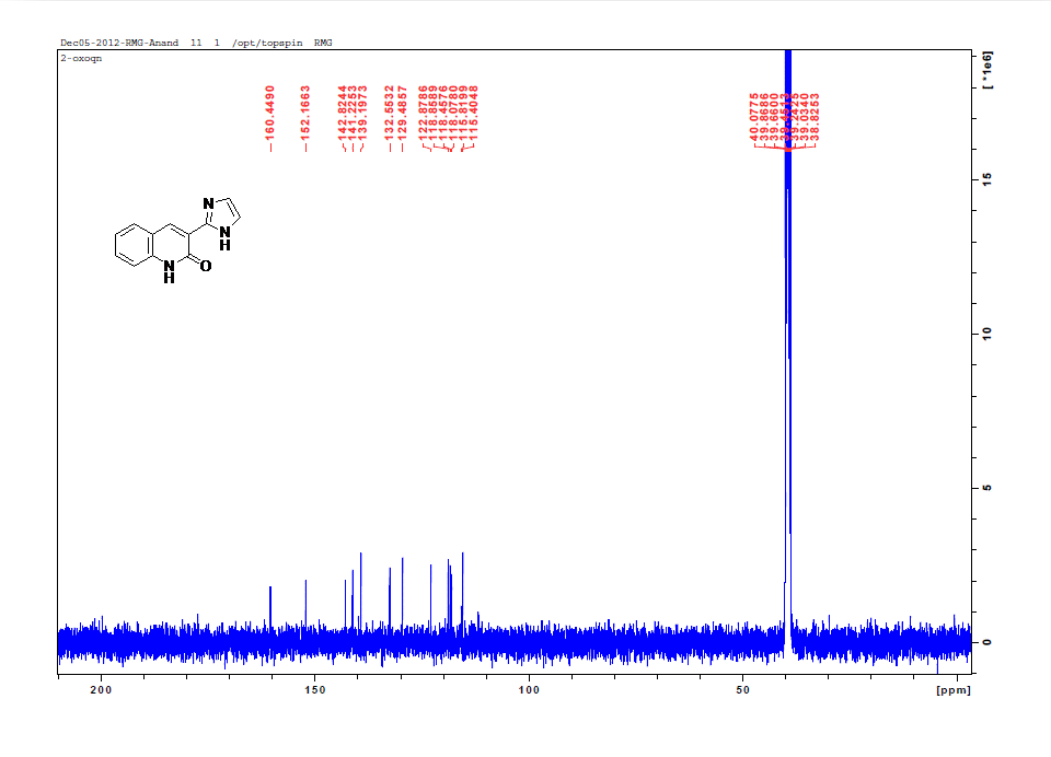

Appendix 5: Table 20: Bond Angles and Bond Lengths of 3-(4,5-Dihydro-1H-imidazol-2-yl)-1H-quinolin-2-one

Atoms	Bond Angle
C(2)-C(1)-C(6)	120
C(2)-C(1)-H(31)	119.998
C(6)-C(1)-H(31)	119.998
C(1)-C(2)-C(3)	120.001
C(1)-C(2)-H(29)	119.998
C(3)-C(2)-H(29)	119.998
C(2)-C(3)-C(4)	119.998
C(2)-C(3)-H(28)	120
C(4)-C(3)-H(28)	120
C(3)-C(4)-C(5)	120.001
C(3)-C(4)-H(32)	119.998
C(5)-C(4)-H(32)	119.998
C(4)-C(5)-C(6)	120
C(4)-C(5)-N(7)	119.998
C(6)-C(5)-N(7)	119.998
C(1)-C(6)-C(5)	120
C(1)-C(6)-C(11)	119.998
C(5)-C(6)-C(11)	119.998
C(5)-N(7)-C(9)	121.764
C(5)-N(7)-H(8)	115.417
H(8)-N(7)-C(9)	122.815
N(7)-C(9)-C(10)	120.558
N(7)-C(9)-O(12)	119.519
C(10)-C(9)-O(12)	119.921
C(9)-C(10)-C(11)	117.601
C(9)-C(10)-C(16)	119.996
C(11)-C(10)-C(16)	122.4
C(6)-C(11)-C(10)	120
C(6)-C(11)-H(30)	119.998
C(10)-C(11)-H(30)	119.998
C(16)-N(13)-C(18)	111
H(14)-N(13)-C(16)	124.497
H(14)-N(13)-C(18)	124.499
C(16)-N(15)-C(17)	104.501
C(10)-C(16)-N(13)	124.504
C(10)-C(16)-N(15)	124.497
N(13)-C(16)-N(15)	110.998

Atoms	Bond Angle
N(15)-C(17)-C(18)	116.814
N(15)-C(17)-C(21)	121.596
C(18)-C(17)-C(21)	121.587
N(13)-C(18)-C(17)	96.685
N(13)-C(18)-C(19)	133.603
C(17)-C(18)-C(19)	129.711
C(18)-C(19)-H(25)	109.996
C(18)-C(19)-H(26)	109.998
C(18)-C(19)-H(27)	109.998
H(25)-C(19)-H(26)	109
H(25)-C(19)-H(27)	109
H(26)-C(19)-H(27)	108.814
C(21)-C(20)-H(22)	120.5
C(21)-C(20)-H(23)	120.498
H(22)-C(20)-H(23)	119.001
C(17)-C(21)-C(20)	120.003
C(17)-C(21)-H(24)	119.996
C(20)-C(21)-H(24)	119.998

Atoms	Bond Lengths
C(1)-C(2)	1.42
C(1)-C(6)	1.42
C(1)-H(31)	1.1
C(2)-C(3)	1.42
C(2)-H(29)	1.1
C(3)-C(4)	1.42
C(3)-H(28)	1.1
C(4)-C(5)	1.42
C(4)-H(32)	1.1
C(5)-C(6)	1.42
C(5)-N(7)	1.345
C(6)-C(11)	1.503
N(7)-C(9)	1.397
N(7)-H(8)	1.012
C(9)-C(10)	1.517
C(9)-O(12)	1.208
C(10)-C(11)	1.337
C(10)-C(16)	1.503
C(11)-H(30)	1.1
N(13)-C(16)	1.462
N(13)-C(18)	1.462
N(13)-H(14)	1.05
N(15)-C(16)	1.26
N(15)-C(17)	1.456
C(17)-C(18)	1.414
C(17)-C(21)	1.503
C(18)-C(19)	1.497
C(19)-H(25)	1.113
C(19)-H(26)	1.113
C(19)-H(27)	1.113
C(20)-C(21)	1.337
C(20)-H(22)	1.1
C(20)-H(23)	1.1
C(21)-H(24)	1.1
C(2)-C(1)-C(6)	120
C(2)-C(1)-H(31)	119.998
C(6)-C(1)-H(31)	119.998

Atoms	Bond Lengths
C(1)-C(2)-C(3)	120.001
C(1)-C(2)-H(29)	119.998
C(3)-C(2)-H(29)	119.998
C(2)-C(3)-C(4)	119.998
C(2)-C(3)-H(28)	120
C(4)-C(3)-H(28)	120
C(3)-C(4)-C(5)	120.001
C(3)-C(4)-H(32)	119.998
C(5)-C(4)-H(32)	119.998
C(4)-C(5)-C(6)	120
C(4)-C(5)-N(7)	119.998
C(6)-C(5)-N(7)	119.998
C(1)-C(6)-C(5)	120
C(1)-C(6)-C(11)	119.998
C(5)-C(6)-C(11)	119.998
C(5)-N(7)-C(9)	121.764
C(5)-N(7)-H(8)	115.417
H(8)-N(7)-C(9)	122.815
N(7)-C(9)-C(10)	120.558
N(7)-C(9)-O(12)	119.519
C(10)-C(9)-O(12)	119.921
C(9)-C(10)-C(11)	117.601
C(9)-C(10)-C(16)	119.996
C(11)-C(10)-C(16)	122.4
C(6)-C(11)-C(10)	120
C(6)-C(11)-H(30)	119.998
C(10)-C(11)-H(30)	119.998
C(16)-N(13)-C(18)	111
H(14)-N(13)-C(16)	124.497
H(14)-N(13)-C(18)	124.499
C(16)-N(15)-C(17)	104.501
C(10)-C(16)-N(13)	124.504

Atoms	Bond Lengths
N(13)-C(18)-C(17)	96.685
N(13)-C(18)-C(19)	133.603
C(17)-C(18)-C(19)	129.711
C(18)-C(19)-H(25)	109.996
C(18)-C(19)-H(26)	109.998
C(18)-C(19)-H(27)	109.998
H(25)-C(19)-H(26)	109
H(25)-C(19)-H(27)	109
H(26)-C(19)-H(27)	108.814
C(21)-C(20)-H(22)	120.5
C(21)-C(20)-H(23)	120.498
H(22)-C(20)-H(23)	119.001
C(17)-C(21)-C(20)	120.003
C(17)-C(21)-H(24)	119.996
C(20)-C(21)-H(24)	119.998

C(10)-C(16)-N(15)	124.497
N(13)-C(16)-N(15)	110.998
N(15)-C(17)-C(18)	116.814
N(15)-C(17)-C(21)	121.596
C(18)-C(17)-C(21)	121.587

Appendix 6: IR Spectra of 3-(1H-Benzoimidazol-2-yl)-1H-quinolin-2-one

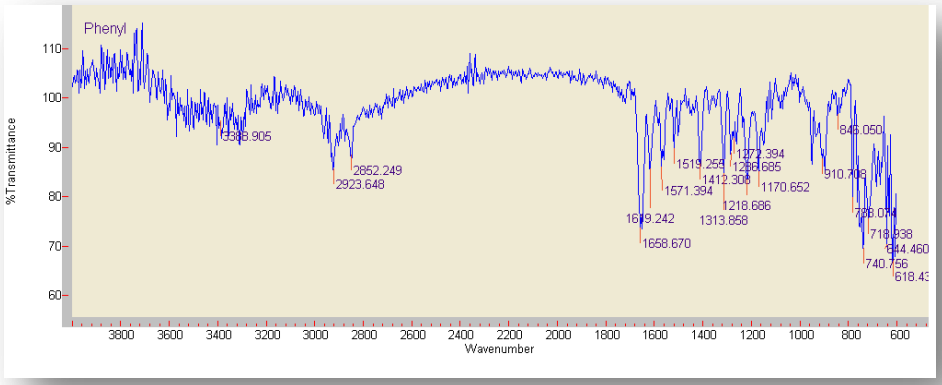

Appendix 7: H-NMR of 3-(1H-Benzoimidazol-2-yl)-1H-quinolin-2-one

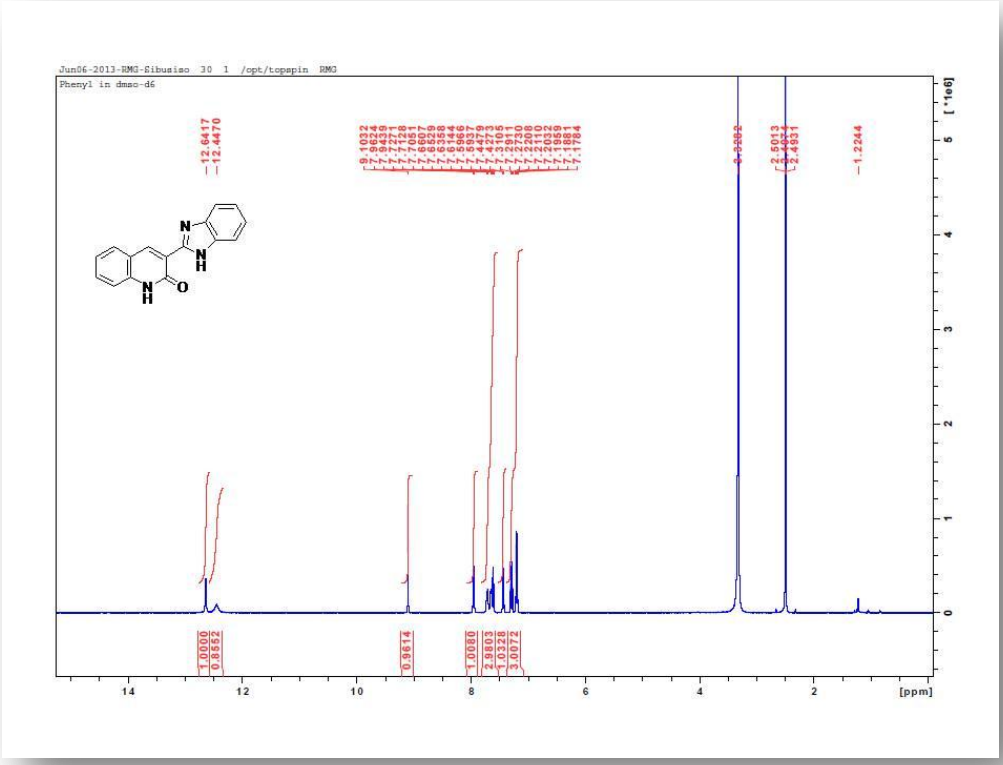

Appendix 8: Expanded Spectra of 3-(1H-Benzoimidazol-2-yl)-1H-quinolin-2-one

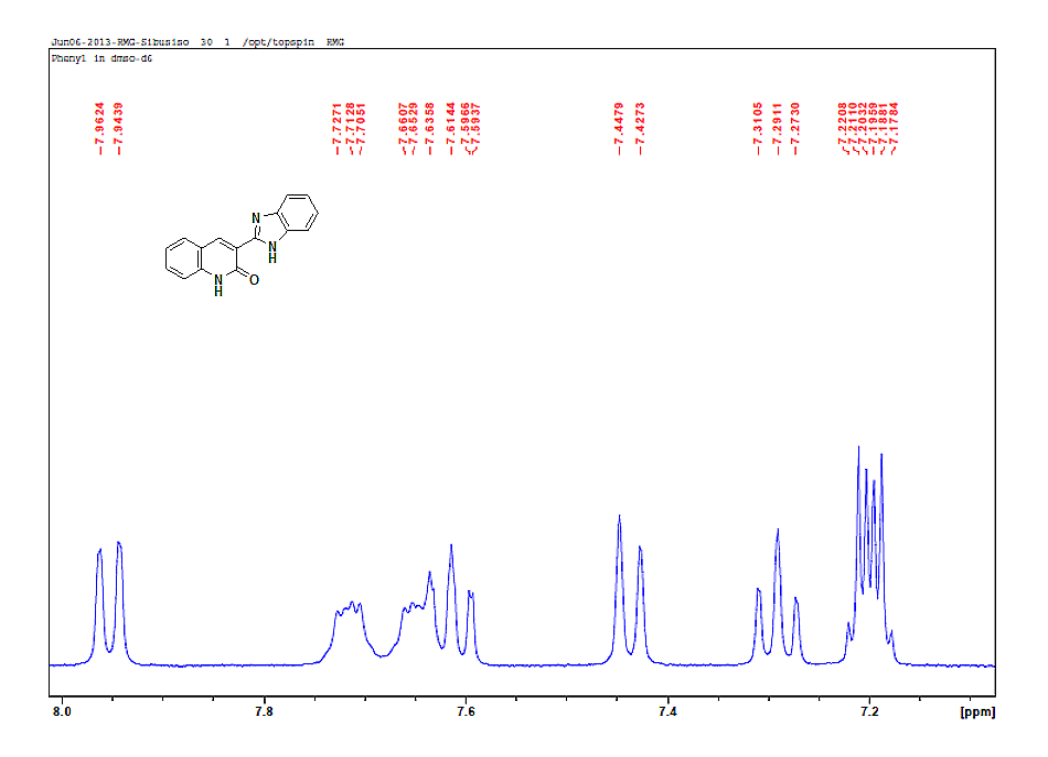

Appendix 9: C-NMR of 3-(1H-Benzoimidazol-2-yl)-1H-quinolin-2-one

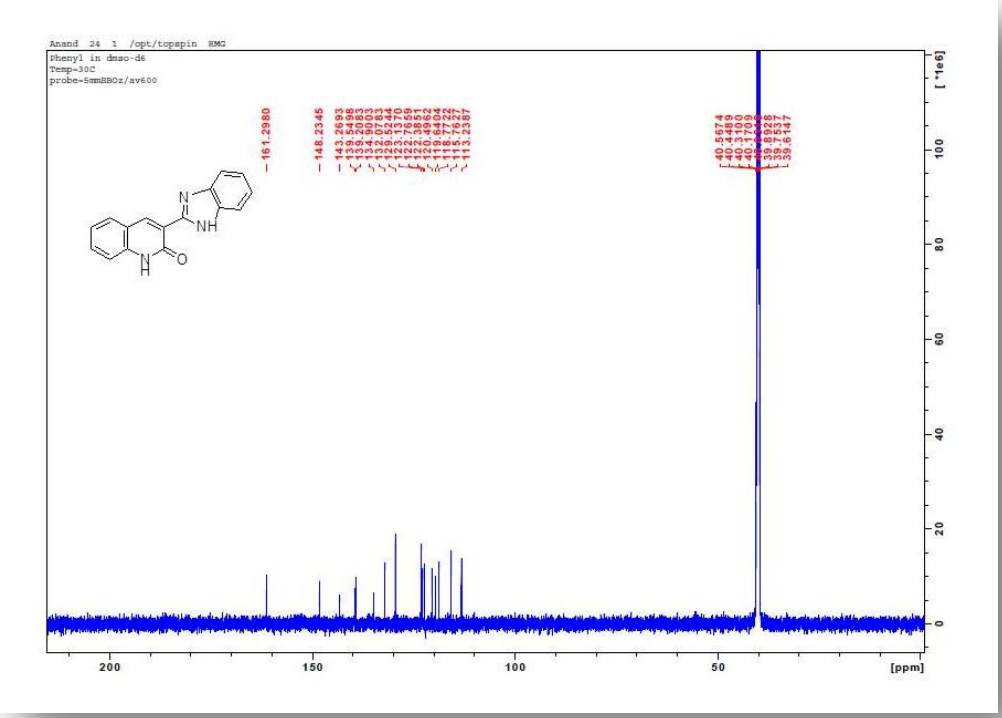

Appendix 10: Table 21: Bond Angles and Bond Lengths of 3-(1H-Benzoimidazol-2-yl)-1H-quinolin-2-one

Atoms	Bond Angle
C(2)-C(1)-C(6)	119.741
C(2)-C(1)-H(26)	120.129
C(6)-C(1)-H(26)	120.127
C(1)-C(2)-C(3)	119.942
C(1)-C(2)-H(23)	120.028
C(3)-C(2)-H(23)	120.028
C(2)-C(3)-C(4)	120.147
C(2)-C(3)-H(22)	119.923
C(4)-C(3)-H(22)	119.925
C(3)-C(4)-C(5)	119.809
C(3)-C(4)-H(27)	120.092
C(5)-C(4)-H(27)	120.094
C(4)-C(5)-C(6)	120.01
C(4)-C(5)-N(7)	120.921
C(6)-C(5)-N(7)	119.068
C(1)-C(6)-C(5)	120.344
C(1)-C(6)-C(11)	121.07
C(5)-C(6)-C(11)	118.585
C(5)-N(7)-C(9)	126.078
C(5)-N(7)-H(8)	113.261
H(8)-N(7)-C(9)	120.661
N(7)-C(9)-C(10)	115.971
N(7)-C(9)-O(12)	121.79
C(10)-C(9)-O(12)	122.219
C(9)-C(10)-C(11)	119.888
C(9)-C(10)-C(18)	119.409
C(11)-C(10)-C(18)	120.697
C(6)-C(11)-C(10)	119.982
C(6)-C(11)-H(25)	120.008
C(10)-C(11)-H(25)	120.008
C(15)-N(13)-C(18)	105.169
H(14)-N(13)-C(15)	109.47
H(14)-N(13)-C(18)	109.47
N(13)-C(15)-C(16)	102.116
N(13)-C(15)-H(19)	108.8
N(13)-C(15)-H(20)	108.799
C(16)-C(15)-H(19)	109.409
C(16)-C(15)-H(20)	109.411
H(19)-C(15)-H(20)	117.234
C(15)-C(16)-N(17)	118.365
C(15)-C(16)-H(21)	121.664
N(17)-C(16)-H(21)	119.967
C(16)-N(17)-C(18)	103.557
C(10)-C(18)-N(13)	111.369
C(10)-C(18)-N(17)	110.596
C(10)-C(18)-H(24)	109.39
N(13)-C(18)-N(17)	110.432
N(13)-C(18)-H(24)	107.423
N(17)-C(18)-H(24)	107.501

Atoms	Bond Lengths
C(1)-C(2)	1.421
C(1)-C(6)	1.419
C(1)-H(26)	1.1
C(2)-C(3)	1.42
C(2)-H(23)	1.099
C(3)-C(4)	1.421
C(3)-H(22)	1.1
C(4)-C(5)	1.42
C(4)-H(27)	1.1
C(5)-C(6)	1.416
C(5)-N(7)	1.344
C(6)-C(11)	1.5
N(7)-C(9)	1.372
N(7)-H(8)	1.012
C(9)-C(10)	1.521
C(9)-O(12)	1.208
C(10)-C(11)	1.338
C(10)-C(18)	1.497
C(11)-H(25)	1.1
N(13)-C(15)	1.452
N(13)-C(18)	1.46
N(13)-H(14)	1.02
C(15)-C(16)	1.489
C(15)-H(19)	1.113
C(15)-H(20)	1.113
C(16)-N(17)	1.256
C(16)-H(21)	1.1
N(17)-C(18)	1.476
C(18)-H(24)	1.113
C(2)-C(1)-C(6)	119.741
C(2)-C(1)-H(26)	120.129
C(6)-C(1)-H(26)	120.127
C(1)-C(2)-C(3)	119.942
C(1)-C(2)-H(23)	120.028
C(3)-C(2)-H(23)	120.028
C(2)-C(3)-C(4)	120.147
C(2)-C(3)-H(22)	119.923

Atoms	Bond Lengths
C(4)-C(3)-H(22)	119.925
C(3)-C(4)-C(5)	119.809
C(3)-C(4)-H(27)	120.092
C(5)-C(4)-H(27)	120.094
C(4)-C(5)-C(6)	120.01
C(4)-C(5)-N(7)	120.921
C(6)-C(5)-N(7)	119.068
C(1)-C(6)-C(5)	120.344
C(1)-C(6)-C(11)	121.07
C(5)-C(6)-C(11)	118.585
C(5)-N(7)-C(9)	126.078
C(5)-N(7)-H(8)	113.261
H(8)-N(7)-C(9)	120.661
N(7)-C(9)-C(10)	115.971
N(7)-C(9)-O(12)	121.79
C(10)-C(9)-O(12)	122.219
C(9)-C(10)-C(11)	119.888
C(9)-C(10)-C(18)	119.409
C(11)-C(10)-C(18)	120.697
C(6)-C(11)-C(10)	119.982
C(6)-C(11)-H(25)	120.008
C(10)-C(11)-H(25)	120.008
C(15)-N(13)-C(18)	105.169
H(14)-N(13)-C(15)	109.47
H(14)-N(13)-C(18)	109.47
N(13)-C(15)-C(16)	102.116
N(13)-C(15)-H(19)	108.8
N(13)-C(15)-H(20)	108.799
C(16)-C(15)-H(19)	109.409
C(16)-C(15)-H(20)	109.411
H(19)-C(15)-H(20)	117.234

Atoms	Bond Lengths
C(15)-C(16)-N(17)	118.365
C(15)-C(16)-H(21)	121.664
N(17)-C(16)-H(21)	119.967
C(16)-N(17)-C(18)	103.557
C(10)-C(18)-N(13)	111.369
C(10)-C(18)-N(17)	110.596
C(10)-C(18)-H(24)	109.39
N(13)-C(18)-N(17)	110.432
N(13)-C(18)-H(24)	107.423
N(17)-C(18)-H(24)	107.501

Appendix 11: IR spectra of 3-(6-Nitro-1H-Benzoimidazol-2-yl)-1H-quinolin-2-one

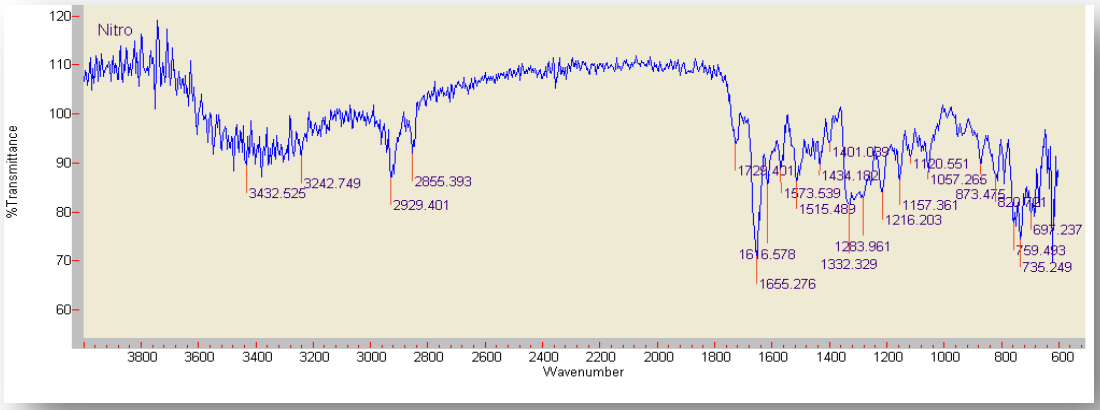

Appendix 12: H-NMR of the 3-(6-Nitro-1H-Benzoimidazol-2-yl)-1H-quinolin-2-one

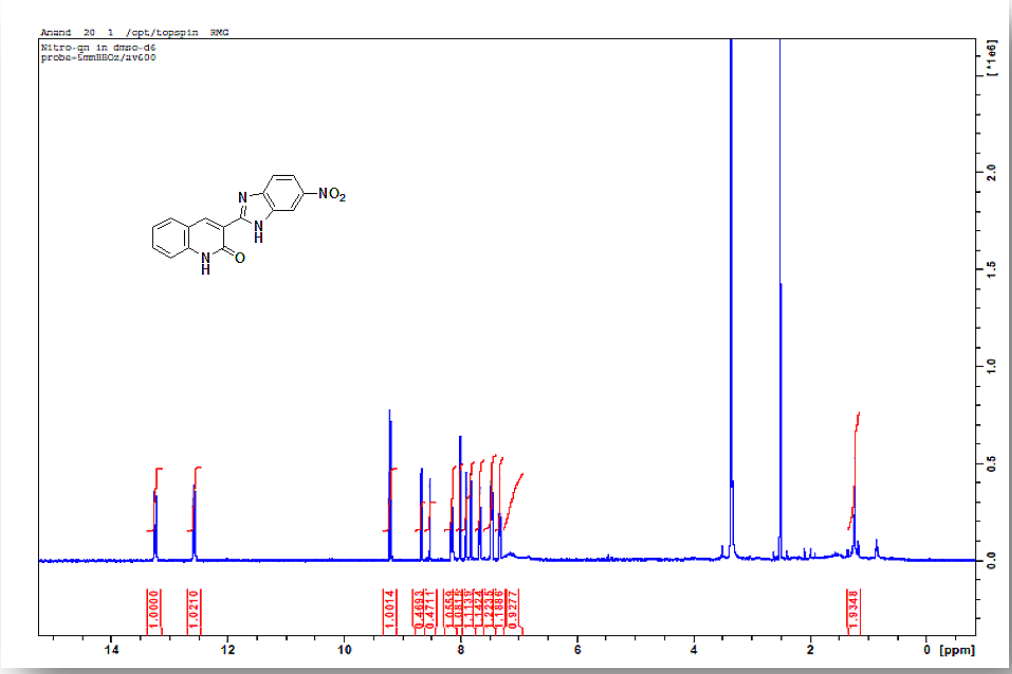

Appendix 13: Expanded Spectra of Expanded Spectra of 3-(6-Nitro-1H-Benzoimidazol-2-yl)-1H-quinolin-2-one

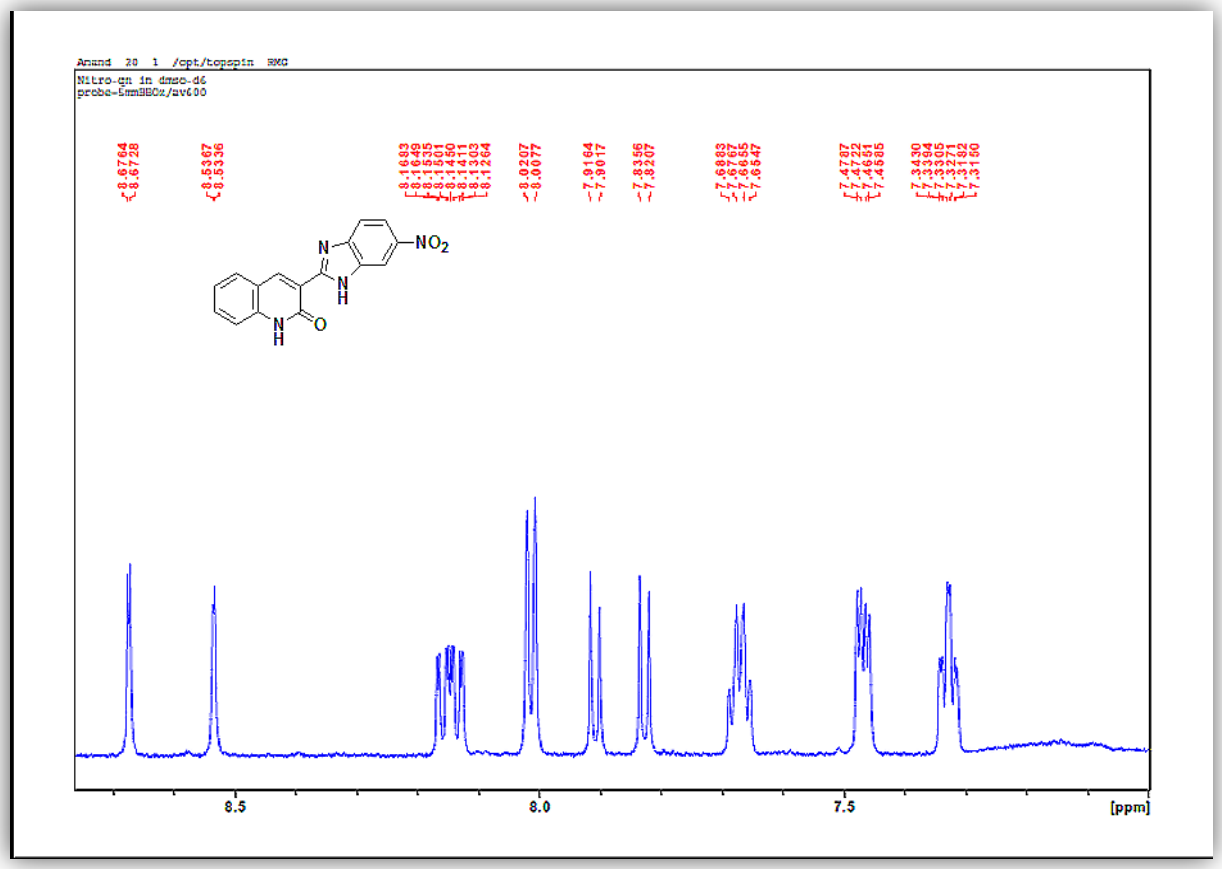

Appendix 14: Expanded Spectra of 3-(6-Nitro-1H-Benzoimidazol-2-yl)-1H-quinolin-2-one - Part 2

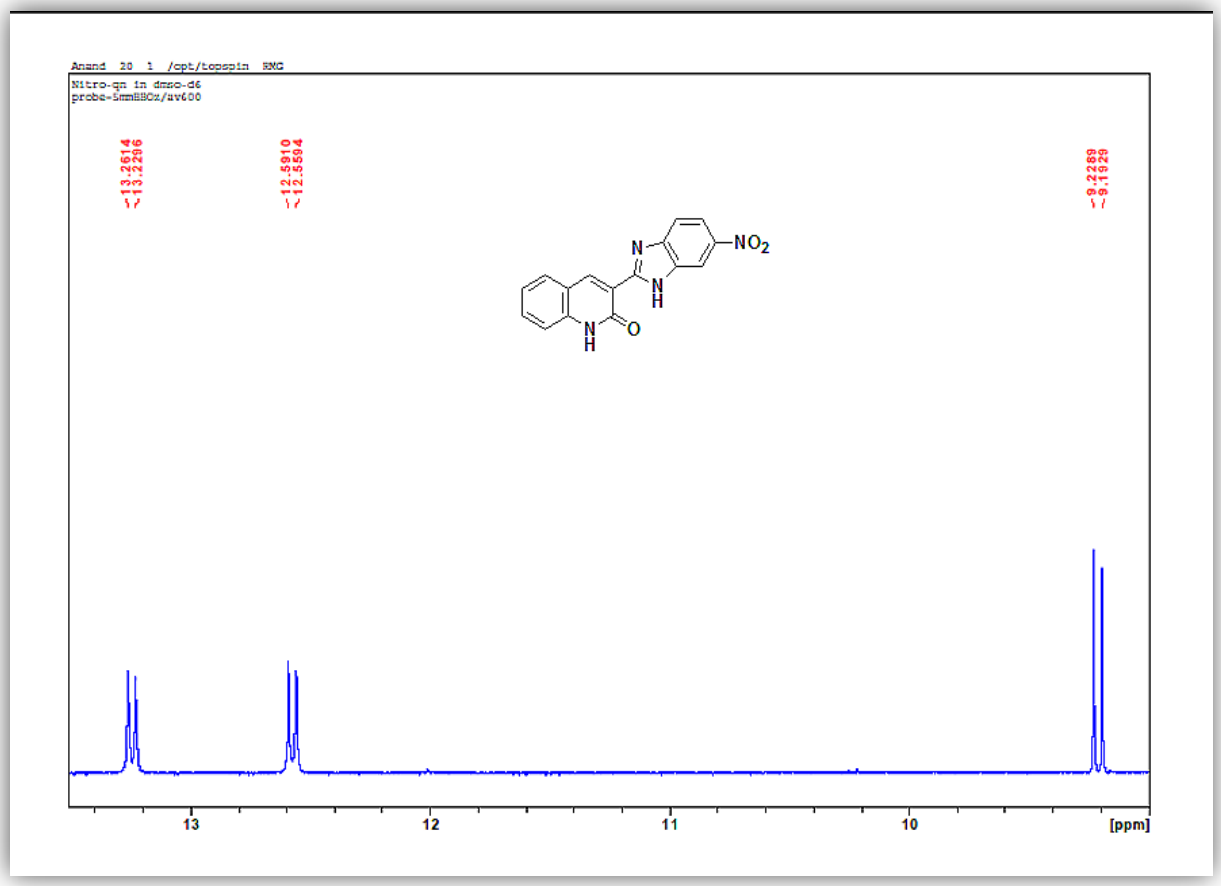

Appendix 15: ^{13}C-NMR of the 3-(6-Nitro-1H-Benzoimidazol-2-yl)-1H-quinolin-2-one

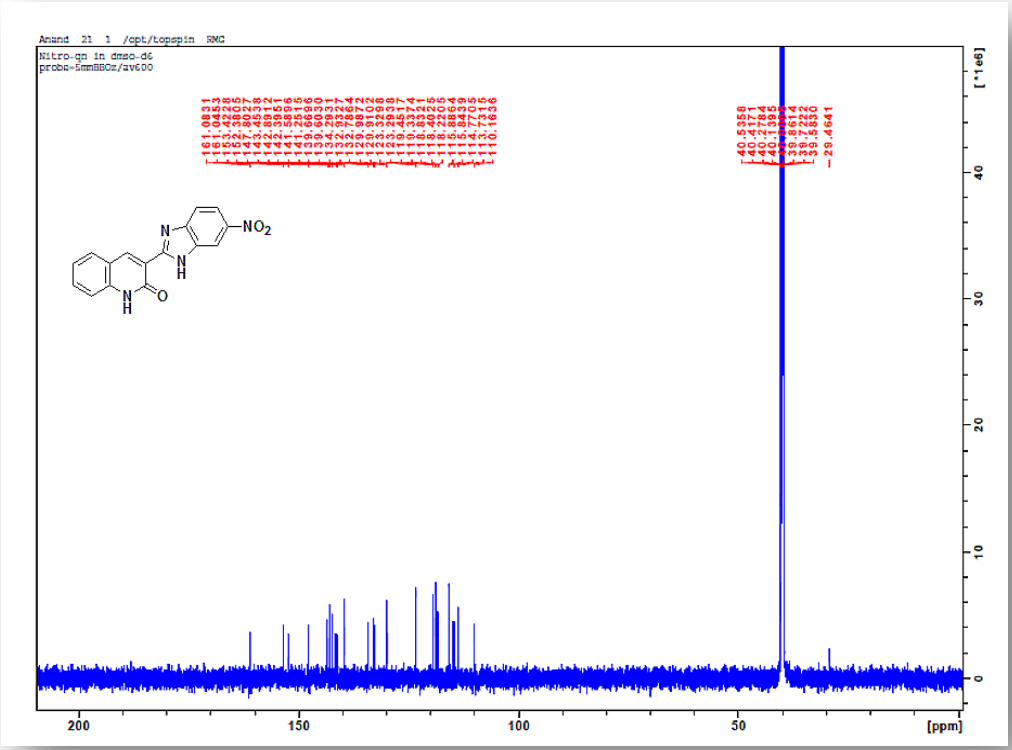

Appendix 16: Table 22: Bond Angles and Bond Lengths of 3-(6-Nitro-1H-Benzoimidazol-2-yl)-1H-quinolin-2-one

Atoms	Bond Length
C(1)-C(2)	1.42
C(1)-C(6)	1.42
C(1)-H(32)	1.1
C(2)-C(3)	1.42
C(2)-H(28)	1.1
C(3)-C(4)	1.42
C(3)-H(27)	1.1
C(4)-C(5)	1.42
C(4)-H(33)	1.1
C(5)-C(6)	1.42
C(5)-N(7)	1.345
C(6)-C(11)	1.42
N(7)-C(9)	1.36
N(7)-H(8)	1.012
C(9)-C(10)	1.517
C(9)-O(12)	1.208
C(10)-C(11)	1.42
C(10)-C(16)	1.42
C(11)-H(31)	1.1
N(13)-C(16)	1.462
N(13)-C(18)	1.318
N(13)-H(14)	1.05
N(15)-C(16)	1.358
N(15)-C(17)	1.358
C(17)-C(18)	1.42
C(17)-C(22)	1.42
C(18)-C(19)	1.42
C(19)-C(20)	1.42
C(19)-H(29)	1.1
C(20)-C(21)	1.42
C(20)-H(26)	1.1
C(21)-C(22)	1.42
C(21)-N(23)	1.496
C(22)-H(30)	1.1
N(23)-O(24)	1.143
N(23)-O(25)	1.316

Atoms	Atom Angles
C(2)-C(1)-C(6)	120
C(2)-C(1)-H(32)	119.998
C(6)-C(1)-H(32)	119.998
C(1)-C(2)-C(3)	120.001
C(1)-C(2)-H(28)	119.998
C(3)-C(2)-H(28)	119.998
C(2)-C(3)-C(4)	119.998
C(2)-C(3)-H(27)	120
C(4)-C(3)-H(27)	120
C(3)-C(4)-C(5)	120.001
C(3)-C(4)-H(33)	119.998
C(5)-C(4)-H(33)	119.998
C(4)-C(5)-C(6)	120
C(4)-C(5)-N(7)	119.998
C(6)-C(5)-N(7)	119.998
C(1)-C(6)-C(5)	120
C(1)-C(6)-C(11)	119.998
C(5)-C(6)-C(11)	119.998
C(5)-N(7)-C(9)	124.843
C(5)-N(7)-H(8)	113.878
H(8)-N(7)-C(9)	121.278
N(7)-C(9)-C(10)	117.477
N(7)-C(9)-O(12)	121.061
C(10)-C(9)-O(12)	121.462
C(9)-C(10)-C(11)	117.597
C(9)-C(10)-C(16)	119.998
C(11)-C(10)-C(16)	122.4
C(6)-C(11)-C(10)	120
C(6)-C(11)-H(31)	119.998
C(10)-C(11)-H(31)	119.998
C(16)-N(13)-C(18)	104.996
H(14)-N(13)-C(16)	127.501
H(14)-N(13)-C(18)	127.501
C(16)-N(15)-C(17)	104.501
C(10)-C(16)-N(13)	124.497
C(10)-C(16)-N(15)	124.5
N(13)-C(16)-N(15)	110.998
N(15)-C(17)-C(18)	111

Atoms	Atom Angles
N(15)-C(17)-C(22)	128.998
C(18)-C(17)-C(22)	120
N(13)-C(18)-C(17)	108.498
N(13)-C(18)-C(19)	131.5
C(17)-C(18)-C(19)	119.998
C(18)-C(19)-C(20)	119.998
C(18)-C(19)-H(29)	120
C(20)-C(19)-H(29)	120
C(19)-C(20)-C(21)	119.988
C(19)-C(20)-H(26)	120.005
C(21)-C(20)-H(26)	120.003
C(20)-C(21)-C(22)	119.988
C(20)-C(21)-N(23)	120.007
C(22)-C(21)-N(23)	120.005
C(17)-C(22)-C(21)	119.998
C(17)-C(22)-H(30)	119.998
C(21)-C(22)-H(30)	119.998
C(21)-N(23)-O(24)	119.998
C(21)-N(23)-O(25)	119.998
O(24)-N(23)-O(25)	120

Appendix 17: IR Spectra of of 4,4-difluoro-4-bora-3a,4a-diaza-s-indacene-2-chloro-quinoline

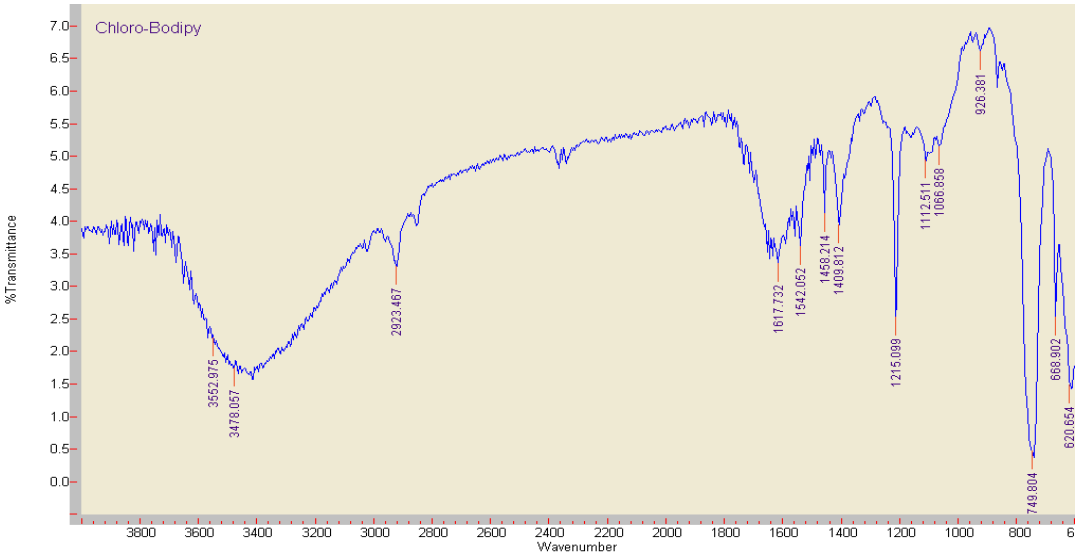

Appendix 18: H-NMR of 4,4-difluoro-4-bora-3a,4a-diaza-s-indacene-2-chloro-quinoline

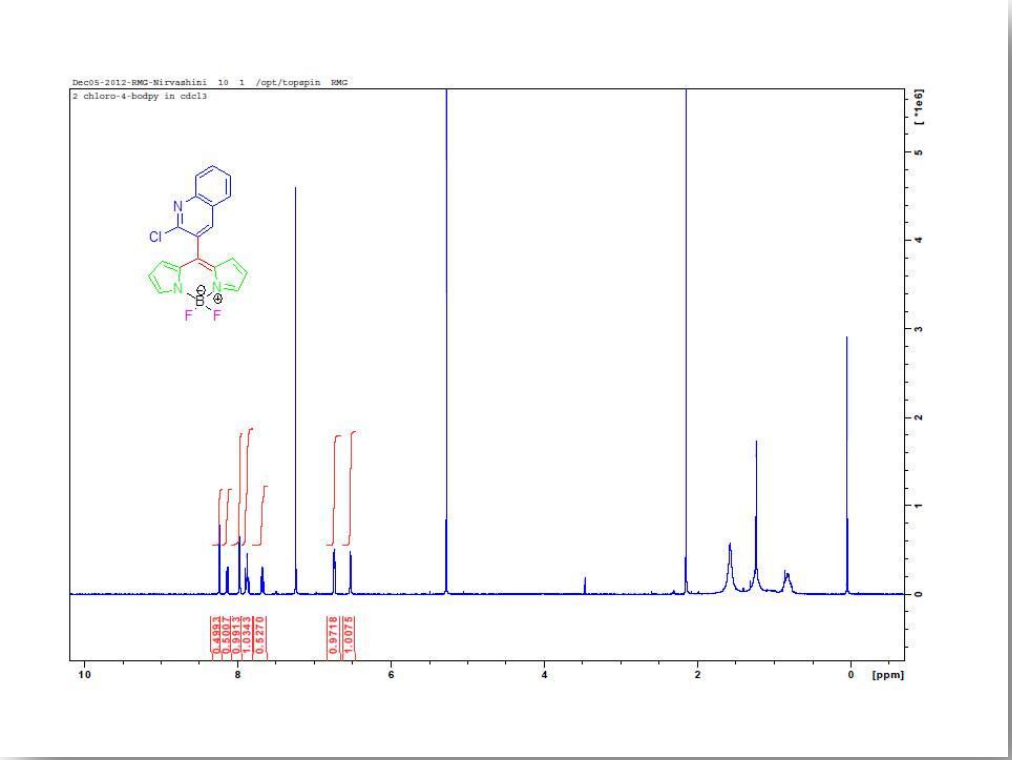

Appendix 19: Expanded H-NMR of 4,4-difluoro-4-bora-3a,4a-diaza-s-indacene-2-chloro-quinoline

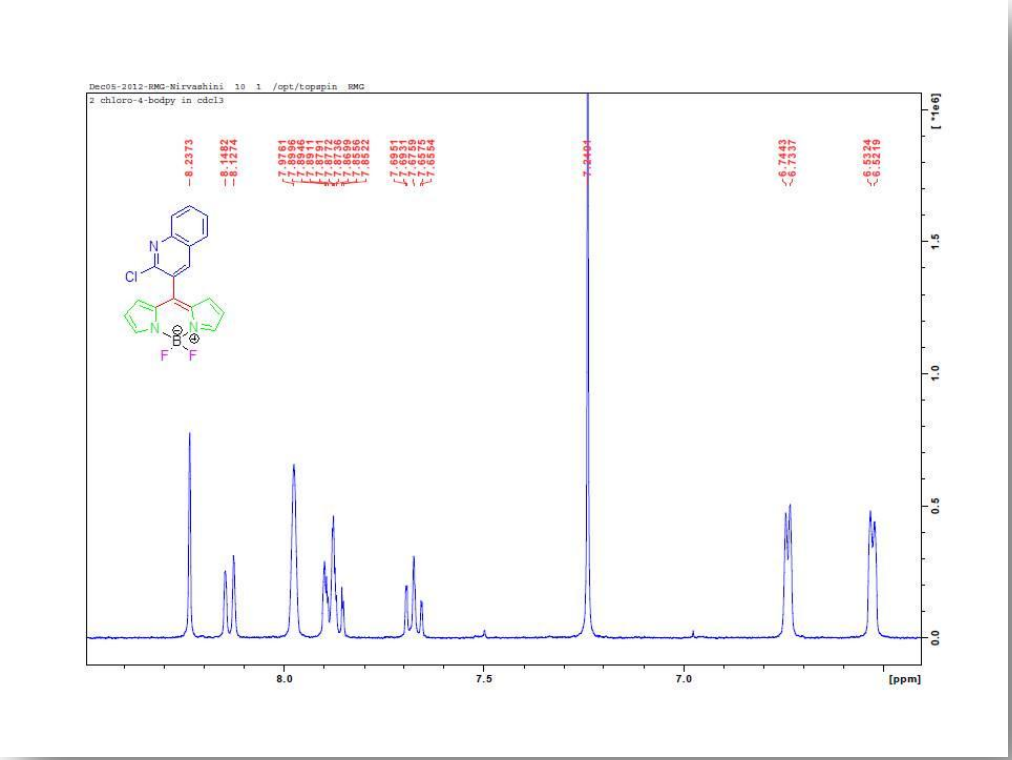

Appendix 20: C-NMR of 4,4-difluoro-4-bora-3a,4a-diaza-s-indacene-2-chloro-quinoline

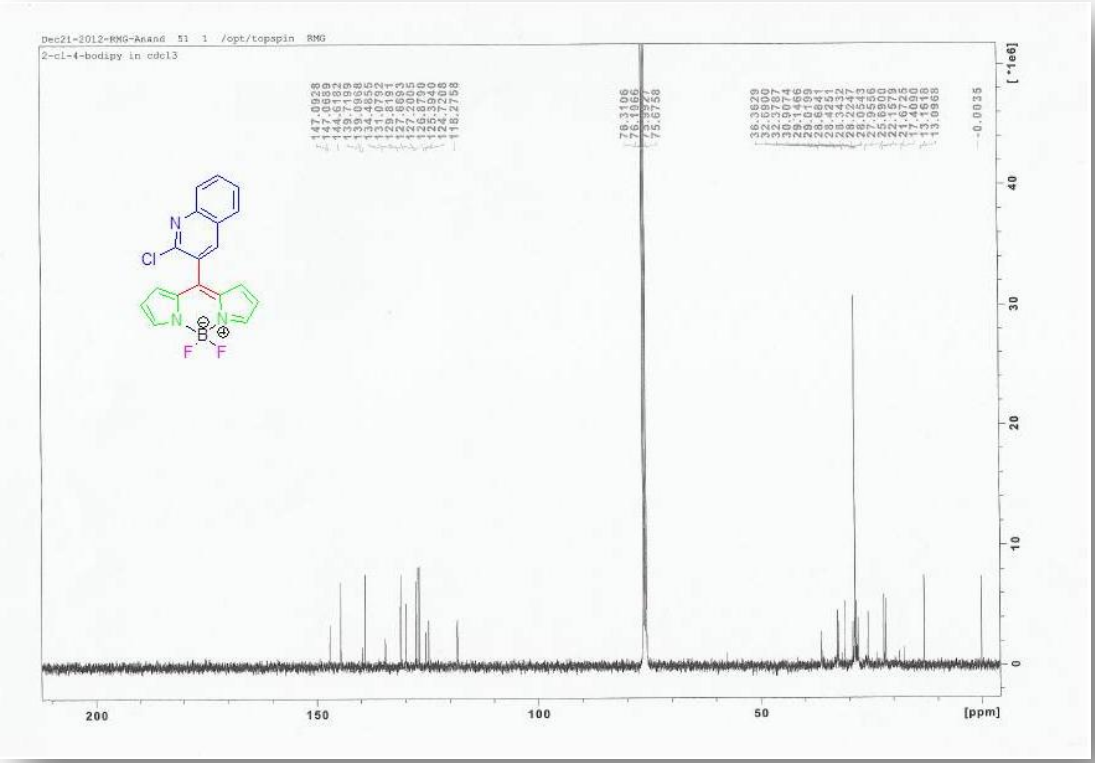

Appendix 21: F-NMR of 4,4-difluoro-4-bora-3a,4a-diaza-s-indacene-2-chloro-quinoline

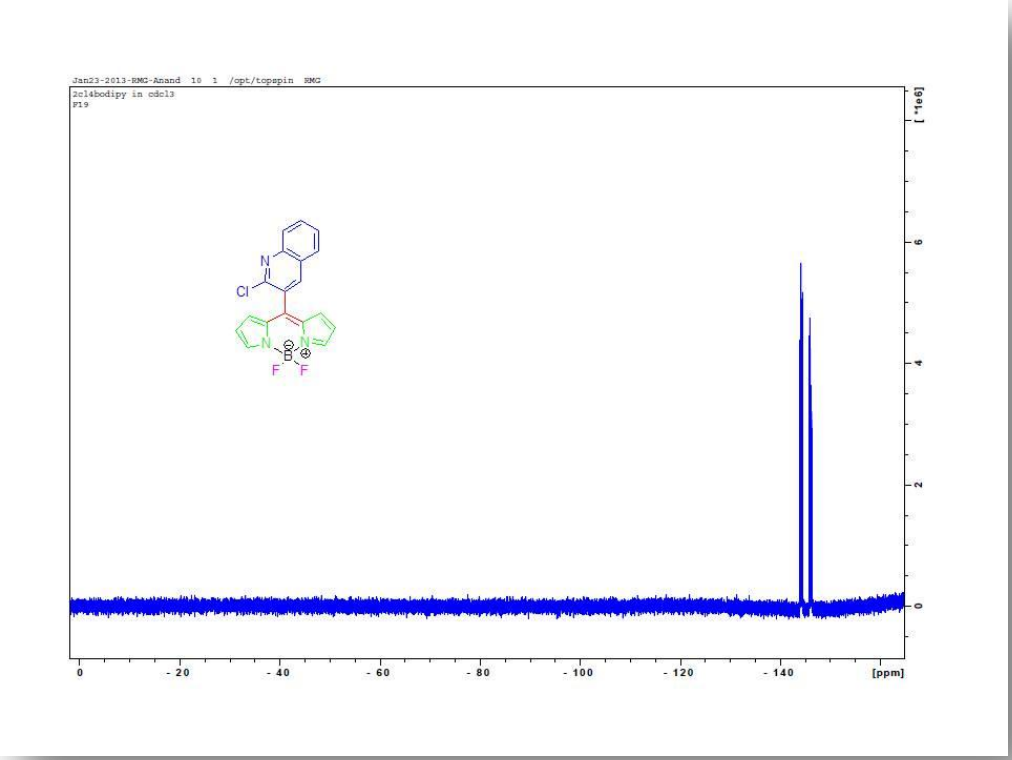

Appendix 22: Table 23: Bond Angles and Bond Lengths for 4,4-difluoro-4-bora-3a,4a-diaza-s-indacene-2-chloro-quinoline (7)

Atom	Bond Angle
C(2)-C(1)-N(5)	111
C(2)-C(1)-C(11)	119.998
N(5)-C(1)-C(11)	120
C(1)-C(2)-C(3)	111
C(1)-C(2)-H(36)	124.497
C(3)-C(2)-H(36)	124.499
C(2)-C(3)-C(4)	104.597
C(2)-C(3)-H(34)	127.697
C(4)-C(3)-H(34)	127.699
C(3)-C(4)-N(5)	102.401
C(3)-C(4)-H(33)	132.047
N(5)-C(4)-H(33)	125.546
C(1)-N(5)-C(4)	111
C(1)-N(5)-B(23)	116.943
C(4)-N(5)-B(23)	117.267
C(7)-C(6)-N(10)	104.436
C(7)-C(6)-H(32)	129.279
N(10)-C(6)-H(32)	126.28
C(6)-C(7)-C(8)	102.25
C(6)-C(7)-H(31)	128.874
C(8)-C(7)-H(31)	128.872
C(7)-C(8)-C(9)	111
C(7)-C(8)-H(35)	124.497
C(9)-C(8)-H(35)	124.497
C(8)-C(9)-N(10)	111
C(8)-C(9)-C(11)	128.998
N(10)-C(9)-C(11)	119.998
C(6)-N(10)-C(9)	110.998
C(6)-N(10)-B(23)	128.998
C(9)-N(10)-B(23)	120.003
C(1)-C(11)-C(9)	120
C(1)-C(11)-C(12)	119.998
C(9)-C(11)-C(12)	119.998
C(11)-C(12)-C(20)	119.998
C(11)-C(12)-C(21)	119.998
C(20)-C(12)-C(21)	120
C(14)-C(13)-C(18)	119.998
C(14)-C(13)-H(29)	120

Atom	Bond Angle
C(18)-C(13)-H(29)	120
C(13)-C(14)-C(15)	120.003
C(13)-C(14)-H(27)	119.998
C(15)-C(14)-H(27)	119.998
C(14)-C(15)-C(16)	119.998
C(14)-C(15)-H(26)	120.001
C(16)-C(15)-H(26)	120
C(15)-C(16)-C(17)	120.003
C(15)-C(16)-H(28)	119.998
C(17)-C(16)-H(28)	119.998
C(16)-C(17)-C(18)	120
C(16)-C(17)-N(19)	119.998
C(18)-C(17)-N(19)	120
C(13)-C(18)-C(17)	119.998
C(13)-C(18)-C(21)	119.998
C(17)-C(18)-C(21)	120
C(17)-N(19)-C(20)	122.119
C(12)-C(20)-N(19)	117.882
C(12)-C(20)-Cl(22)	120.458
N(19)-C(20)-Cl(22)	121.656
C(12)-C(21)-C(18)	120
C(12)-C(21)-H(30)	119.998
C(18)-C(21)-H(30)	119.998
N(5)-B(23)-N(10)	121.114
N(5)-B(23)-F(24)	109.479
N(5)-B(23)-F(25)	109.468
N(10)-B(23)-F(24)	109.482
N(10)-B(23)-F(25)	109.453
F(24)-B(23)-F(25)	94.611

Atoms	Bond Length
C(1)-C(2)	1.337
C(1)-N(5)	1.462
C(1)-C(11)	1.503
C(2)-C(3)	1.503
C(2)-H(36)	1.1
C(3)-C(4)	1.615
C(3)-H(34)	1.1
C(4)-N(5)	1.462
C(4)-H(33)	1.1
N(5)-B(23)	1.413
C(6)-C(7)	1.671
C(6)-N(10)	1.398
C(6)-H(32)	1.1
C(7)-C(8)	1.42
C(7)-H(31)	1.1
C(8)-C(9)	1.42
C(8)-H(35)	1.1
C(9)-N(10)	1.398
C(9)-C(11)	1.42
N(10)-B(23)	1.496
C(11)-C(12)	1.42
C(12)-C(20)	1.42
C(12)-C(21)	1.42
C(13)-C(14)	1.42
C(13)-C(18)	1.42
C(13)-H(29)	1.1
C(14)-C(15)	1.42
C(14)-H(27)	1.1
C(15)-C(16)	1.42
C(15)-H(26)	1.1
C(16)-C(17)	1.42
C(16)-H(28)	1.1
C(17)-C(18)	1.42
C(17)-N(19)	1.358
C(18)-C(21)	1.42
N(19)-C(20)	1.452
C(20)-Cl(22)	1.719
C(21)-H(30)	1.1
B(23)-F(24)	1.54
B(23)-F(25)	1.54
C(2)-C(1)-N(5)	111
C(2)-C(1)-C(11)	119.998

Atoms	Bond Length
N(5)-C(1)-C(11)	120
C(1)-C(2)-C(3)	111
C(1)-C(2)-H(36)	124.497
C(3)-C(2)-H(36)	124.499
C(2)-C(3)-C(4)	104.597
C(2)-C(3)-H(34)	127.697
C(4)-C(3)-H(34)	127.699
C(3)-C(4)-N(5)	102.401
C(3)-C(4)-H(33)	132.047
N(5)-C(4)-H(33)	125.546
C(1)-N(5)-C(4)	111
C(1)-N(5)-B(23)	116.943
C(4)-N(5)-B(23)	117.267
C(7)-C(6)-N(10)	104.436
C(7)-C(6)-H(32)	129.279
N(10)-C(6)-H(32)	126.28
C(6)-C(7)-C(8)	102.25
C(6)-C(7)-H(31)	128.874
C(8)-C(7)-H(31)	128.872
C(7)-C(8)-C(9)	111
C(7)-C(8)-H(35)	124.497
C(9)-C(8)-H(35)	124.497
C(8)-C(9)-N(10)	111
C(8)-C(9)-C(11)	128.998
N(10)-C(9)-C(11)	119.998
C(6)-N(10)-C(9)	110.998
C(6)-N(10)-B(23)	128.998
C(9)-N(10)-B(23)	120.003
C(1)-C(11)-C(9)	120
C(1)-C(11)-C(12)	119.998
C(9)-C(11)-C(12)	119.998
C(11)-C(12)-C(20)	119.998
C(11)-C(12)-C(21)	119.998
C(20)-C(12)-C(21)	120
C(14)-C(13)-C(18)	119.998
C(14)-C(13)-H(29)	120
C(18)-C(13)-H(29)	120

Atoms	Bond Length
C(16)-C(15)-H(26)	120
C(15)-C(16)-C(17)	120.003
C(15)-C(16)-H(28)	119.998
C(17)-C(16)-H(28)	119.998
C(16)-C(17)-C(18)	120
C(16)-C(17)-N(19)	119.998
C(18)-C(17)-N(19)	120
C(13)-C(18)-C(17)	119.998
C(13)-C(18)-C(21)	119.998
C(17)-C(18)-C(21)	120
C(17)-N(19)-C(20)	122.119
C(12)-C(20)-N(19)	117.882
C(12)-C(20)-Cl(22)	120.458
N(19)-C(20)-Cl(22)	121.656
C(12)-C(21)-C(18)	120
C(12)-C(21)-H(30)	119.998
C(18)-C(21)-H(30)	119.998
N(5)-B(23)-N(10)	121.114
N(5)-B(23)-F(24)	109.479
N(5)-B(23)-F(25)	109.468
N(10)-B(23)-F(24)	109.482
N(10)-B(23)-F(25)	109.453
F(24)-B(23)-F(25)	94.611

C(13)-C(14)-C(15)	120.003
C(13)-C(14)-H(27)	119.998
C(15)-C(14)-H(27)	119.998
C(14)-C(15)-C(16)	119.998
C(14)-C(15)-H(26)	120.001

Appendix 23: IR Spectra of 4,4-difluoro-4-bora-3a,4a-diaza-s-indacene-2-oxo-quinoline

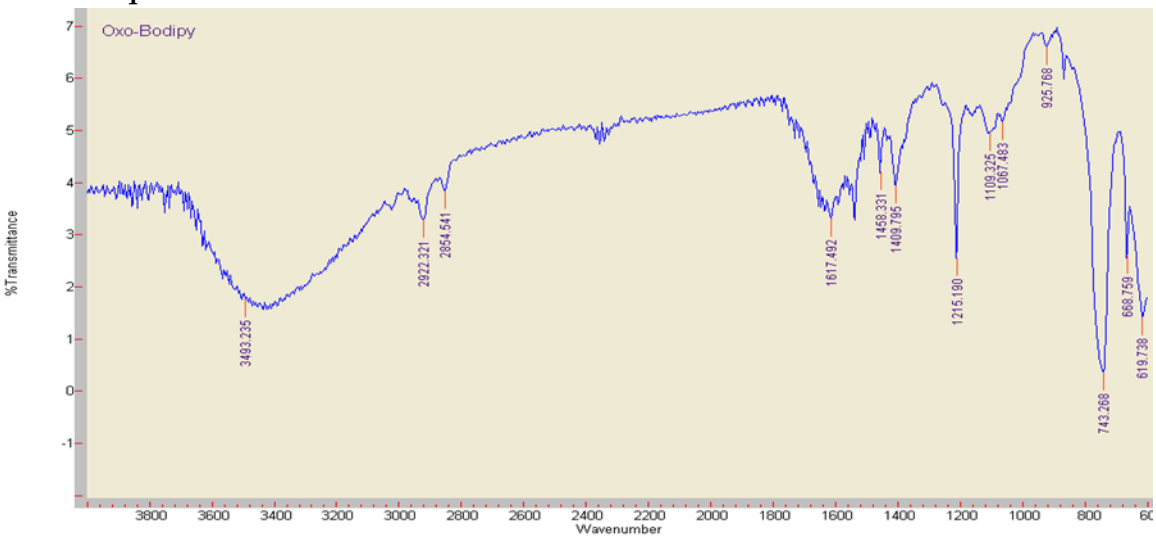

Appendix 24: H-NMR of 4,4-difluoro-4-bora-3a,4a-diaza-s-indacene-2-oxo-quinoline

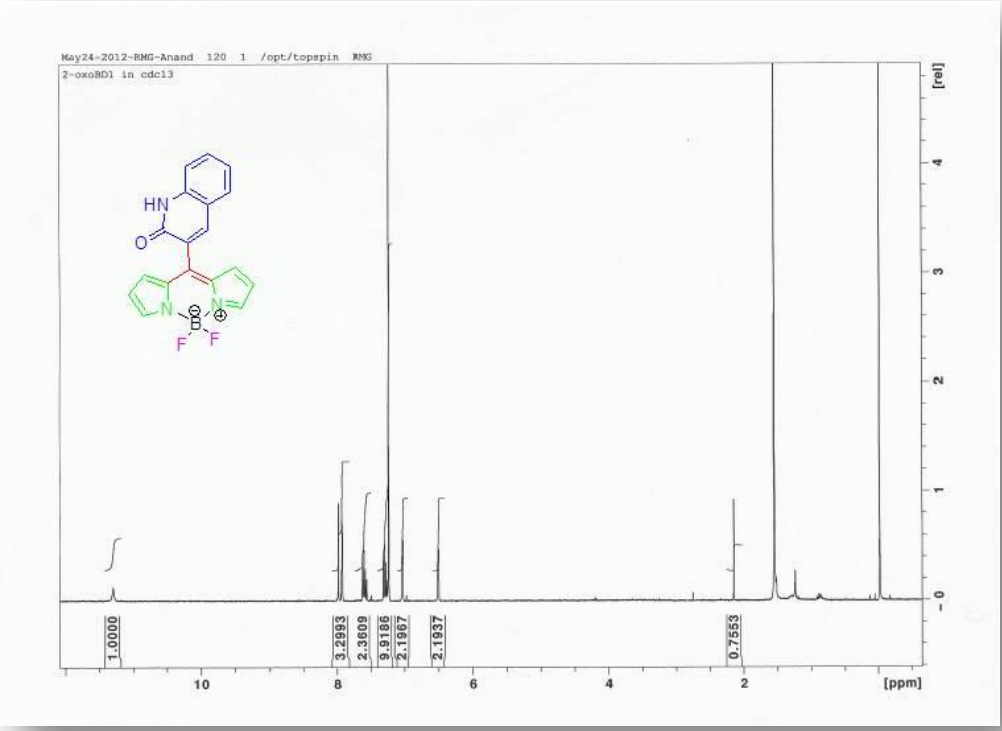

Appendix 25: Expanded H-NMR of 4,4-difluoro-4-bora-3a,4a-diaza-s-indacene-2-oxo-quinoline

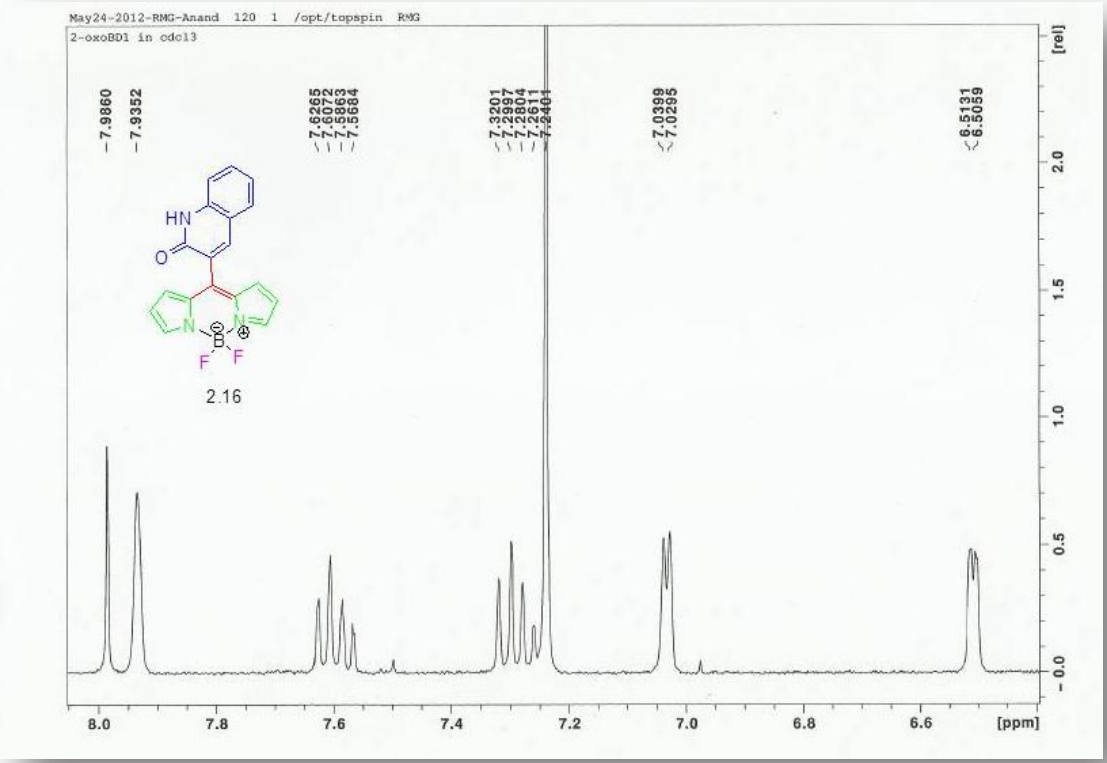

Appendix 26: C-NMR of 4,4-difluoro-4-bora-3a,4a-diaza-s-indacene-2-oxo-quinoline

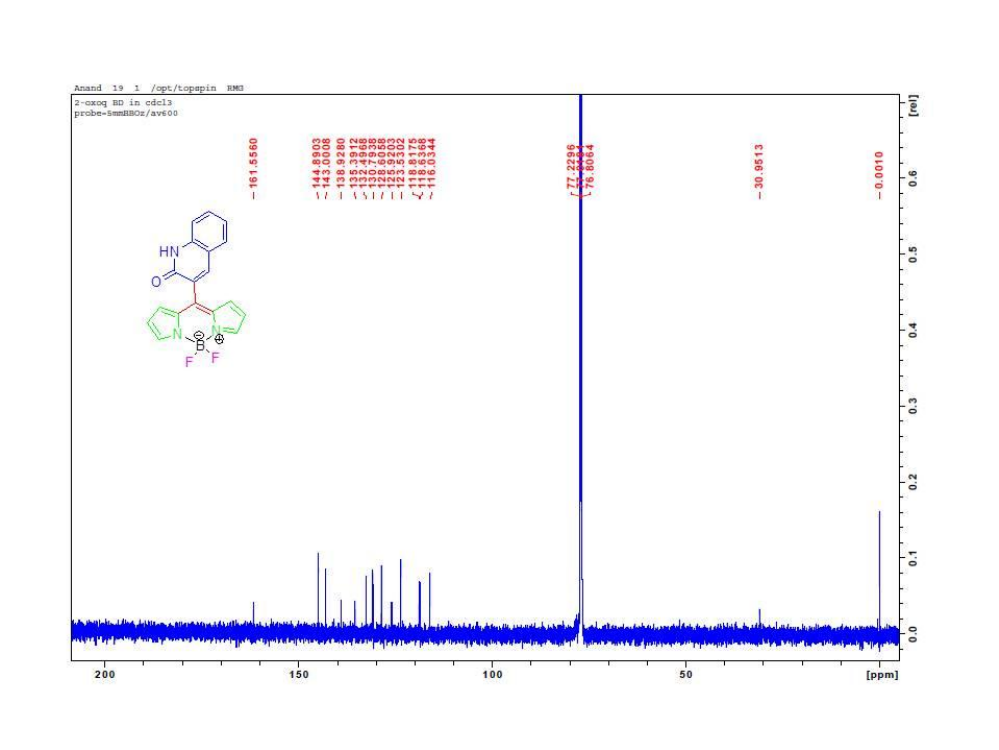

Appendix 27: F-NMR of 4,4-difluoro-4-bora-3a,4a-diaza-s-indacene-2-oxo-quinoline

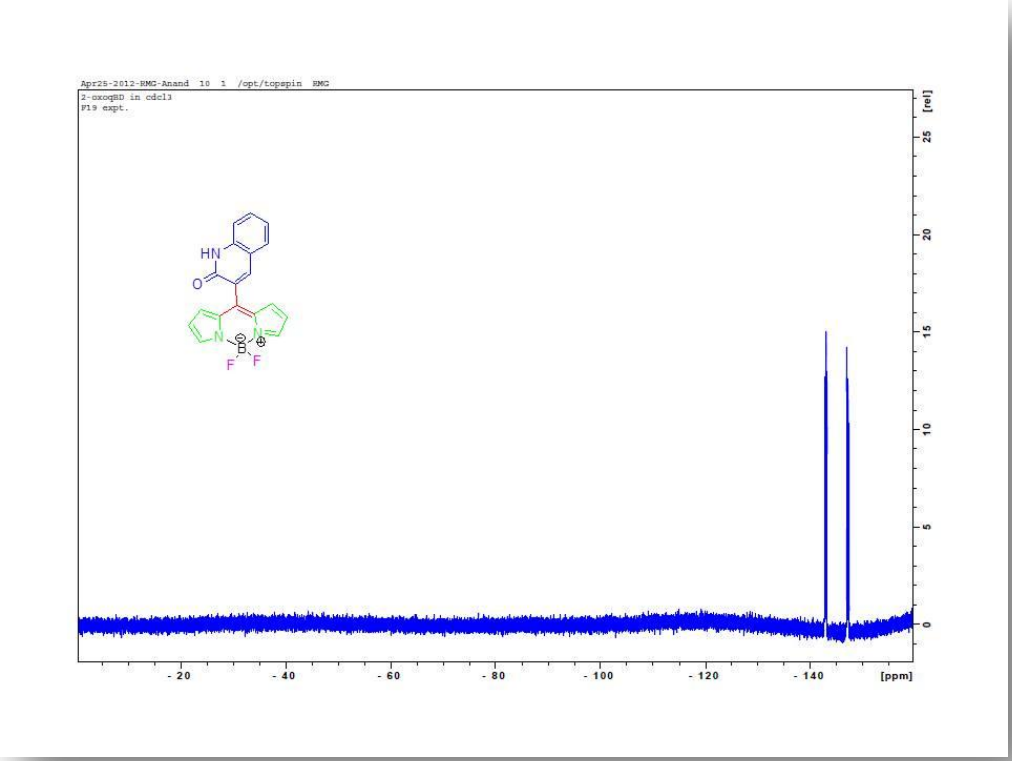

Appendix 28: Expanded F-NMR of 4,4-difluoro-4-bora-3a,4a-diaza-s-indacene-2-oxo-quinoline

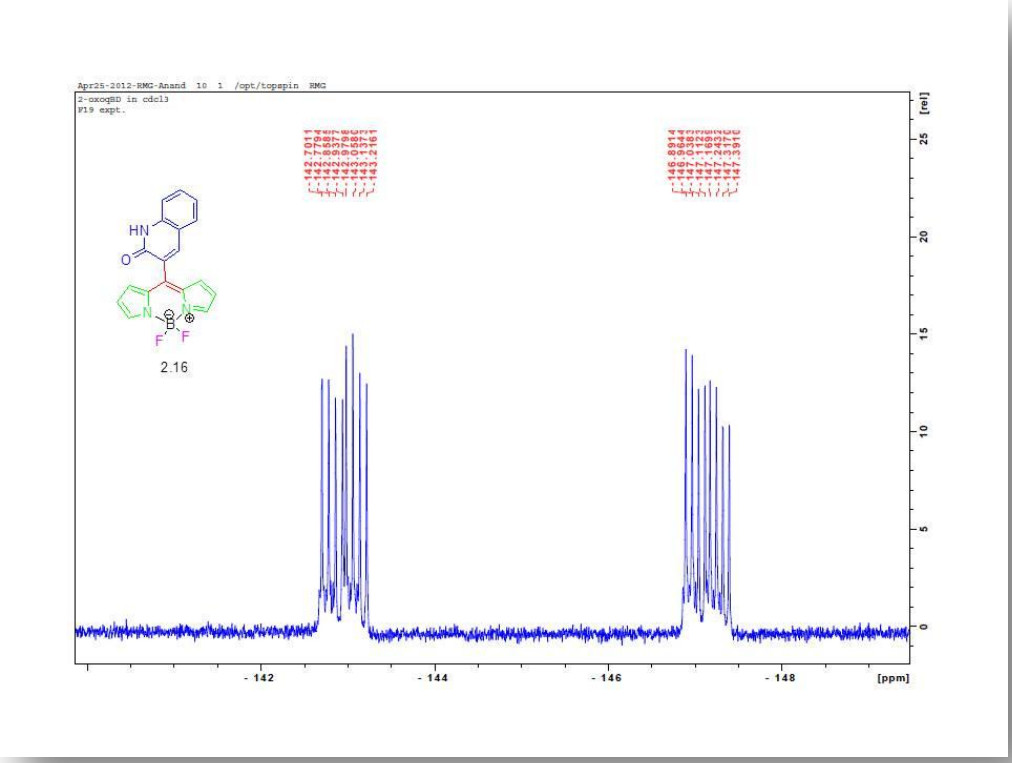

Appendix 29: Table 24: Bond Angles and Bond Lengths for 4,4-difluoro-4-bora-3a,4a-diaza-s-indacene-quinolin-2-one

Atoms	Bond Angles
C(2)-C(1)-N(5)	107.896
C(2)-C(1)-C(11)	130.185
N(5)-C(1)-C(11)	121.914
C(1)-C(2)-C(3)	108.204
C(1)-C(2)-H(37)	125.891
C(3)-C(2)-H(37)	125.905
C(2)-C(3)-C(4)	108.643
C(2)-C(3)-H(35)	125.684
C(4)-C(3)-H(35)	125.67
C(3)-C(4)-N(5)	107.463
C(3)-C(4)-H(34)	129.526
N(5)-C(4)-H(34)	123.009
C(1)-N(5)-C(4)	107.792
C(1)-N(5)-B(24)	123.829
C(4)-N(5)-B(24)	128.379
C(7)-C(6)-N(10)	110.804
C(7)-C(6)-H(33)	126.114
N(10)-C(6)-H(33)	123.082
C(6)-C(7)-C(8)	106.311
C(6)-C(7)-H(32)	126.829
C(8)-C(7)-H(32)	126.857
C(7)-C(8)-C(9)	107.127
C(7)-C(8)-H(36)	126.426
C(9)-C(8)-H(36)	126.448
C(8)-C(9)-N(10)	110.017
C(8)-C(9)-C(11)	126.964
N(10)-C(9)-C(11)	123.019
C(6)-N(10)-C(9)	105.741
C(6)-N(10)-B(24)	127.186
C(9)-N(10)-B(24)	127.074
C(1)-C(11)-C(9)	114.709
C(1)-C(11)-C(12)	122.516
C(9)-C(11)-C(12)	122.776
C(11)-C(12)-C(21)	118.753
C(11)-C(12)-C(22)	121.481
C(21)-C(12)-C(22)	119.765
C(14)-C(13)-C(18)	119.912
C(14)-C(13)-H(30)	120.021

Atoms	Bond Angles
C(18)-C(13)-H(30)	120.066
C(13)-C(14)-C(15)	119.991
C(13)-C(14)-H(28)	120.022
C(15)-C(14)-H(28)	119.984
C(14)-C(15)-C(16)	120.01
C(14)-C(15)-H(27)	120.012
C(16)-C(15)-H(27)	119.977
C(15)-C(16)-C(17)	120.029
C(15)-C(16)-H(29)	120.007
C(17)-C(16)-H(29)	119.965
C(16)-C(17)-C(18)	119.916
C(16)-C(17)-N(19)	119.8
C(18)-C(17)-N(19)	120.285
C(13)-C(18)-C(17)	120.14
C(13)-C(18)-C(22)	120.437
C(17)-C(18)-C(22)	119.423
C(17)-N(19)-C(21)	126.277
C(17)-N(19)-H(20)	112.548
H(20)-N(19)-C(21)	119.981
C(12)-C(21)-N(19)	114.691
C(12)-C(21)-O(23)	122.857
N(19)-C(21)-O(23)	122.444
C(12)-C(22)-C(18)	119.556
C(12)-C(22)-H(31)	120.21
C(18)-C(22)-H(31)	120.238
N(5)-B(24)-N(10)	109.451
N(5)-B(24)-F(25)	109.549
N(5)-B(24)-F(26)	109.409
N(10)-B(24)-F(25)	109.699
N(10)-B(24)-F(26)	109.218
F(25)-B(24)-F(26)	109.5

Atoms	Bond Length
C(1)-C(2)	1.338
C(1)-N(5)	1.456
C(1)-C(11)	1.498
C(2)-C(3)	1.508
C(2)-H(37)	1.1
C(3)-C(4)	1.339
C(3)-H(35)	1.1
C(4)-N(5)	1.458
C(4)-H(34)	1.1
N(5)-B(24)	1.497
C(6)-C(7)	1.418
C(6)-N(10)	1.399
C(6)-H(33)	1.1
C(7)-C(8)	1.418
C(7)-H(32)	1.1
C(8)-C(9)	1.421
C(8)-H(36)	1.1
C(9)-N(10)	1.404
C(9)-C(11)	1.418
N(10)-B(24)	1.501
C(11)-C(12)	1.42
C(12)-C(21)	1.518
C(12)-C(22)	1.42
C(13)-C(14)	1.42
C(13)-C(18)	1.42
C(13)-H(30)	1.1
C(14)-C(15)	1.42
C(14)-H(28)	1.1
C(15)-C(16)	1.42
C(15)-H(27)	1.1
C(16)-C(17)	1.42
C(16)-H(29)	1.1
C(17)-C(18)	1.419
C(17)-N(19)	1.345
C(18)-C(22)	1.419
N(19)-C(21)	1.37
N(19)-H(20)	1.012
C(21)-O(23)	1.208
C(22)-H(31)	1.1
B(24)-F(25)	1.54

Atoms	Bond Length
B(24)-F(26)	1.54
C(2)-C(1)-N(5)	107.896
C(2)-C(1)-C(11)	130.185
N(5)-C(1)-C(11)	121.914
C(1)-C(2)-C(3)	108.204
C(1)-C(2)-H(37)	125.891
C(3)-C(2)-H(37)	125.905
C(2)-C(3)-C(4)	108.643
C(2)-C(3)-H(35)	125.684
C(4)-C(3)-H(35)	125.67
C(3)-C(4)-N(5)	107.463
C(3)-C(4)-H(34)	129.526
N(5)-C(4)-H(34)	123.009
C(1)-N(5)-C(4)	107.792
C(1)-N(5)-B(24)	123.829
C(4)-N(5)-B(24)	128.379
C(7)-C(6)-N(10)	110.804
C(7)-C(6)-H(33)	126.114
N(10)-C(6)-H(33)	123.082
C(6)-C(7)-C(8)	106.311
C(6)-C(7)-H(32)	126.829
C(8)-C(7)-H(32)	126.857
C(7)-C(8)-C(9)	107.127
C(7)-C(8)-H(36)	126.426
C(9)-C(8)-H(36)	126.448
C(8)-C(9)-N(10)	110.017
C(8)-C(9)-C(11)	126.964
N(10)-C(9)-C(11)	123.019
C(6)-N(10)-C(9)	105.741
C(6)-N(10)-B(24)	127.186
C(9)-N(10)-B(24)	127.074
C(1)-C(11)-C(9)	114.709
C(1)-C(11)-C(12)	122.516
C(9)-C(11)-C(12)	122.776
C(11)-C(12)-C(21)	118.753
C(11)-C(12)-C(22)	121.481
C(21)-C(12)-C(22)	119.765
C(14)-C(13)-C(18)	119.912
C(14)-C(13)-H(30)	120.021
C(18)-C(13)-H(30)	120.066

Atoms	Bond Length
C(13)-C(14)-C(15)	119.991
C(13)-C(14)-H(28)	120.022
C(15)-C(14)-H(28)	119.984
C(14)-C(15)-C(16)	120.01
C(14)-C(15)-H(27)	120.012
C(16)-C(15)-H(27)	119.977
C(15)-C(16)-C(17)	120.029
C(15)-C(16)-H(29)	120.007
C(17)-C(16)-H(29)	119.965
C(16)-C(17)-C(18)	119.916
C(16)-C(17)-N(19)	119.8
C(18)-C(17)-N(19)	120.285
C(13)-C(18)-C(17)	120.14
C(13)-C(18)-C(22)	120.437
C(17)-C(18)-C(22)	119.423
C(17)-N(19)-C(21)	126.277
C(17)-N(19)-H(20)	112.548
H(20)-N(19)-C(21)	119.981
C(12)-C(21)-N(19)	114.691
C(12)-C(21)-O(23)	122.857
N(19)-C(21)-O(23)	122.444
C(12)-C(22)-C(18)	119.556
C(12)-C(22)-H(31)	120.21
C(18)-C(22)-H(31)	120.238

N(5)-B(24)-N(10)	109.451
N(5)-B(24)-F(25)	109.549
N(5)-B(24)-F(26)	109.409
N(10)-B(24)-F(25)	109.699
N(10)-B(24)-F(26)	109.218
F(25)-B(24)-F(26)	109.5

Appendix 30: IR Spectra of Fraction 5-6 of Scheme 9

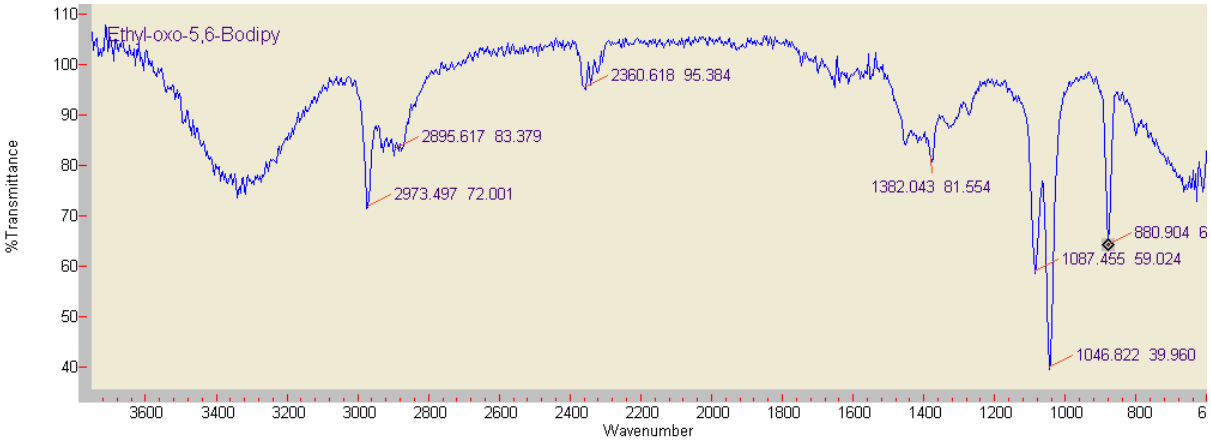

Appendix 31: H-NMR Spectra of Fraction 5-6 of Scheme 9

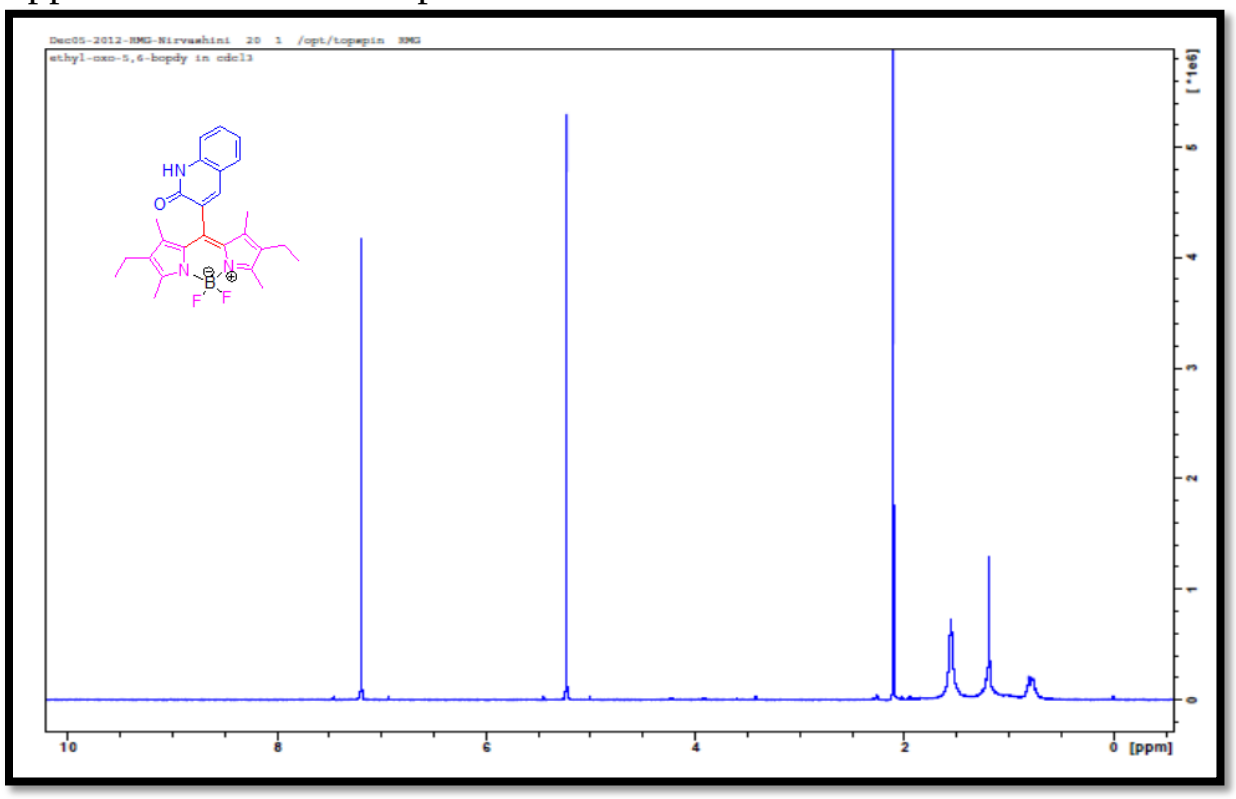

Appendix 32: IR Spectra of Fraction 7 of Scheme 9

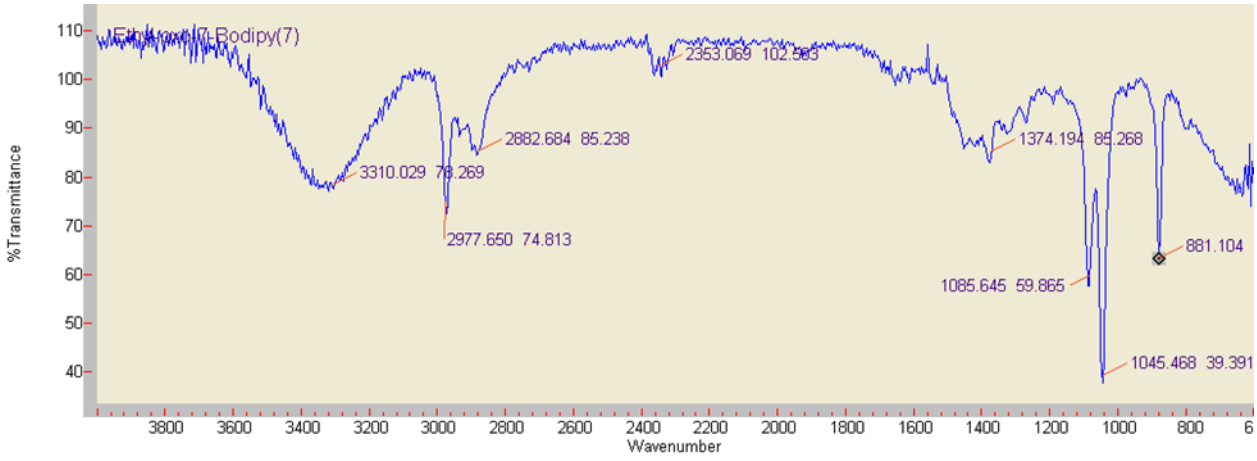

Appendix 33: H-NMR Spectra of Fraction 7 of Scheme 9

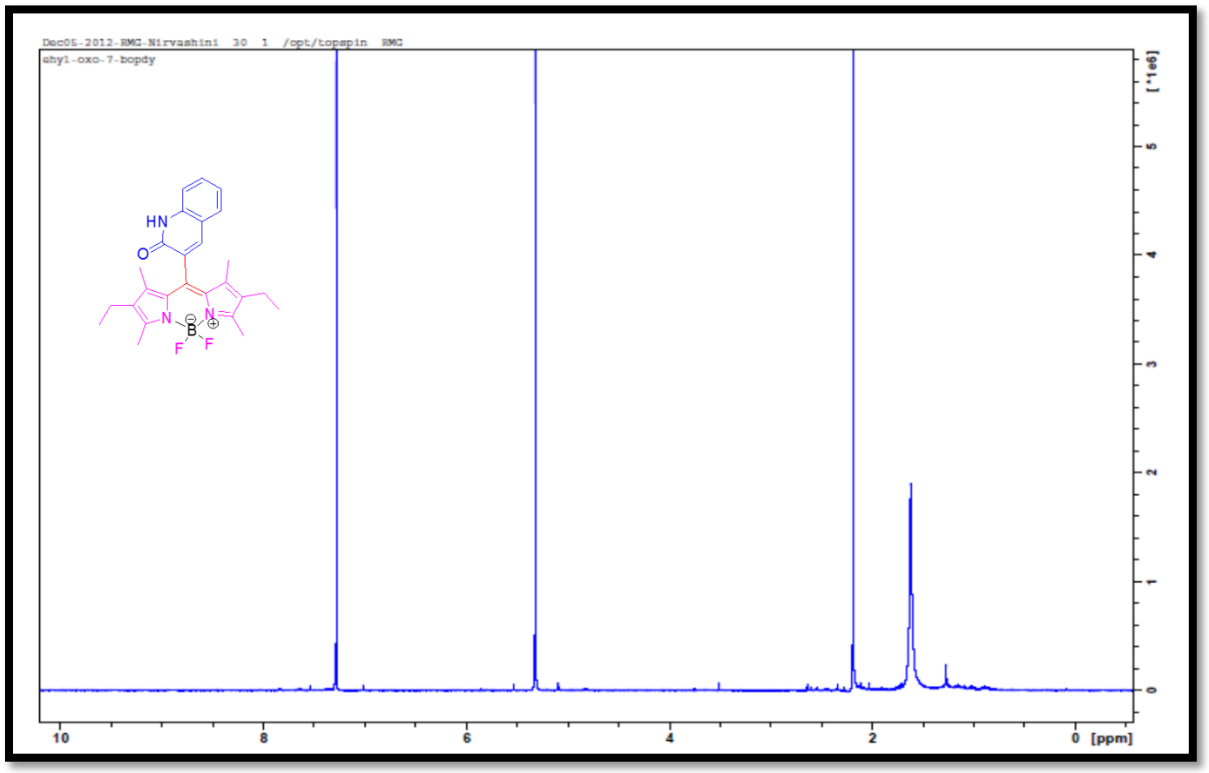

Appendix 34: IR Spectra of Fraction 8 of Scheme 9

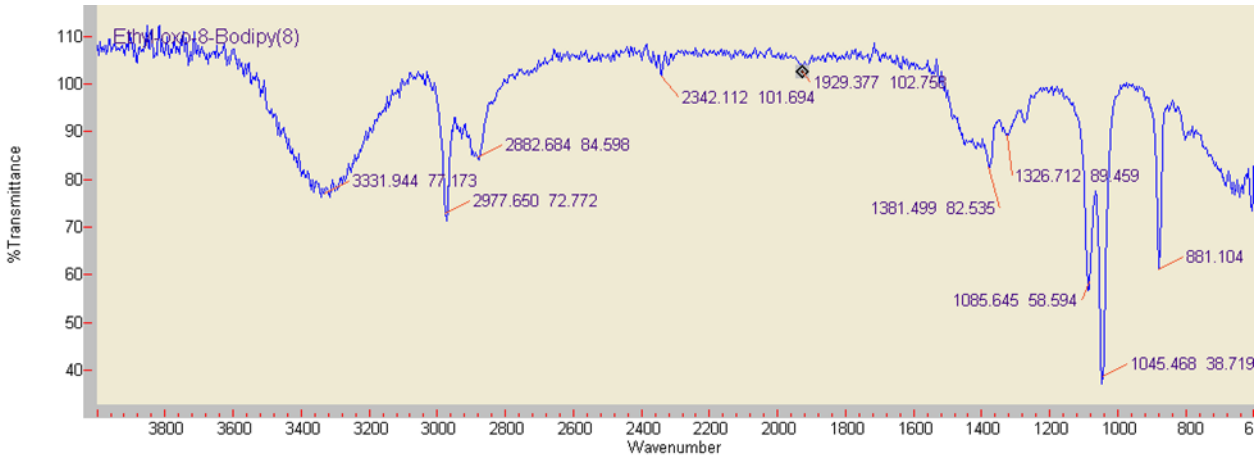

Appendix 35: H-NMR Spectra of Fraction 8 of Scheme 9

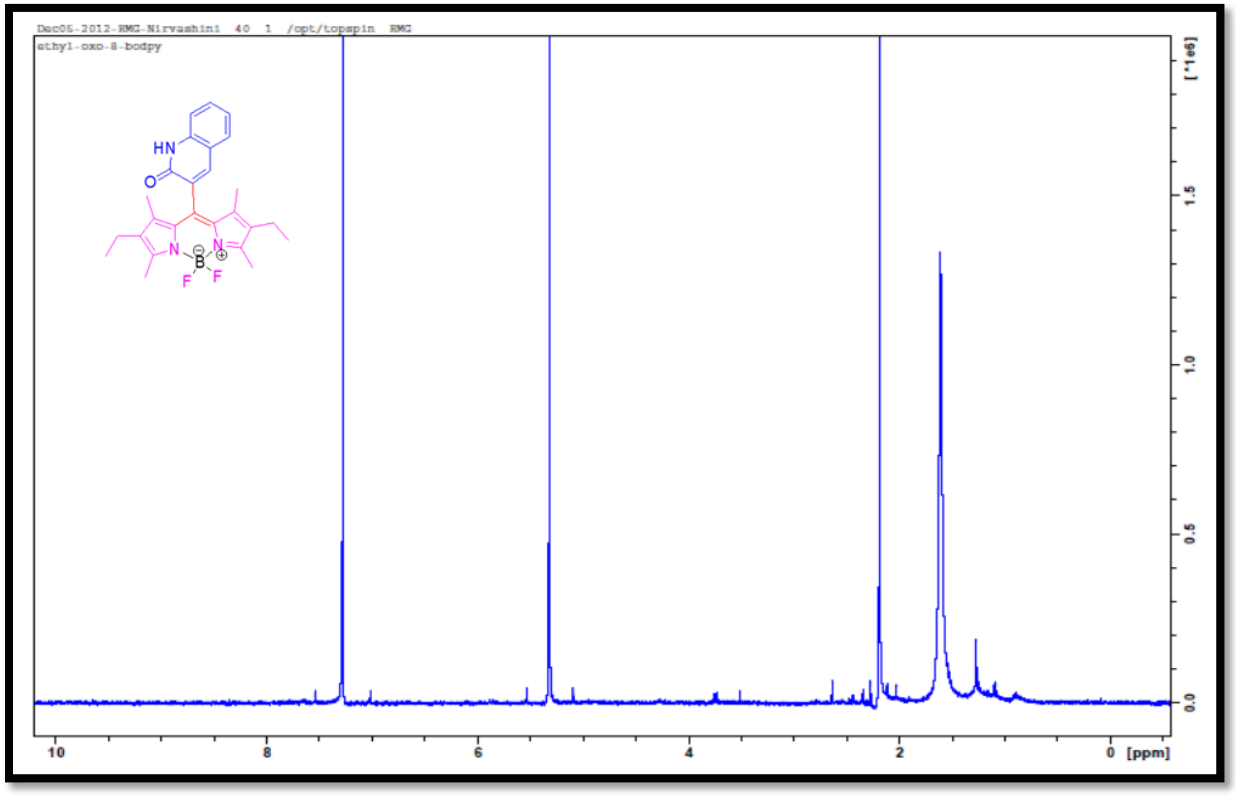

Appendix 36: IR Spectra of Fraction 8 in MeOH of Scheme 9

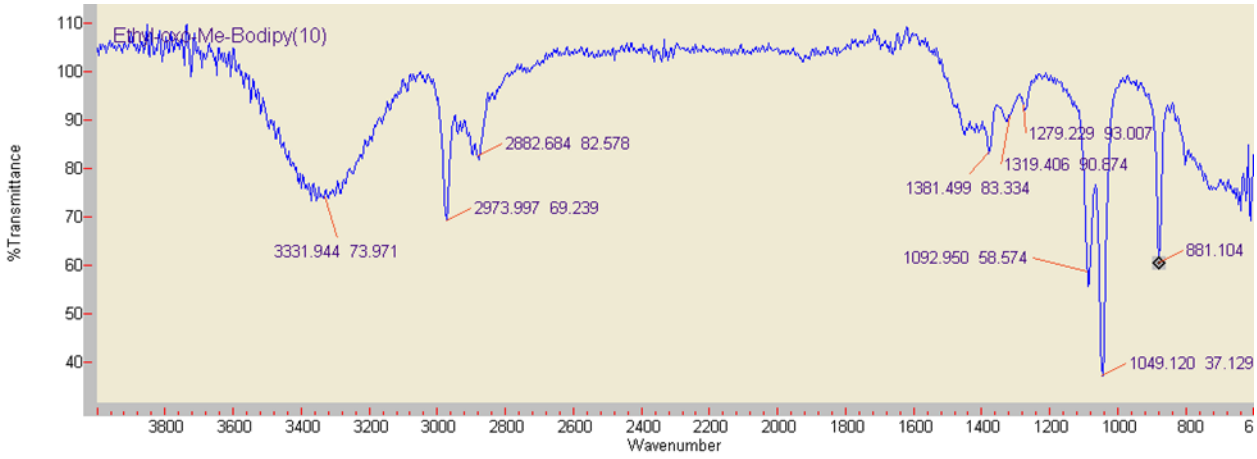

Appendix 37: IR Spectra of Fraction 1 of 84.

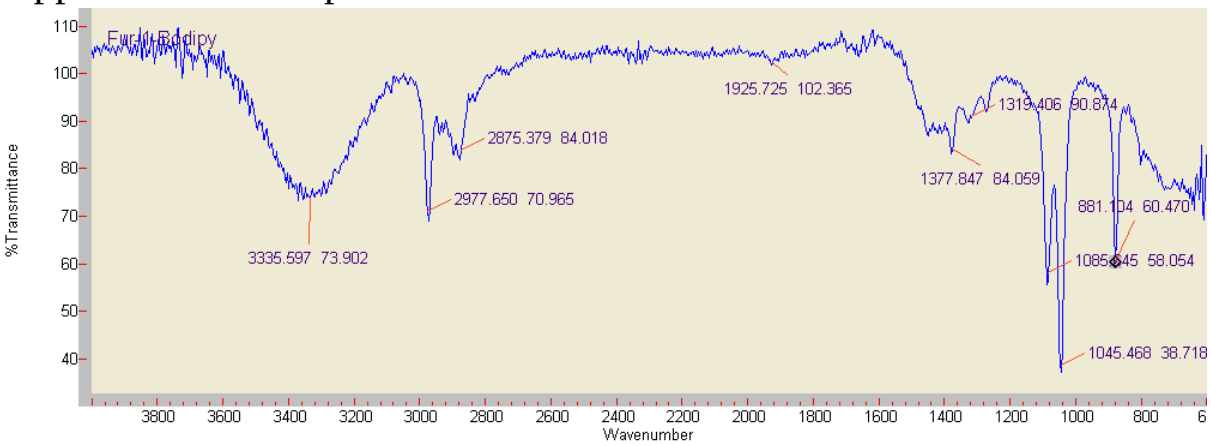

Appendix 38: H-NMR Spectra of Fraction 1 of 84

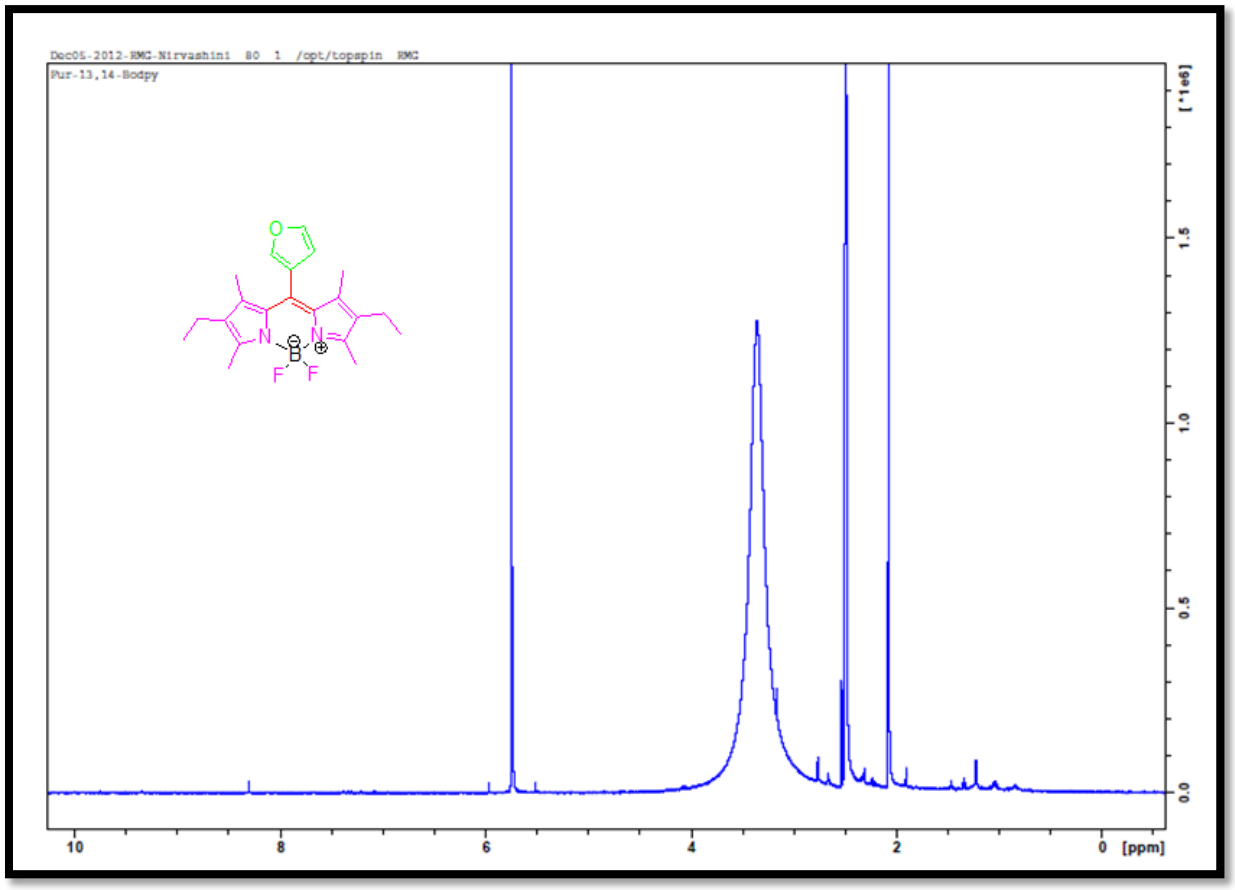

Appendix 39: IR Spectra of Fur-13-Bodipy(12)

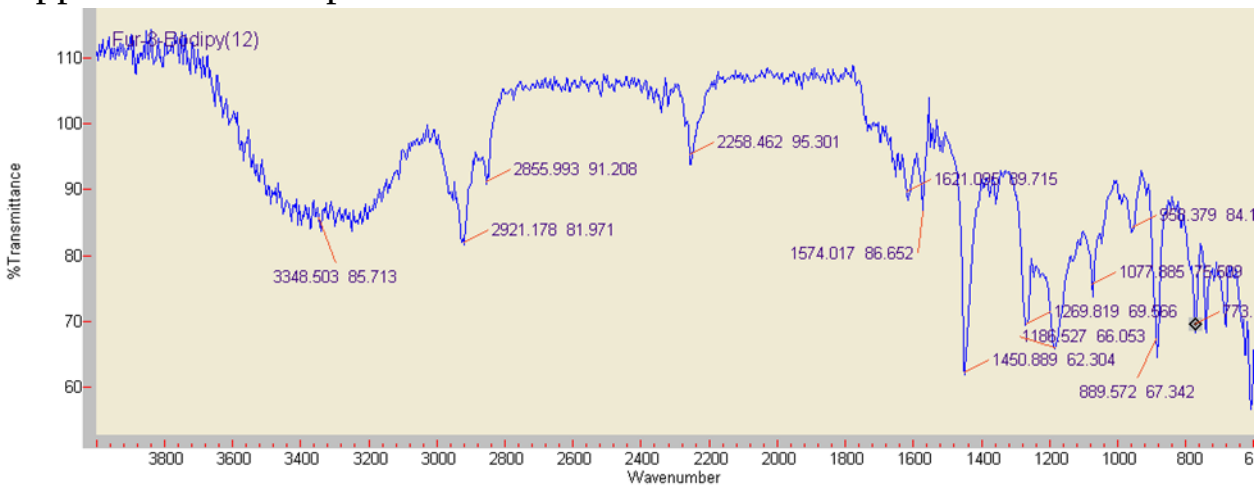

Appendix 40: H-NMR Spectra of Fraction 8 of 84

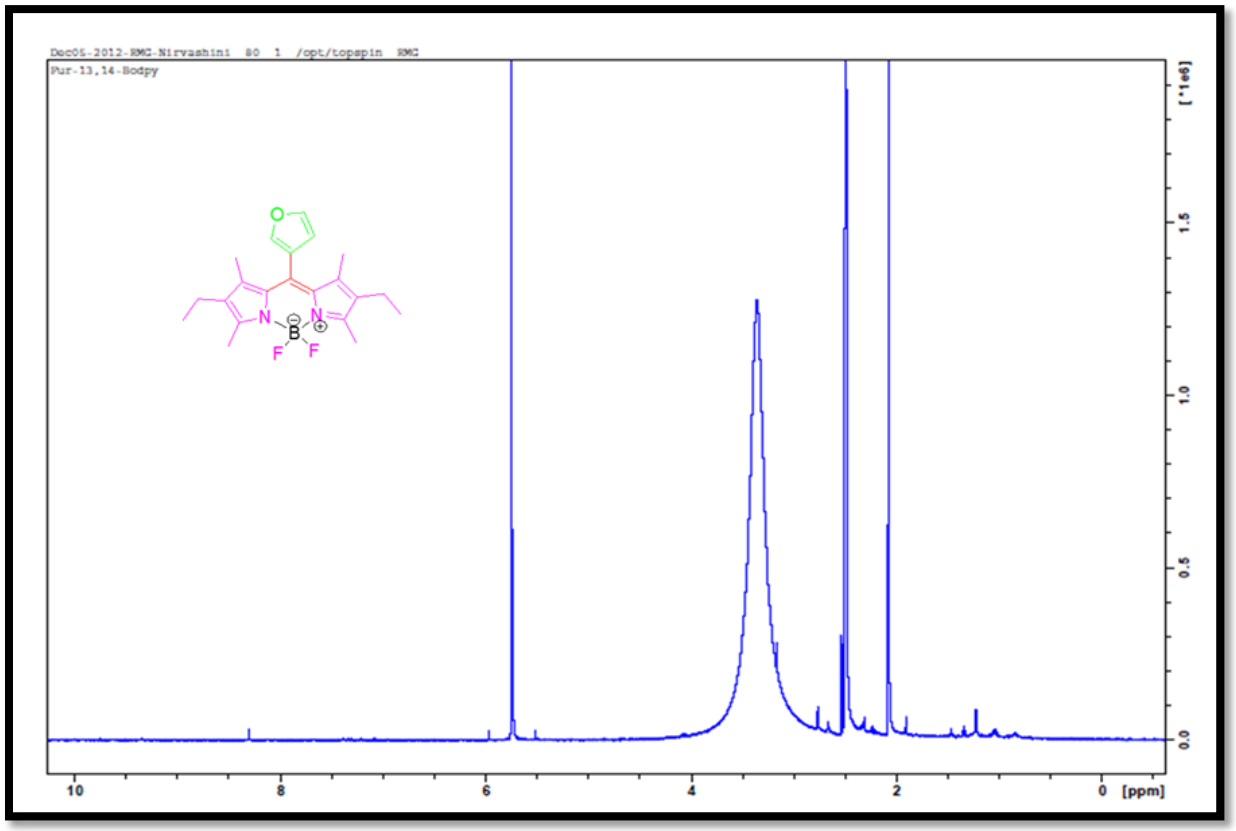

Appendix 41: IR Spectra of Fraction 13-14 of 84

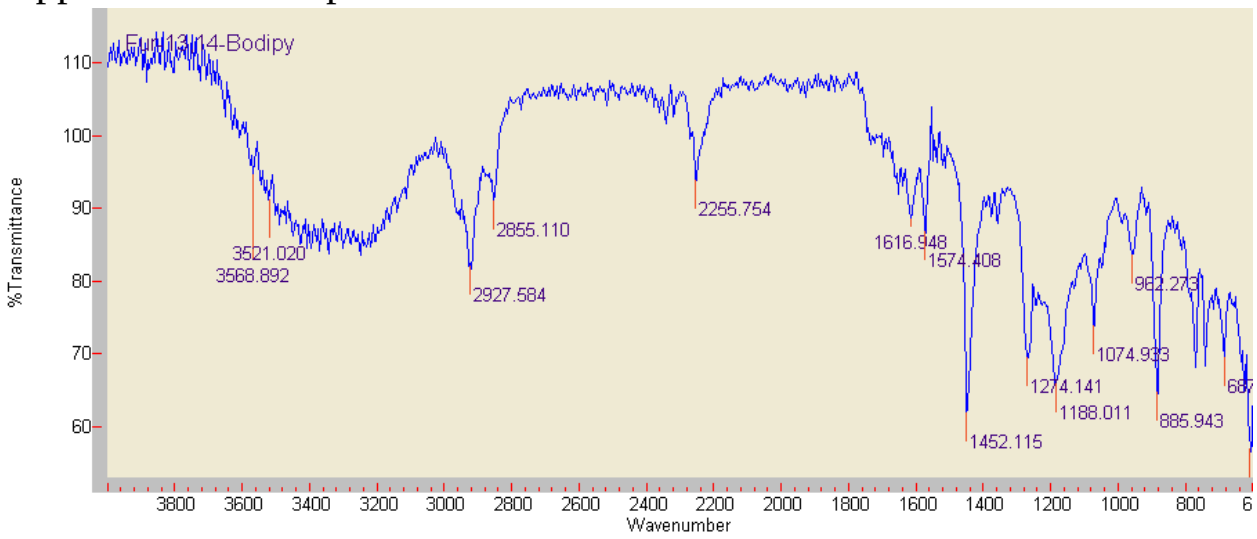

Appendix 42: IR Spectra of Fraction 3 of 86

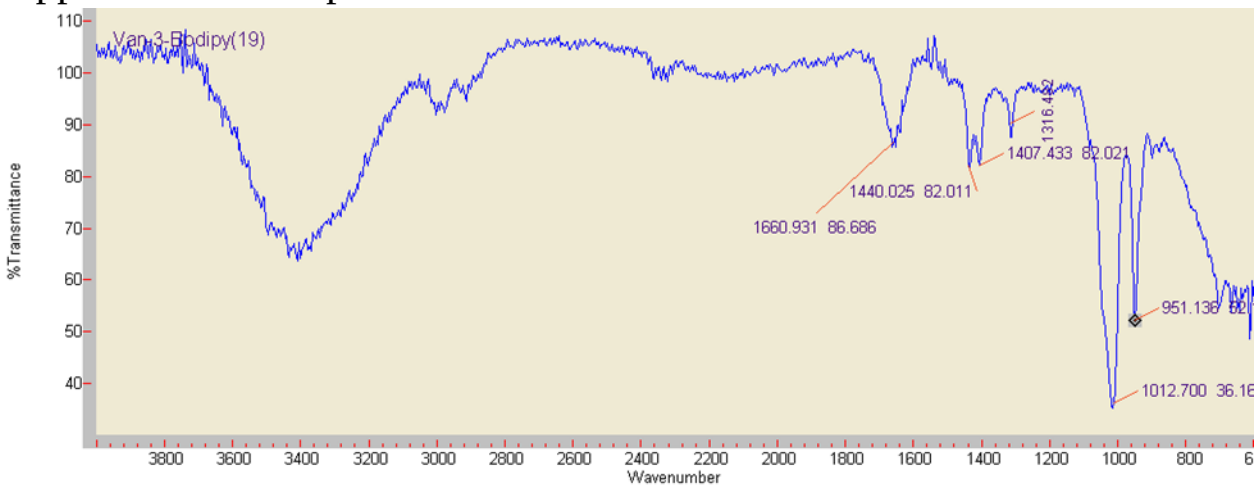

Appendix 43: IR Spectra of Fraction 9 of 86

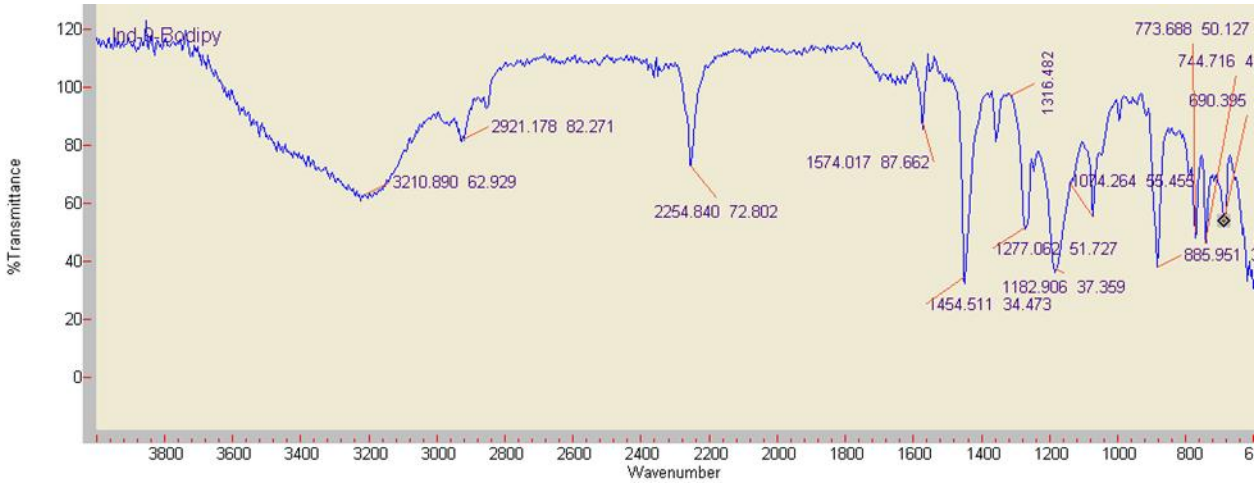

Appendix 44: H-NMR Spectra of Fraction 9 of 88

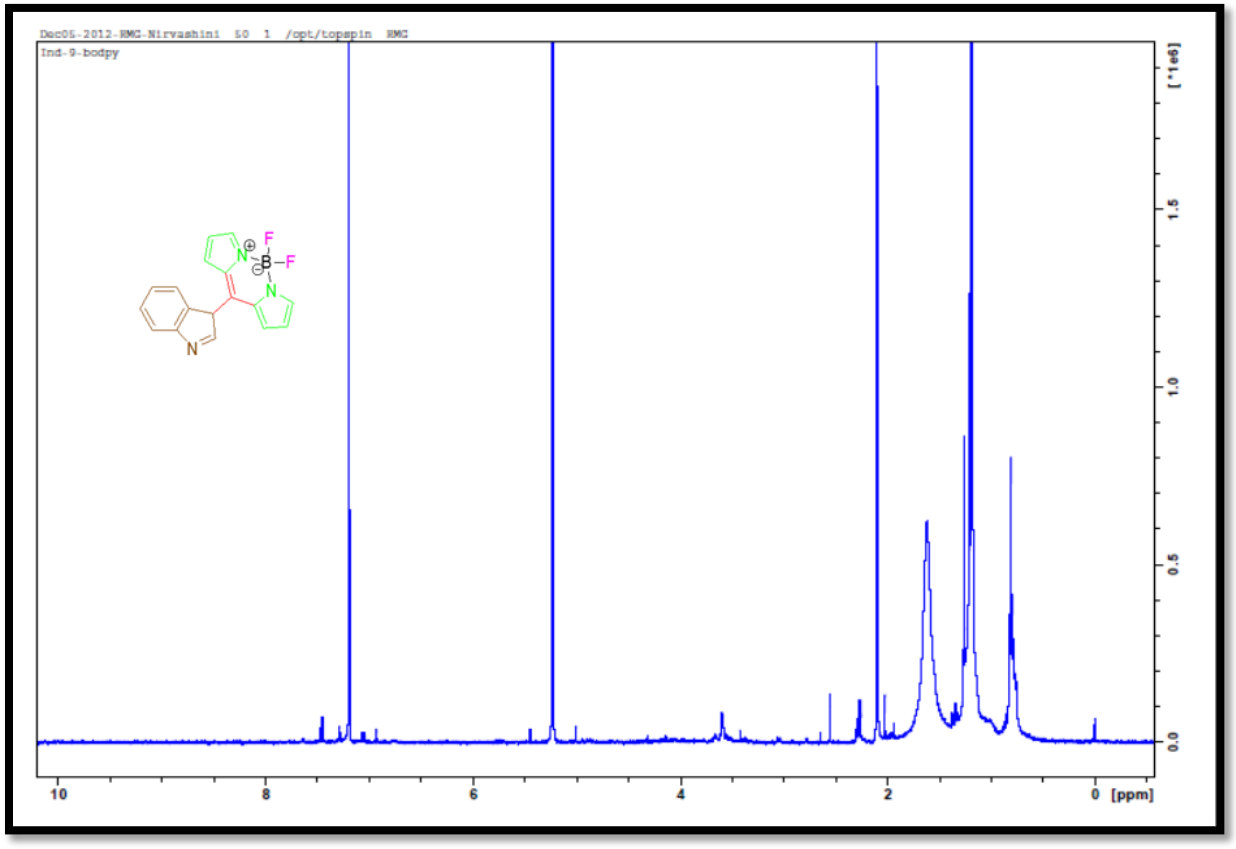

Appendix 45: H-NMR Spectra of Fraction 7 of 88

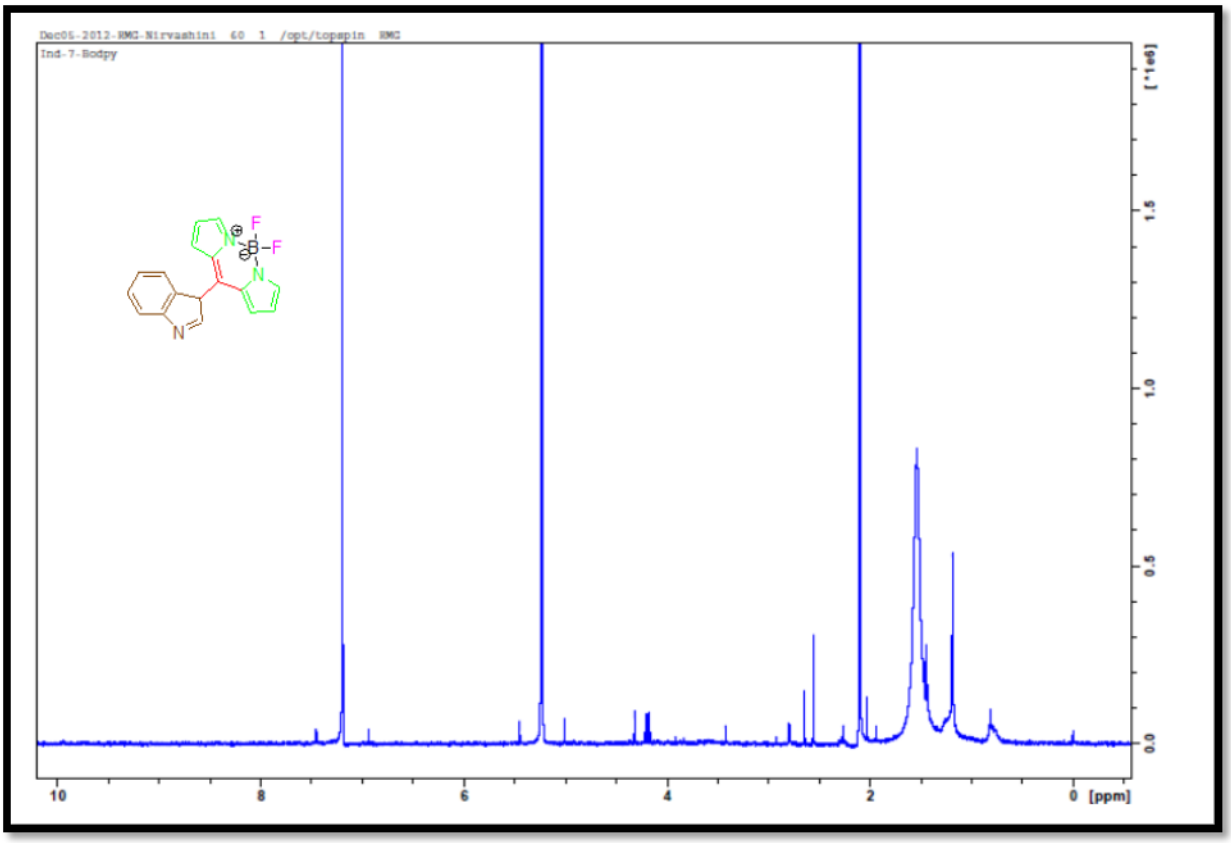

Appendix 46: UV-Visible Spectra of Compound 2 in Different Solvent Systems

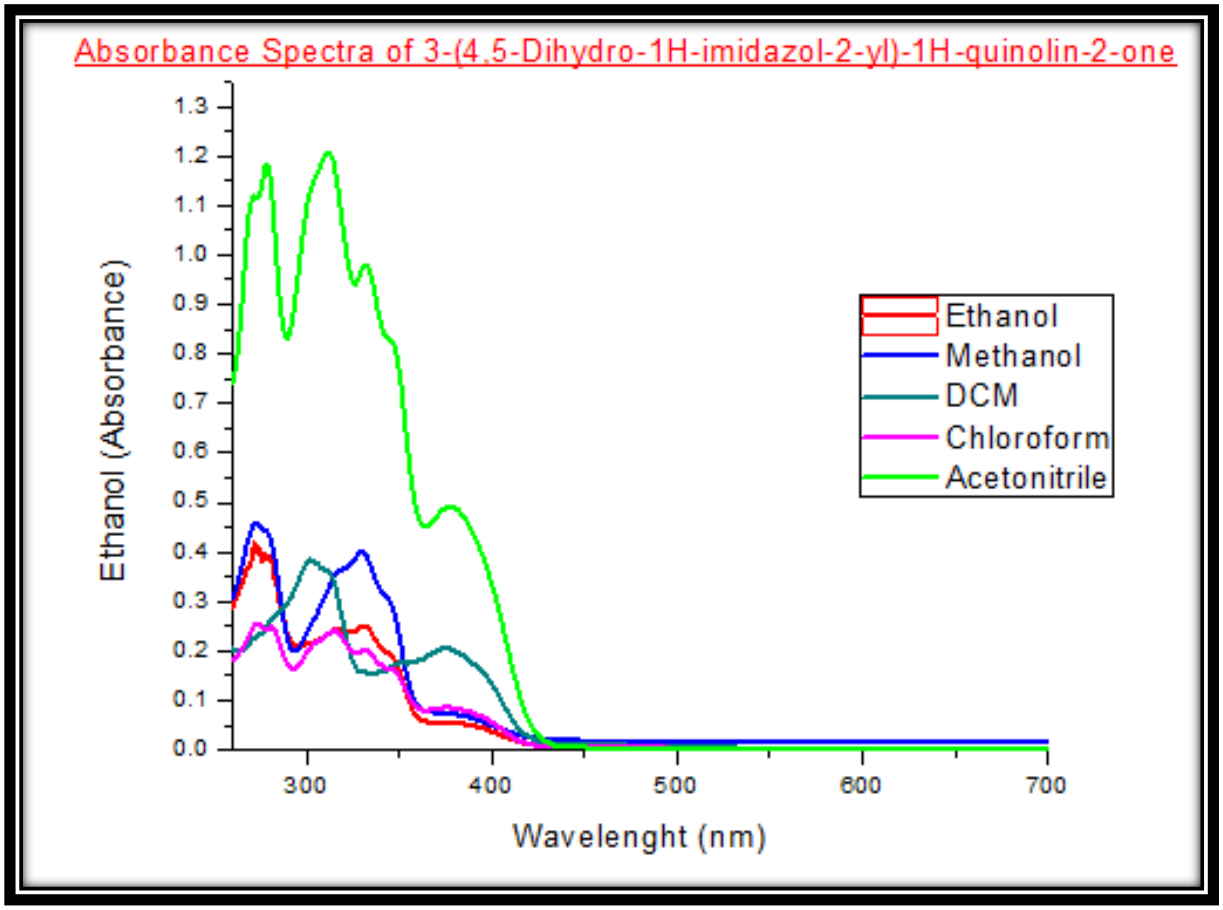

Appendix 47: UV-Visible Spectra of Compound 3 in Different Solvent Systems

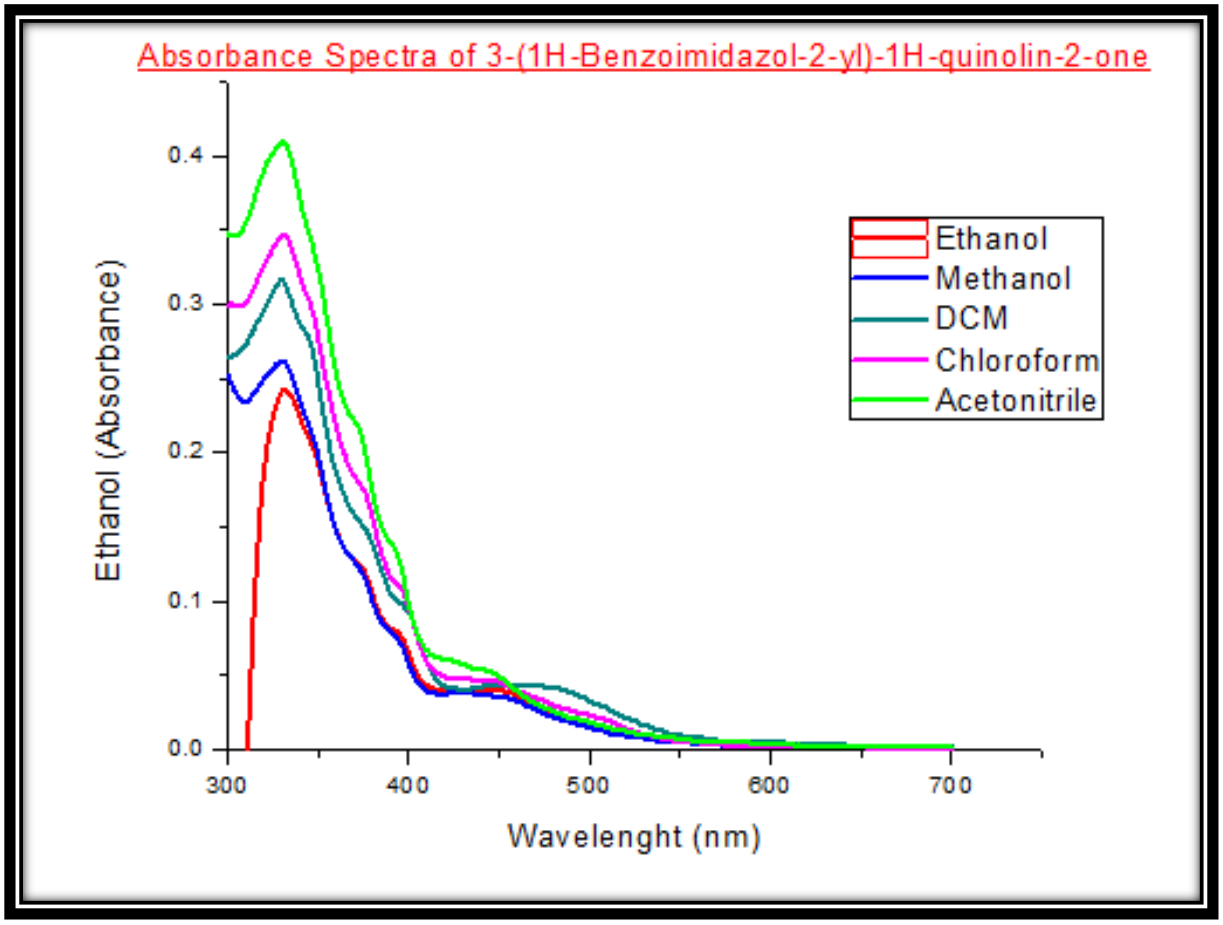

Appendix 48: UV-Visible Spectra of Compound 4 in Different Solvent Systems

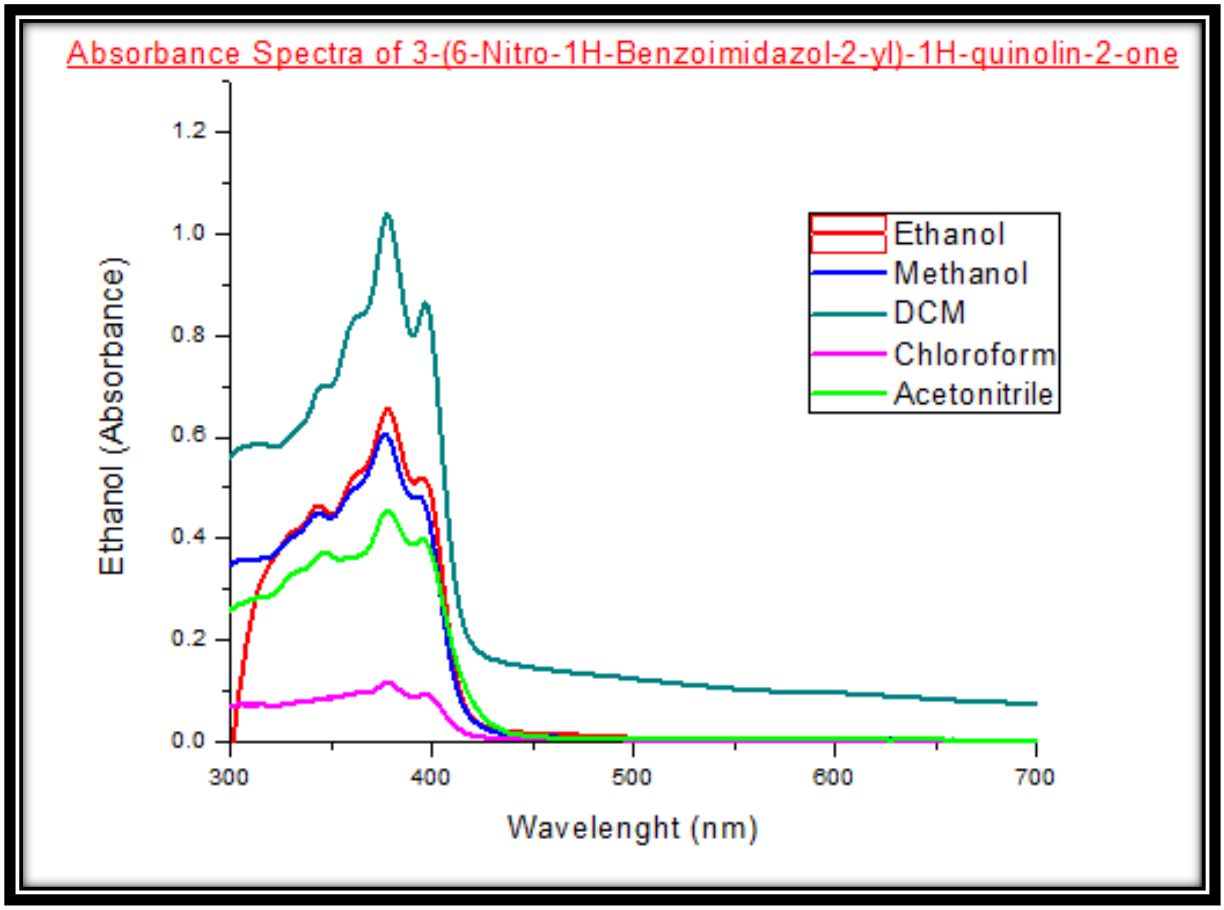

Appendix 49: UV-Visible Spectra of Compound 7 in Different Solvent Systems

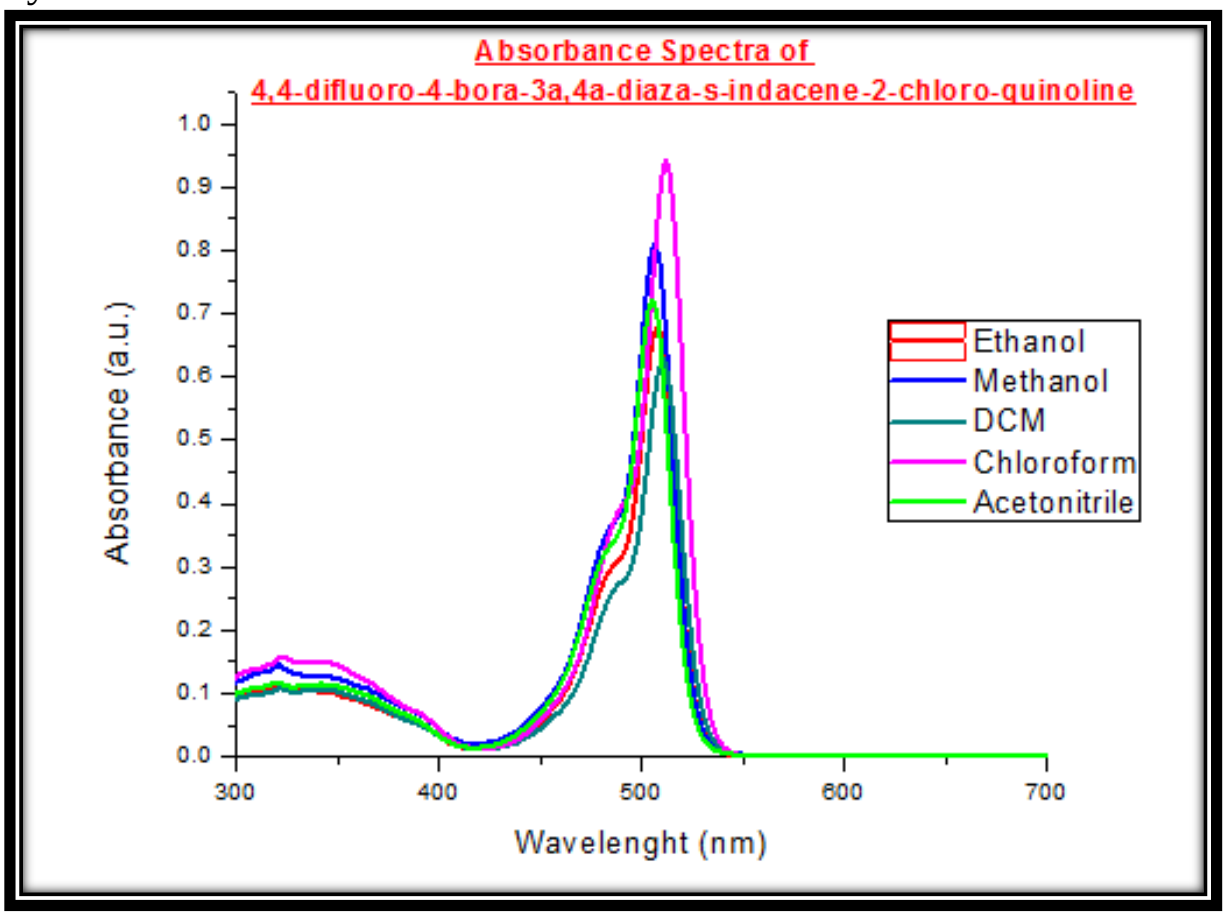

Appendix 50: UV-Visible Spectra of Compound 5 in Different Solvent Systems

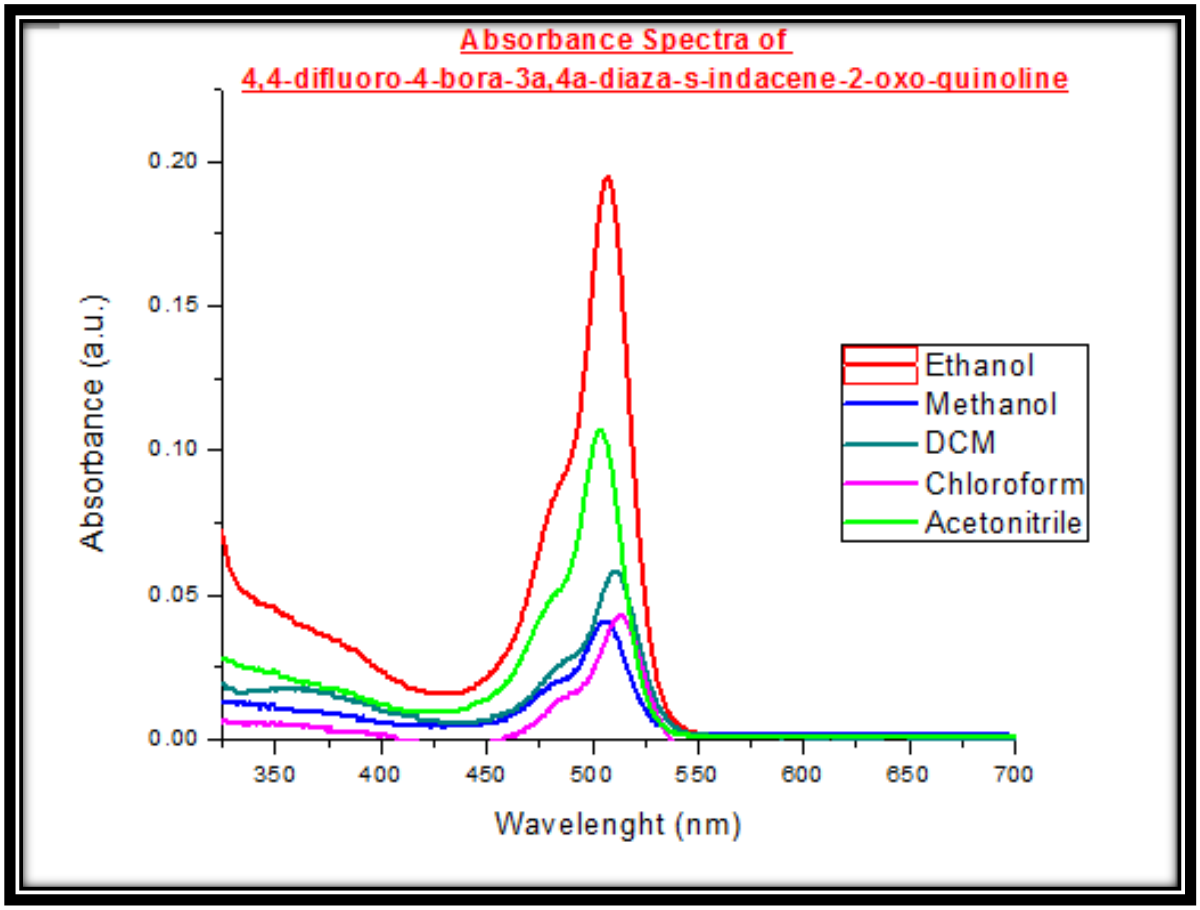

Appendix 51: Fluorescence Spectra of Compound 2 in Different Solvent Systems

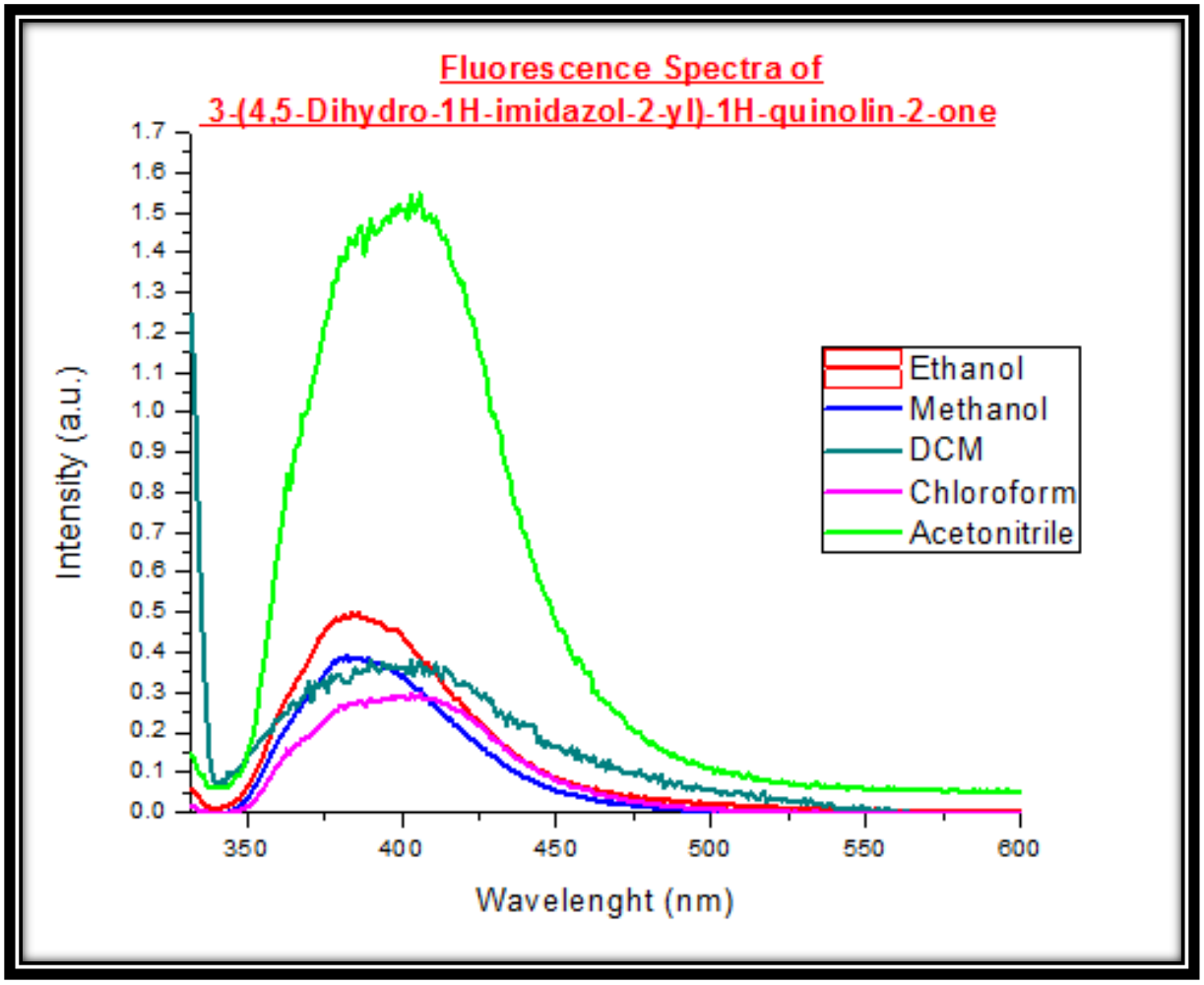

Appendix 52: Fluorescence Spectra of Compound 3 in Different Solvent Systems

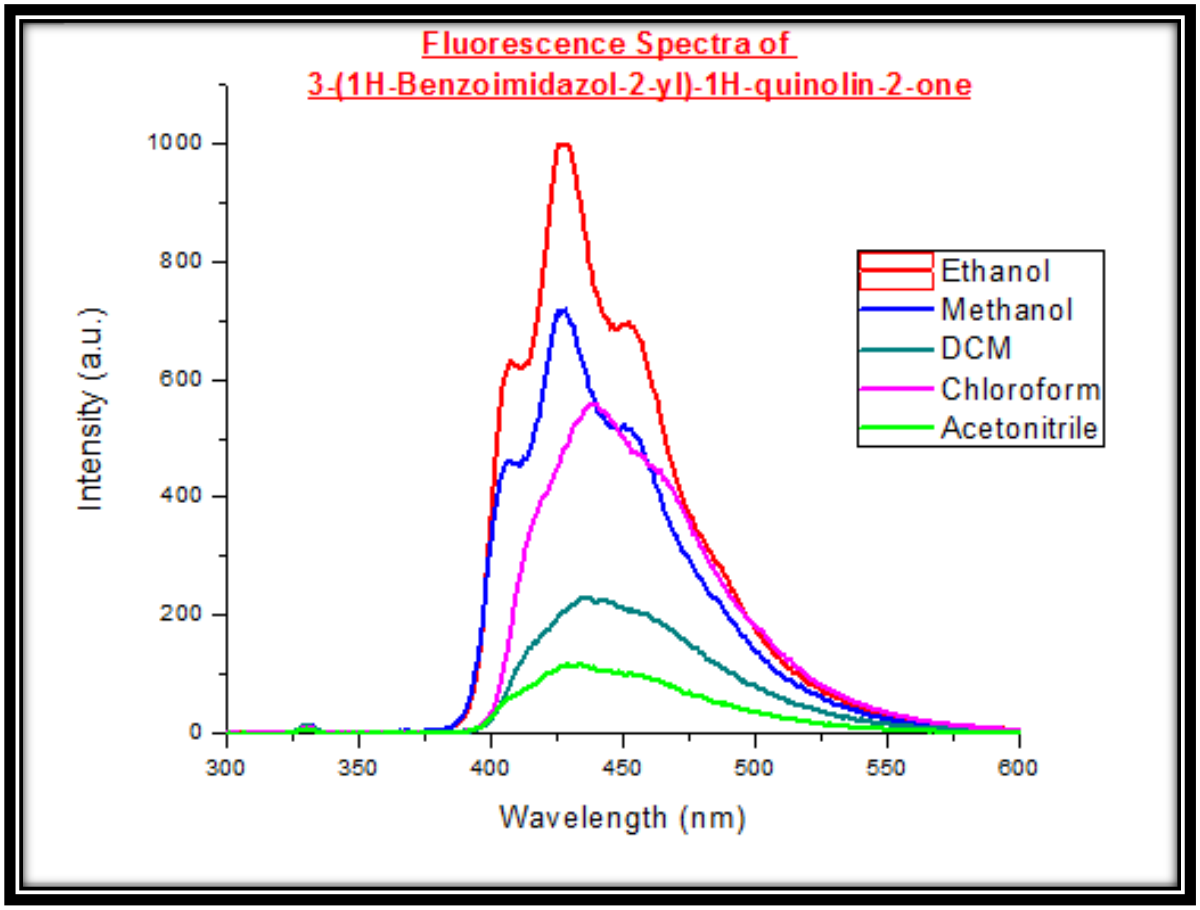

Appendix 53: Fluorescence Spectra of Compound 4 in Different Solvent Systems

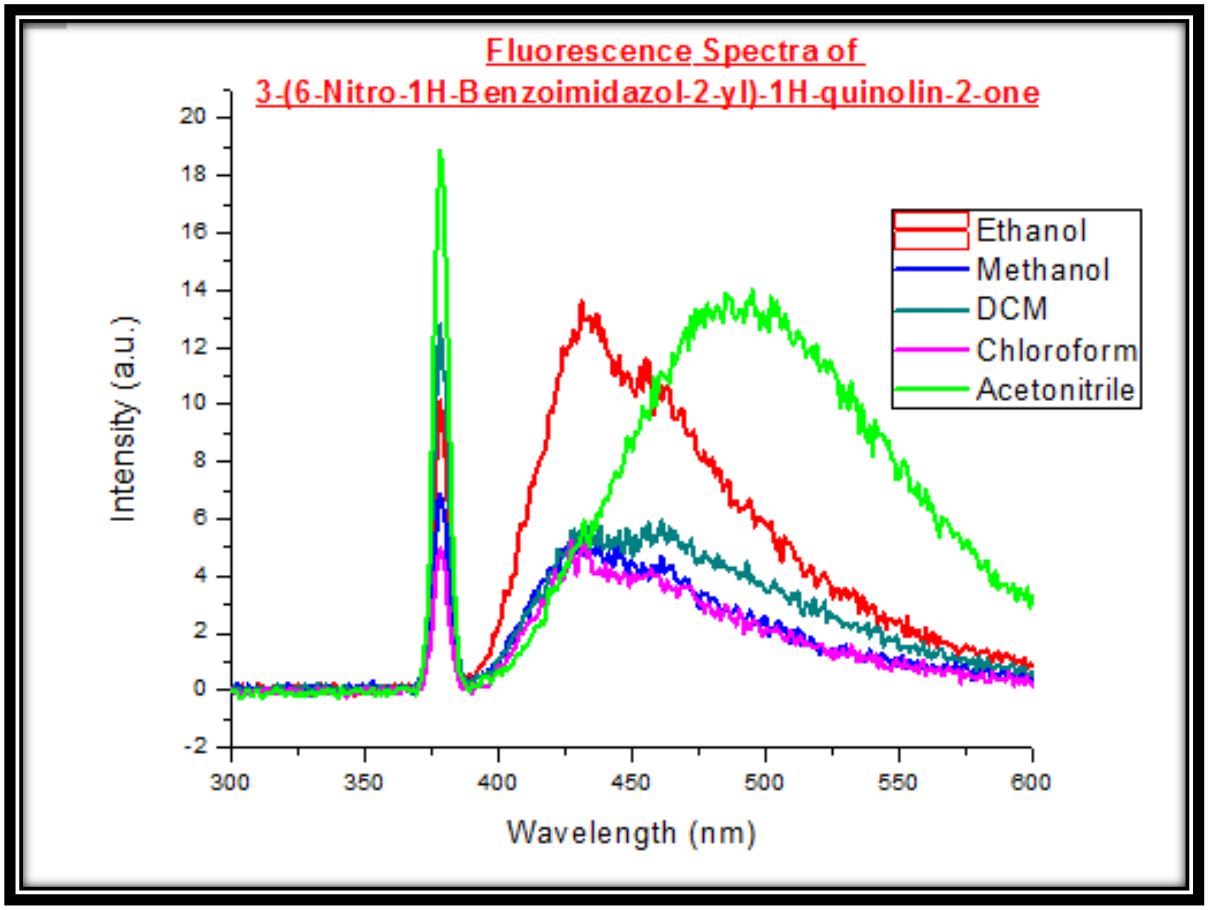

Appendix 54: Fluorescence Spectra of Compound 7 in Different Solvent Systems

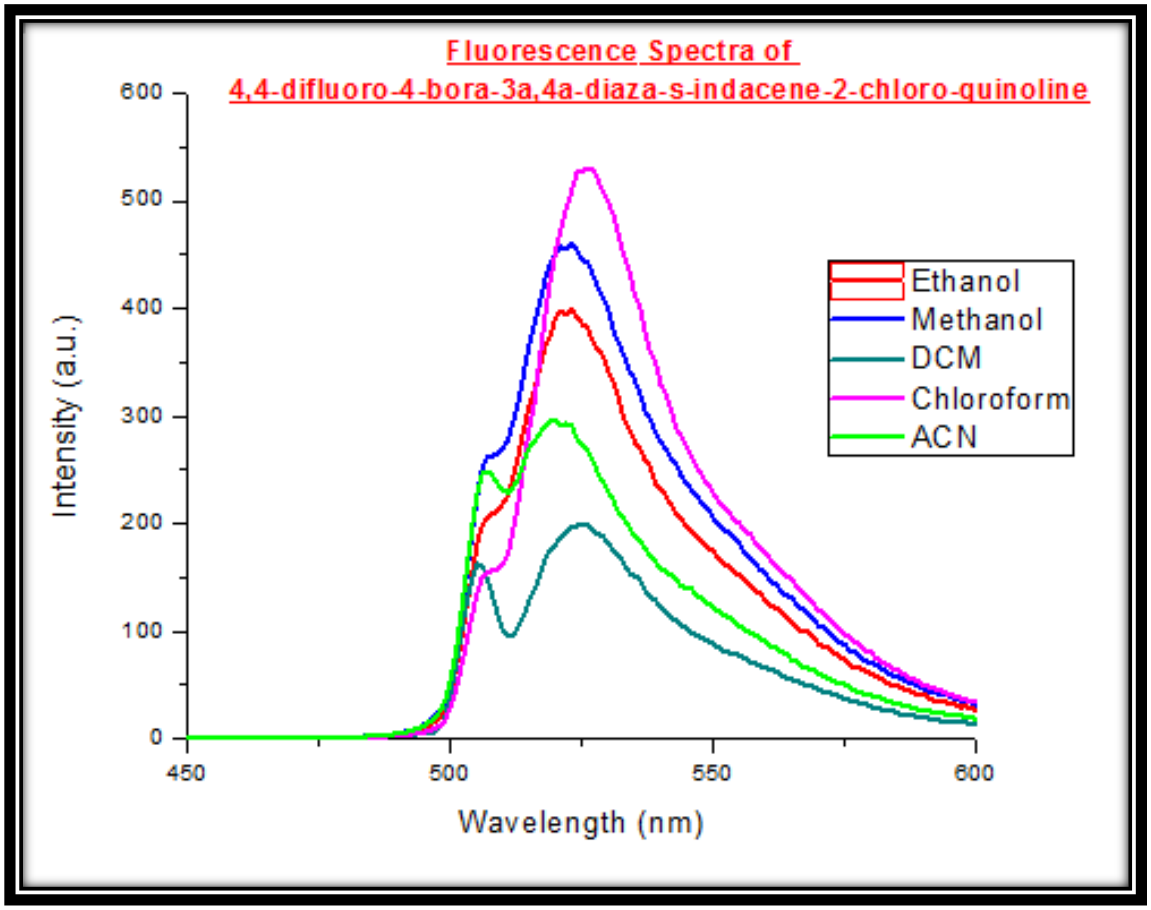

Appendix 55: Fluorescence Spectra of Compound 5 in Different Solvent Systems

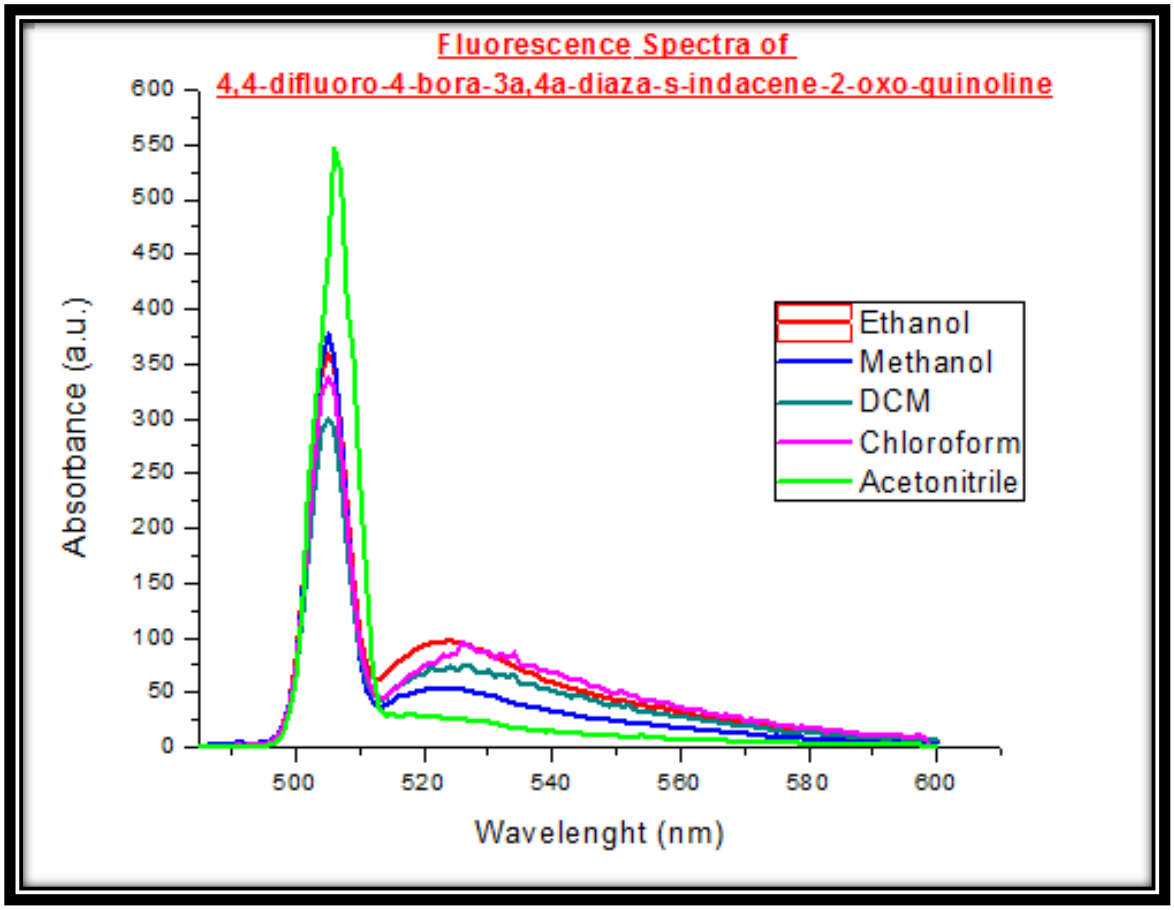

Appendix 56: Stokes Shift of Compound 2 in EtOH

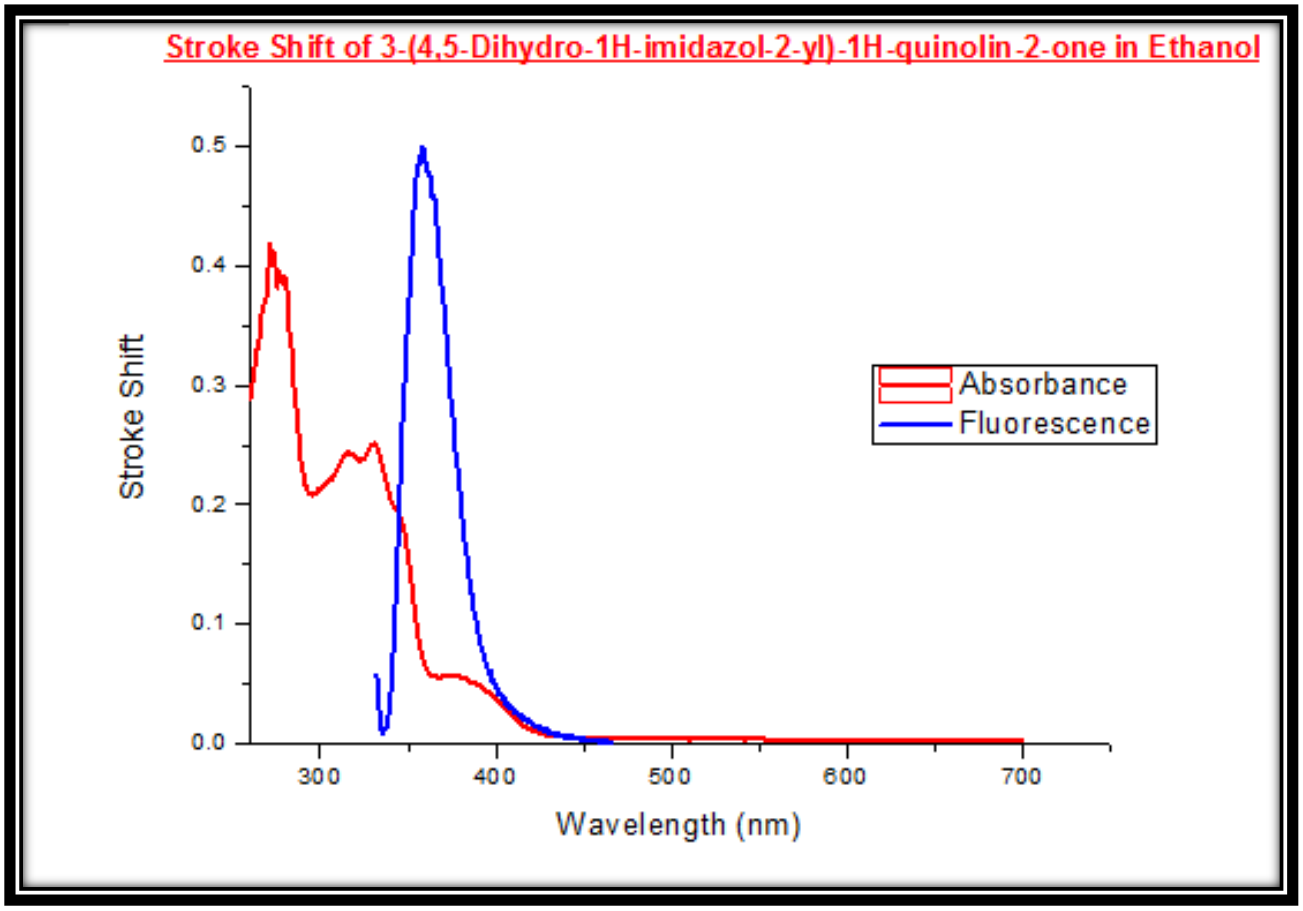

Appendix 57: Stokes Shift of Compound 2 in MeOH

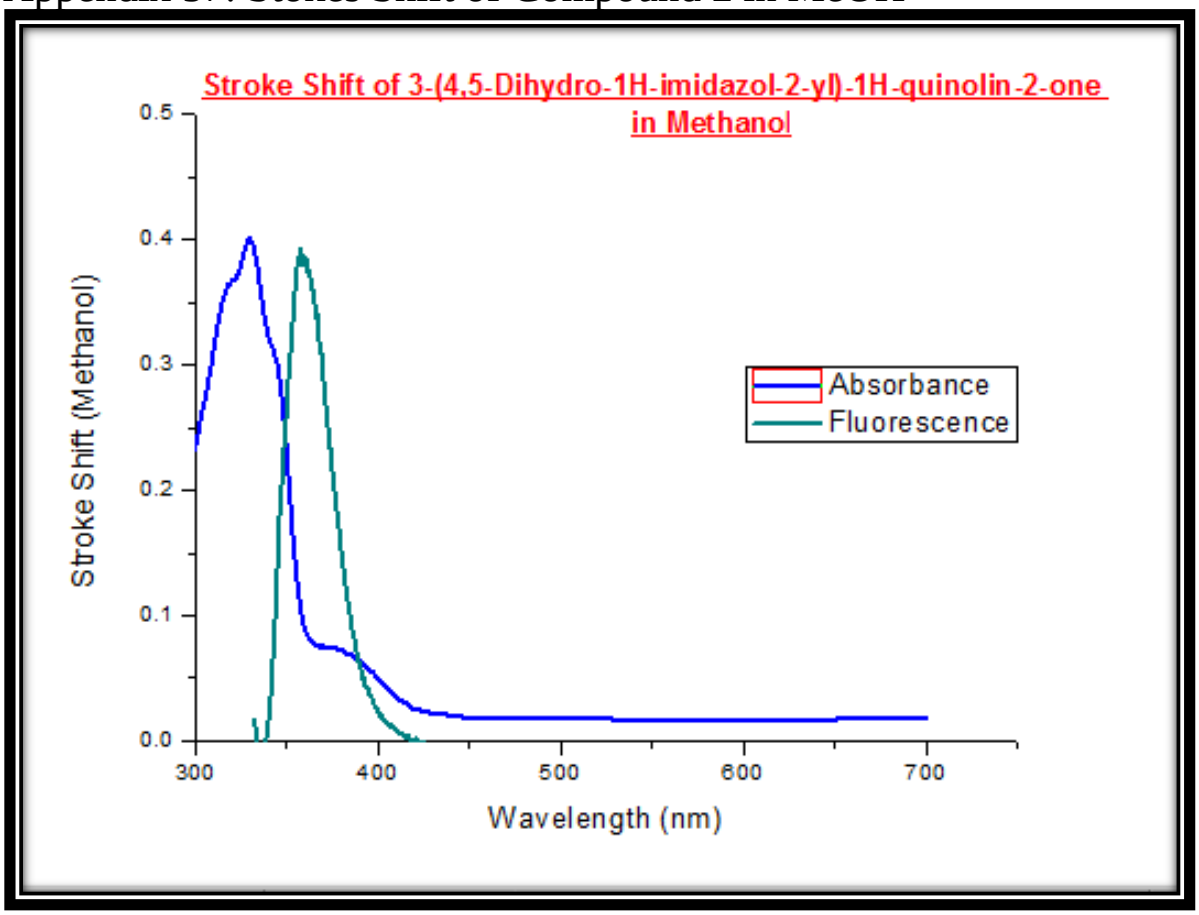

Appendix 58: Stokes Shift of Compound 2 in DCM

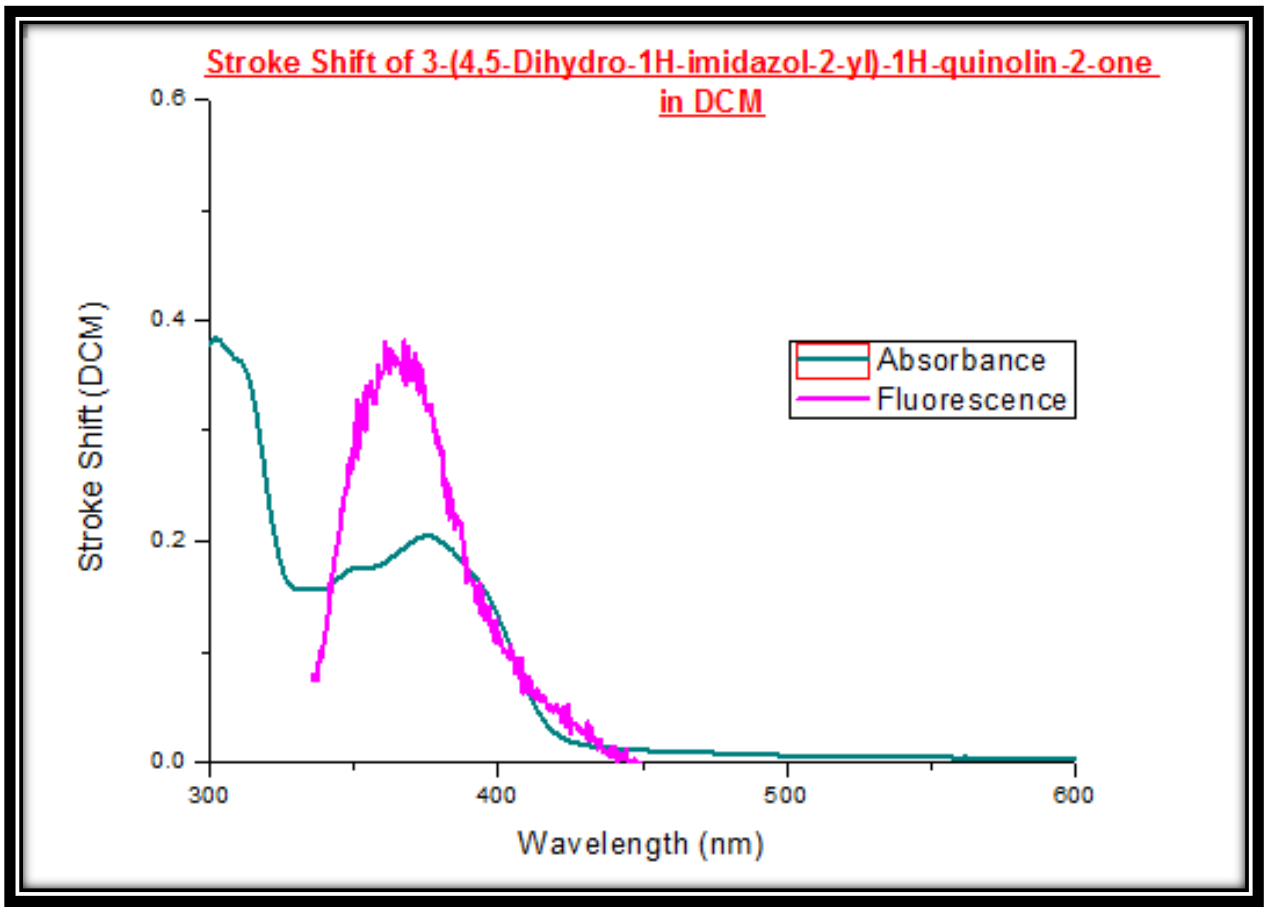

Appendix 59: Stokes Shift of Compound 2 in Chloroform

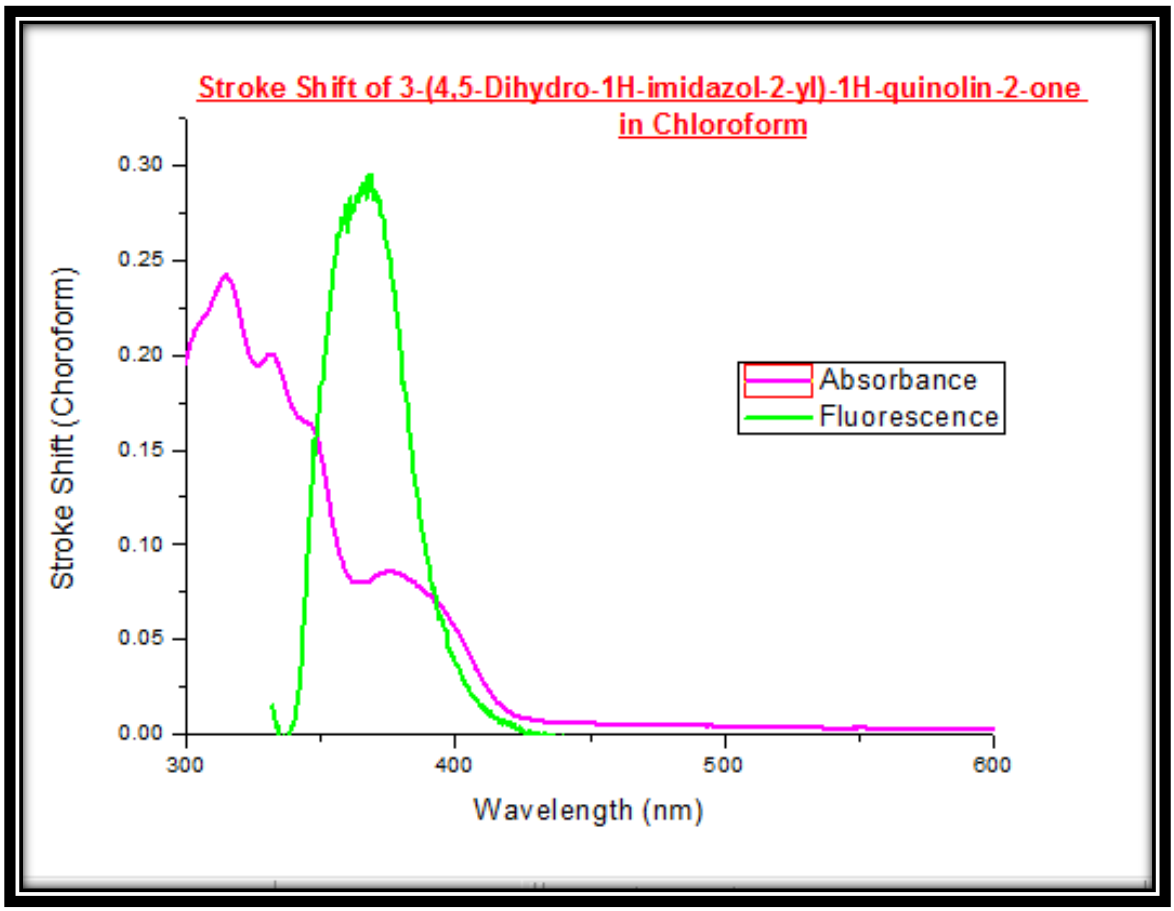

Appendix 60: Stokes Shift of Compound 2 in ACN

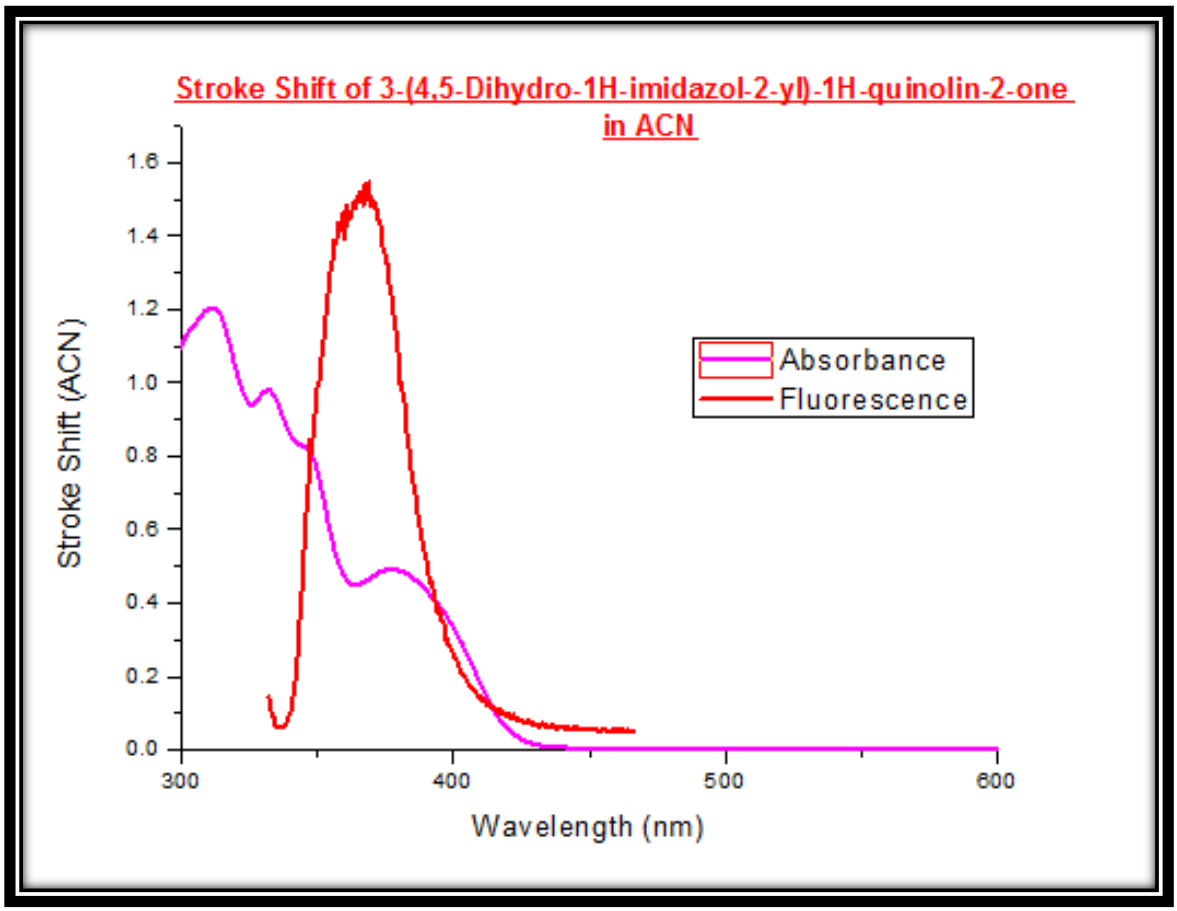

Appendix 61: Stokes Shift of Compound 3 in EtOH

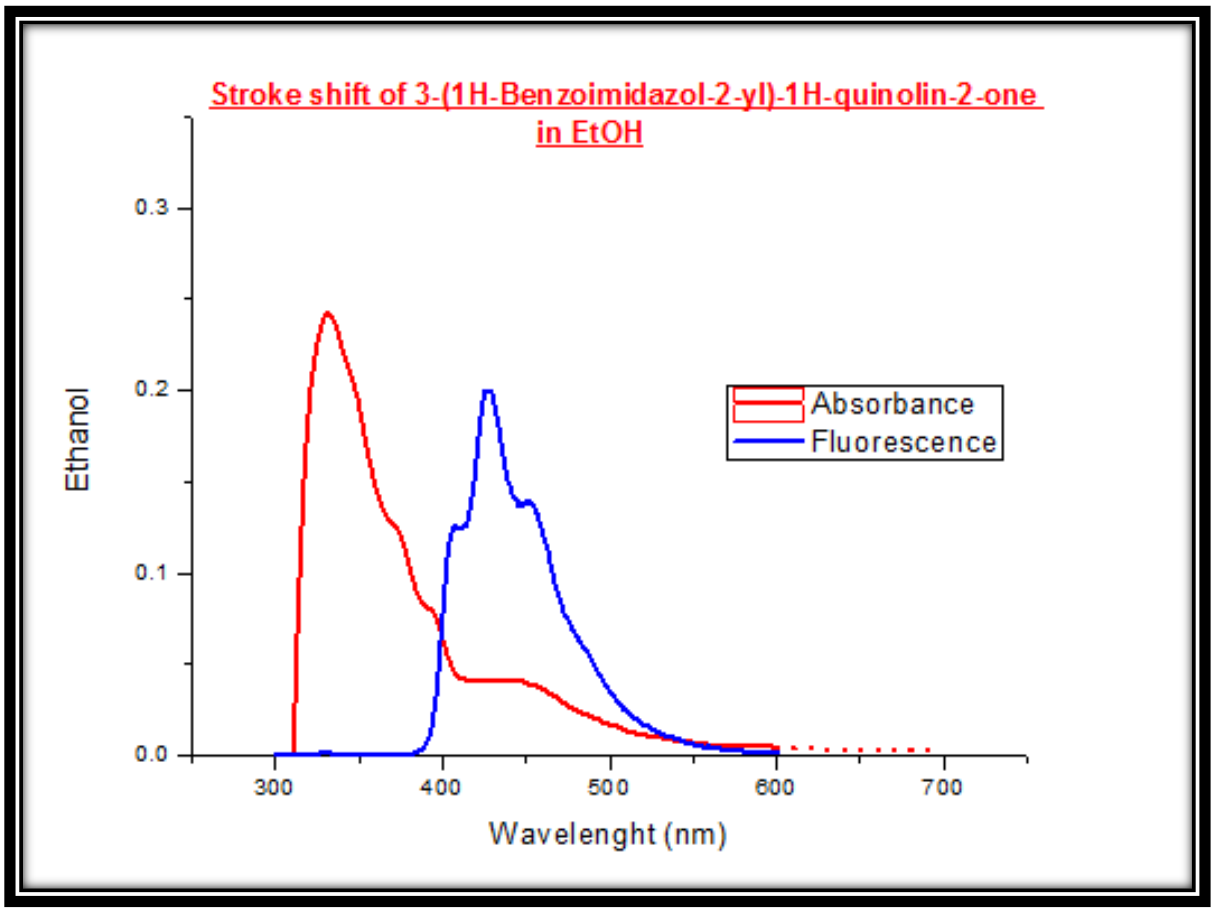

Appendix 62: Stokes Shift of Compound 3 in MeOH

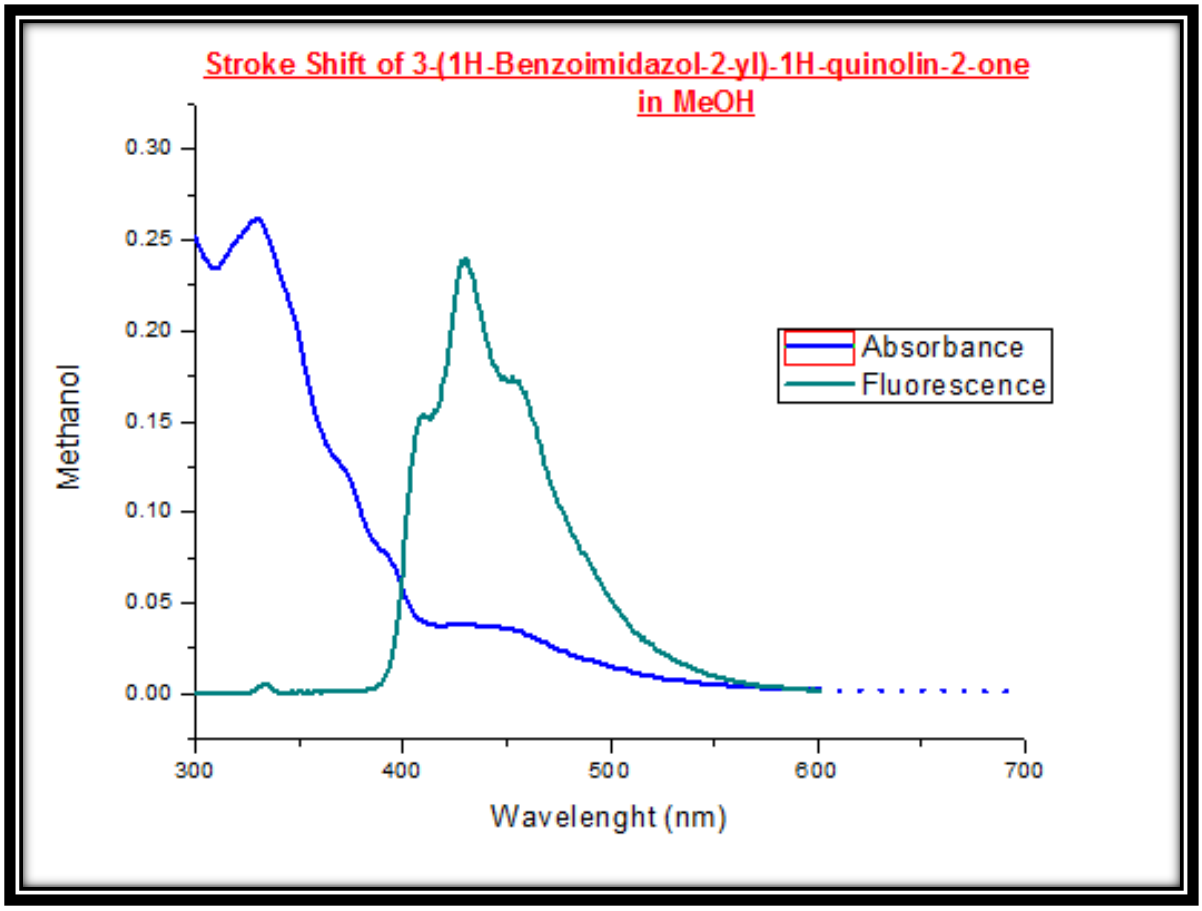

Appendix 63: Stokes Shift of Compound 3 in DCM

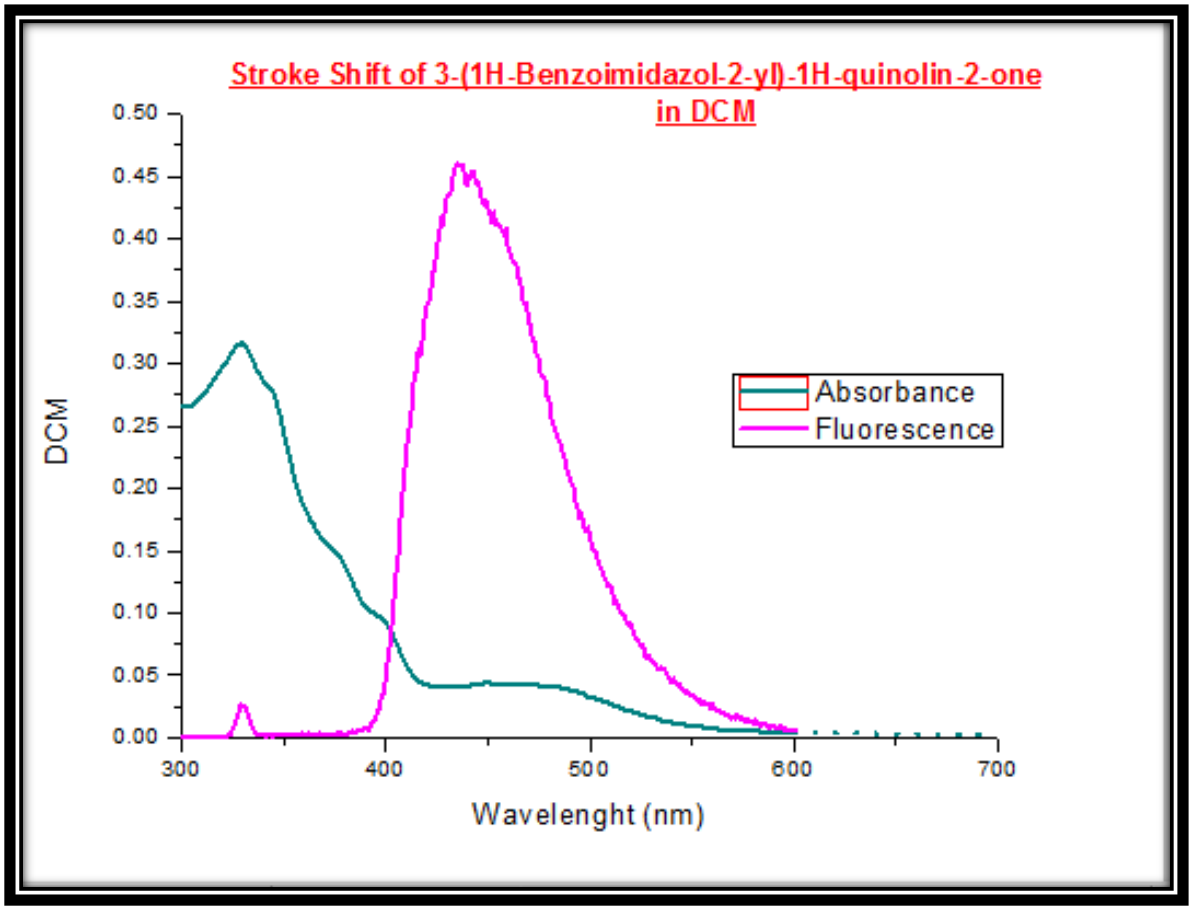

Appendix 64: Stokes Shift of Compound 3 in Chloroform

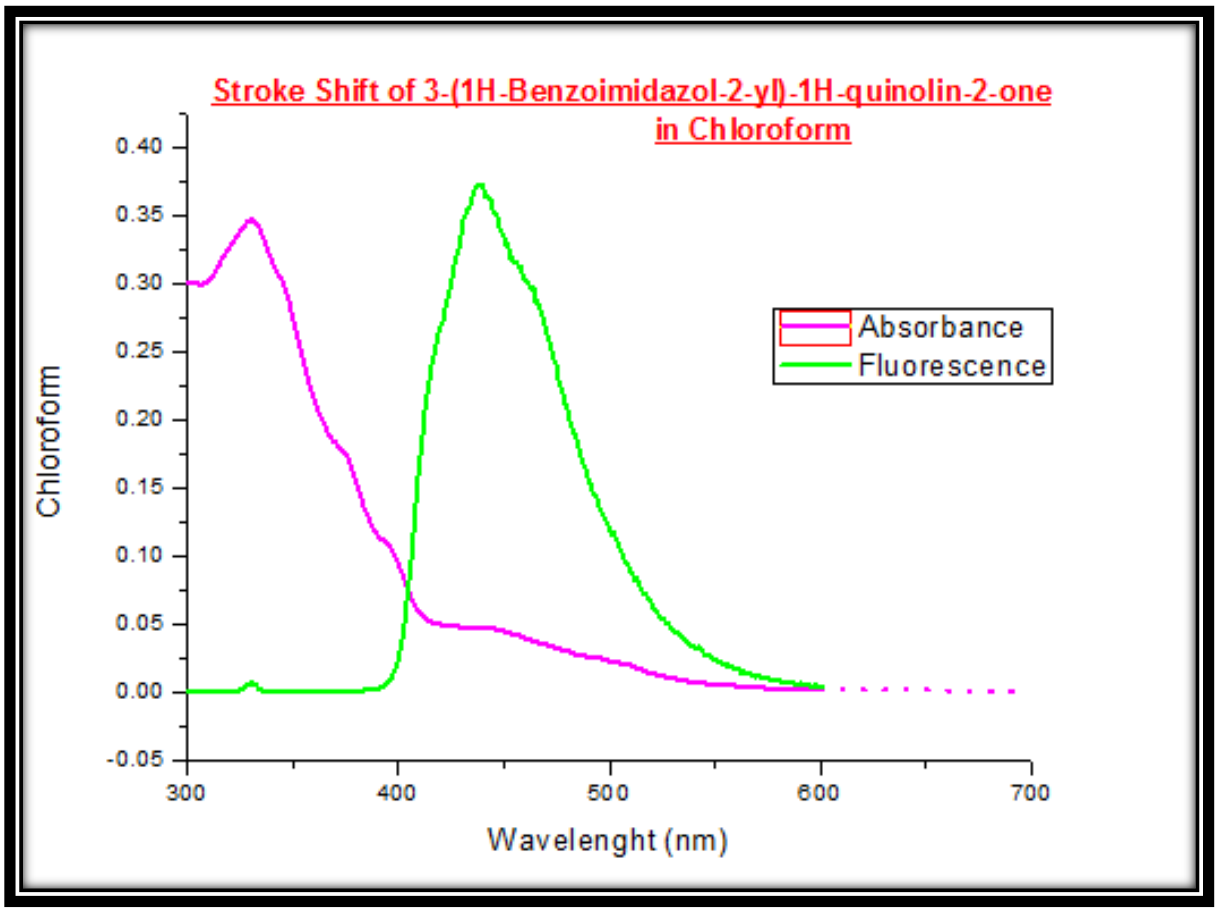

Appendix 65: Stokes Shift of Compound 3 in ACN

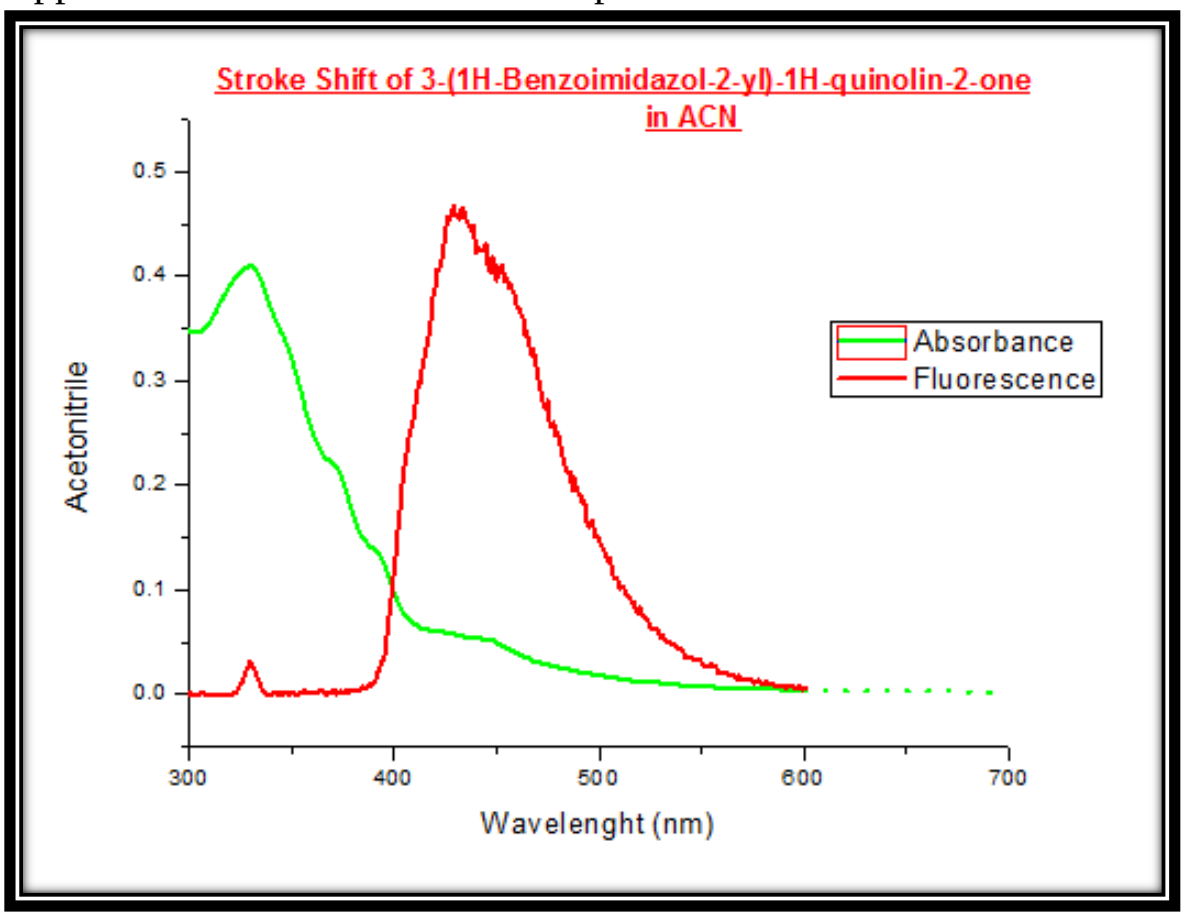

Appendix 66: Stokes Shift of Compound 4 in EtOH

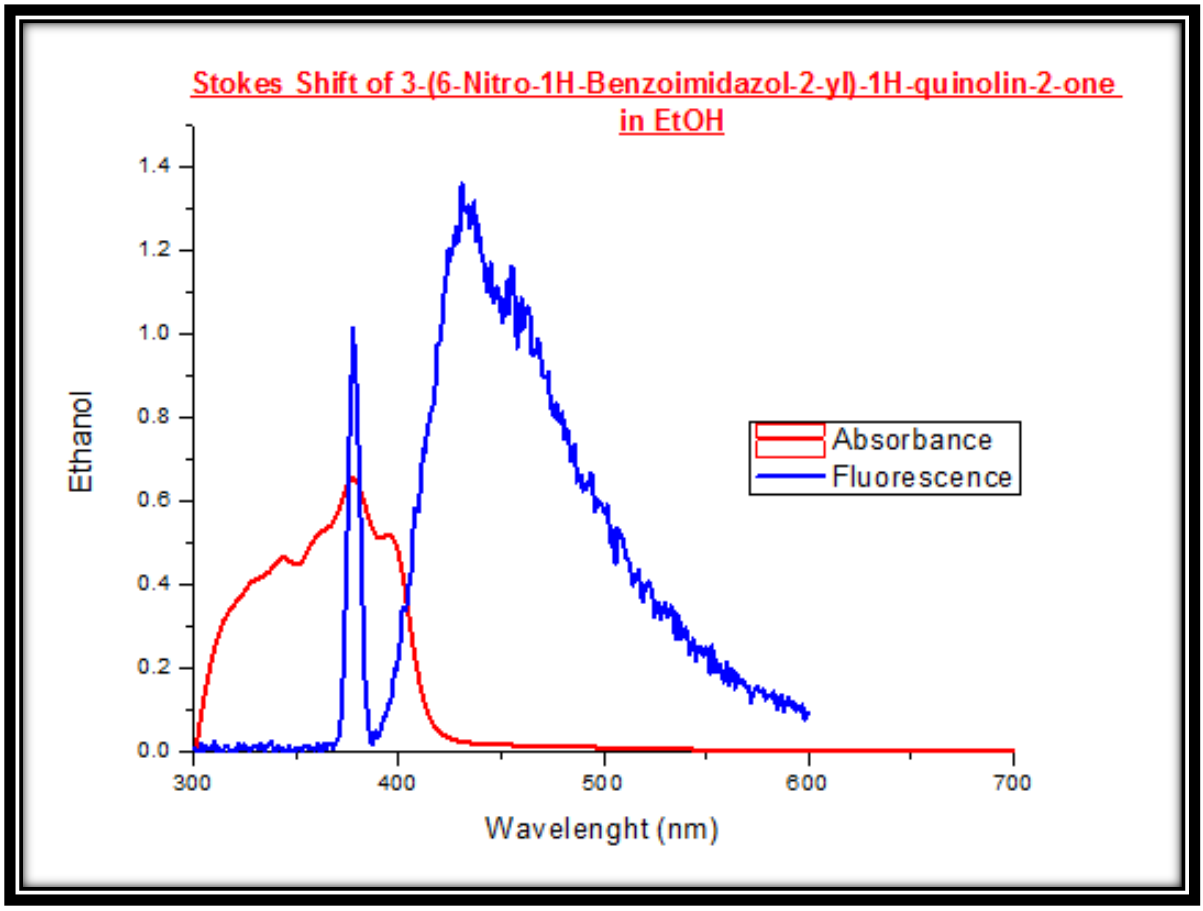

Appendix 67: Stokes Shift of Compound 4 in MeOH

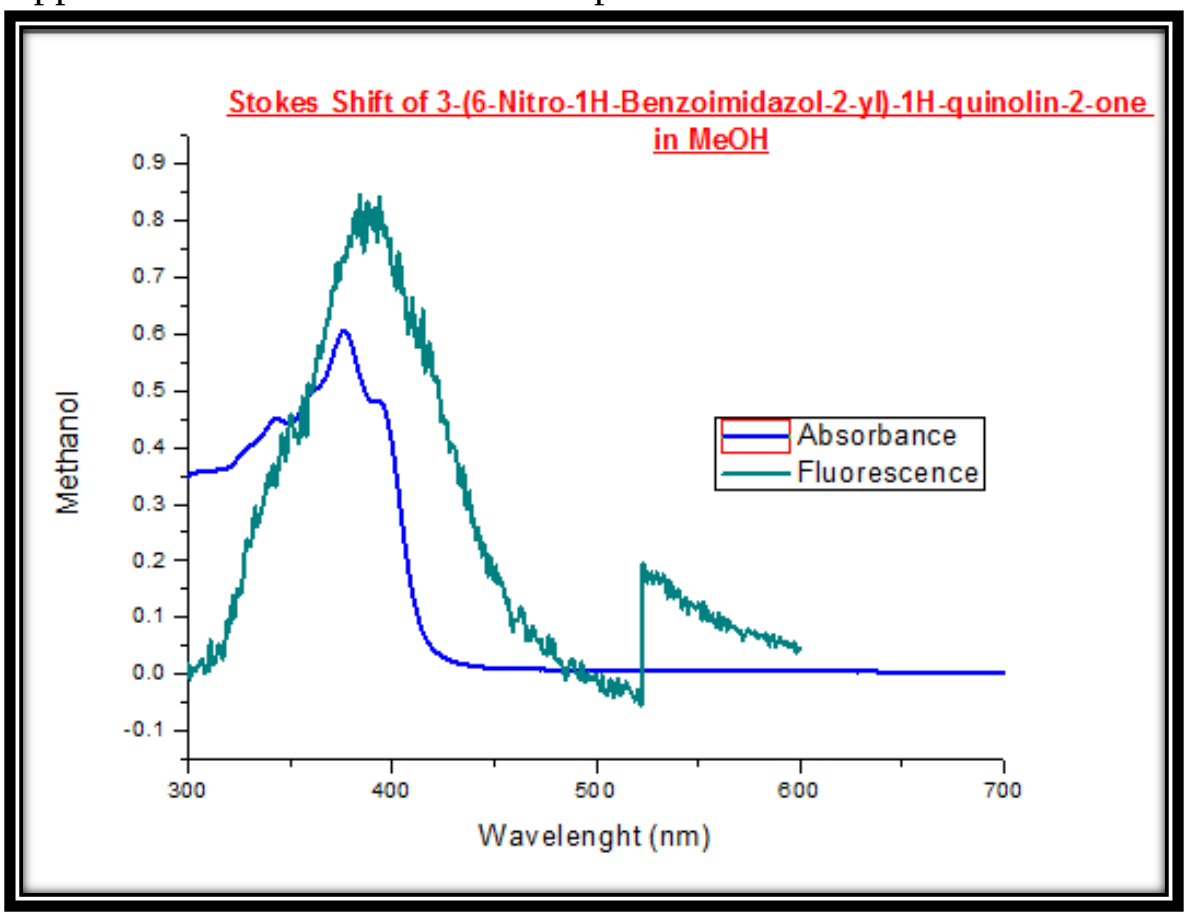

Appendix 68: Stokes Shift of Compound 4 in DCM

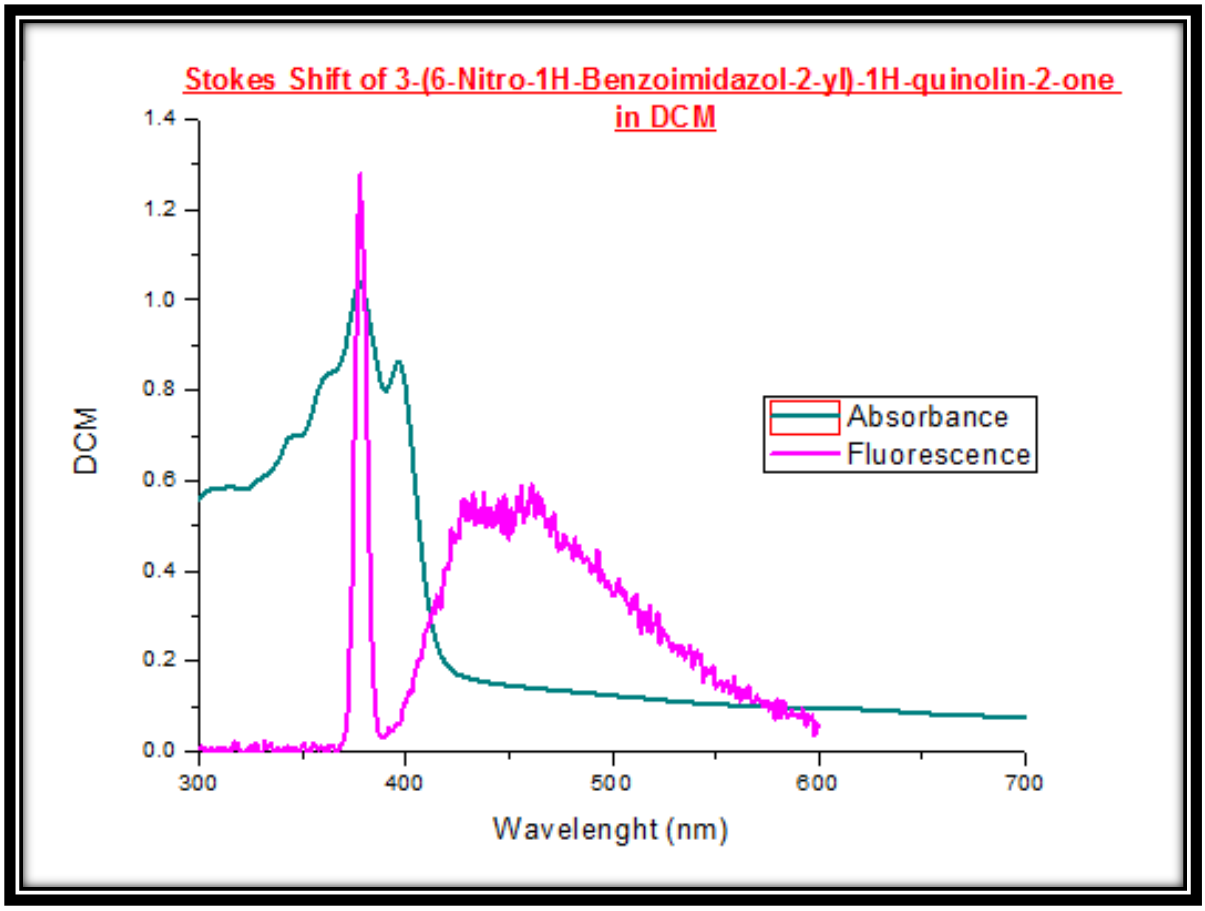

Appendix 69: Stokes Shift of Compound 4 in Chloroform

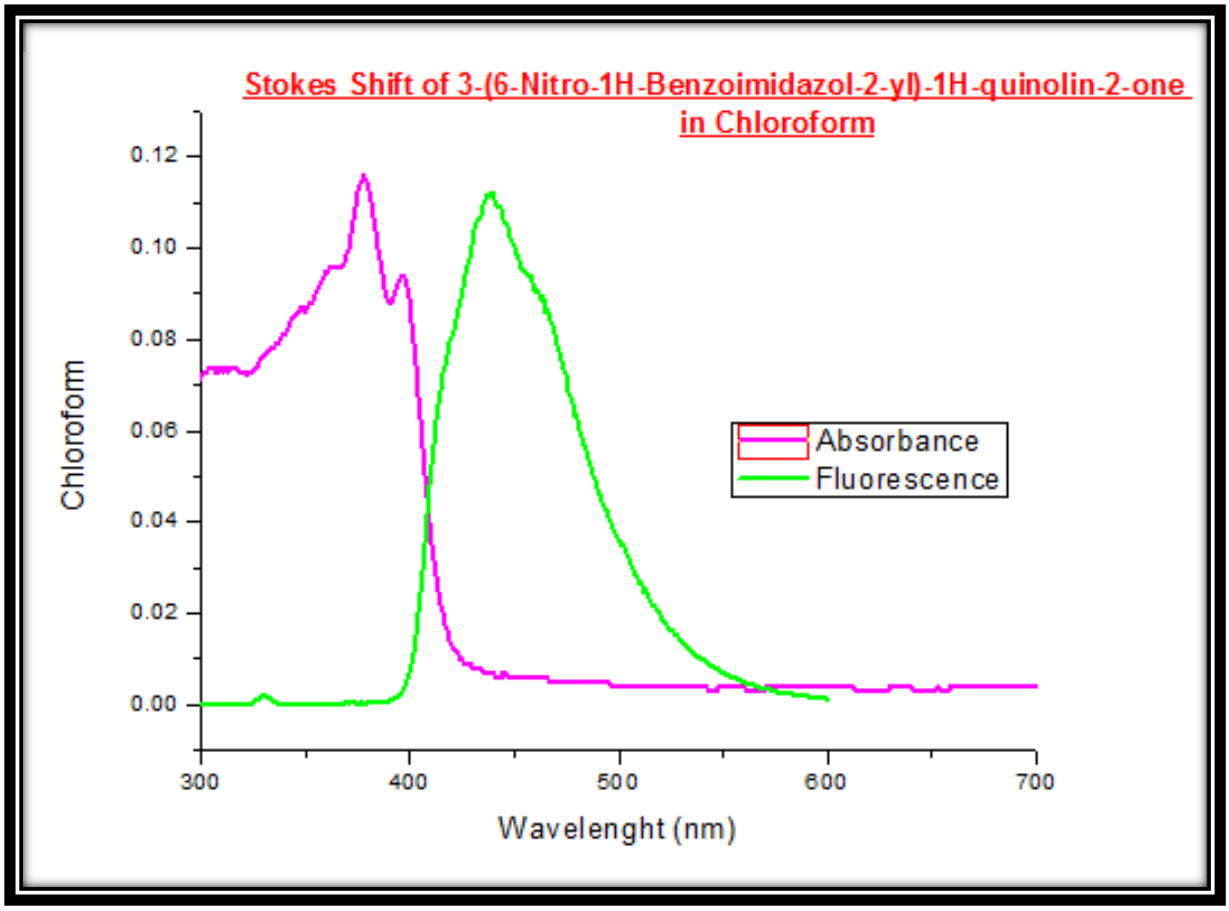

Appendix 70: Stokes Shift of Compound 4 in ACN

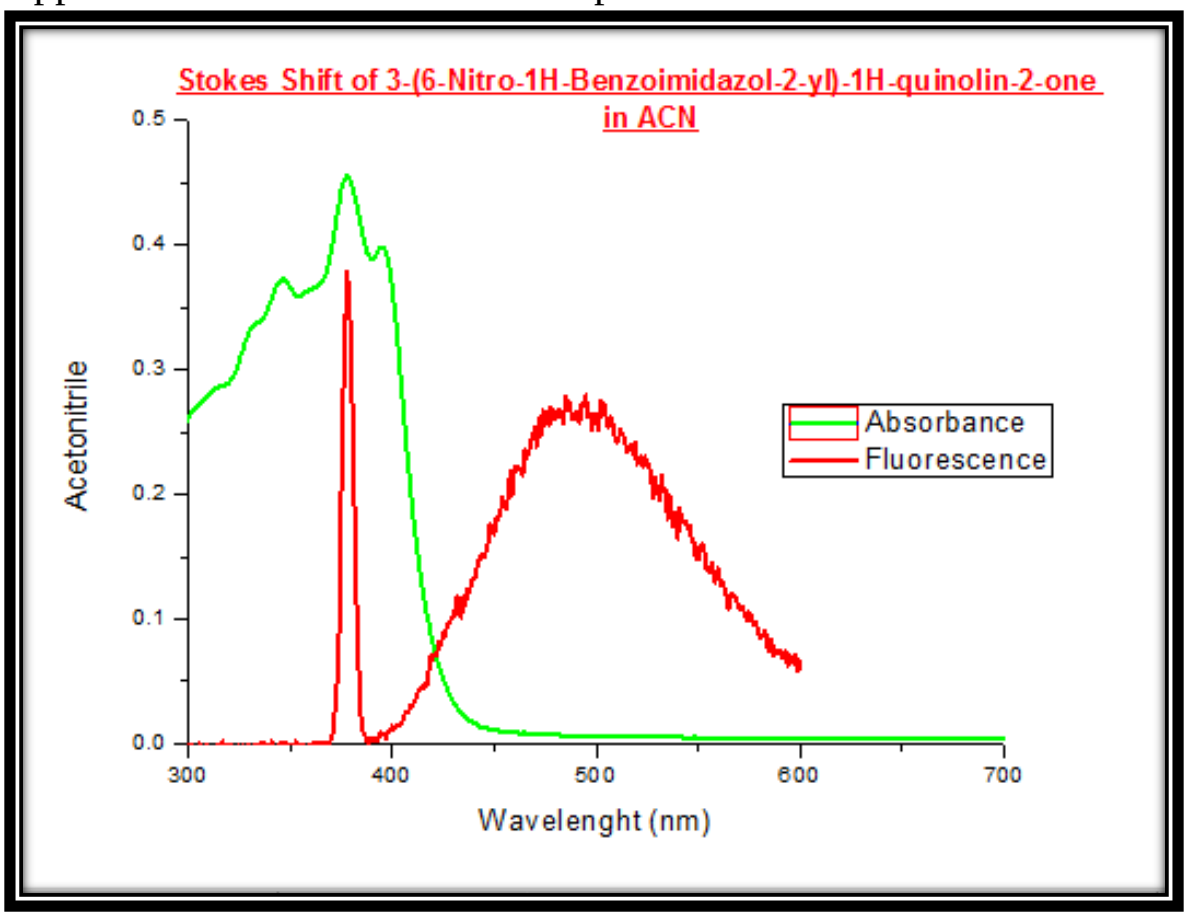

Appendix 71: Stokes Shift of Compound 7 in EtOH

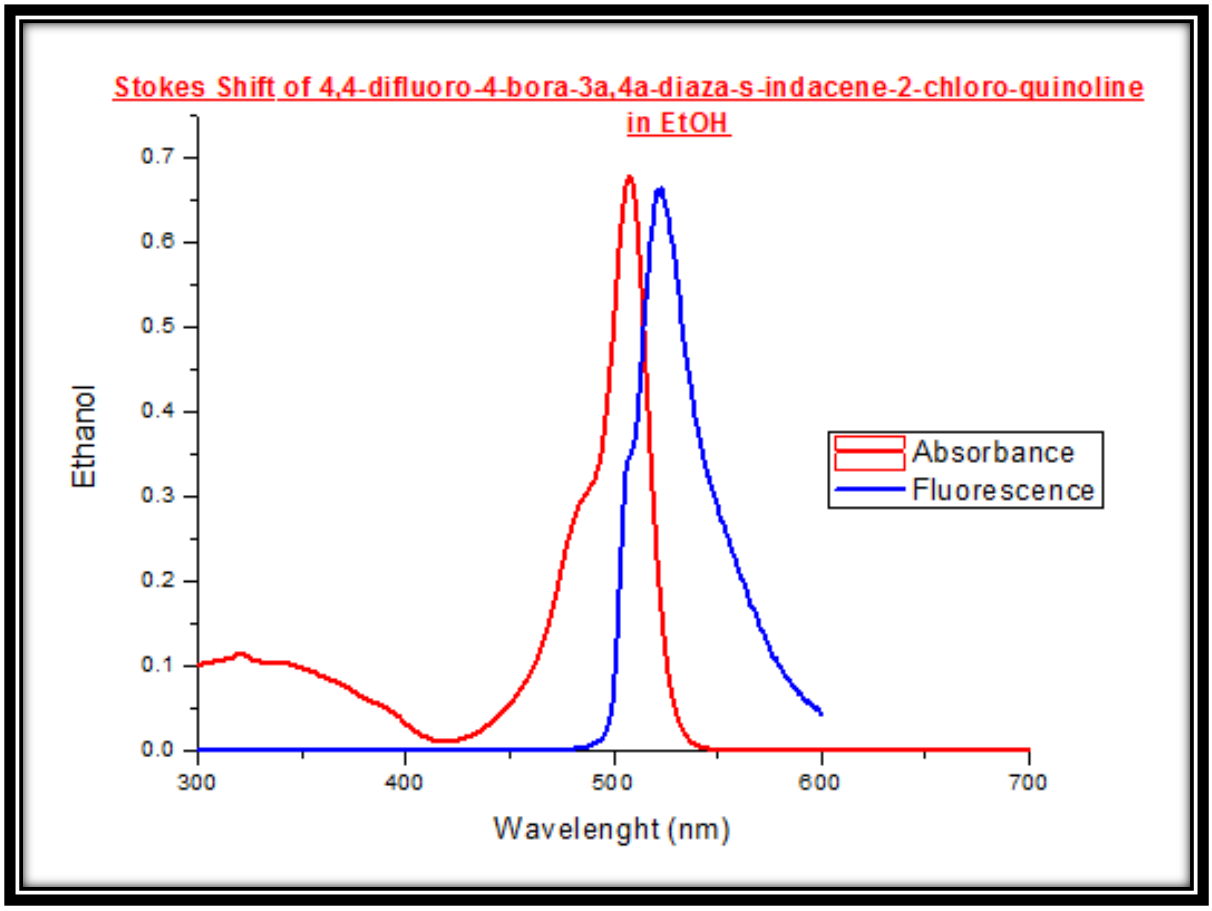

Appendix 72: Stokes Shift of Compound 7 in MeOH

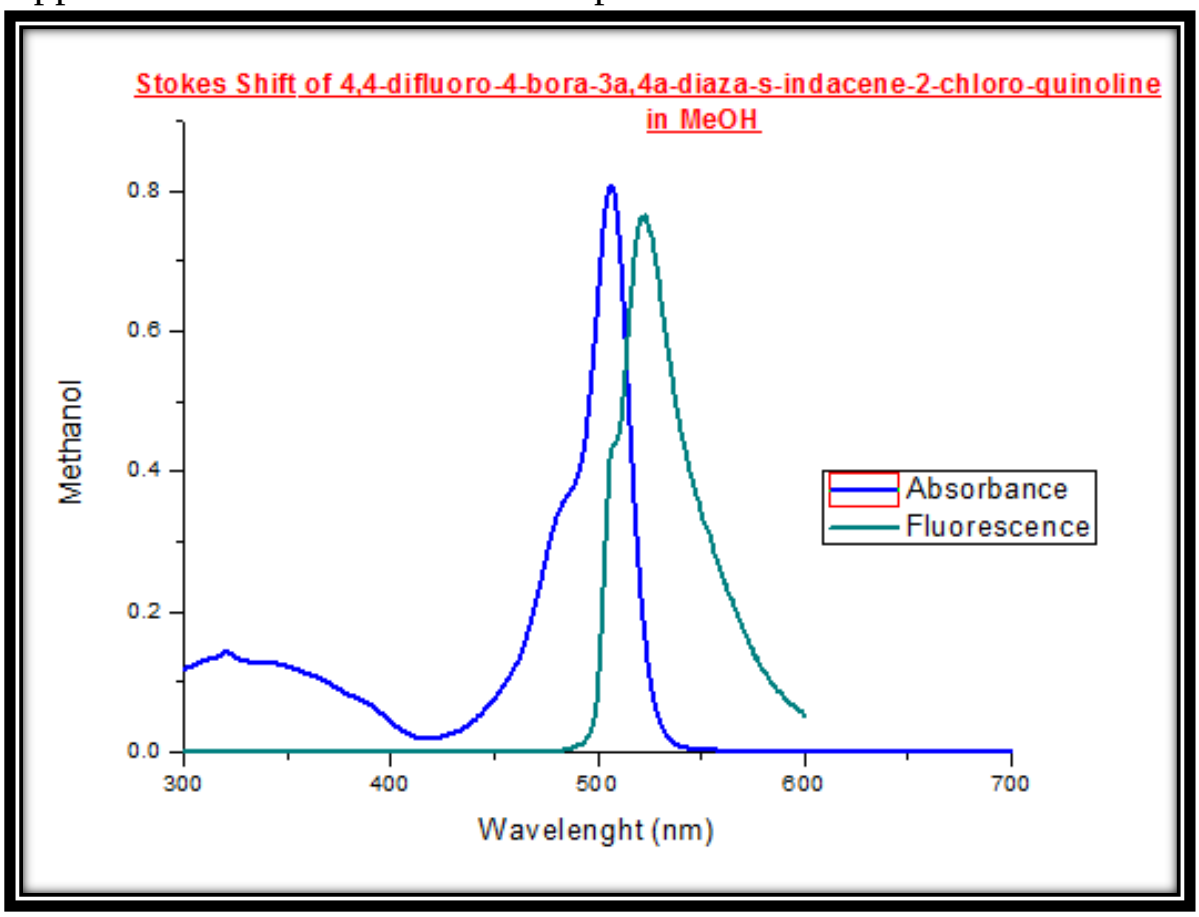

Appendix 73: Stokes Shift of Compound 7 in DCM

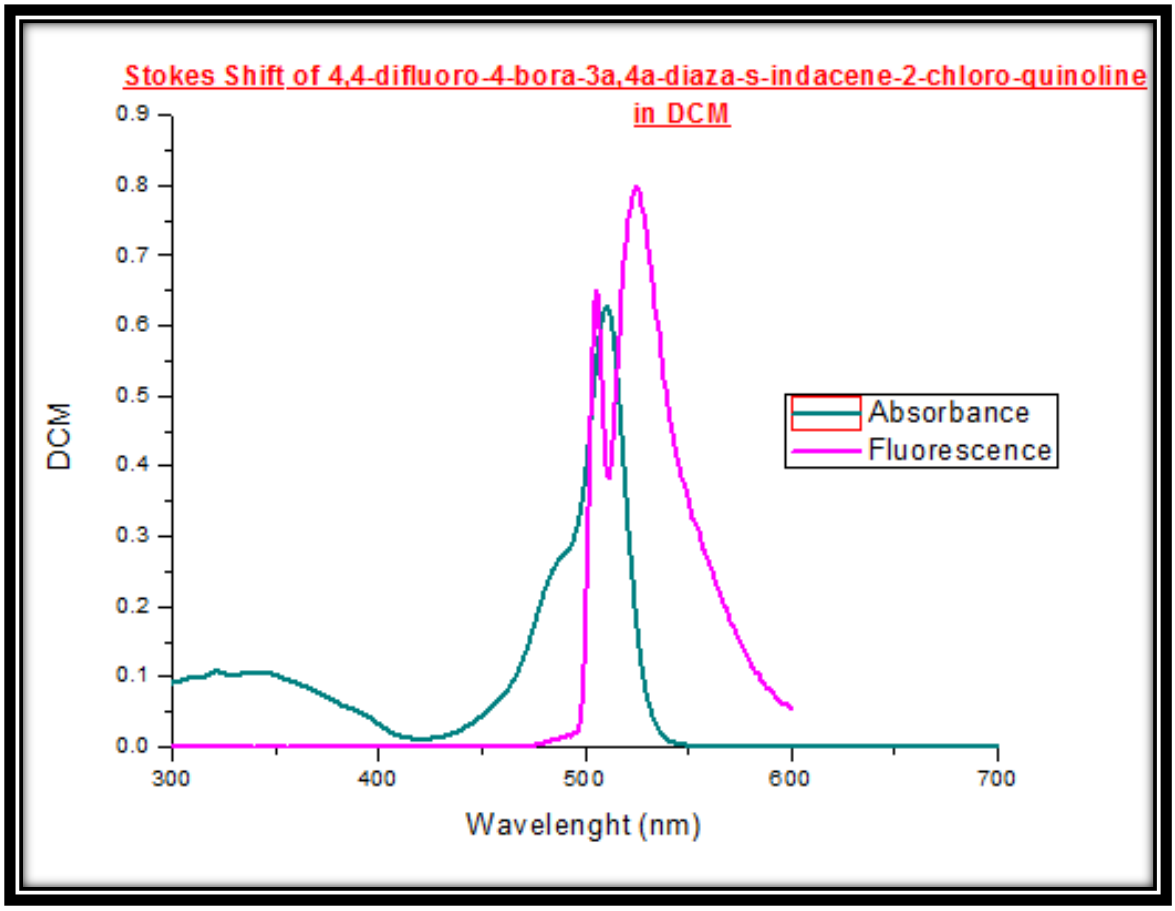

Appendix 74: Stokes Shift of Compound 7 in Chloroform

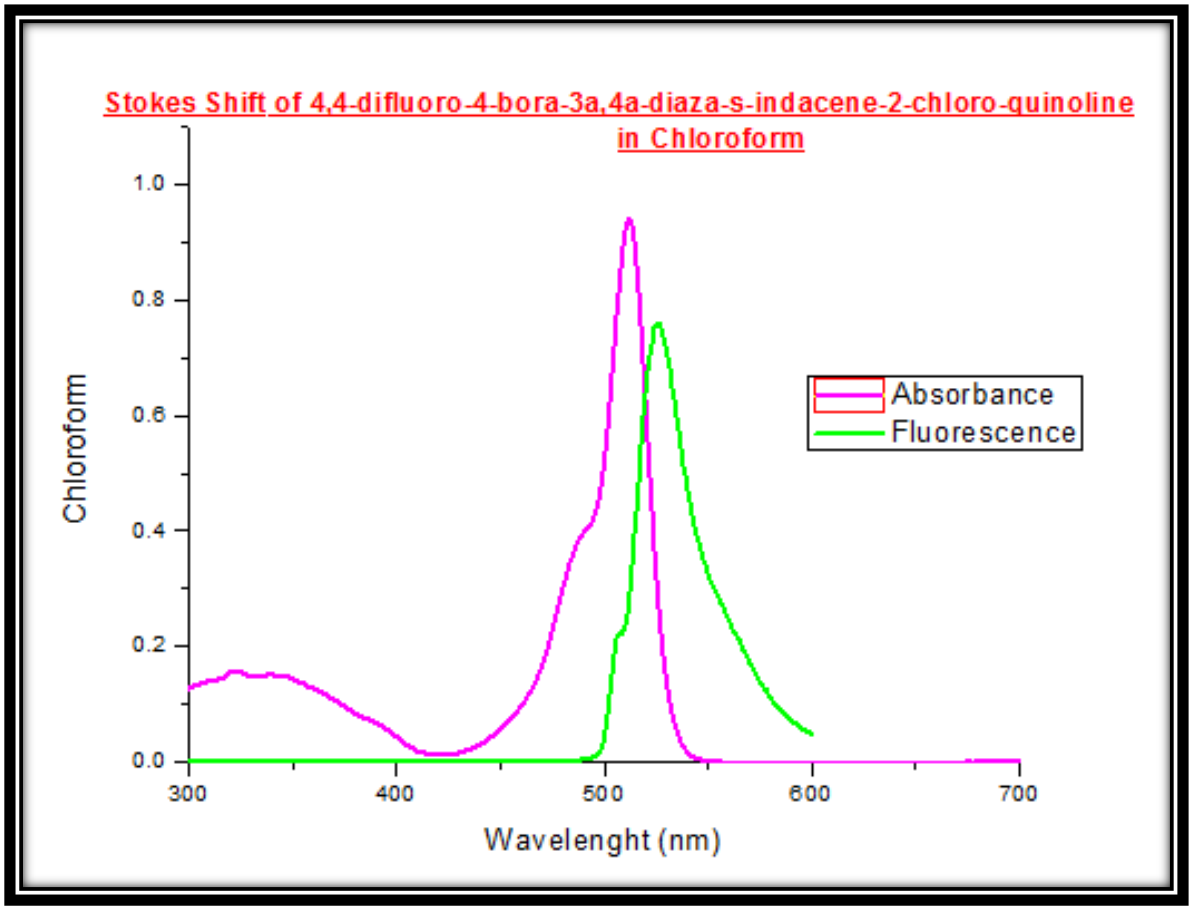

Appendix 75: Stokes Shift of Compound 7 in ACN

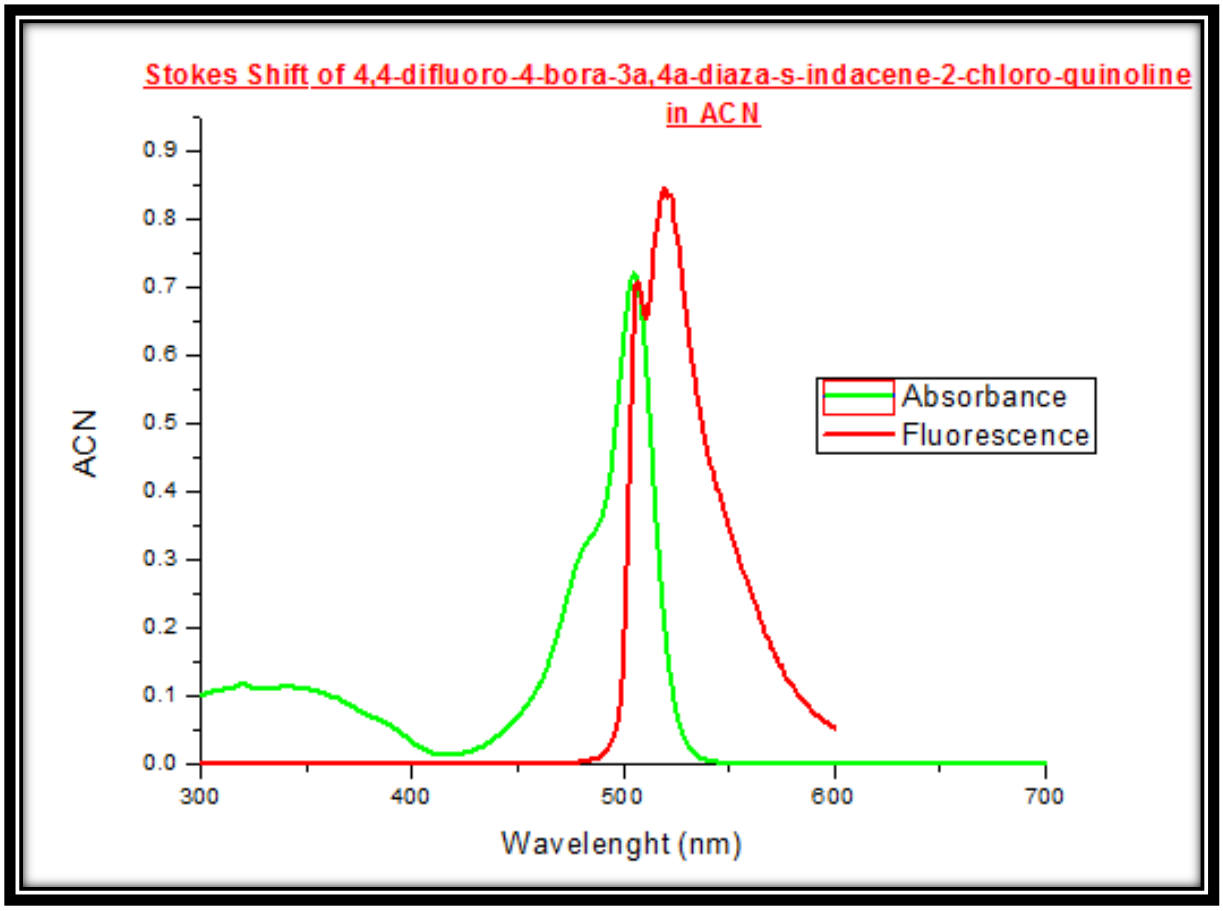

Appendix 76: Stokes Shift of Compound 5 in EtOH

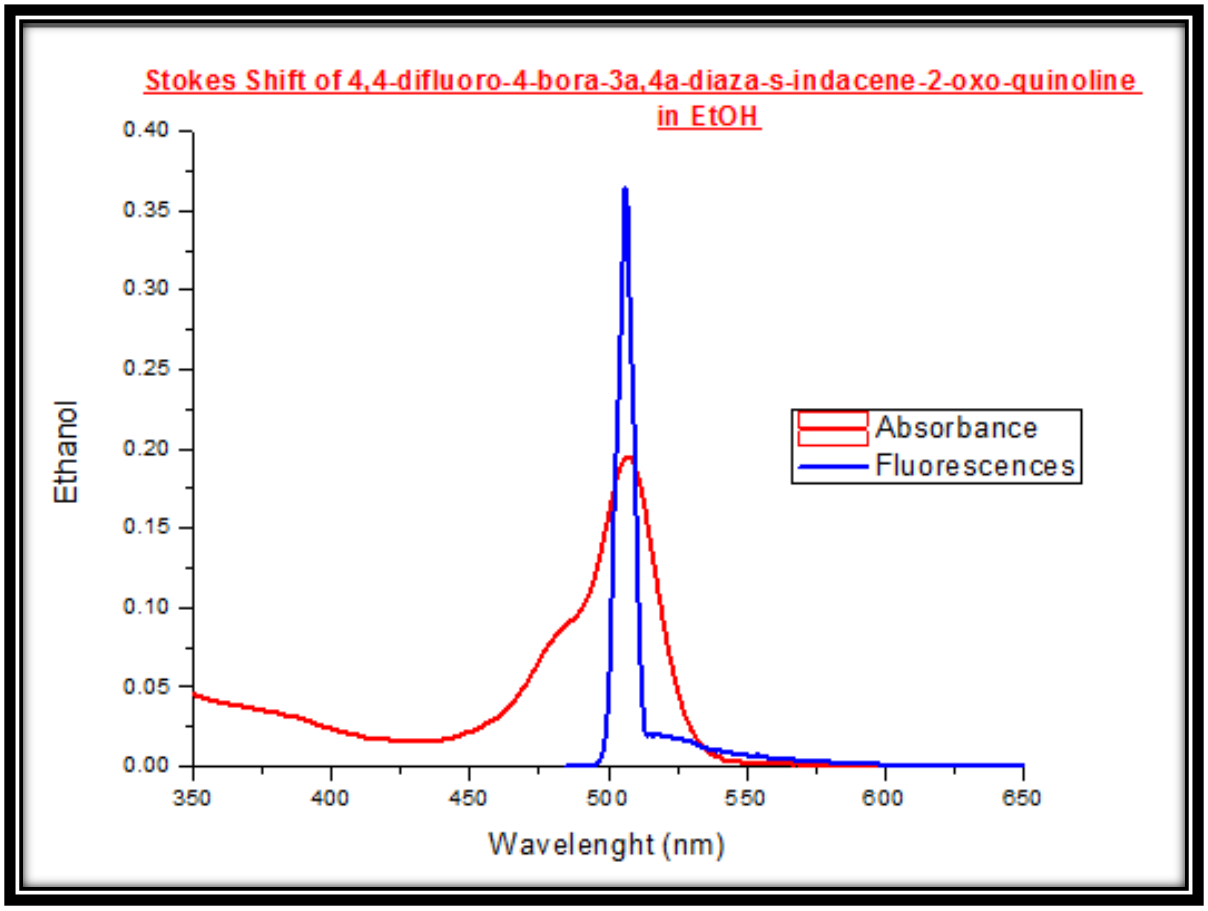

Appendix 77: Stoke Shift of Compound 5 in MeOH

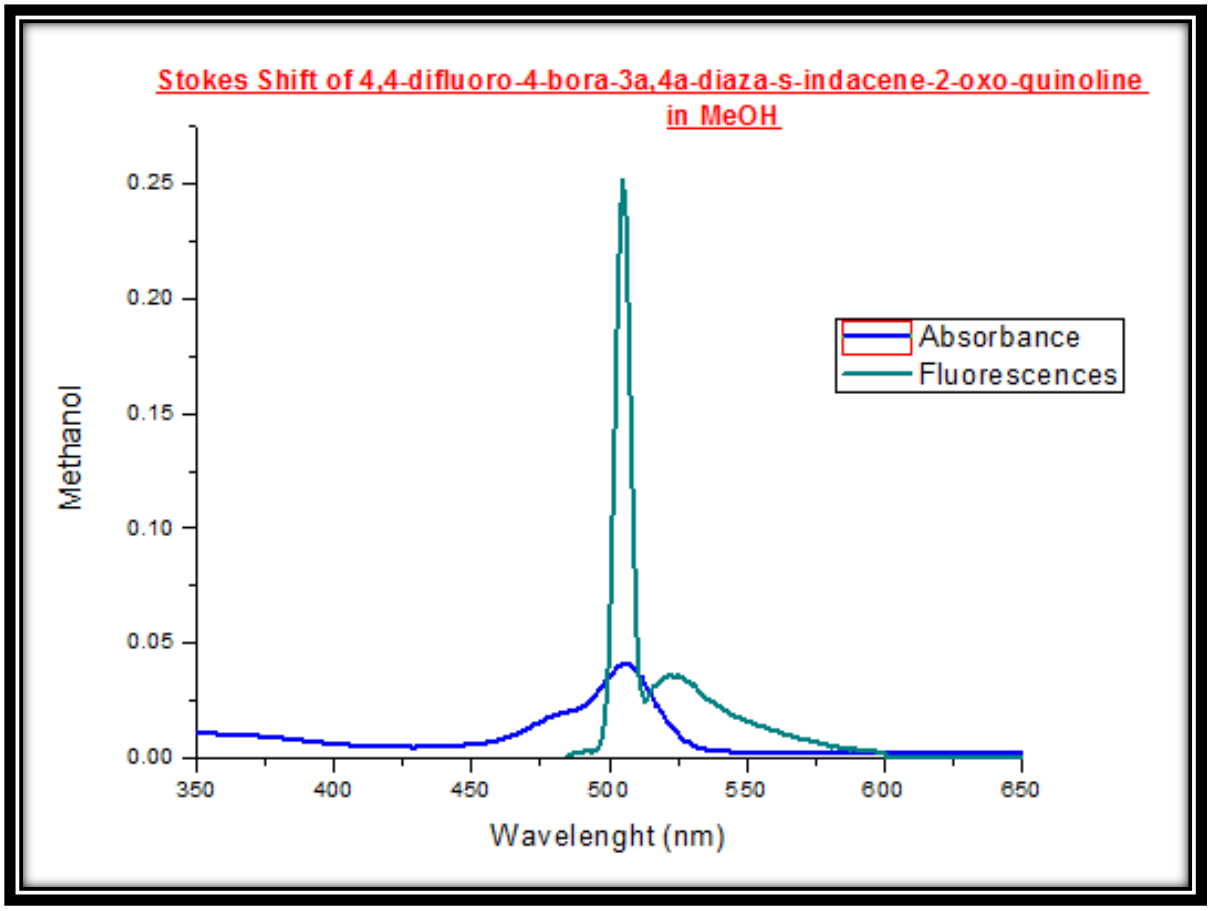

Appendix 78: Stokes Shift of Compound 5 in DCM

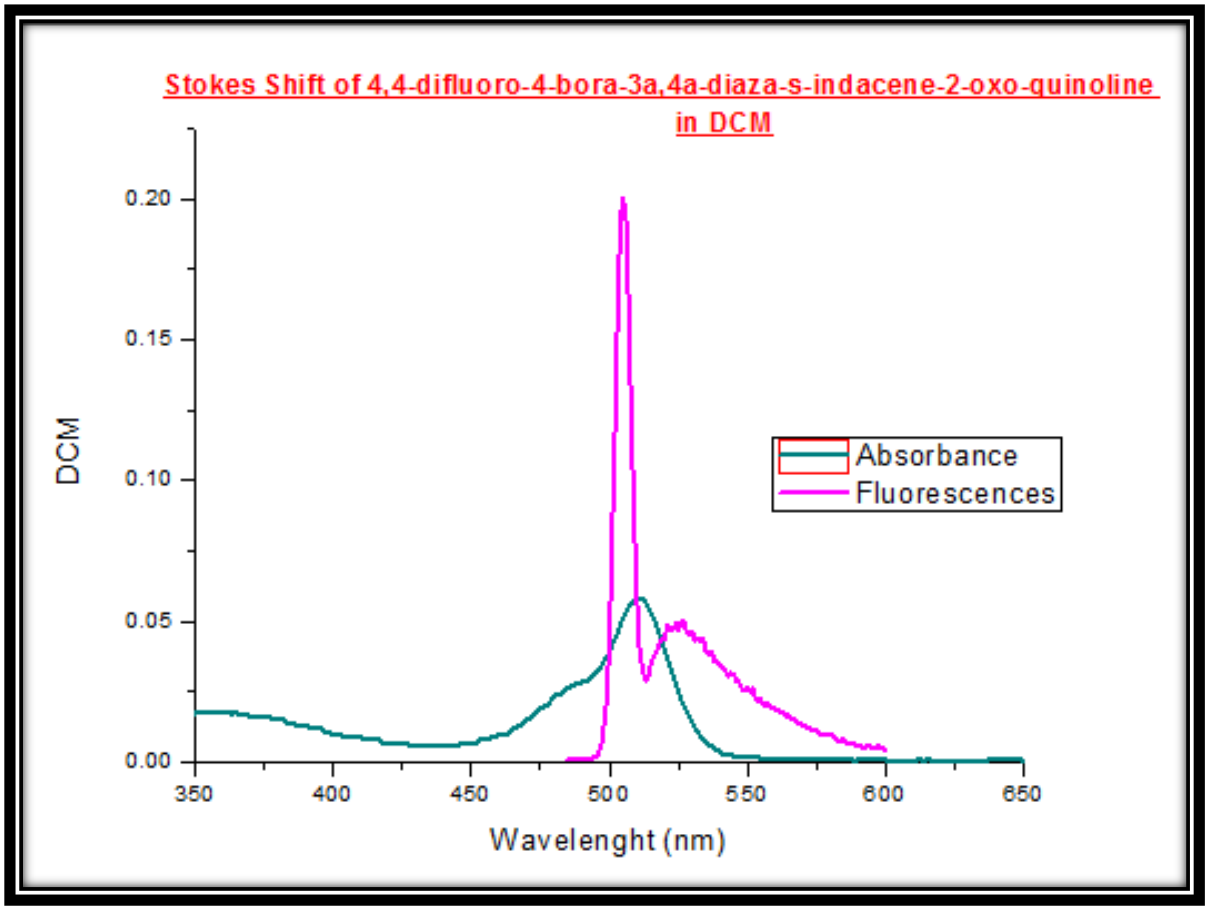

Appendix 79: Stokes Shift of Compound 5 in Chloroform

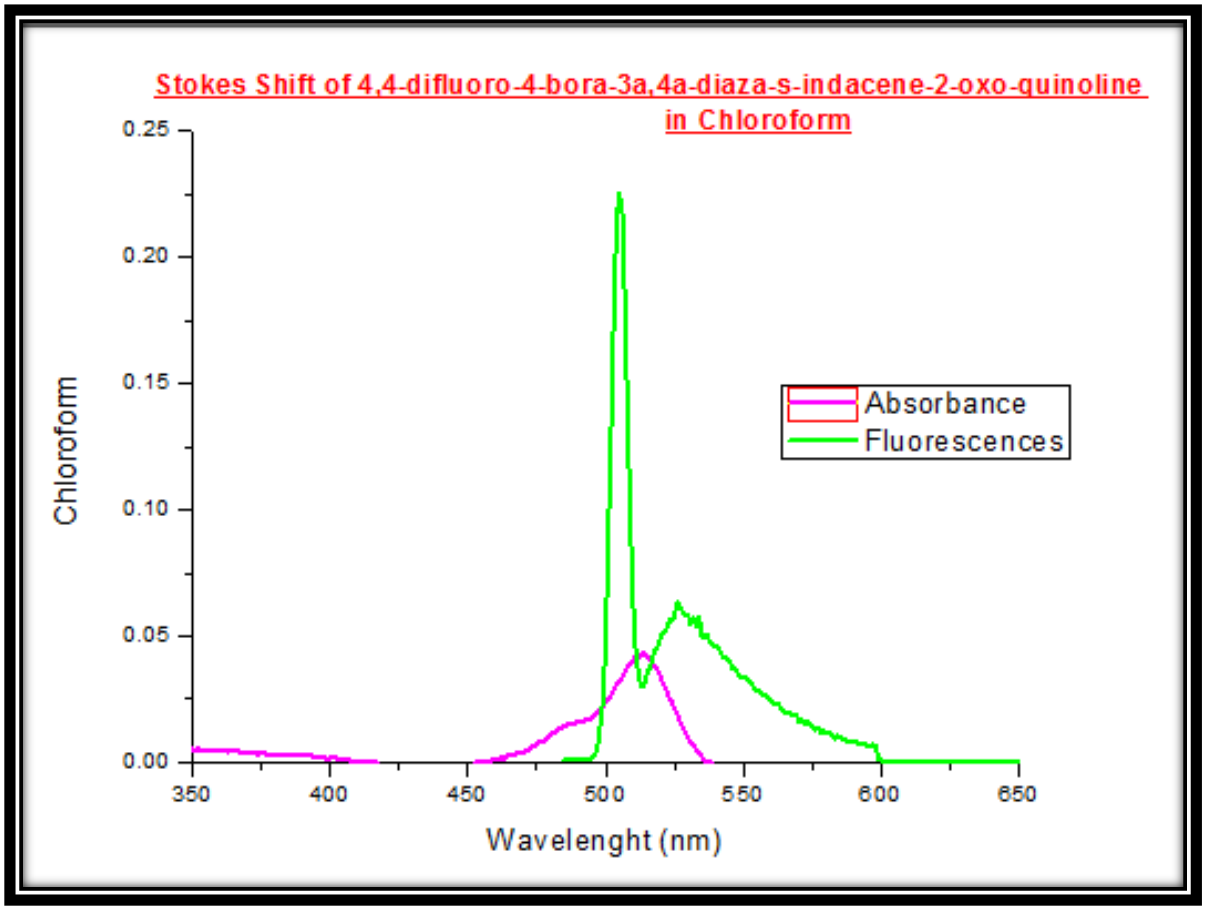

Appendix 80: Stokes Shift of Compound 5 in ACN

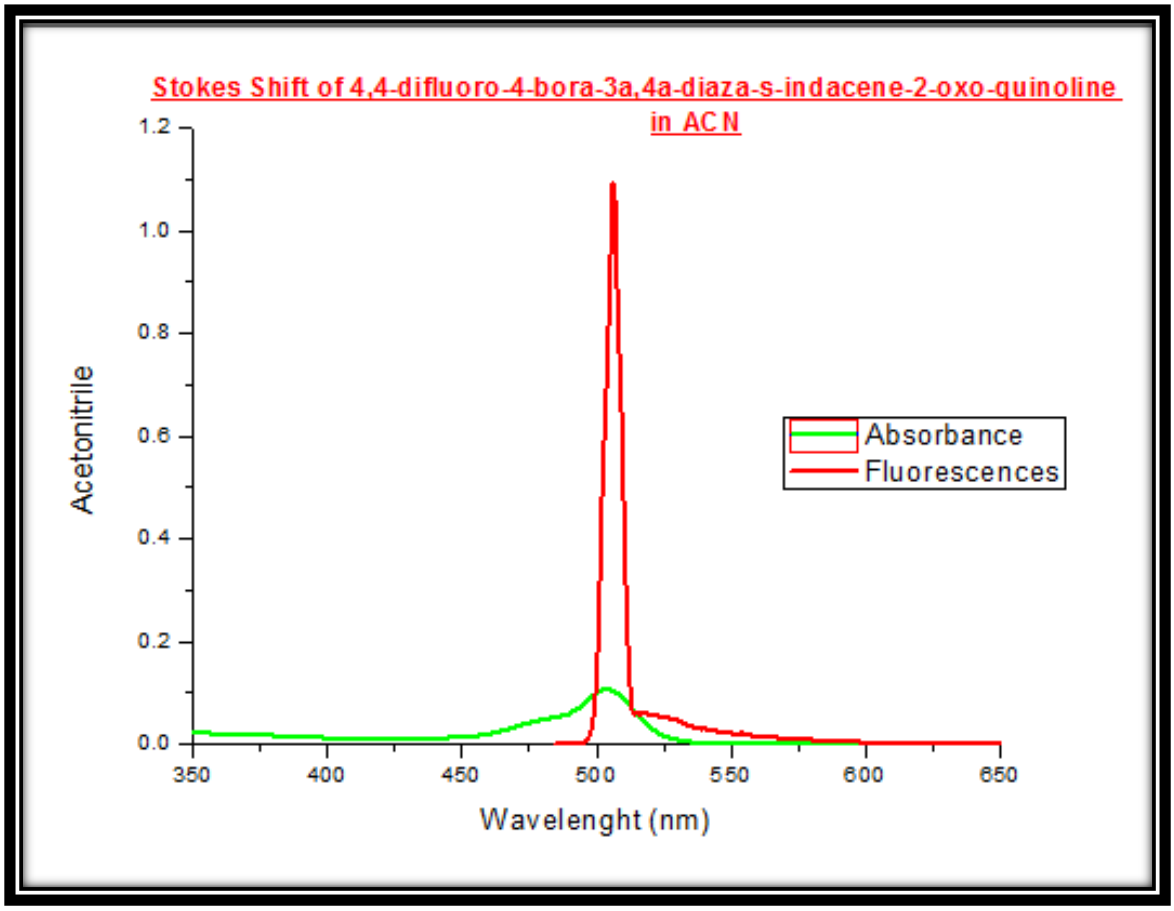

Appendix 81– Quantum Yield: UV/Vis and Fluorescence Data and Plot of UV/Vis vs. Fluorescence of Compound 2

UV/ Vis of Compound 2						
Solvents	**Wavelength**	**0.2**	**0.4**	**0.6**	**0.8**	**1**
EtOH	312	0.157	0.315	0.472	0.629	0.787
MeOH		0.221	0.441	0.662	0.883	1.103
DCM		0.239	0.477	0.716	0.955	1.193
Chloroform		0.157	0.315	0.472	0.629	0.787
Acetonitrile		0.803	1.605	2.408	3.211	4.013
Fluorescence of Compound 2						
Solvents	**Wavelength**	**0.2**	**0.4**	**0.6**	**0.8**	**1**
EtOH	384	2.067749	1.060071	2.122961	2.275541	2.141358
MeOH	382	2.111778	294776	3.052641	2.408623	7.558504
DCM	403	2.665357	2.831483	2.974759	2.864935	2.661082
Chloroform	406	0.148519	1.021828	1.177705	2.005713	1.631453
Acetonitrile	406	1.673867	3.383743	1.697037	1.691251	5.736521

Plot of UV/Vis vs. Fluorescence of Compound 2

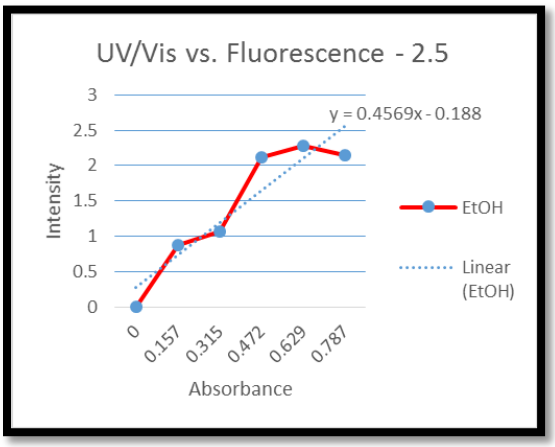

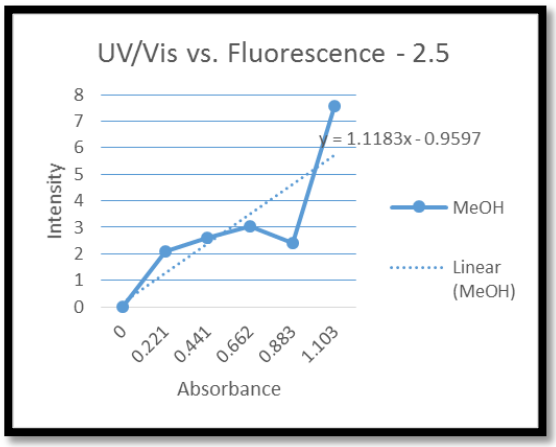

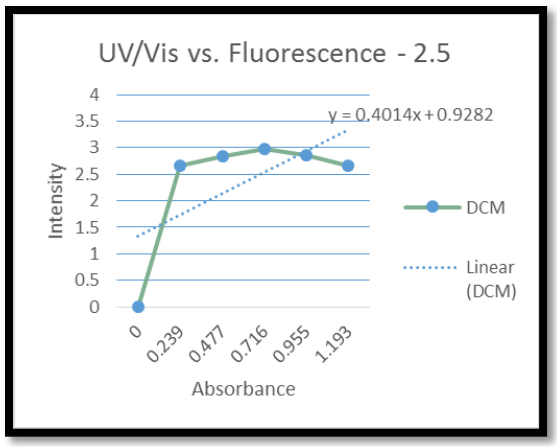
UV/Vis vs. Fluorescence - 2.5
y = 0.4014x + 0.9282
Intensity
Absorbance
DCM
Linear (DCM)
0
0.239
0.477
0.716
0.955
1.193

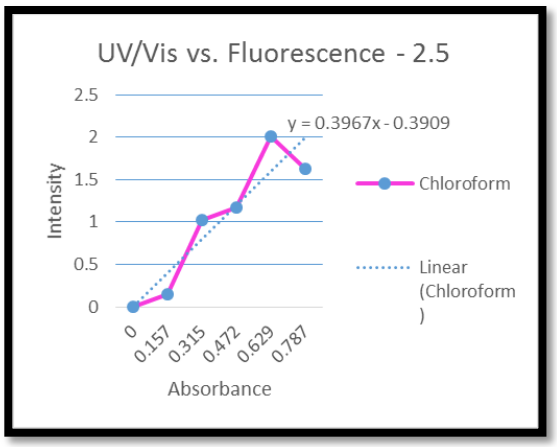
UV/Vis vs. Fluorescence - 2.5
y = 0.3967x - 0.3909
Intensity
Absorbance
Chloroform
Linear (Chloroform)
0
0.157
0.315
0.472
0.629
0.787

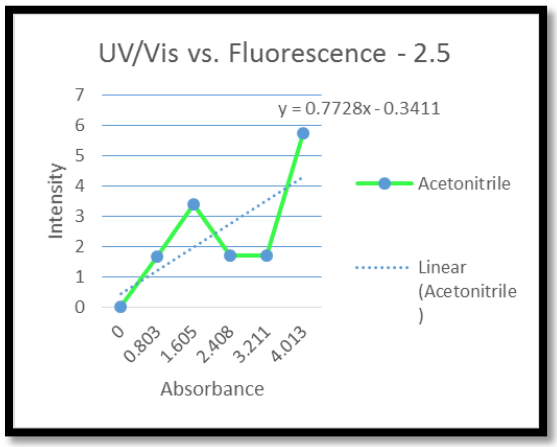
UV/Vis vs. Fluorescence - 2.5
y = 0.7728x - 0.3411
Intensity
Absorbance
Acetonitrile
Linear (Acetonitrile)
0
0.803
1.605
2.408
3.211
4.013

Appendix 82– Quantum Yield: UV/Vis and Fluorescence Data and Plot of UV/Vis vs. Fluorescence of Compound 3

UV/ Vis of Compound 2.7							
Solvents	**Wavelength**	**0**	**0.2**	**0.4**	**0.6**	**0.8**	**1**
EtOH	330	0.000	0.006	0.013	0.019	0.026	0.032
MeOH		0.000	0.005	0.009	0.014	0.018	0.023
DCM		0.000	0.013	0.027	0.040	0.053	0.067
Chloroform		0.000	0.010	0.019	0.029	0.038	0.048
Acetonitrile		0.000	0.013	0.027	0.040	0.053	0.067
Fluorescence of Compound 2.7							
Solvents	**Wavelength**	**0**	**0.2**	**0.4**	**0.6**	**0.8**	**1**
EtOH	430	0	25.42599	33.58843	45.59742	106.6554	67.69821
MeOH	428	0	15.35608	22.23593	30.7813	60.95342	52.22667
DCM	430	0	22.77365	15.8723	20.57736	39.14484	19.35352
Chloroform	430	0	10.55564	18.70501	23.80681	43.05437	35.22449
Acetonitrile	407	0	5.226651	11.48271	12.85164	24.20628	30.61215

Plot of UV/Vis vs. Fluorescence of Compound 3

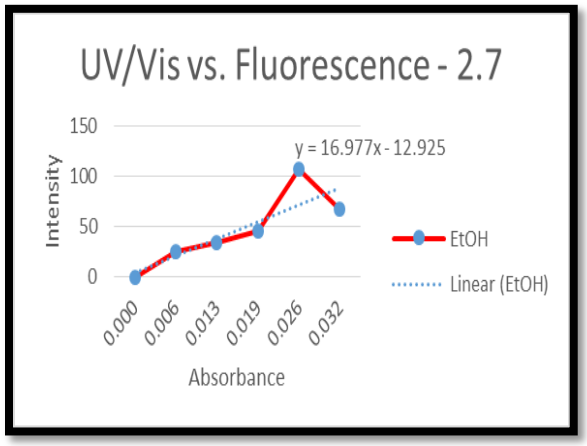

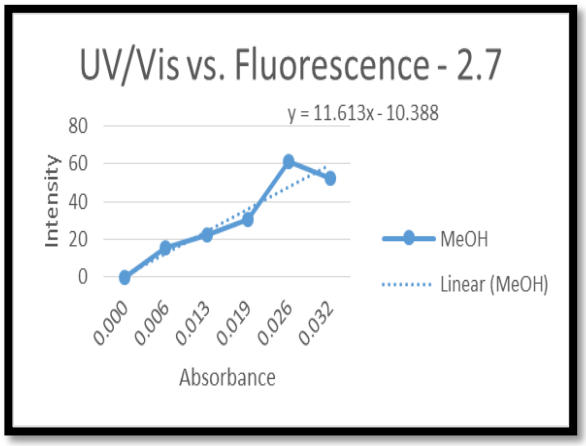

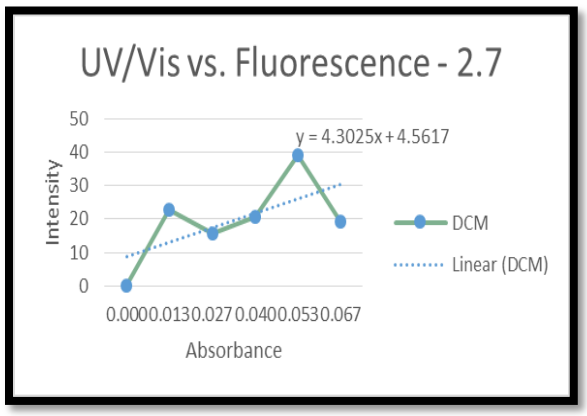

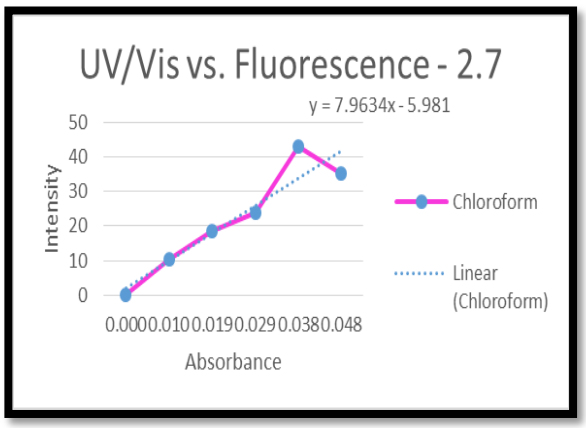

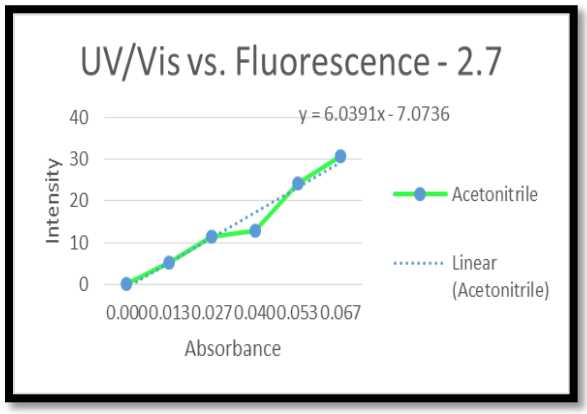

Appendix 83 – Quantum Yield: UV/Vis and Fluorescence Data and Plot of UV/Vis vs. Fluorescence of Compound 4

UV/ Vis of Compound 2.9							
Solvents	**Wavelength**	**0**	**0.2**	**0.4**	**0.6**	**0.8**	**1**
EtOH	378	0.000	0.006	0.013	0.019	0.026	0.032
MeOH		0.000	0.005	0.009	0.014	0.018	0.023
DCM		0.000	0.013	0.027	0.040	0.053	0.067
Chloroform		0.000	0.010	0.019	0.029	0.038	0.048
Acetonitrile		0.000	0.013	0.027	0.040	0.053	0.067
Fluorescence of Compound 2.9							
Solvents	**Wavelength**	**0**	**0.2**	**0.4**	**0.6**	**0.8**	**1**
EtOH	456	0	0.081613	1.129827	0.824337	1.931434	1.560029
MeOH	462	0	1.9278	2.366405	3.019201	2.958035	7.135094
DCM	451	0	2.665357	2.831483	2.974759	2.864935	2.561082
Chloroform	433	0	0.148519	1.021828	1.177705	2.005713	1.631453
Acetonitrile	471	0	1.673867	1.683743	1.697037	1.691251	5.736521

Plot of UV/Vis vs. Fluorescence of Compound 4

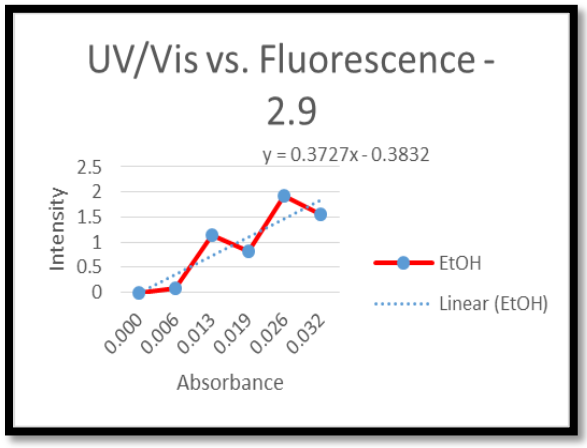

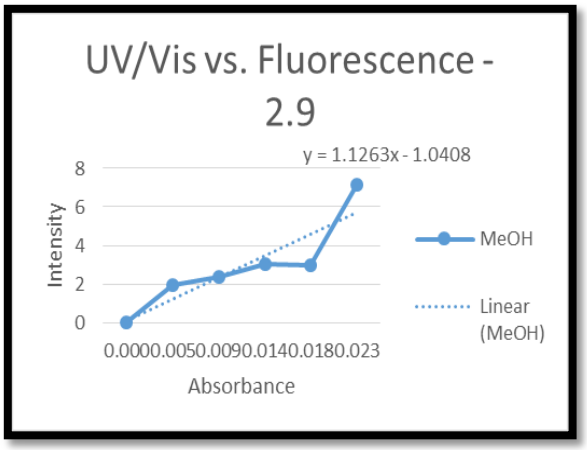

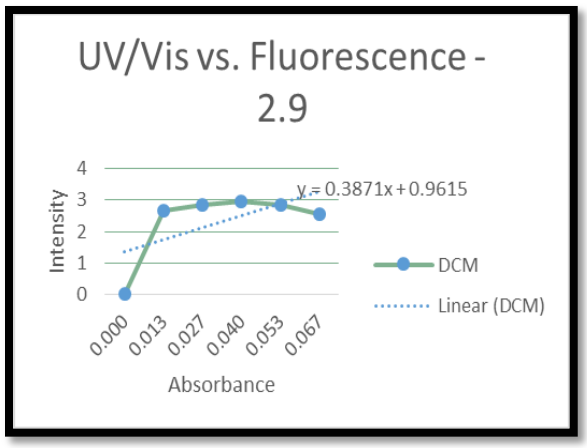

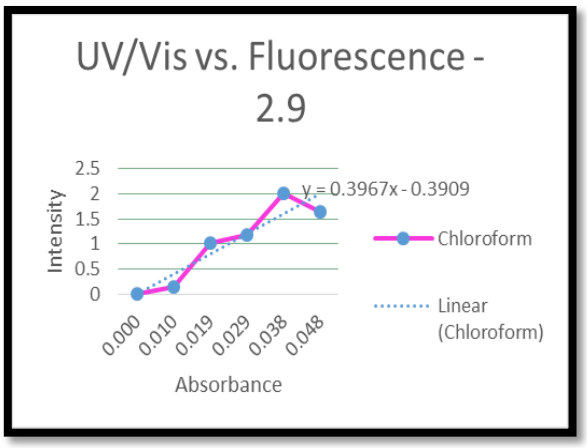

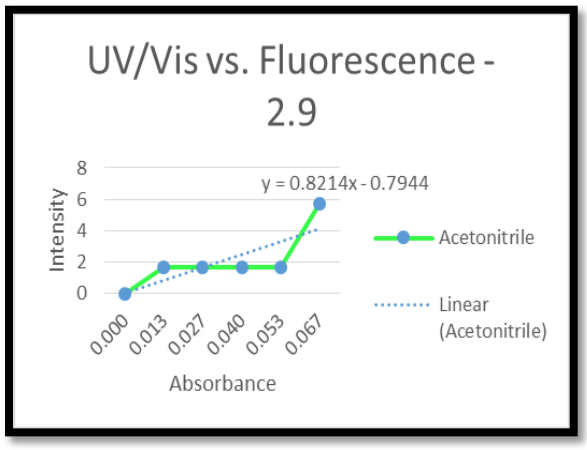

Appendix 84– Quantum Yield: UV/Vis and Fluorescence Data and Plot of UV/Vis vs. Fluorescence of Compound 7

UV/ Vis of Compound 3.13							
Solvents	**Wavelength**	**0**	**0.2**	**0.4**	**0.6**	**0.8**	**1**
EtOH	504	0.000	0.004	0.008	0.012	0.016	0.020
MeOH		0.000	0.005	0.010	0.015	0.020	0.025
DCM		0.000	0.003	0.006	0.009	0.013	0.016
Chloroform		0.000	0.005	0.009	0.014	0.018	0.023
Acetonitrile		0.000	0.005	0.010	0.014	0.019	0.024
Fluorescence of Compound 3.13							
Solvents	**Wavelength**	**0**	**0.2**	**0.4**	**0.6**	**0.8**	**1**
EtOH	521	0	93.64936	144.6947	241.9785	317.8142	397.5224
MeOH	523	0	106.2816	152.3633	247.5977	339.7573	459.6491
DCM	527	0	97.86394	125.9844	179.7191	228.9733	194.1602
Chloroform	527	0	91.72939	203.1931	303.8332	420.6638	530.5707
Acetonitrile	507	0	171.9521	209.8525	220.1203	213.9864	248.2459

Plot of UV/Vis vs. Fluorescence of Compound 7

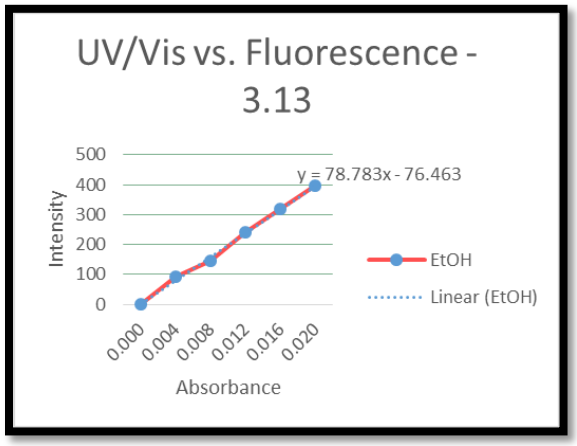

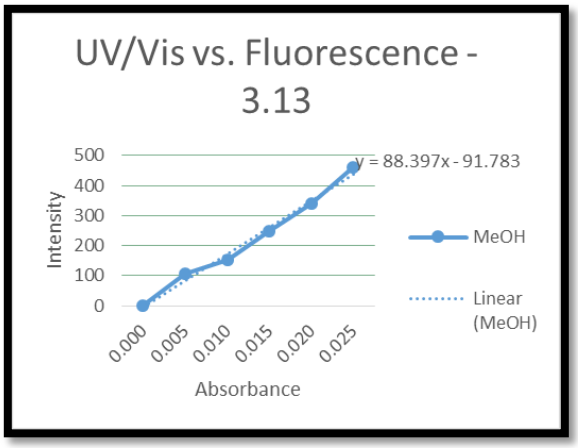

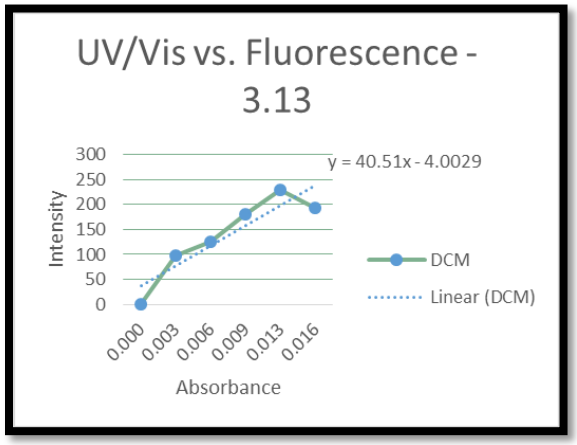

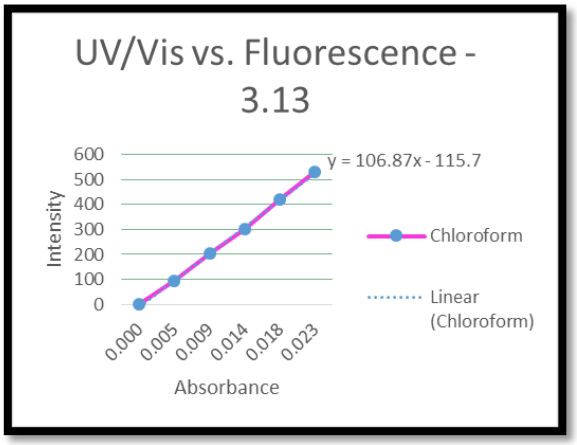

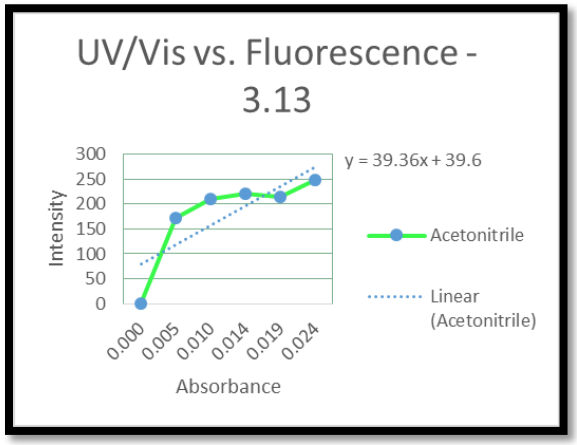

Appendix 85– Quantum Yield: UV/Vis and Fluorescence Data Plot of UV/Vis vs. Fluorescence of Compound 5

UV/ Vis of Compound 3.16							
Solvents	**Wavelength**	**0**	**0.2**	**0.4**	**0.6**	**0.8**	**1**
EtOH	505	0.001	0.003	0.004	0.005	0.006	0.006
MeOH		0.000	0.001	0.001	0.001	0.001	0.001
DCM		0.000	0.001	0.001	0.001	0.002	0.002
Chloroform		0.000	0.000	0.001	0.001	0.001	0.001
Acetonitrile		0.001	0.001	0.002	0.003	0.004	0.004
Fluorescence of Compound 3.16							
Solvents	**Wavelength**	**0**	**0.2**	**0.4**	**0.6**	**0.8**	**1**
EtOH	524	0	19.09992	56.66893	67.05192	42.05141	97.99206
MeOH	525	0	16.98723	22.67521	40.11994	44.05954	54.46032
DCM	526	0	14.08707	42.5972	53.25911	31.51754	74.61356
Chloroform	527	0	18.02207	52.56093	65.2248	39.5668	92.69003
Acetonitrile	518	0	6.070484	18.09638	22.01188	13.3718	31.00457

Plot of UV/Vis vs. Fluorescence of Compound 5

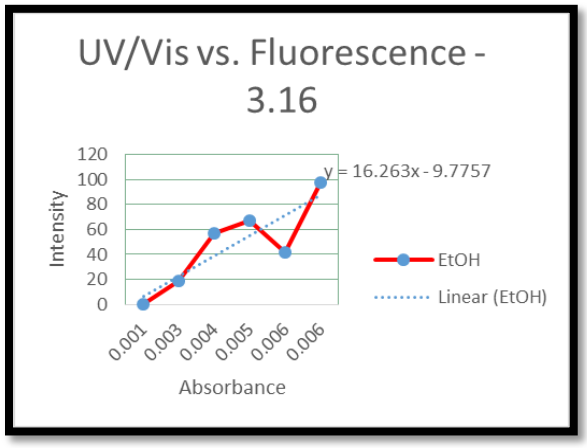

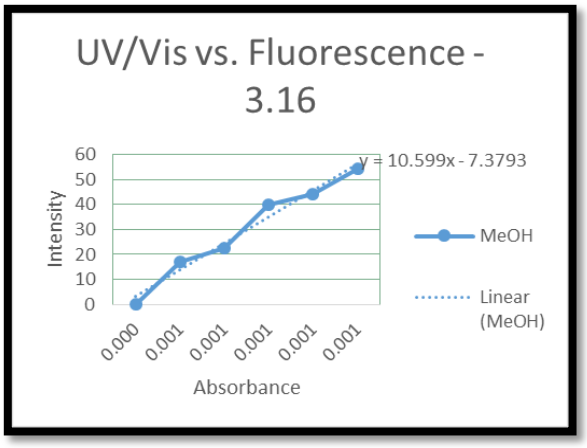

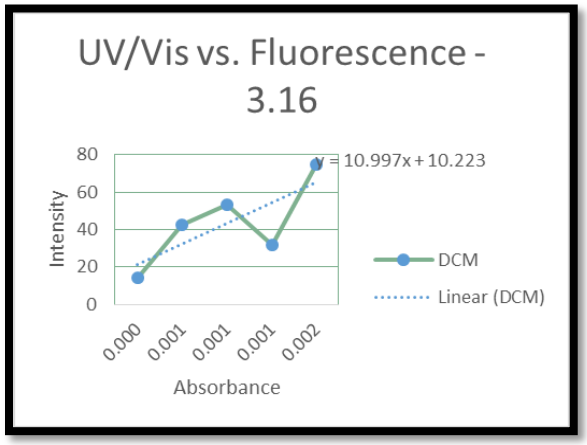

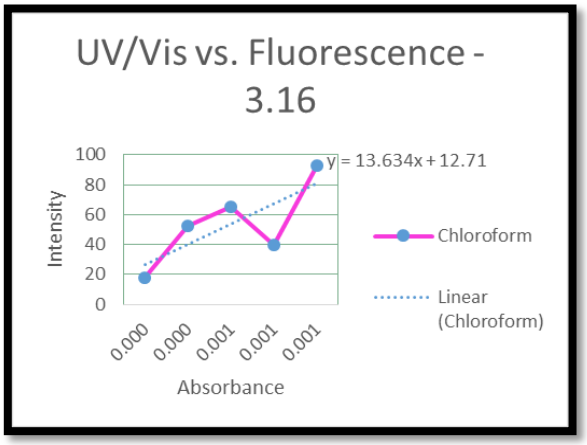

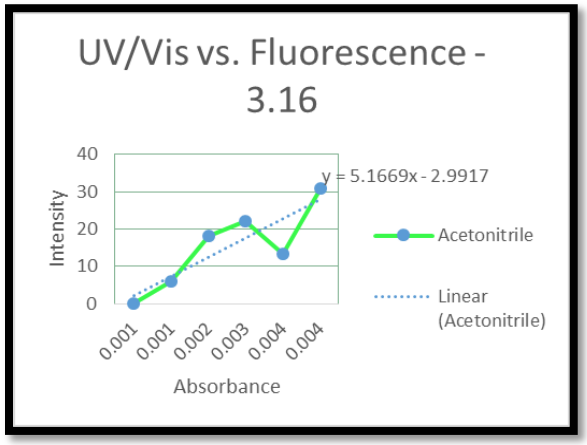

Appendix 86– Quantum Yield: UV/Vis and Fluorescence Data Plot of UV/Vis vs. Fluorescence of Reference Standard- Fluorescein

UV/Vis of Fluorescein							
Compound	**Wavelength (nm)**	**Blank**	**0.20**	**0.40**	**0.60**	**0.80**	**1.00**
2	312	0.0475	0.064	0.068	0.077	0.087	0.094
3	330	0.0443	0.059	0.066	0.079	0.092	0.1
4	378	0.0397	0.043	0.043	0.048	0.053	0.055
7	505	0.035	0.132	0.262	0.369	0.45	0.536
5	504	0.0352	0.134	0.266	0.377	0.46	0.547
Fluorescence of Fluorescein							
Compound	**Wavelength (nm)**	**Blank**	**0.2**	**0.4**	**0.6**	**0.8**	**1**
2	312	0.162886456	38.95909119	42.65011215	62.89025116	57.1101532	46.3876915
3	330	0.101415336	220.067627	243.2561798	222.6515961	218.2761078	186.6099548
4	378	4.324095249	172.6702881	202.8662415	211.8899231	192.7109222	186.5467529
7	505	0.422850728	50.88630676	58.62001343	480.7977905	509.7564087	577.877833
5	504	0.422850728	51.50131836	53.89317627	499.2761536	494.9100037	576.7335205

Plot of UV/Vis vs. Fluorescence of Fluorescein Reference Standard

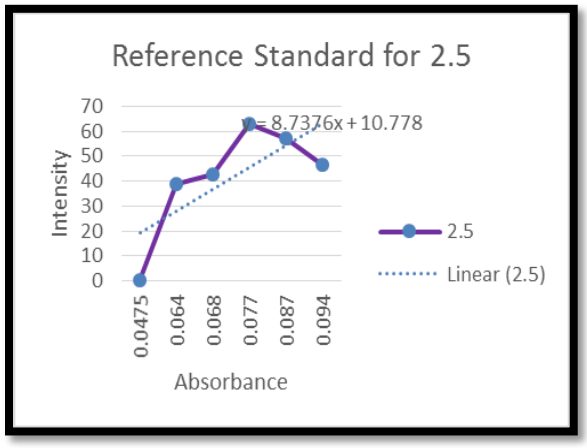

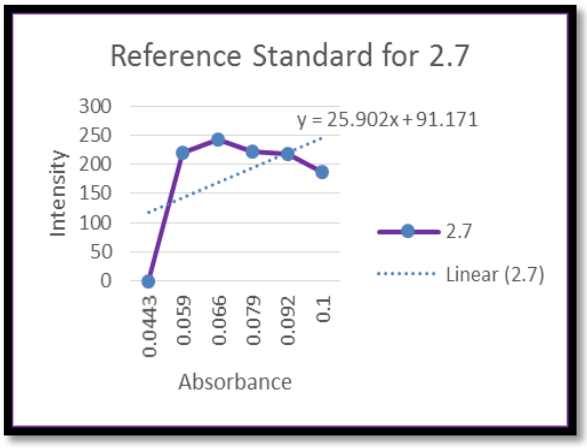

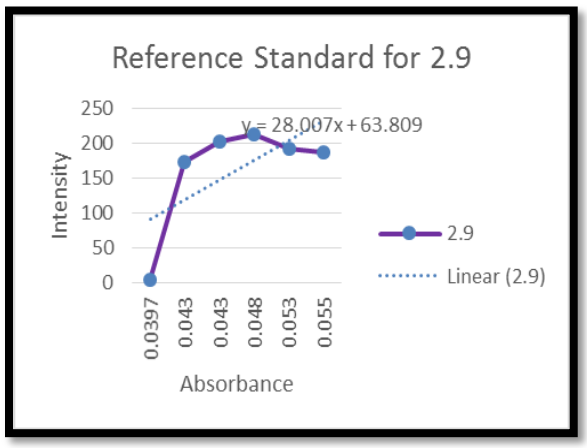

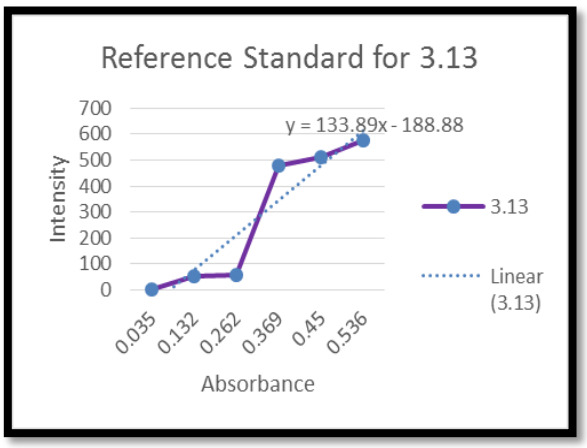

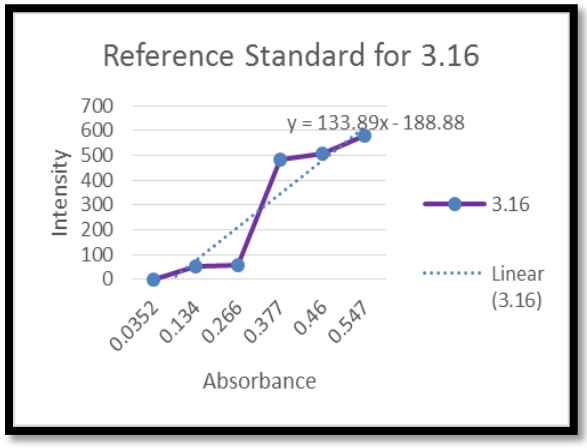

Appendix 87: Refractive Index of Solvents

Solvent	Refractive Index (nD)
Ethanol	1.360
Methanol	1.328
DCM	1.424
Chloroform	1.440
ACN	1.344
Sodium Hydroxide (0.1M)	1.34348

Appendix 88: Absorbance vs. Reflectance Spectra of 3-(4,5-Dihydro-1H-imidazol-2-yl)-1H-quinolin-2-one

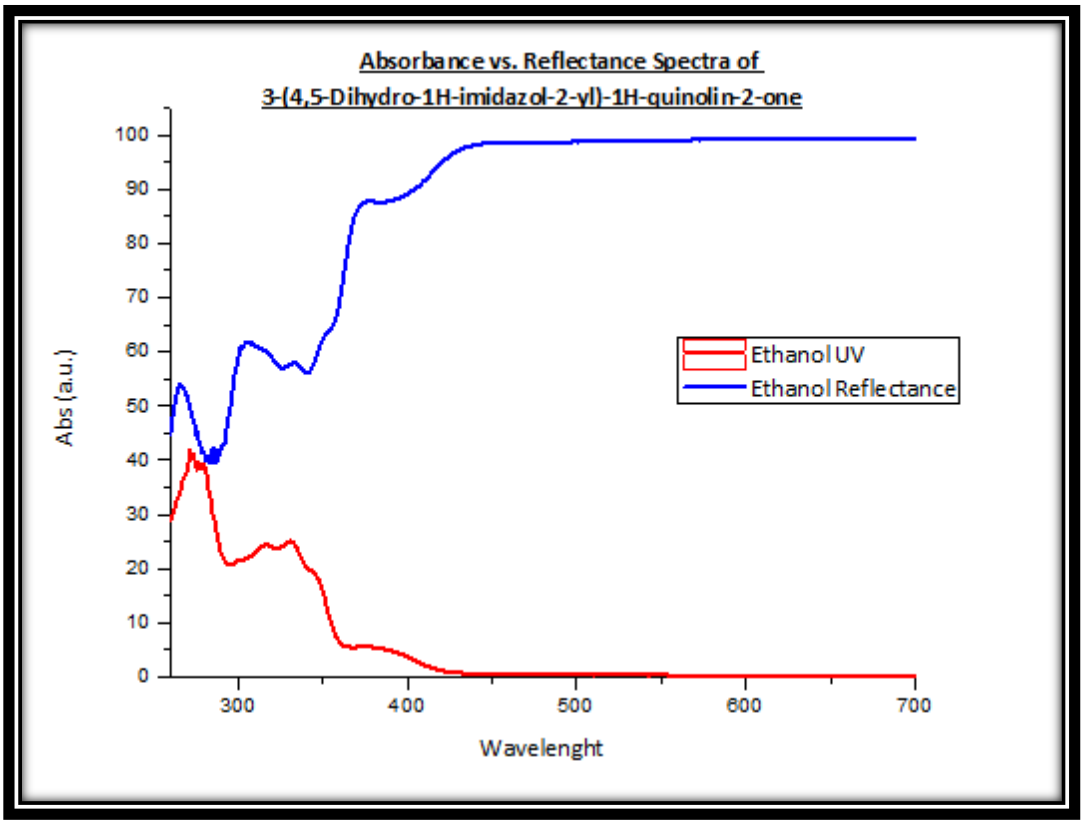

Appendix 89: Absorbance vs. Reflectance Spectra of 3-(4,5-Dihydro-1H-imidazol-2-yl)-1H-quinolin-2-one in Methanol

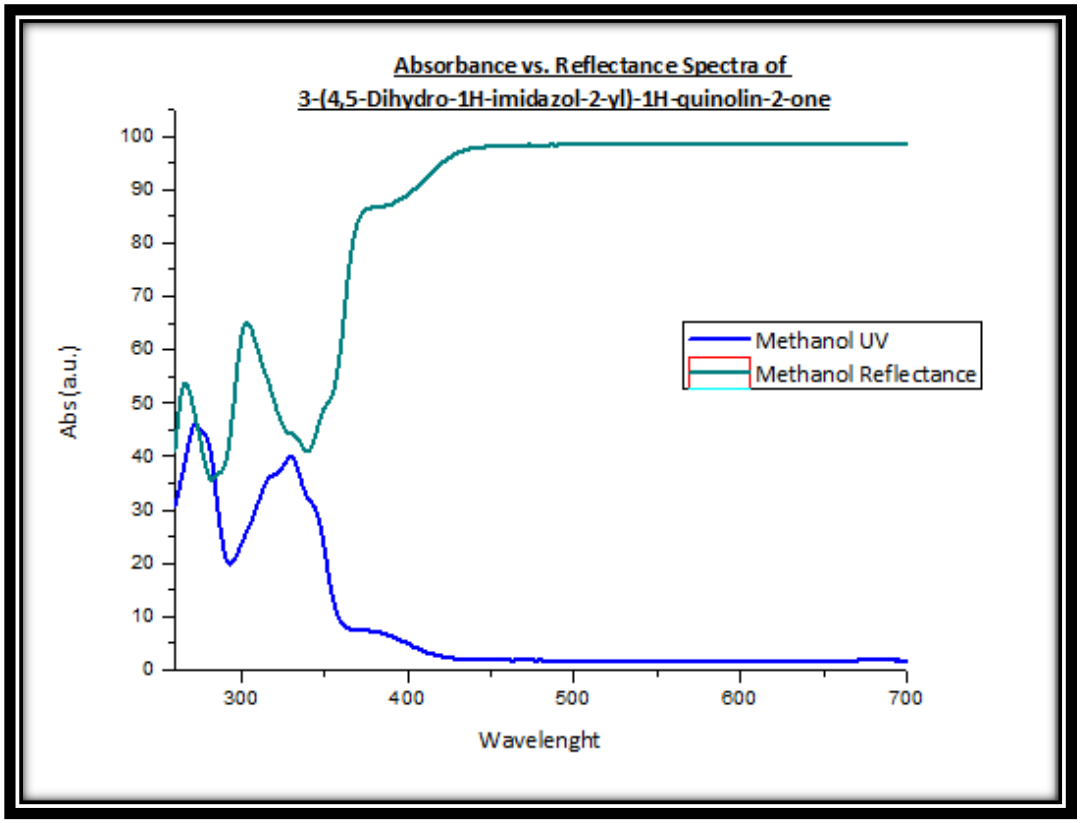

Appendix 90: Absorbance vs. Reflectance Spectra of 3-(4,5-Dihydro-1H-imidazol-2-yl)-1H-quinolin-2-one in DCM

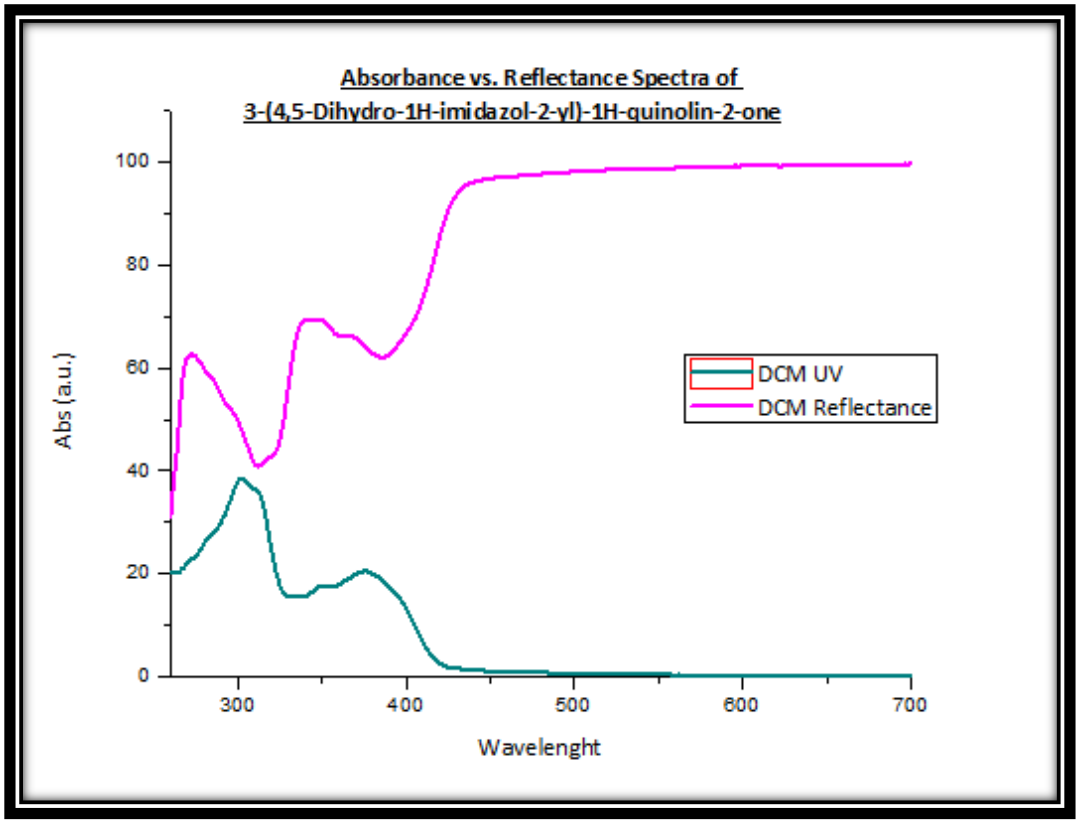

Appendix 91: Absorbance vs. Reflectance Spectra of 3-(4,5-Dihydro-1H-imidazol-2-yl)-1H-quinolin-2-one in Chloroform

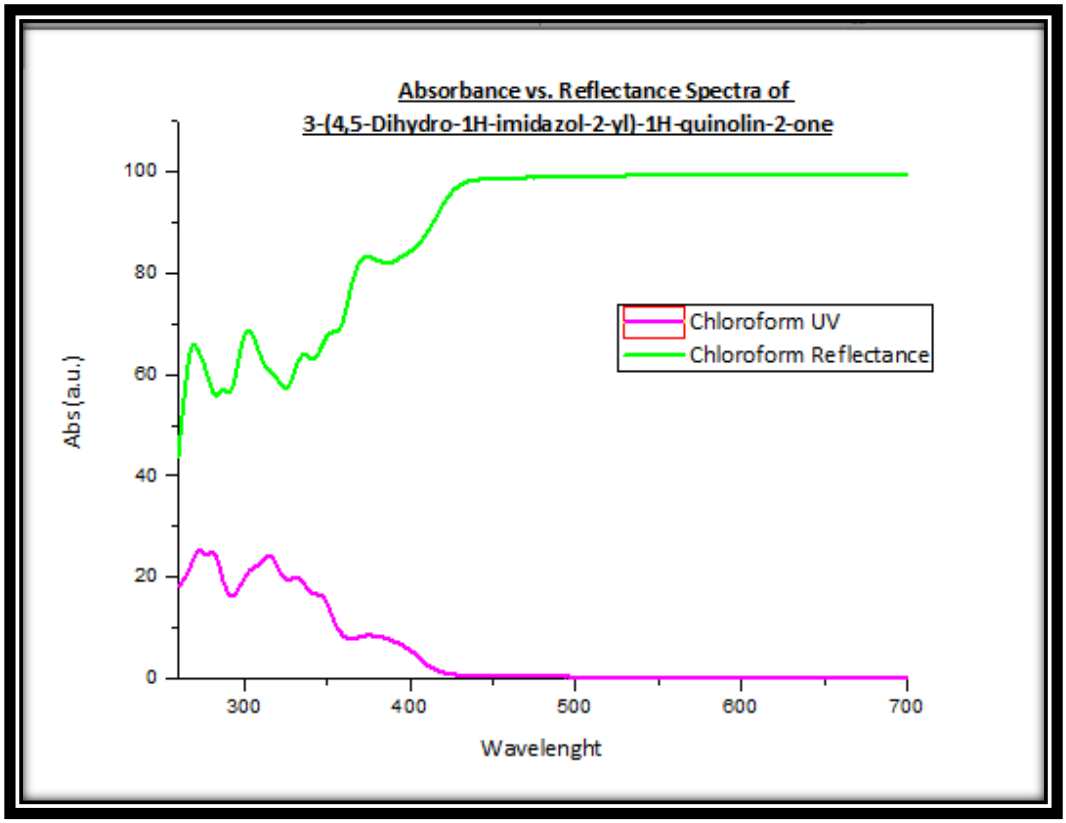

Appendix 92: Absorbance vs. Reflectance Spectra of 3-(4,5-Dihydro-1H-imidazol-2-yl)-1H-quinolin-2-one in Acetonitrile

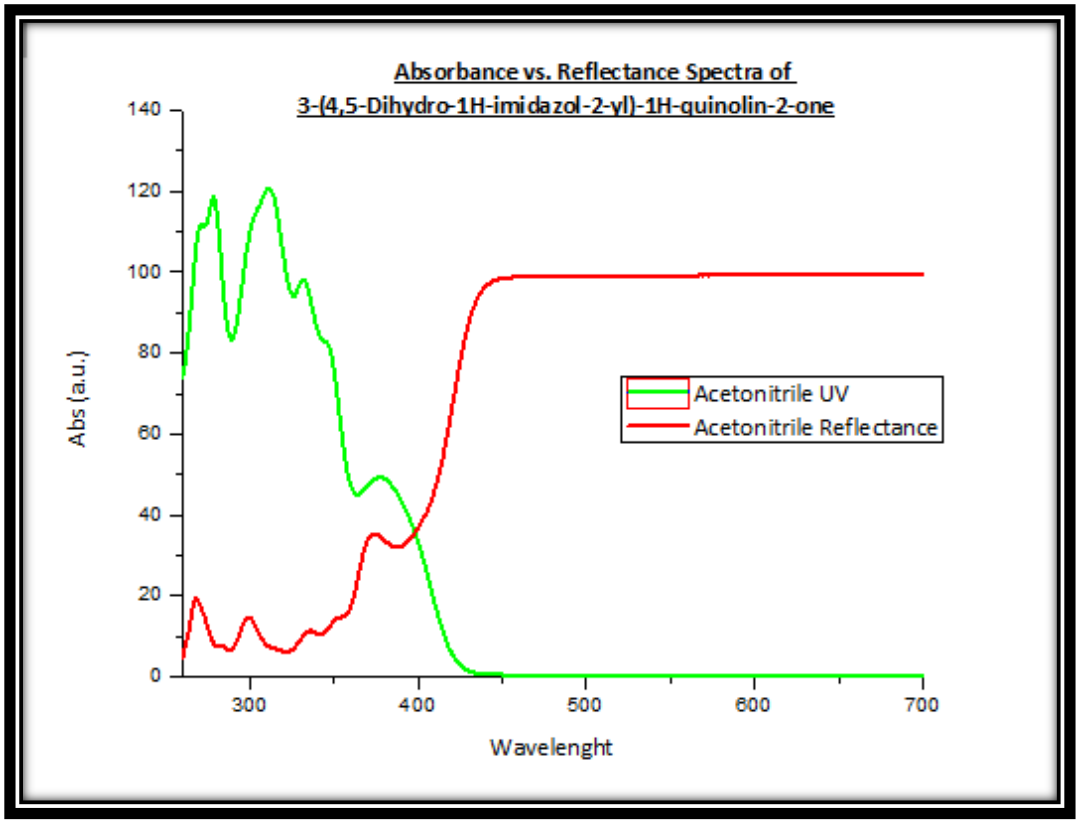

Appendix 93: Absorbance vs. Reflectance Spectra of 3-(-1H-Benzoimidazol-2-yl)-1H-quinolin-2-one in Ethanol

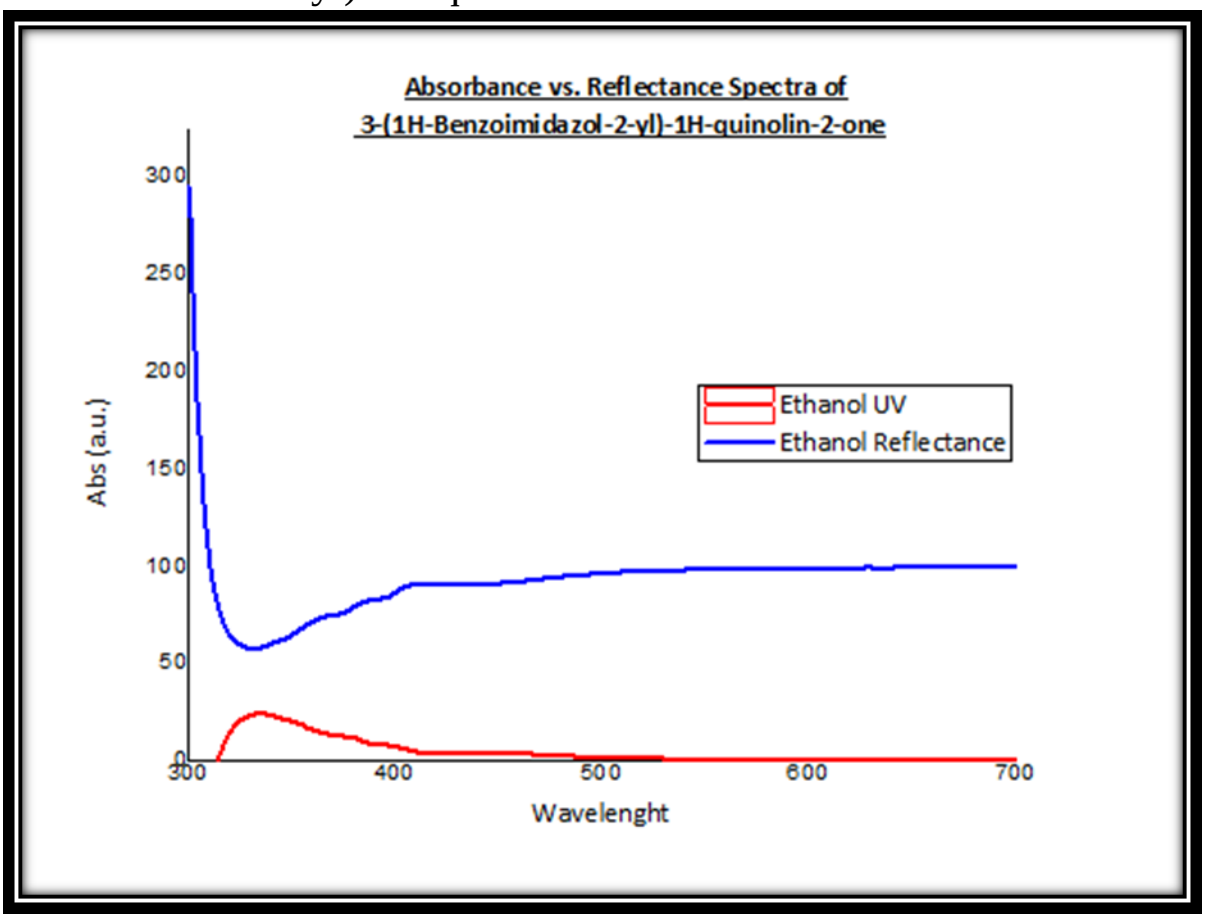

Appendix 94: Absorbance vs. Reflectance Spectra of 3-(-1H-Benzoimidazol-2-yl)-1H-quinolin-2-one in Methanol

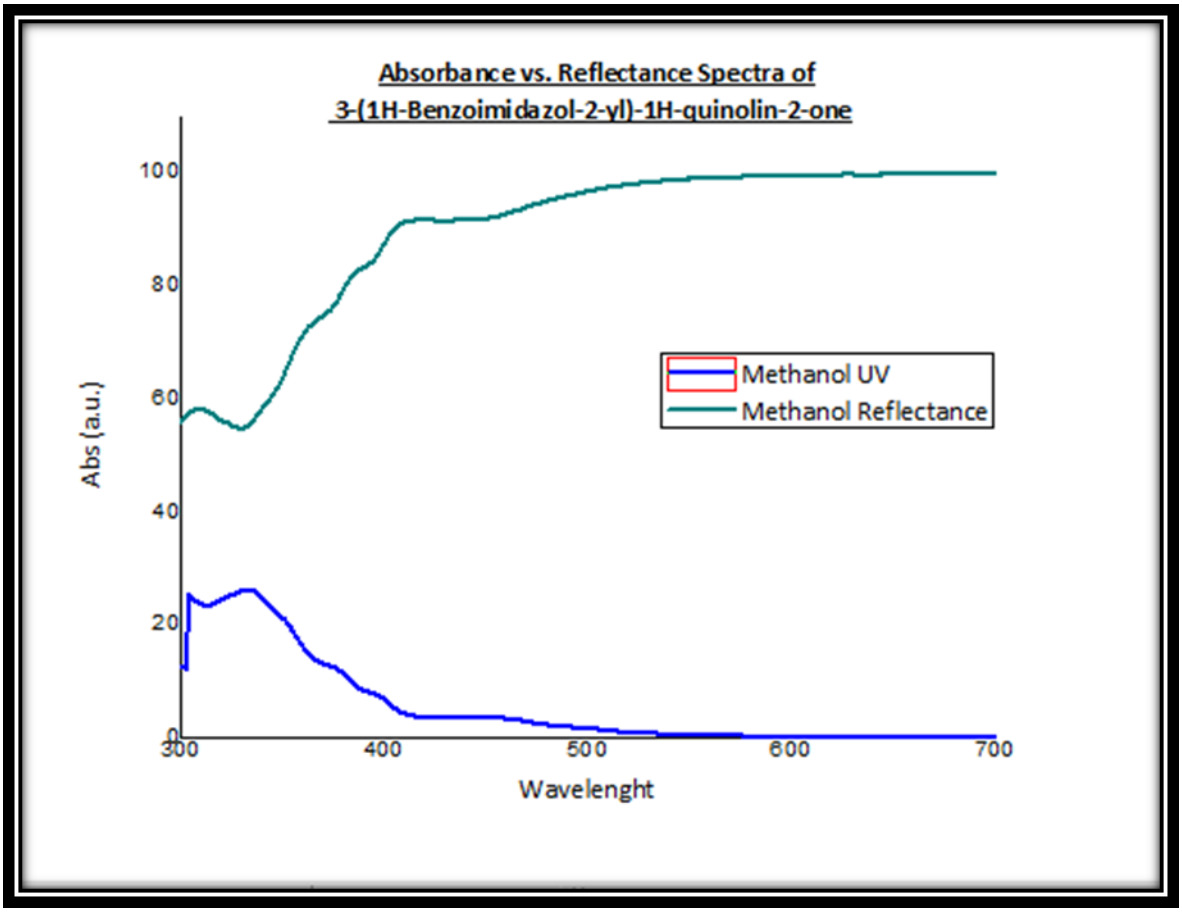

Appendix 95: Absorbance vs. Reflectance Spectra of 3-(-1H-Benzoimidazol-2-yl)-1H-quinolin-2-one in DCM

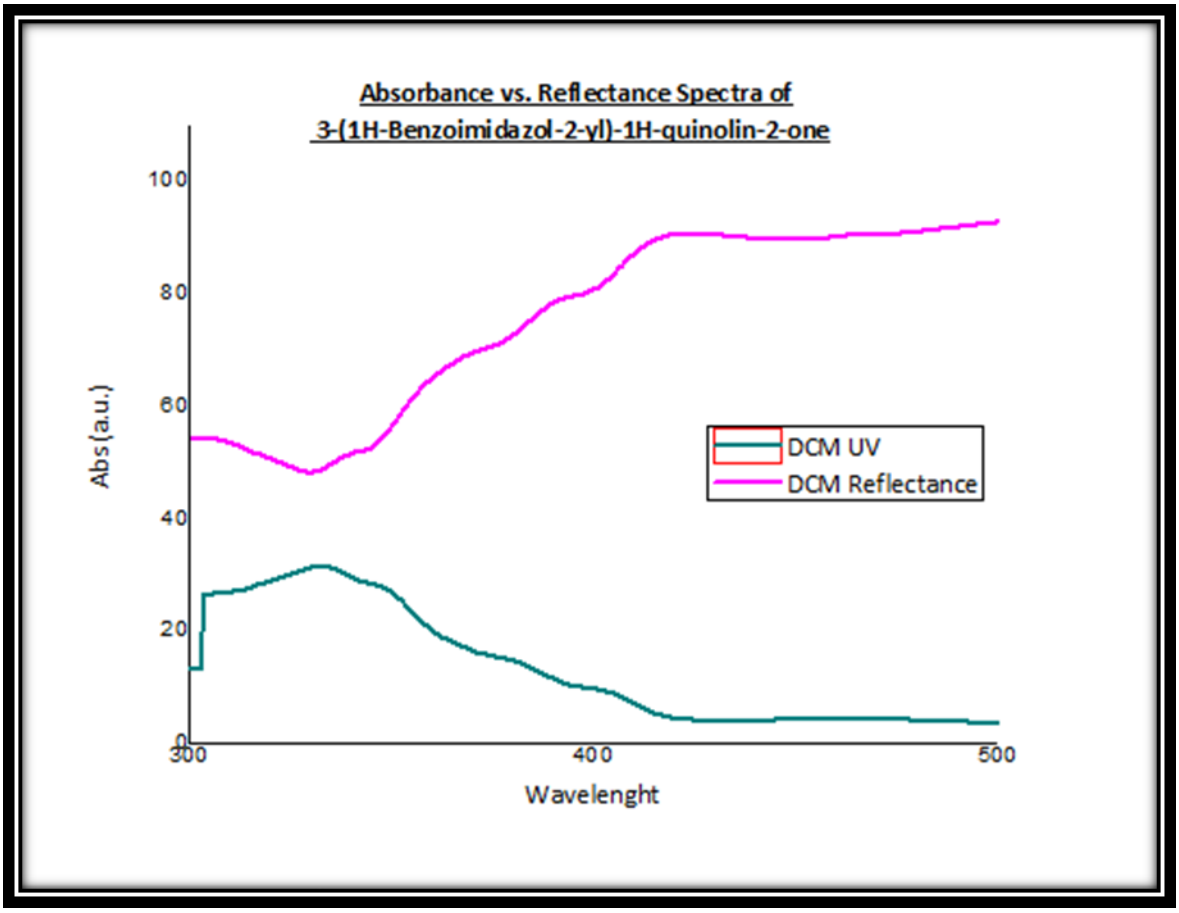

Appendix 96: Absorbance vs. Reflectance Spectra of 3-(-1H-Benzoimidazol-2-yl)-1H-quinolin-2-one in Chloroform

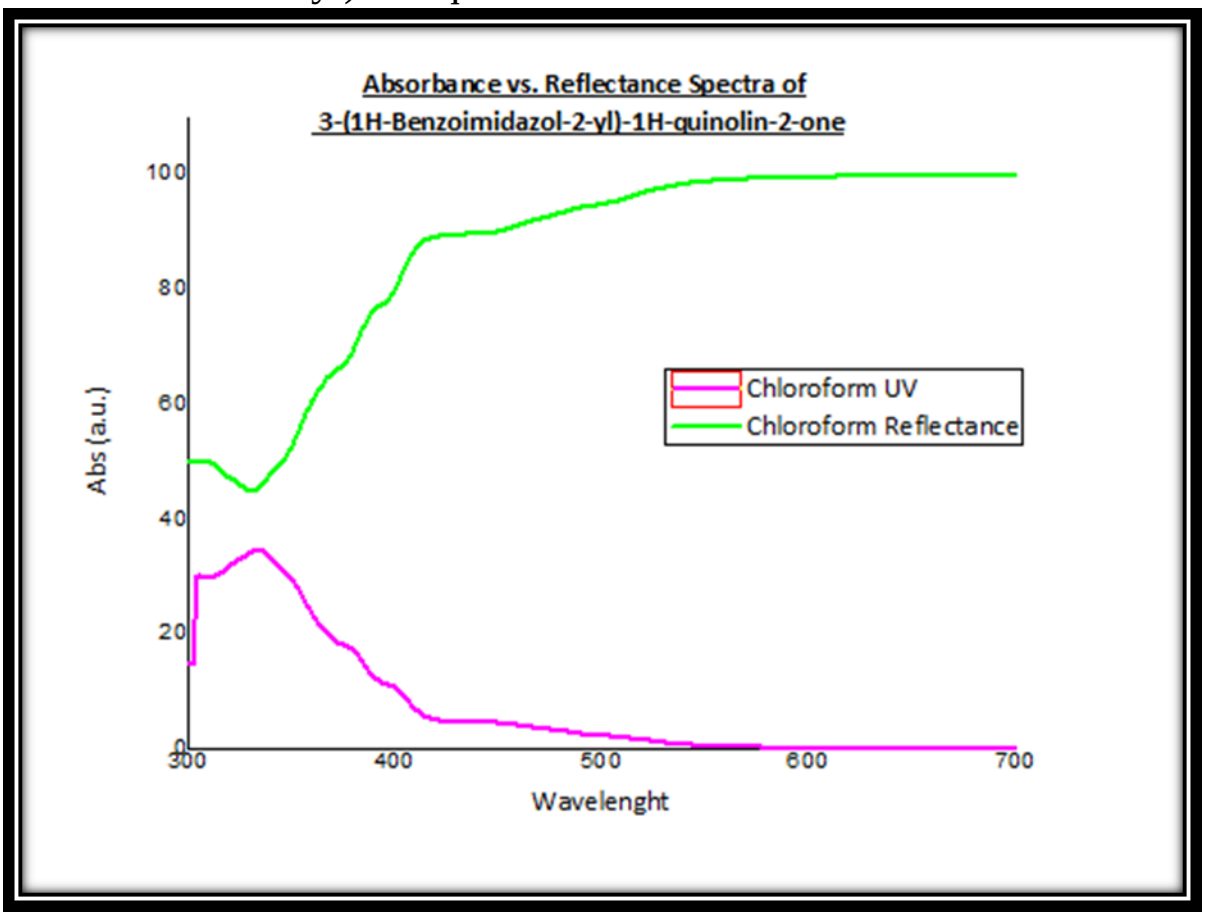

Appendix 97: Absorbance vs. Reflectance Spectra of 3-(-1H-Benzoimidazol-2-yl)-1H-quinolin-2-one in Acetonitrile

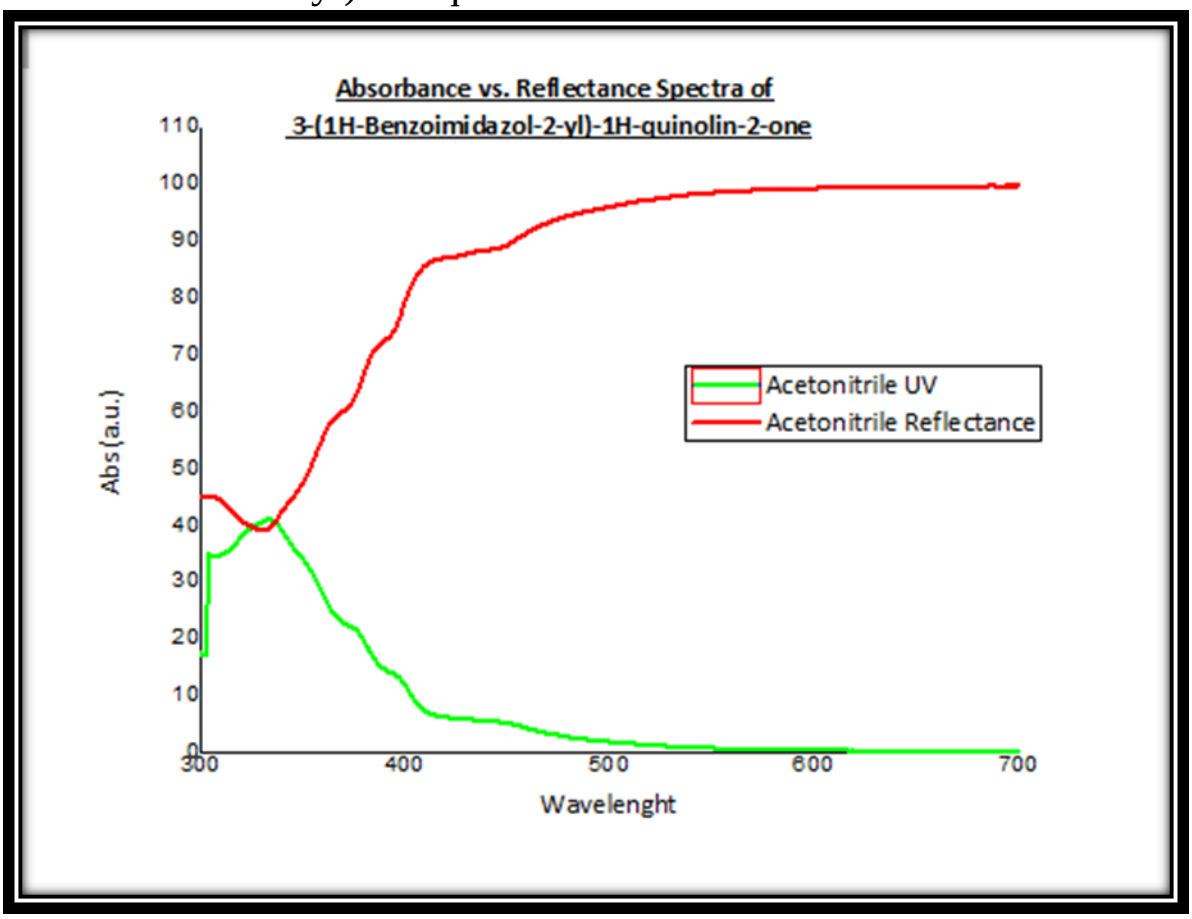

Appendix 98: Absorbance vs. Reflectance Spectra of 3-(6-Nitro-1H-Benzoimidazol-2-yl)-1H-quinolin-2-one in Ethanol

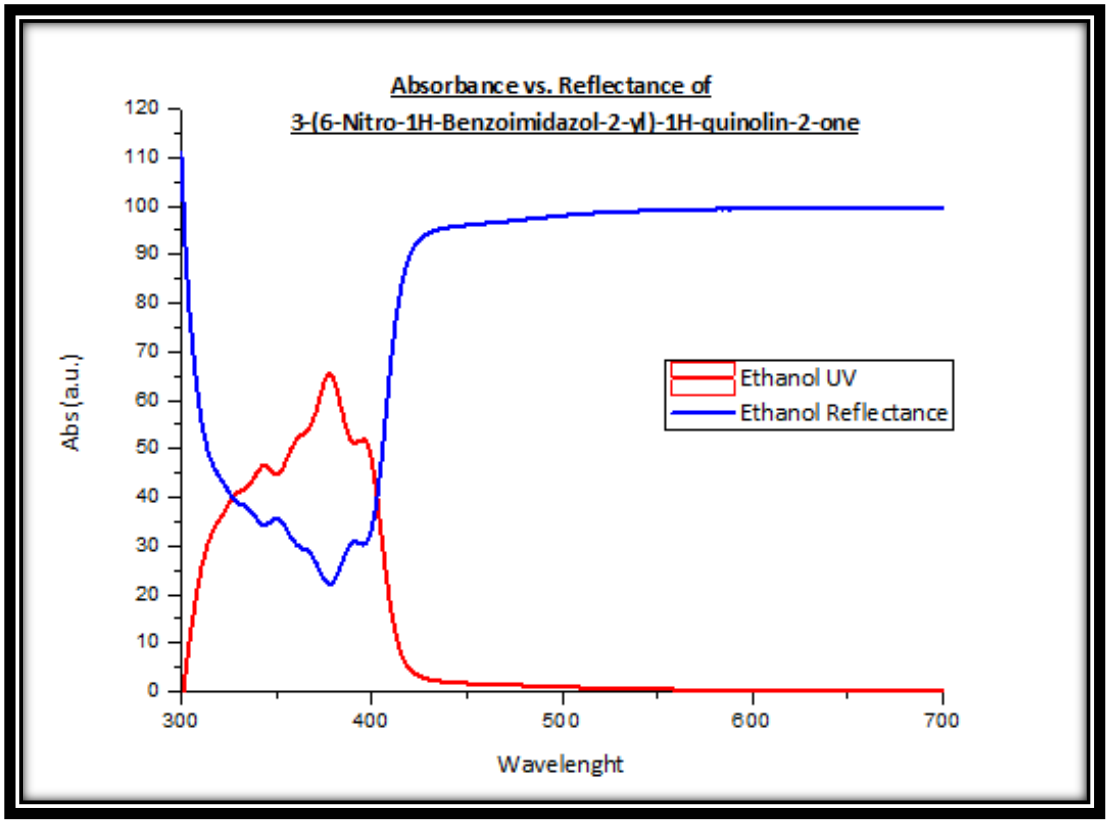

Appendix 99: Absorbance vs. Reflectance Spectra of 3-(6-Nitro-1H-Benzoimidazol-2-yl)-1H-quinolin-2-one in Methanol

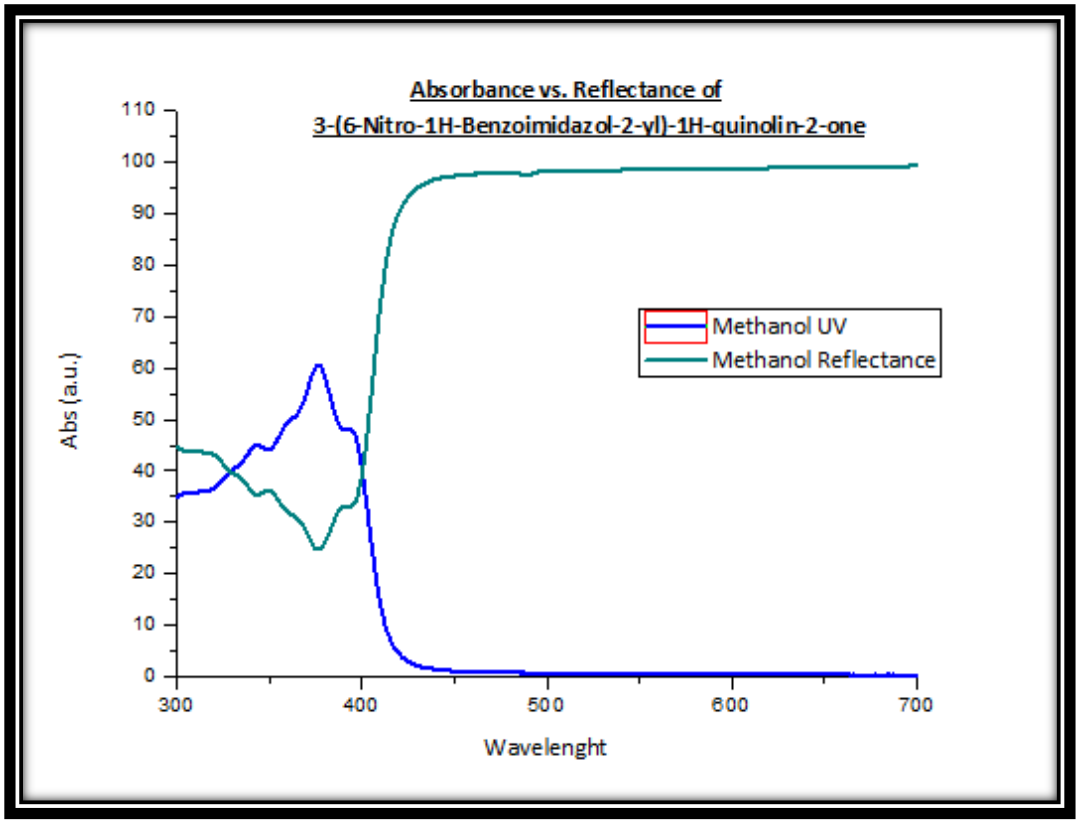

Appendix 100: Absorbance vs. Reflectance Spectra of 3-(6-Nitro-1H-Benzoimidazol-2-yl)-1H-quinolin-2-one in DCM

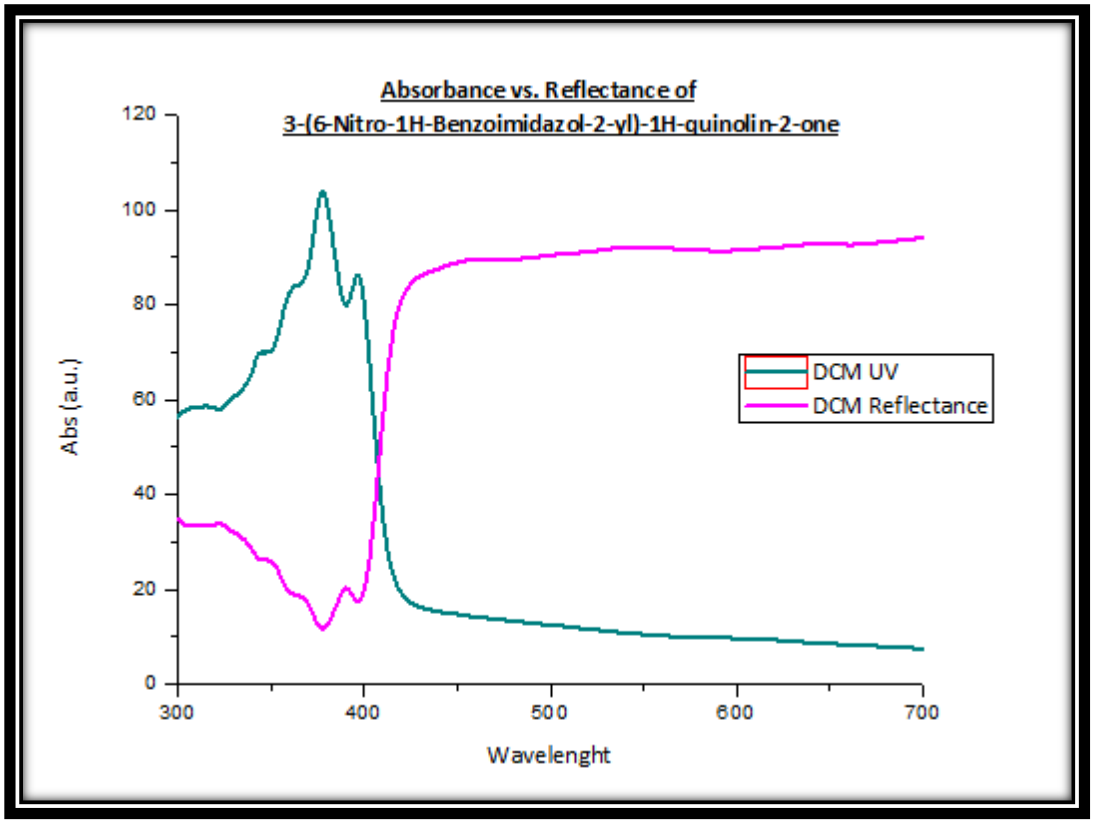

Appendix 101: Absorbance vs. Reflectance Spectra of 3-(6-Nitro-1H-Benzoimidazol-2-yl)-1H-quinolin-2-one in Chloroform

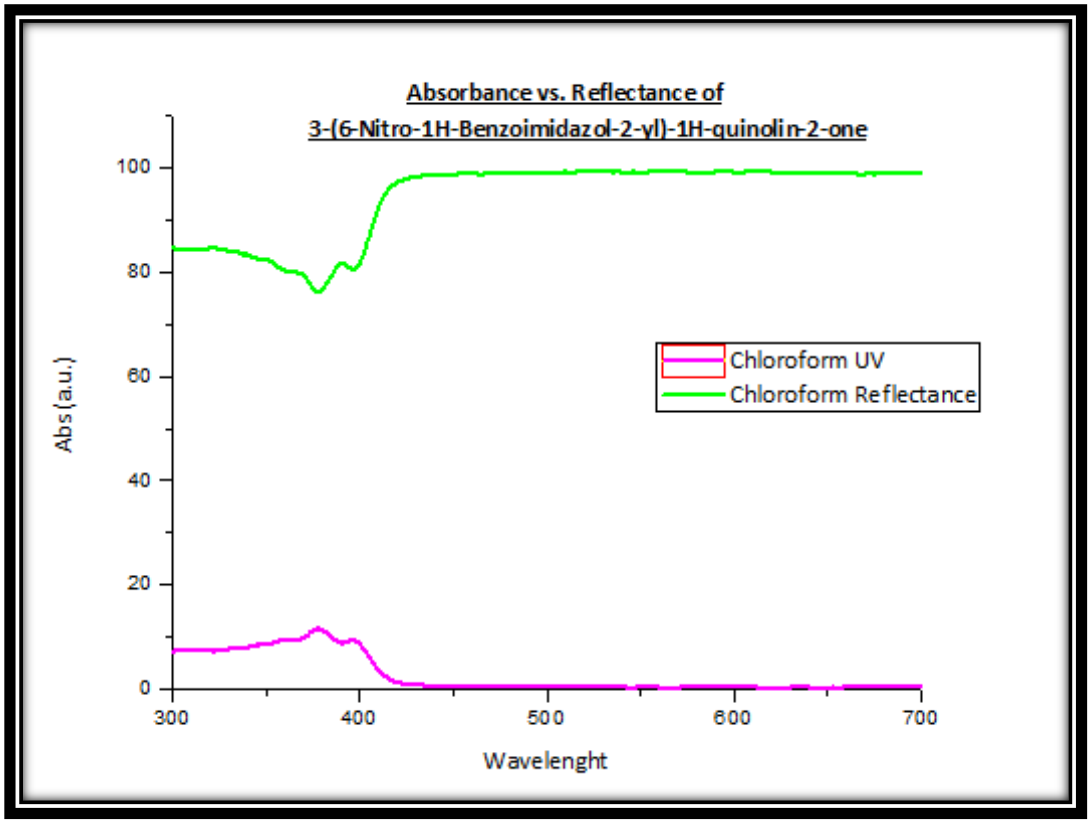

Appendix 102: Absorbance vs. Reflectance Spectra of 3-(6-Nitro-1H-Benzoimidazol-2-yl)-1H-quinolin-2-one in Acetonitrile

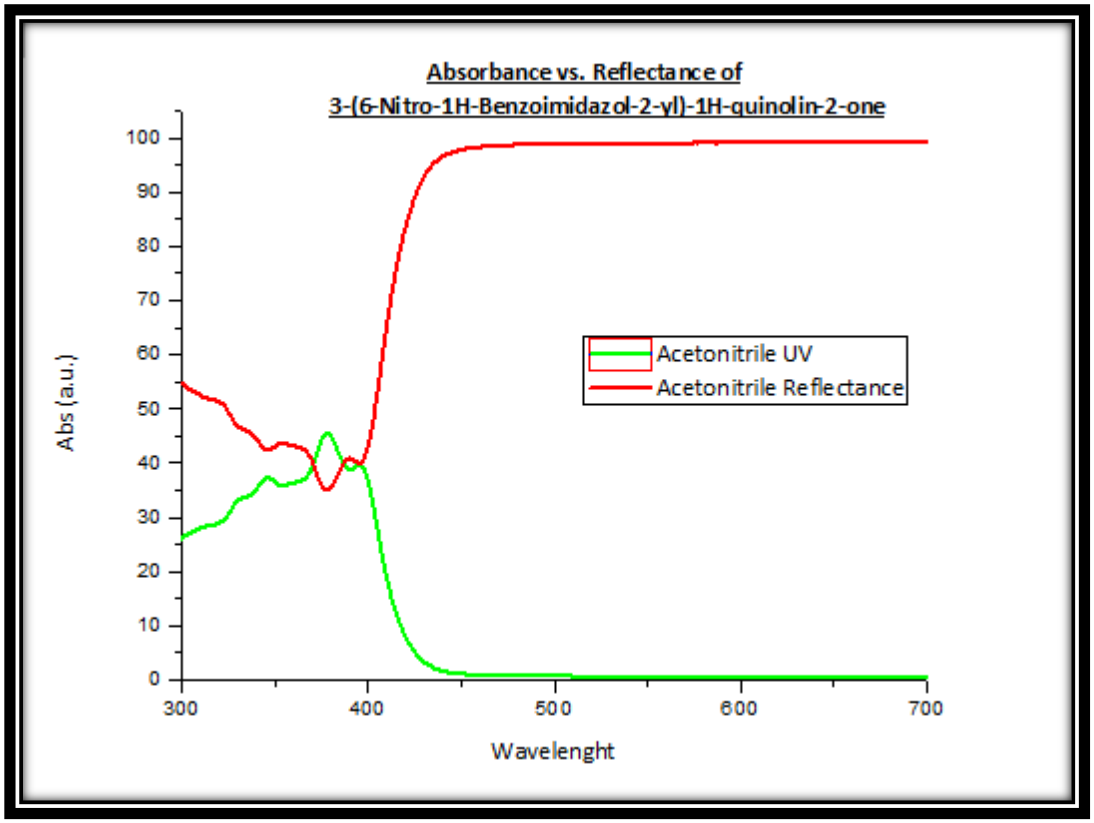

Appendix 103: Absorbance vs. Reflectance Spectra of 4,4-difluoro-4-bora-3a,4a-diaza-s-indacene-2-Chloro-quinoline in Ethanol

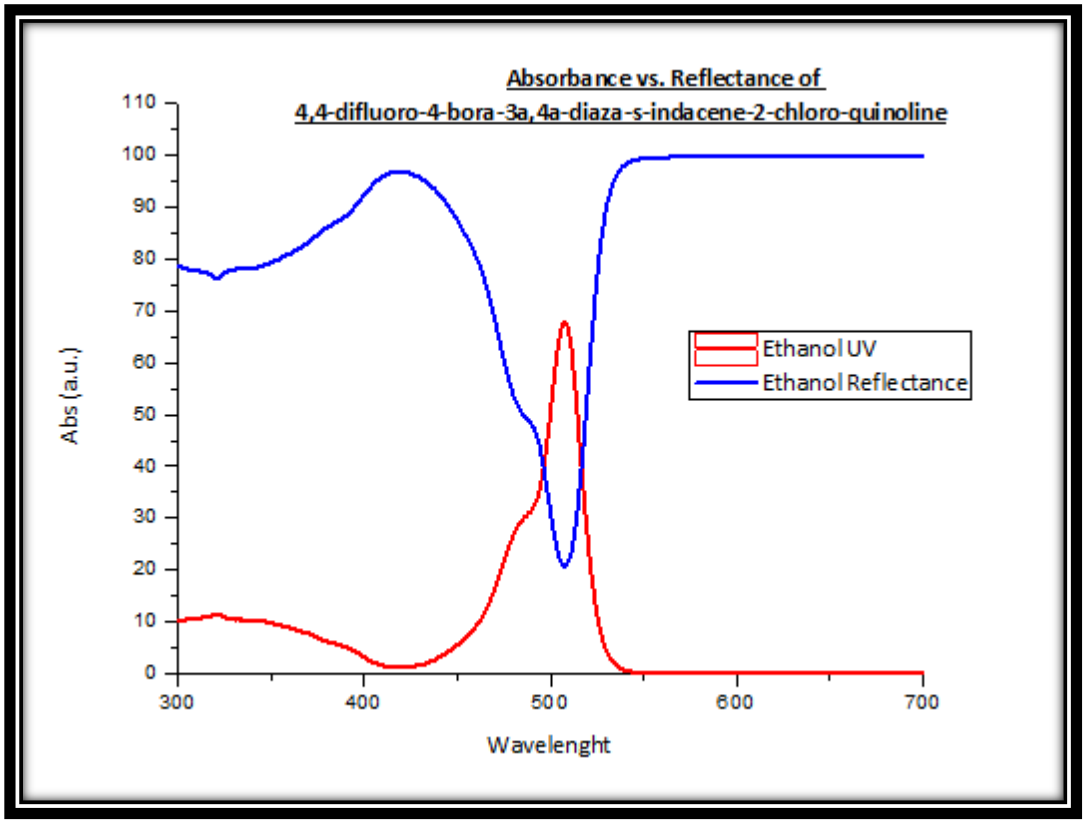

Appendix 104: Absorbance vs. Reflectance Spectra of 4,4-difluoro-4-bora-3a,4a-diaza-s-indacene-2-Chloro-quinoline in Methanol

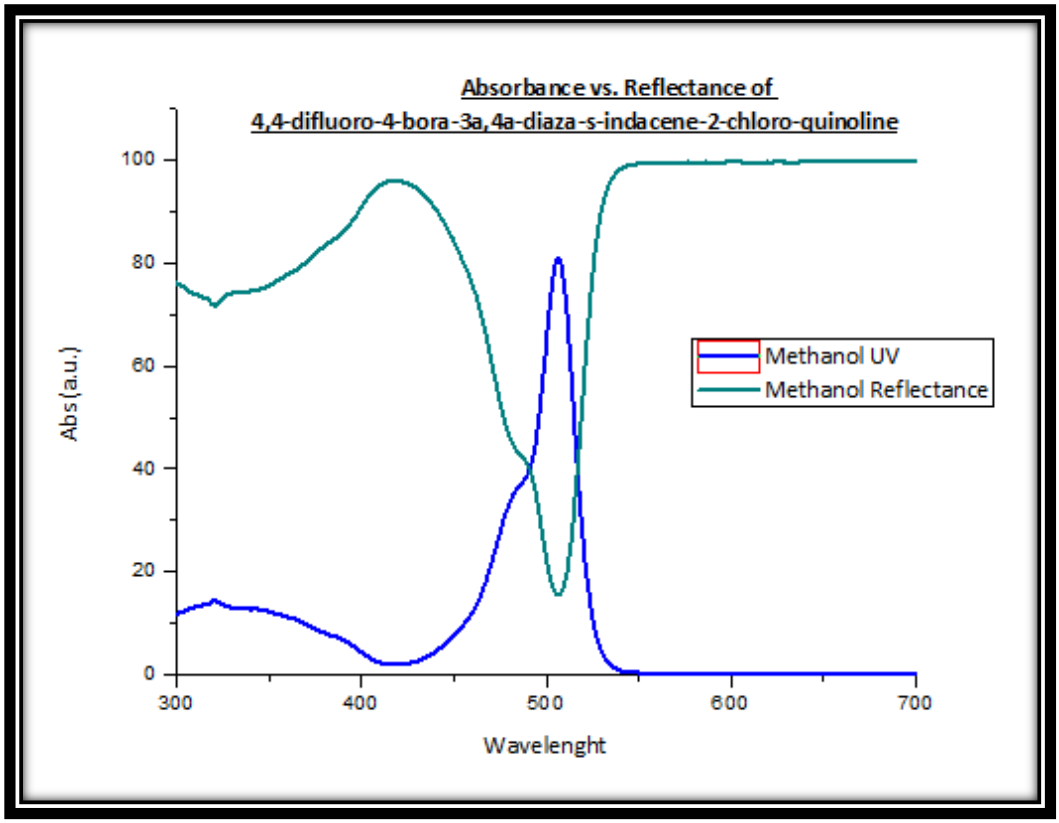

Appendix 105: Absorbance vs. Reflectance Spectra of 4,4-difluoro-4-bora-3a,4a-diaza-s-indacene-2-Chloro-quinoline in DCM

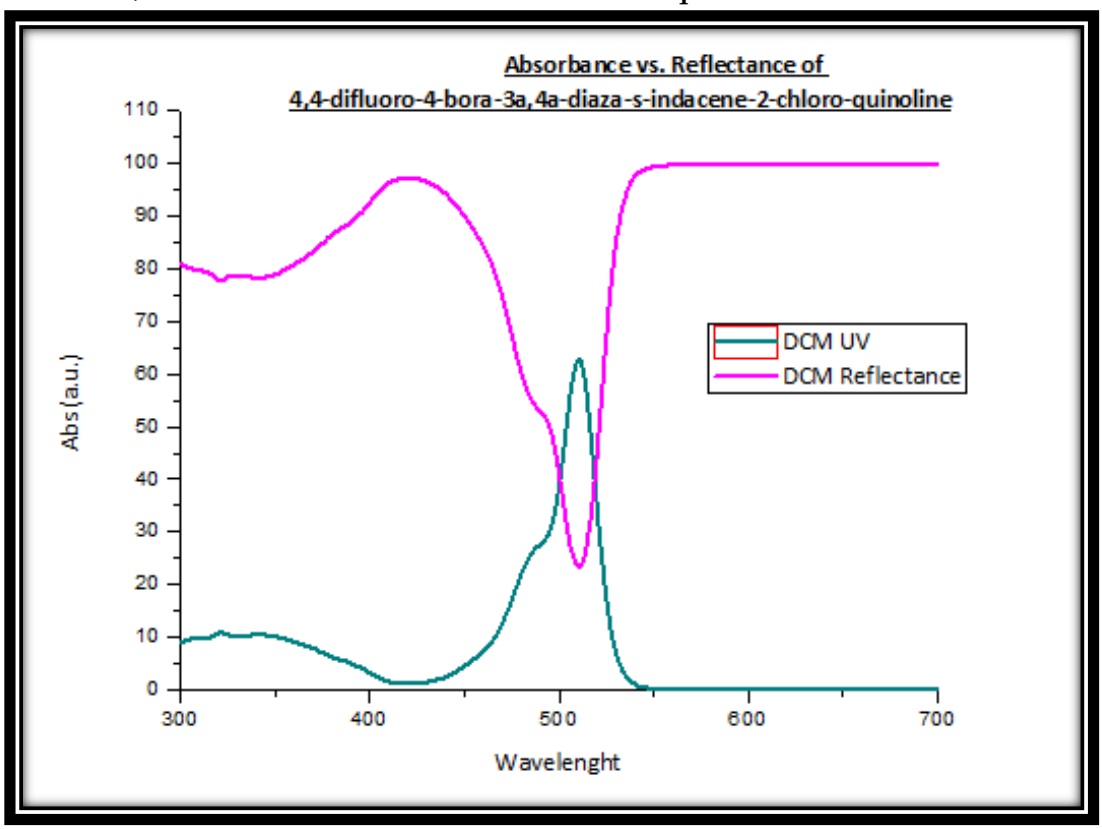

Appendix 106: Absorbance vs. Reflectance Spectra of 4,4-difluoro-4-bora-3a,4a-diaza-s-indacene-2-Chloro-quinoline in Chloroform

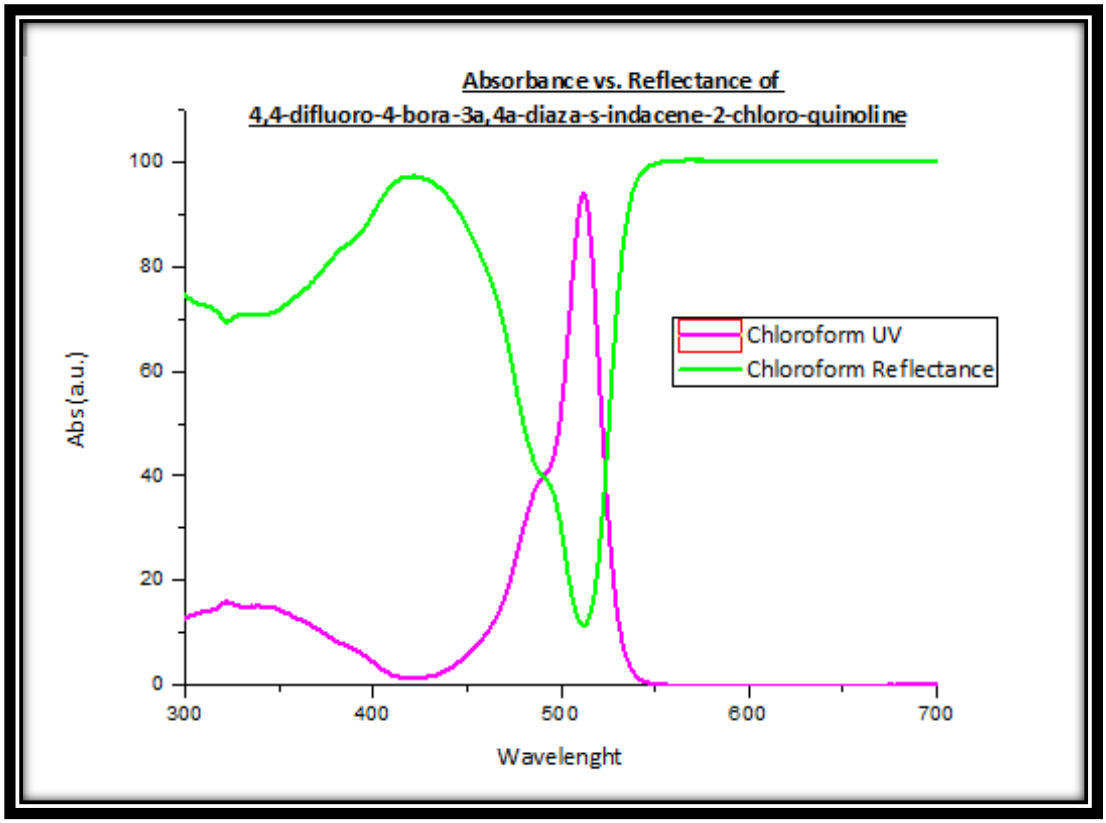

Appendix 107: Absorbance vs. Reflectance Spectra of 4,4-difluoro-4-bora-3a,4a-diaza-s-indacene-2-Chloro-quinoline in Acetonitrile

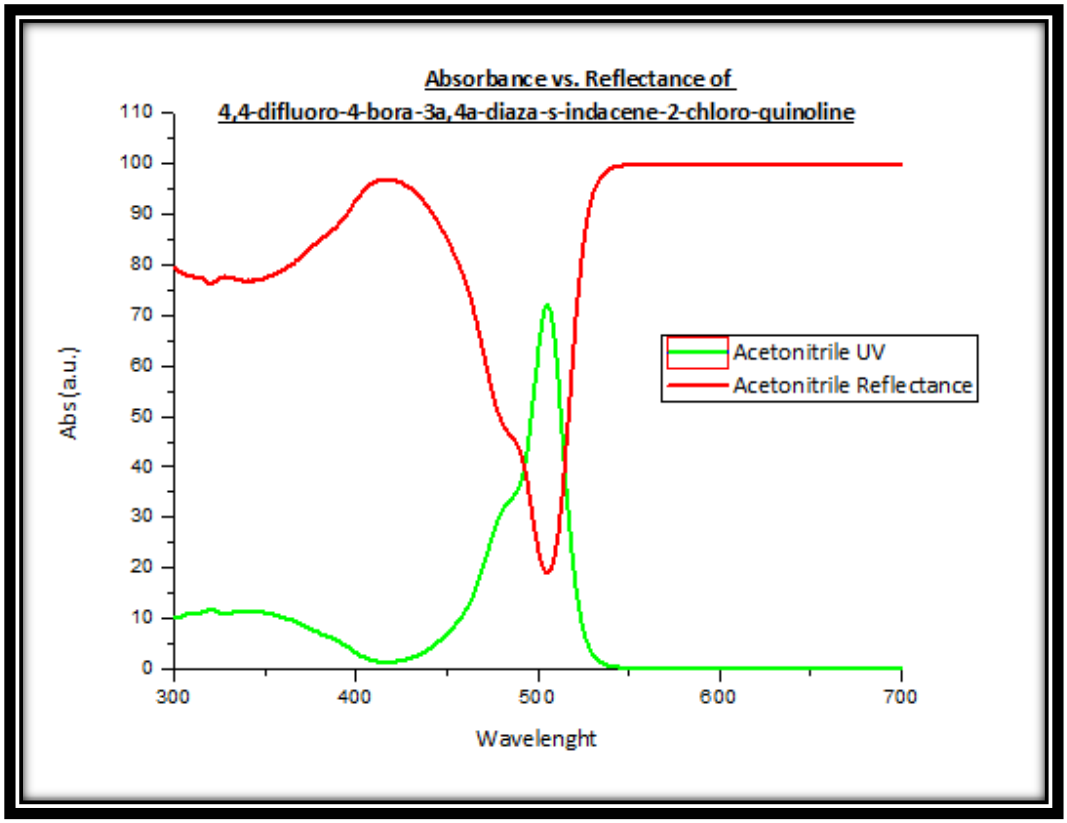

Appendix 108: Absorbance vs. Reflectance Spectra of 4,4-difluoro-4-bora-3a,4a-diaza-s-indacene-2-oxo-quinoline in Ethanol

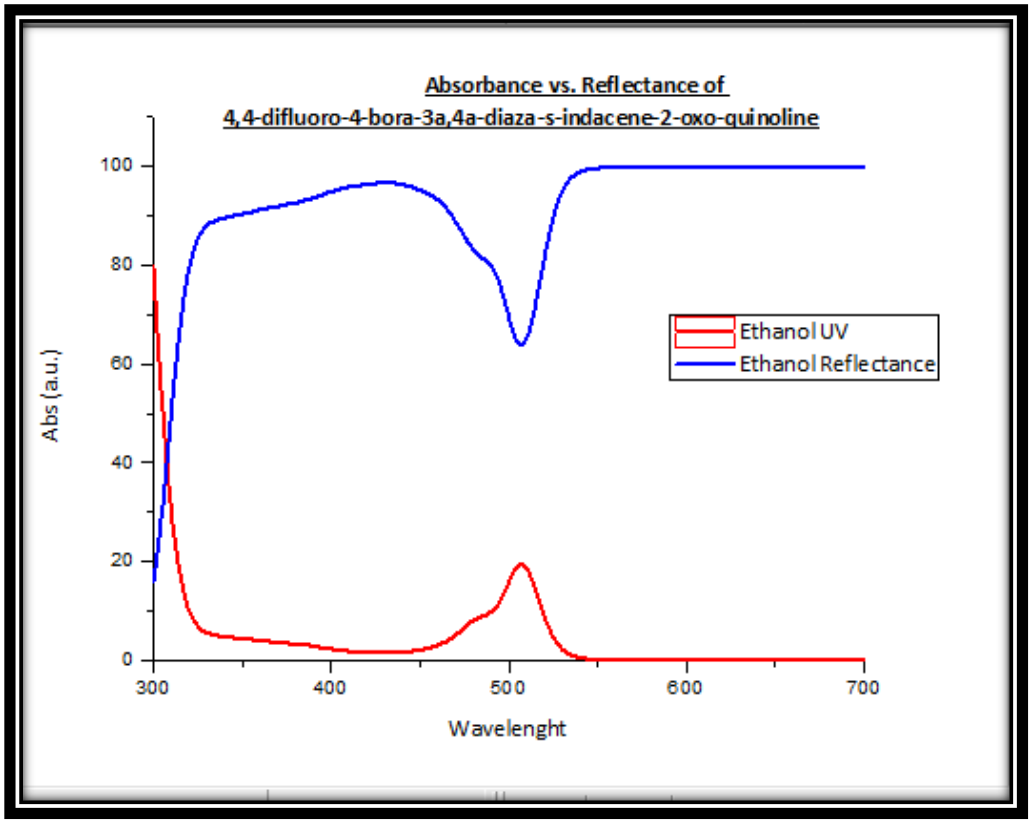

Appendix 109: Absorbance vs. Reflectance Spectra of 4,4-difluoro-4-bora-3a,4a-diaza-s-indacene-2-oxo-quinoline in Methanol

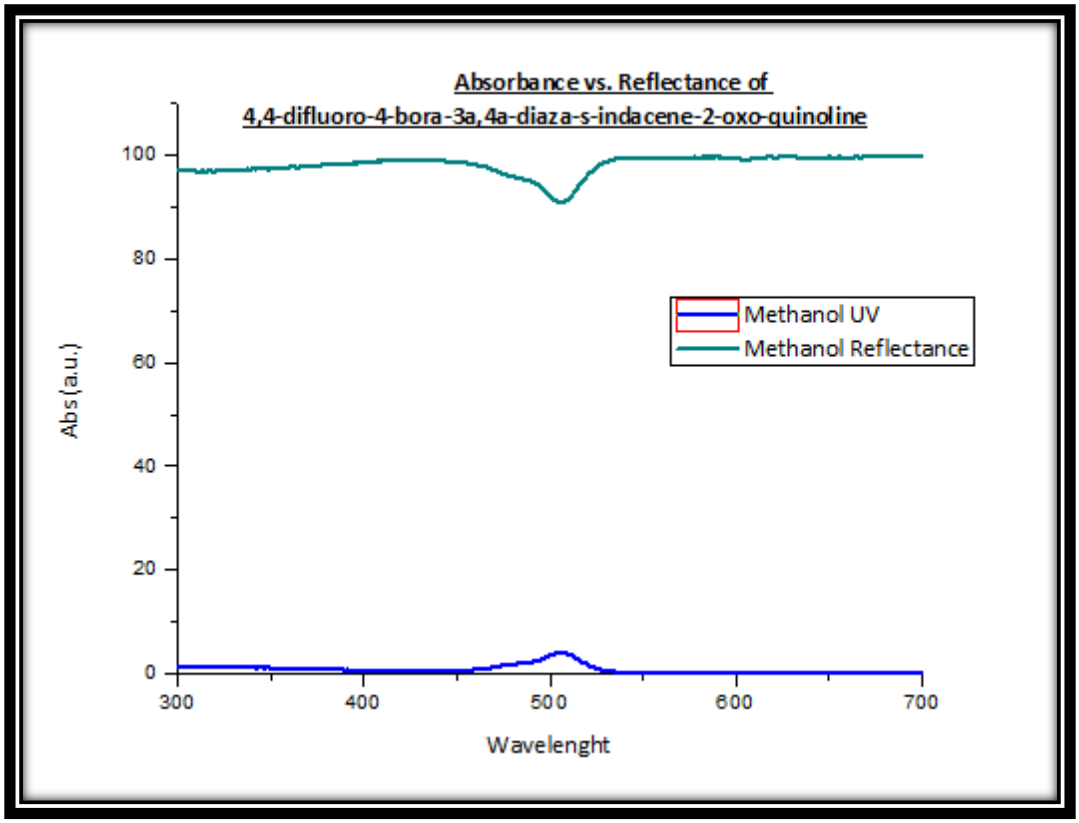

Appendix 110: Absorbance vs. Reflectance Spectra of 4,4-difluoro-4-bora-3a,4a-diaza-s-indacene-2-oxo-quinoline in DCM

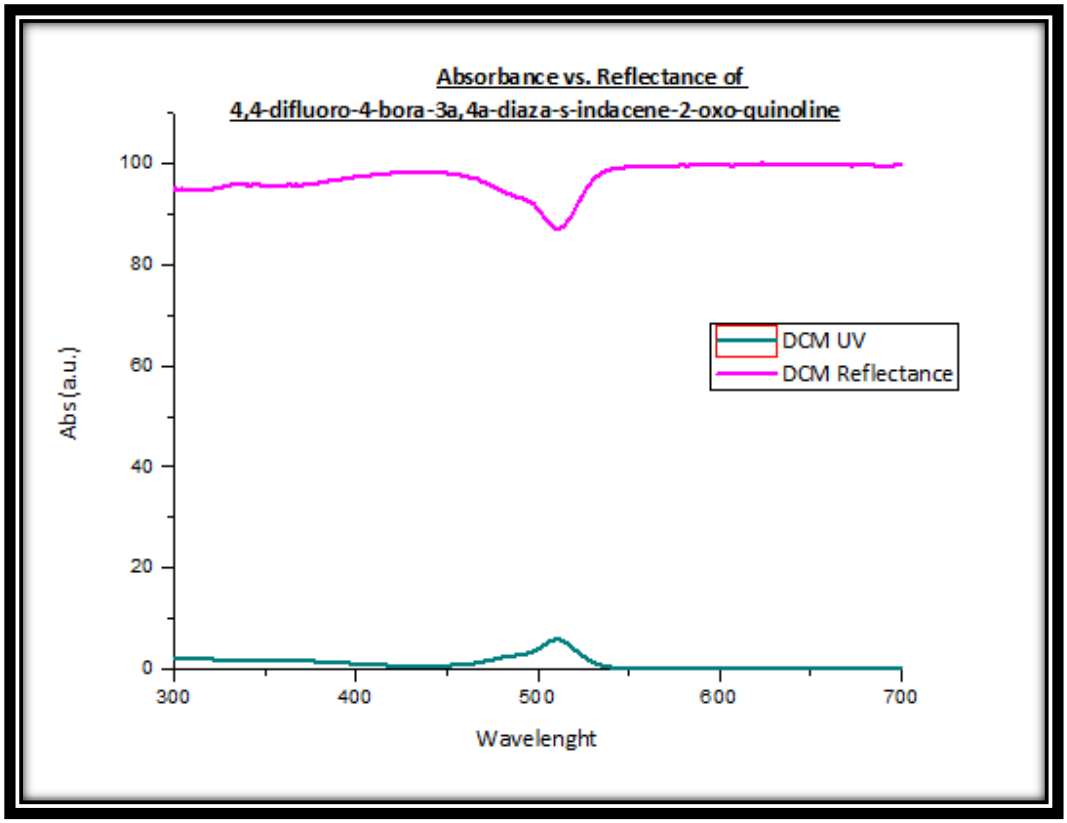

Appendix 111: Absorbance vs. Reflectance Spectra of 4,4-difluoro-4-bora-3a,4a-diaza-s-indacene-2-oxo-quinoline in Chloroform

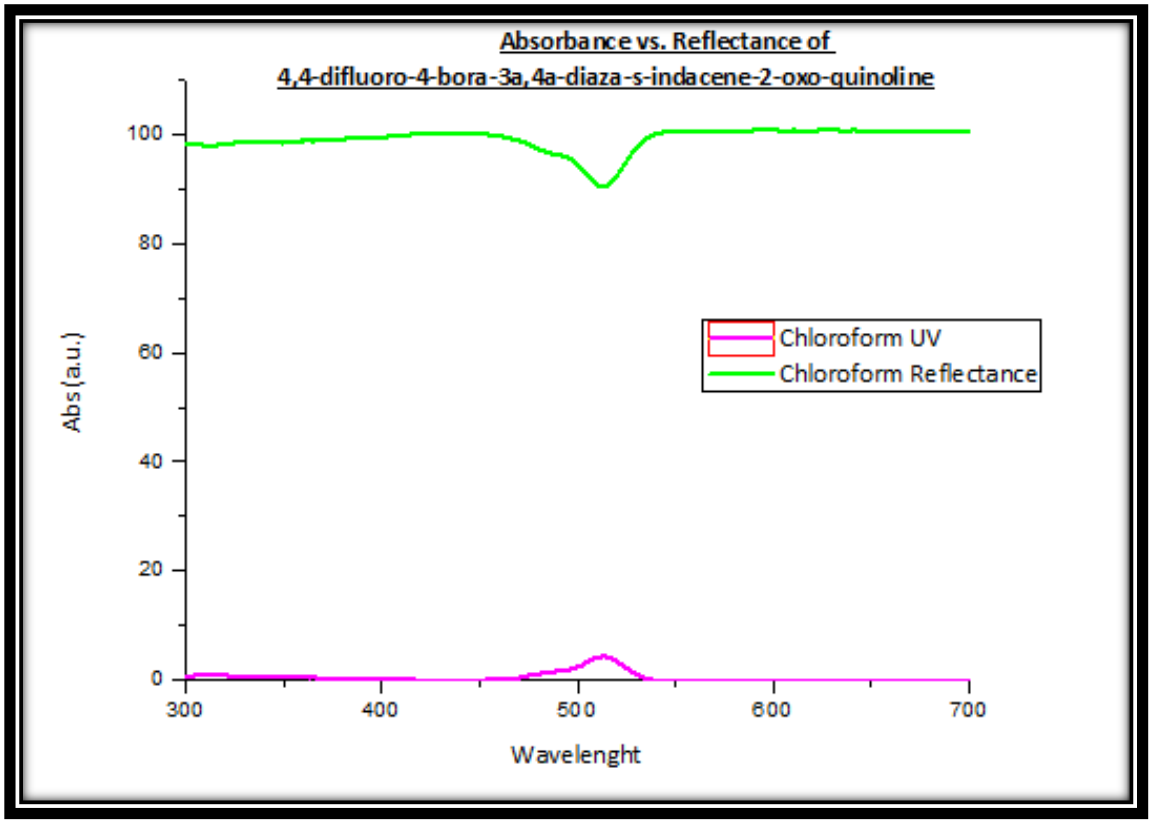

Appendix 112: Absorbance vs. Reflectance Spectra of 4,4-difluoro-4-bora-3a,4a-diaza-s-indacene-2-oxo-quinoline in Acetonitrile

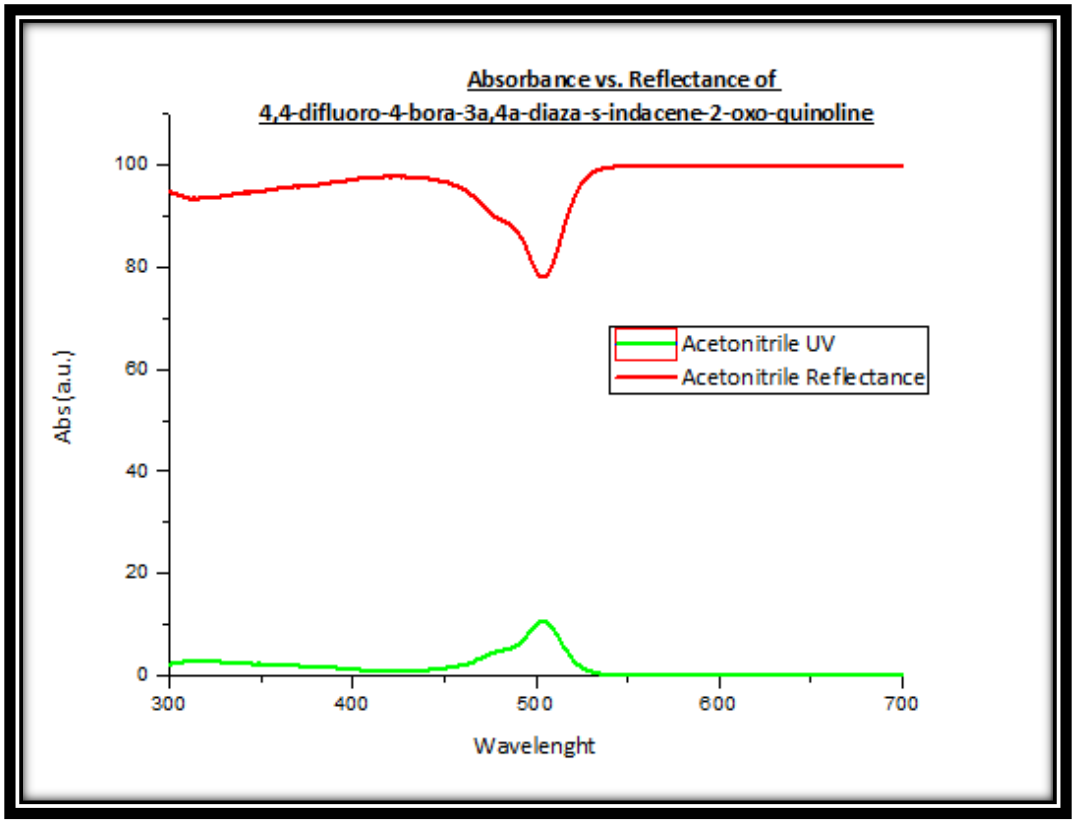

Appendix 113: Reflectance Spectra of 3-(4,5-Dihydro-1H-imidazol-2-yl)-1H-quinolin-2-one

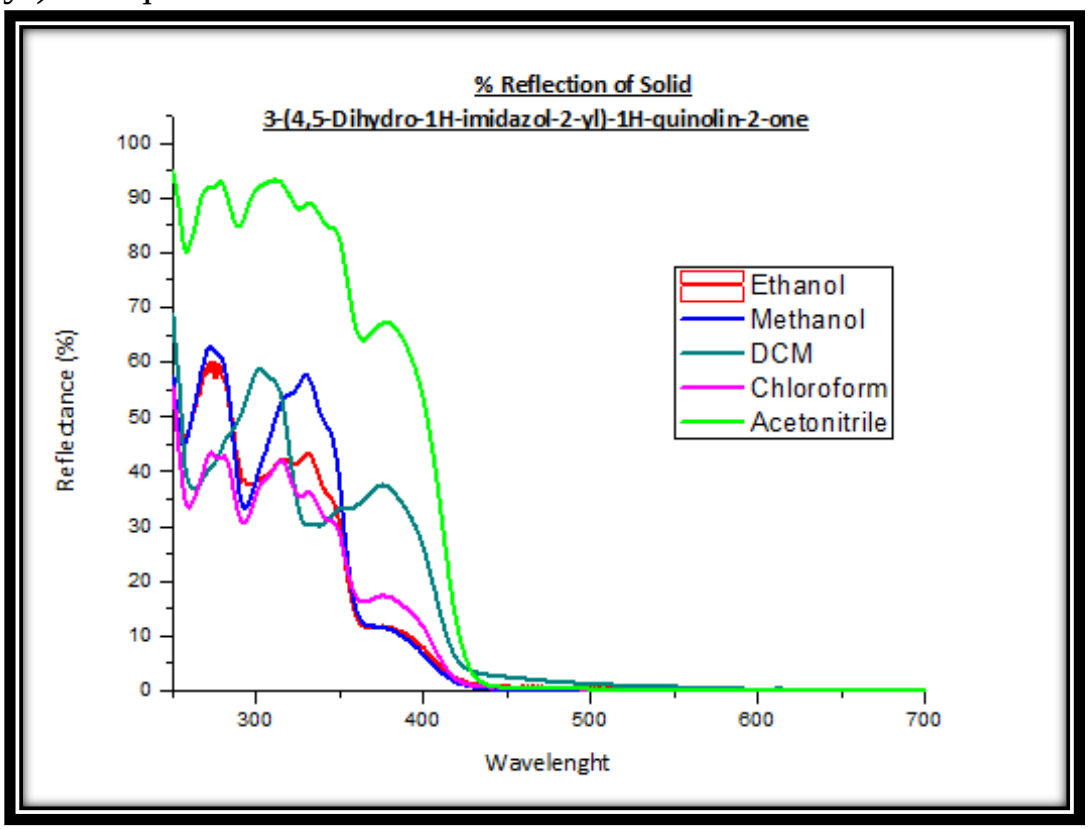

Appendix 114: Reflectance Spectra of 3-(-1H-Benzoimidazol-2-yl)-1H-quinolin-2-one

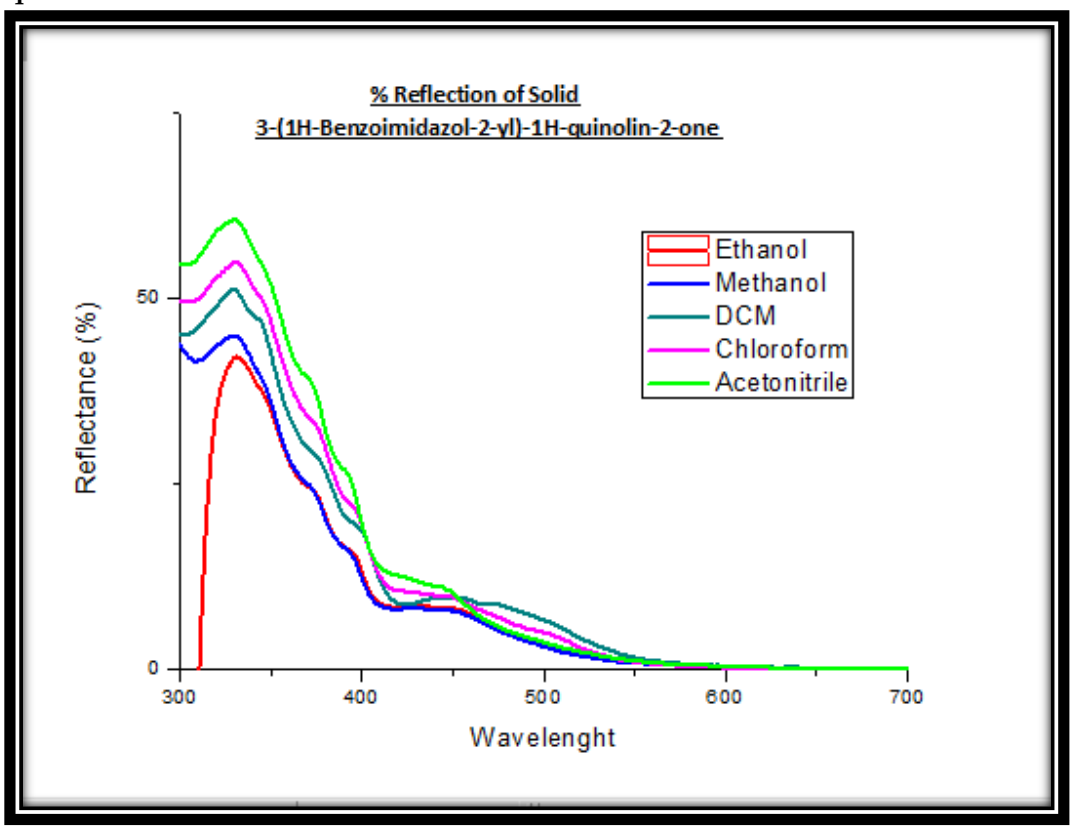

Appendix 115: Reflectance Spectra of 3-(6-Nitro-1H-Benzoimidazol-2-yl)-1H-quinolin-2-one

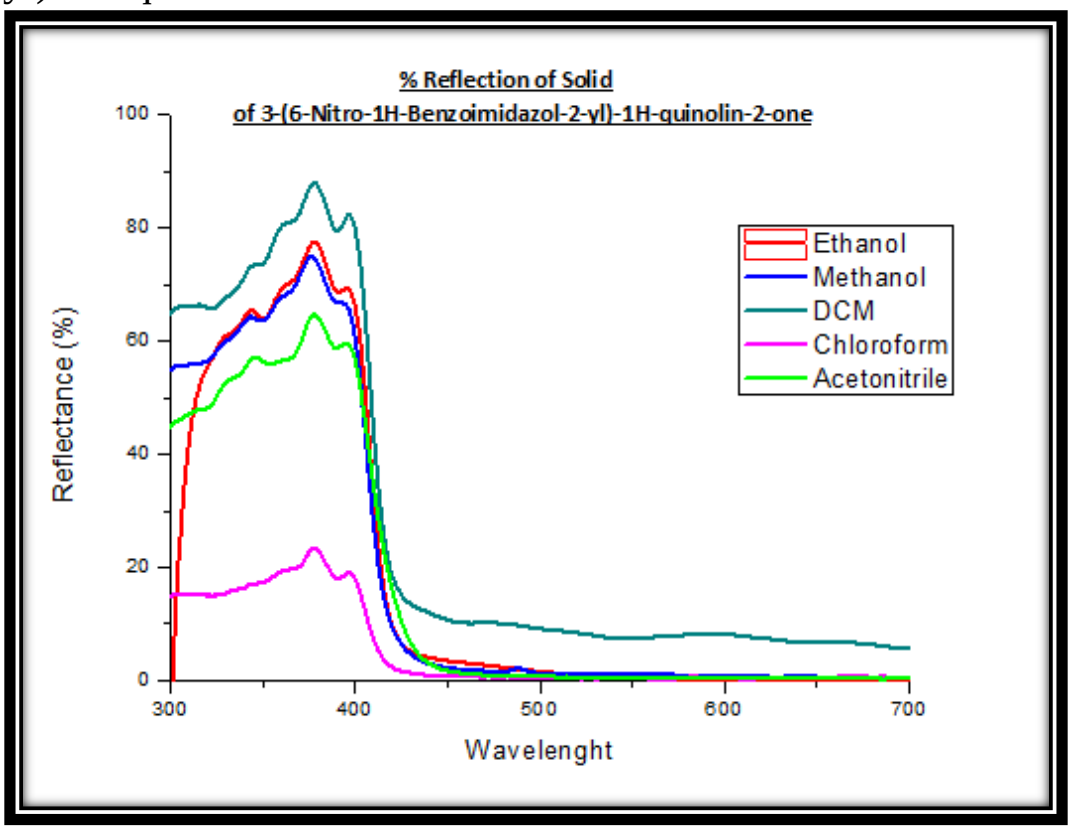

Appendix 116: Reflectance Spectra of 4,4-difluoro-4-bora-3a,4a-diaza-s-indacene-2-Chloro-quinoline

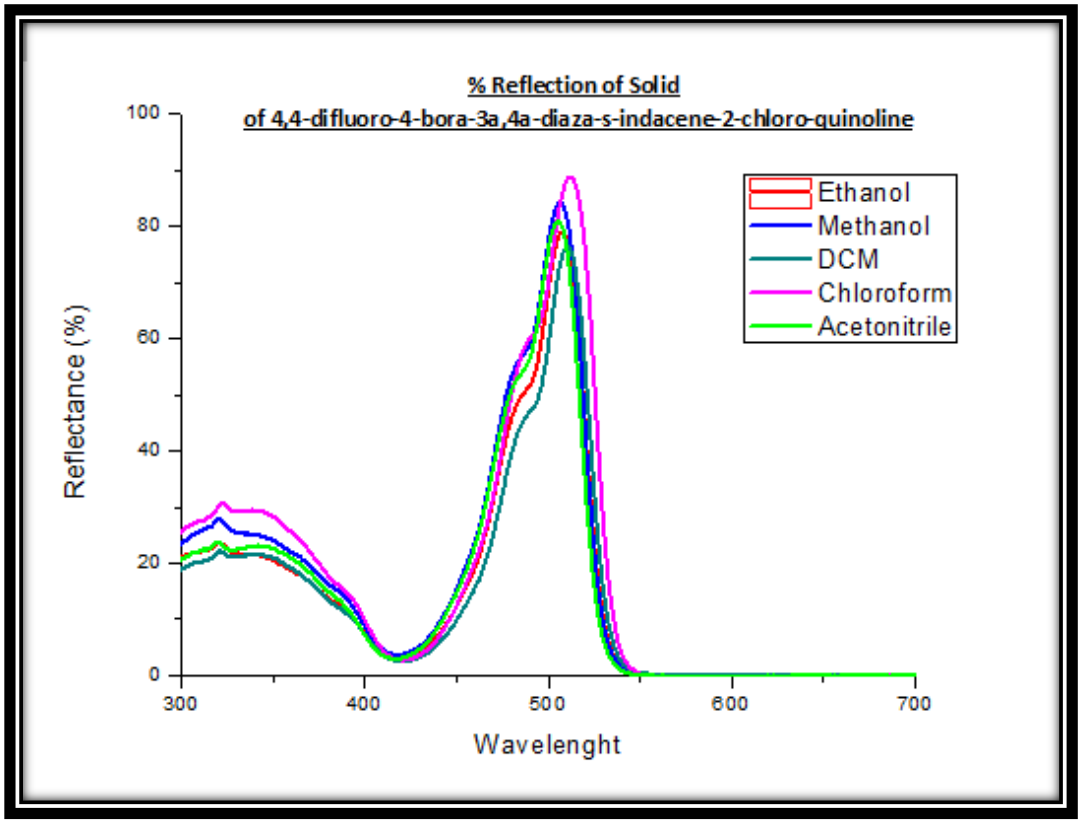

Appendix 117: Reflectance Spectra of 4,4-difluoro-4-bora-3a,4a-diaza-s-indacene-2-oxo-quinoline

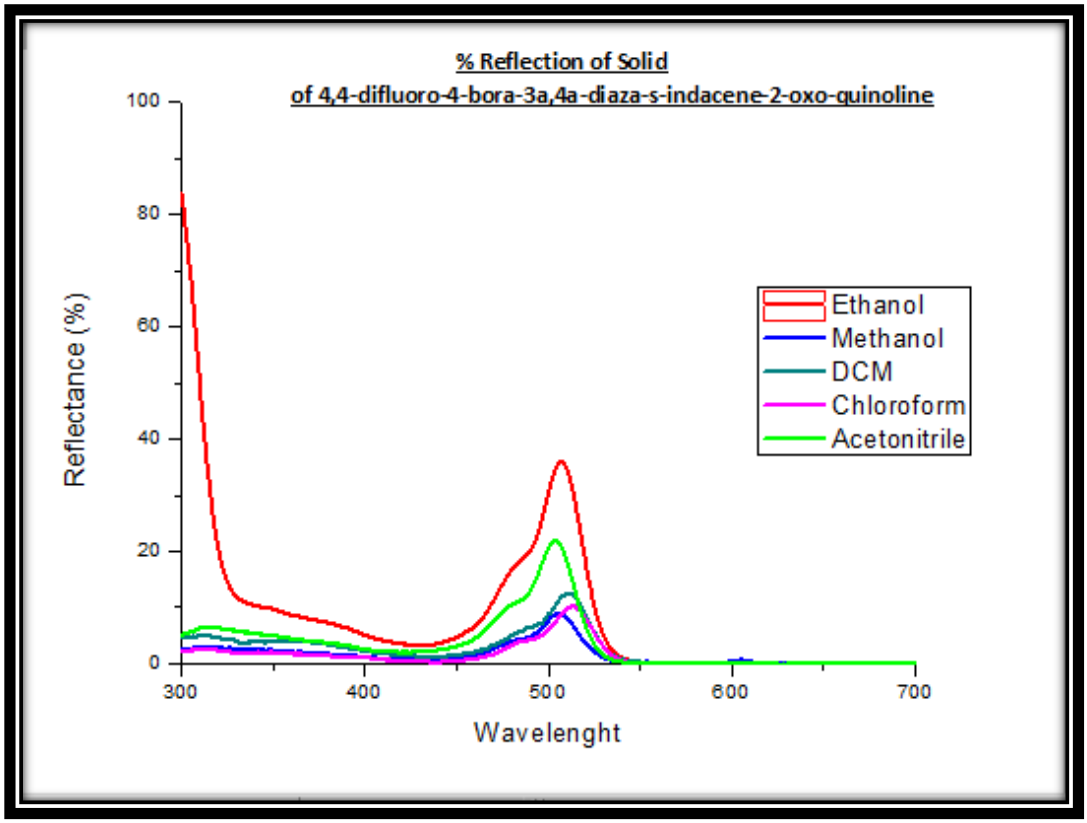

Appendix 118: Transmittance Spectra of 3-(4,5-Dihydro-1H-imidazol-2-yl)-1H-quinolin-2-one

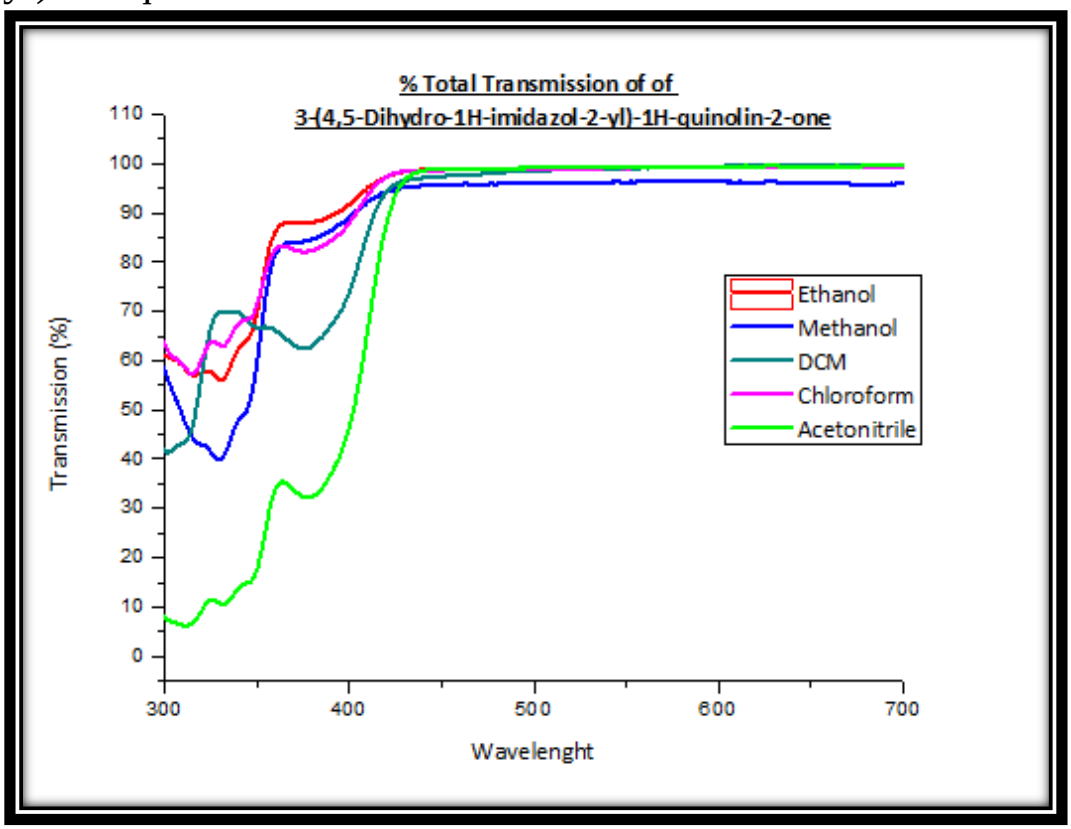

Appendix 119: Transmittance Spectra of 3-(-1H-Benzoimidazol-2-yl)-1H-quinolin-2-one

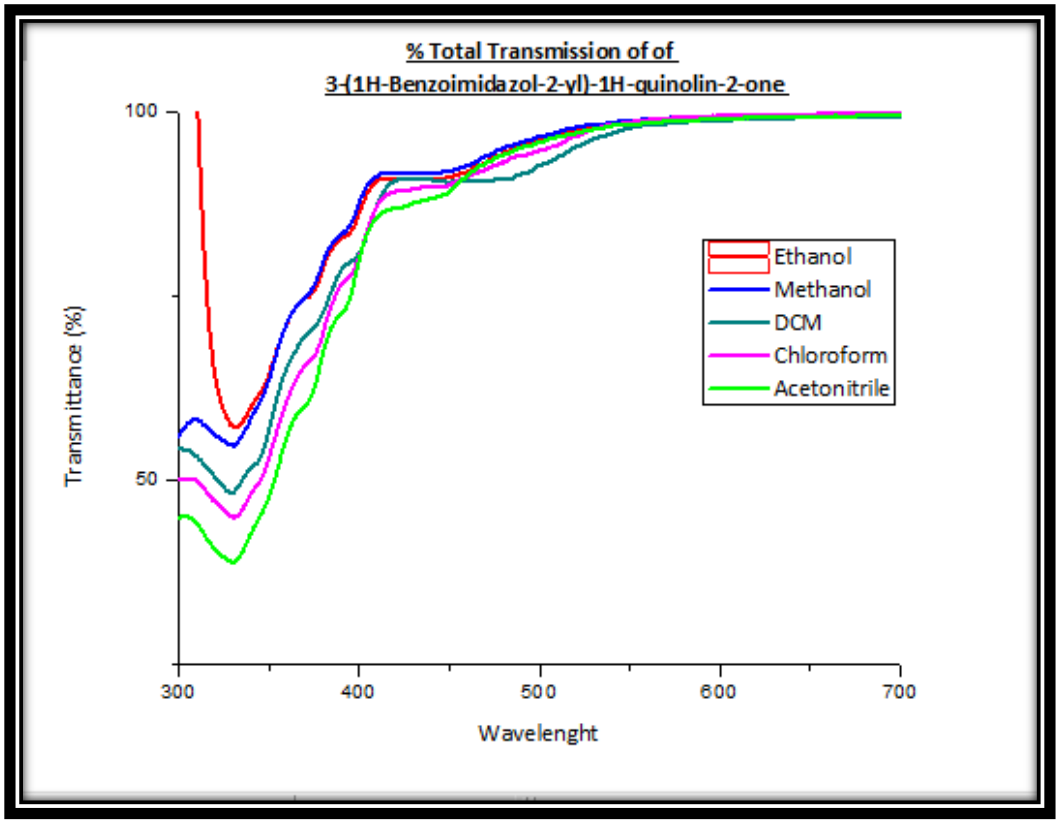

Appendix 120: Transmittance Spectra of 3-(6-Nitro-1H-Benzoimidazol-2-yl)-1H-quinolin-2-one

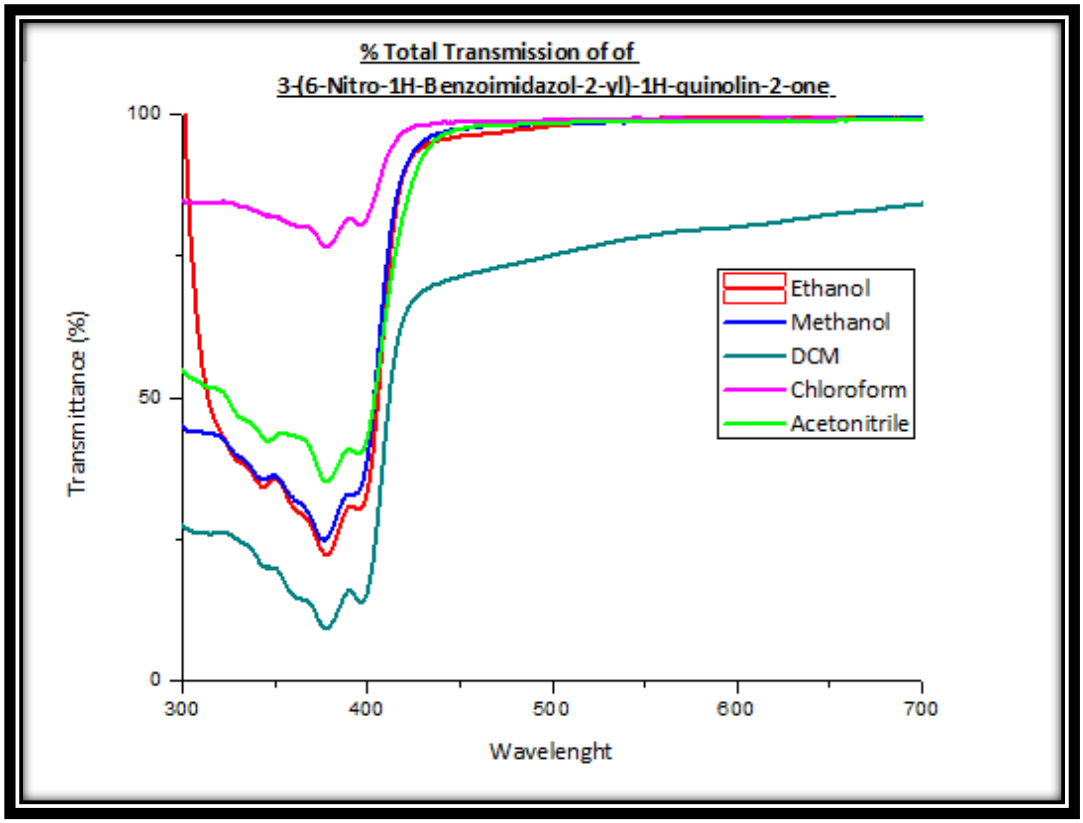

Appendix 121: Transmittance Spectra of 4,4-difluoro-4-bora-3a,4a-diaza-s-indacene-2-Chloro-quinoline

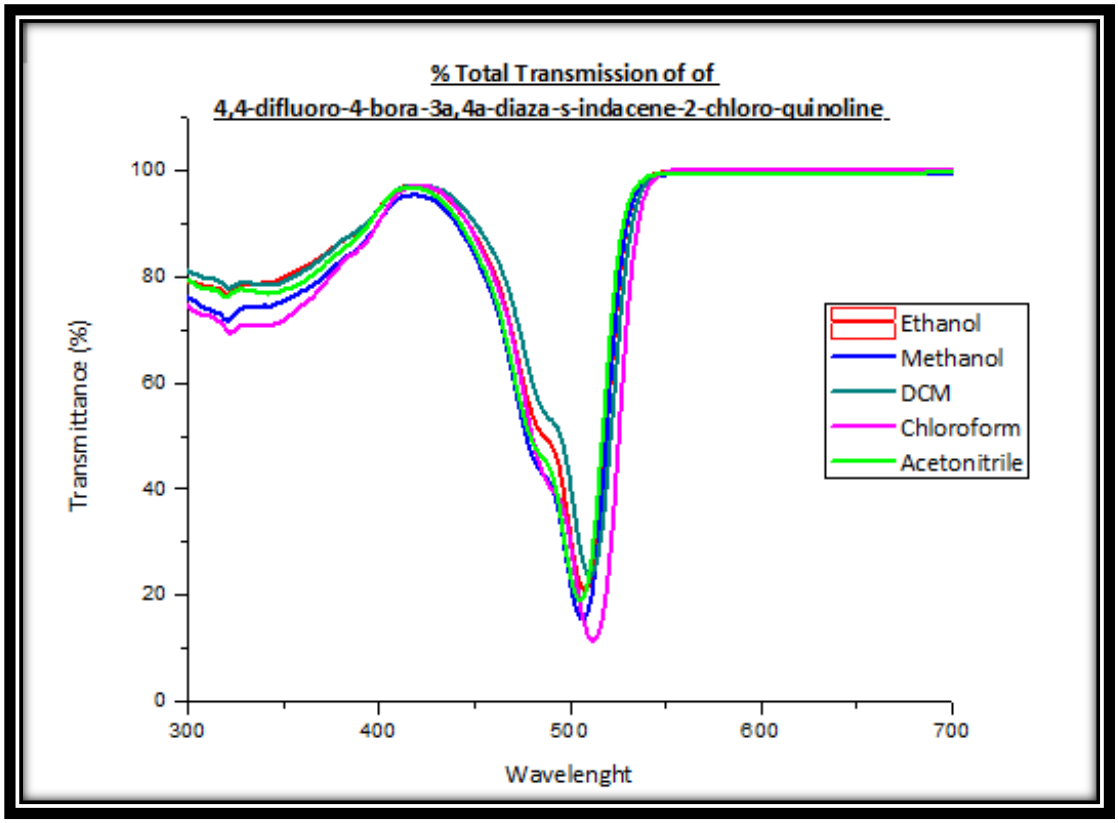

Appendix 122: Transmittance Spectra of 4,4-difluoro-4-bora-3a,4a-diaza-s-indacene-2-oxo-quinoline

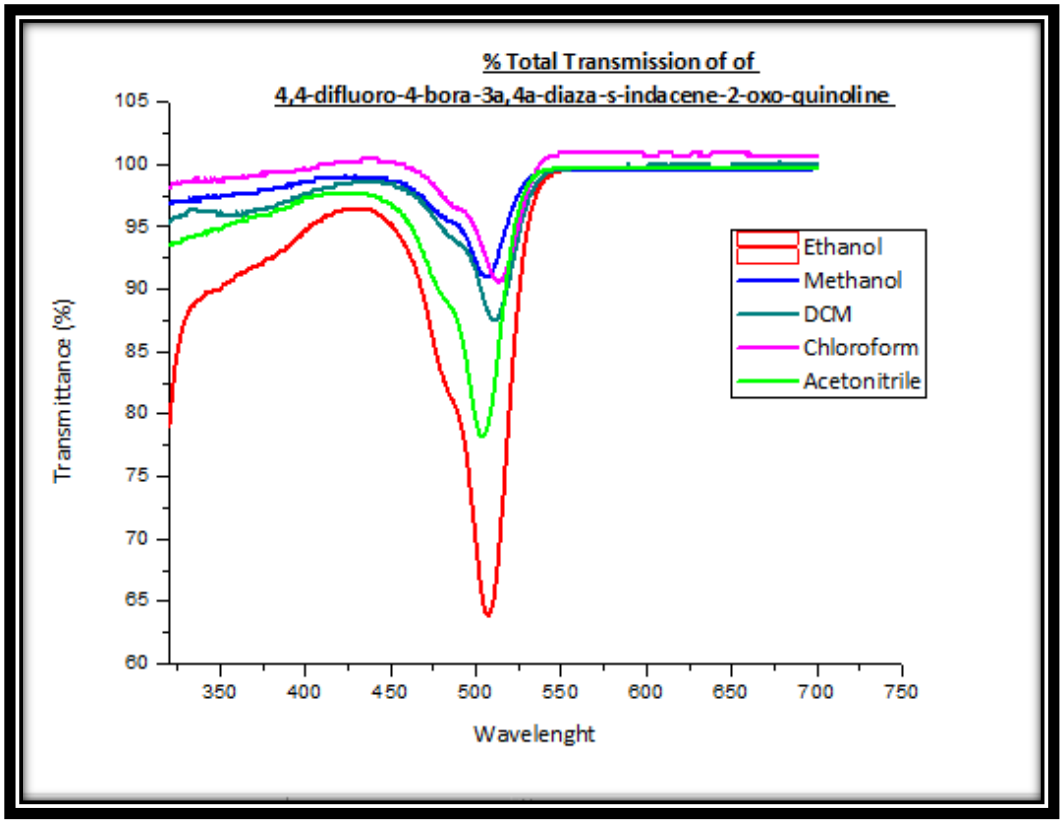

Appendix 123: Reflectance Spectra of 3-(4,5-Dihydro-1H-imidazol-2-yl)-1H-quinolin-2-one

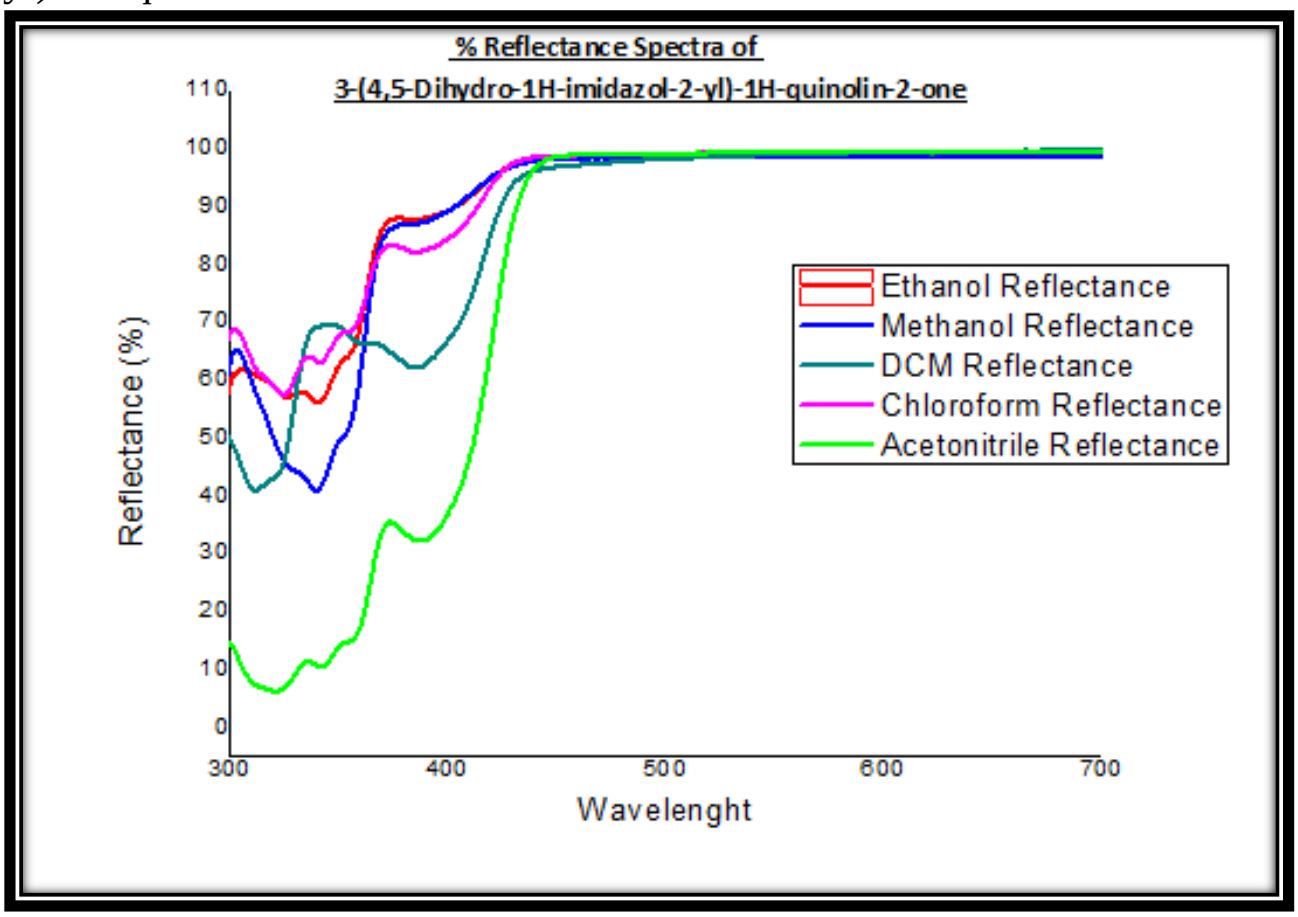

Appendix 124: Reflectance Spectra of 3-(-1H-Benzoimidazol-2-yl)-1H-quinolin-2-one

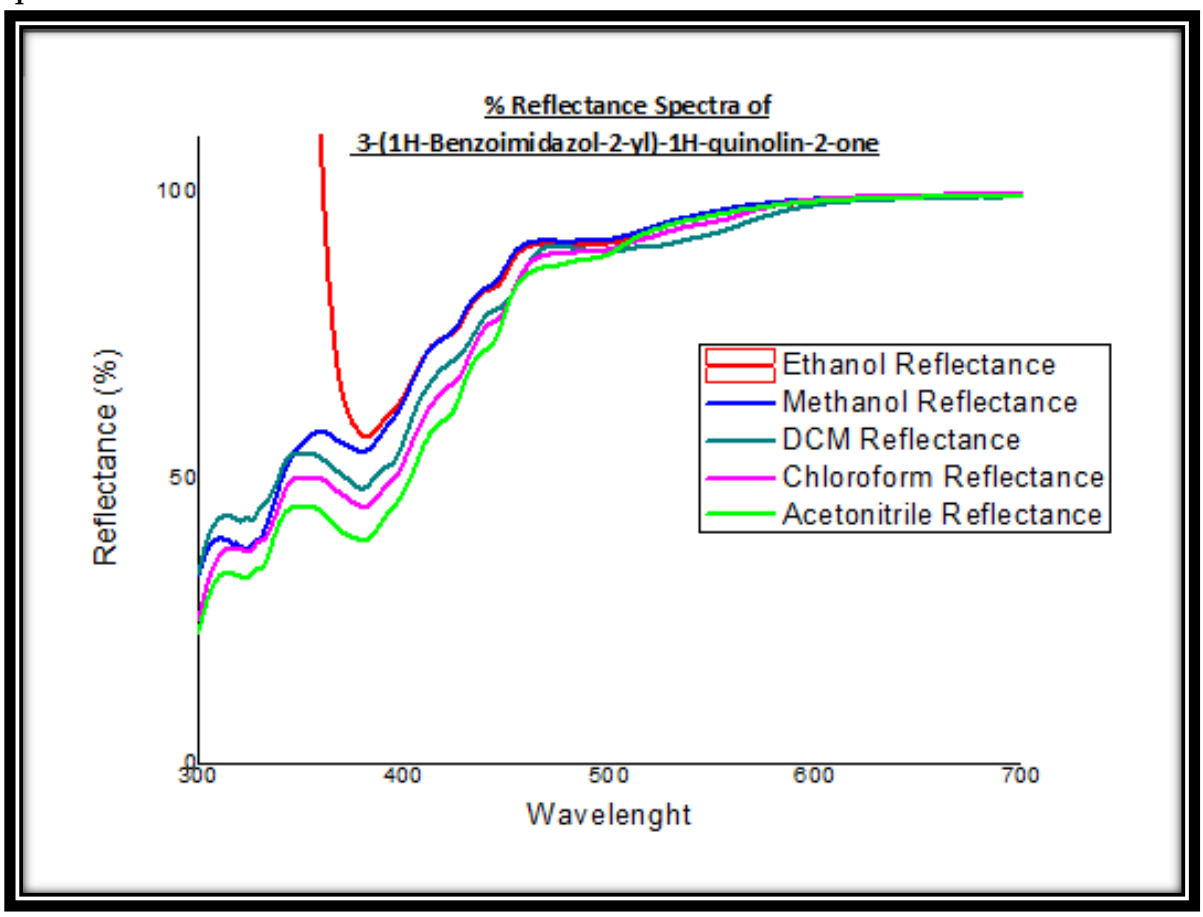

Appendix 125: Reflectance Spectra of 3-(6-Nitro-1H-Benzoimidazol-2-yl)-1H-quinolin-2-one

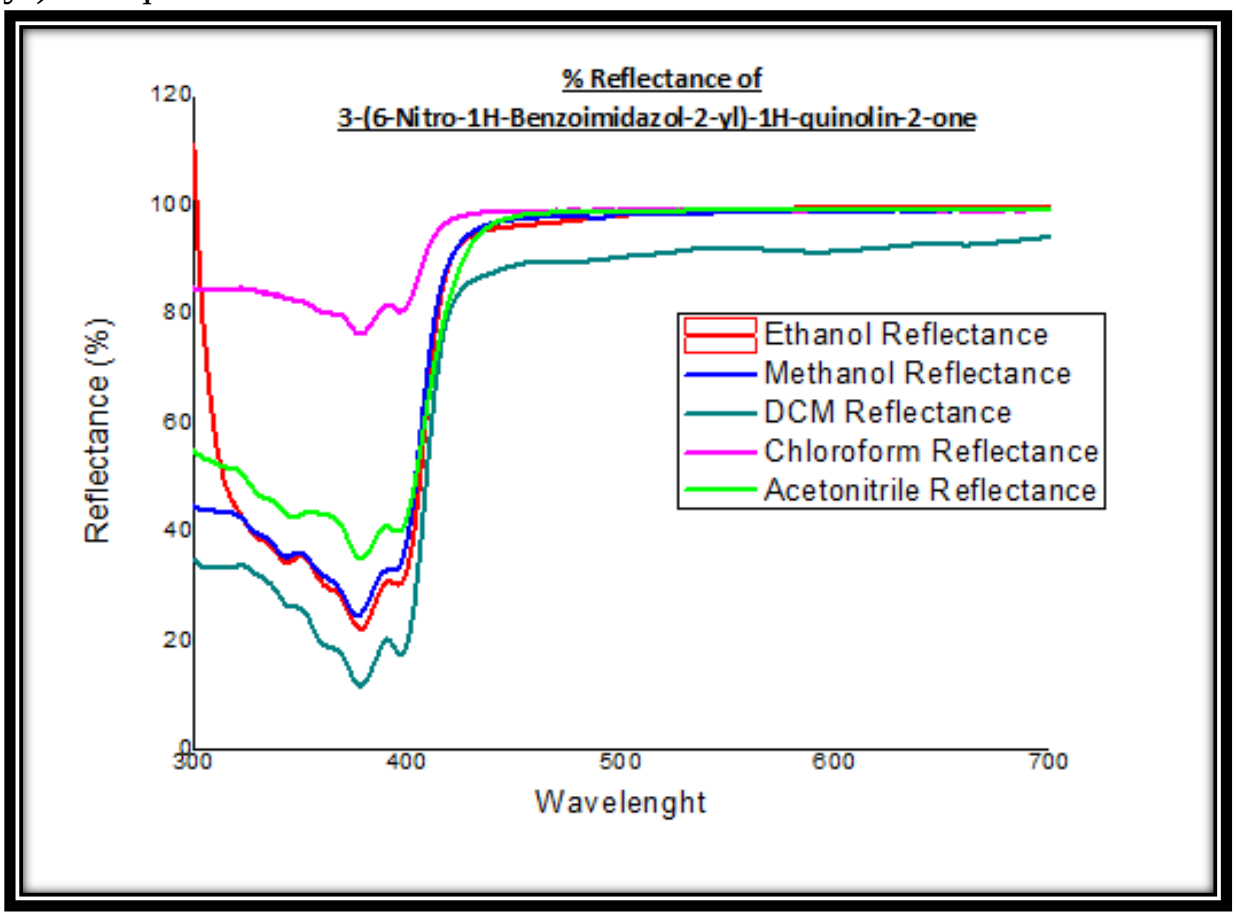

Appendix 126: Reflectance Spectra of 4,4-difluoro-4-bora-3a,4a-diaza-s-indacene-2-Chloro-quinoline

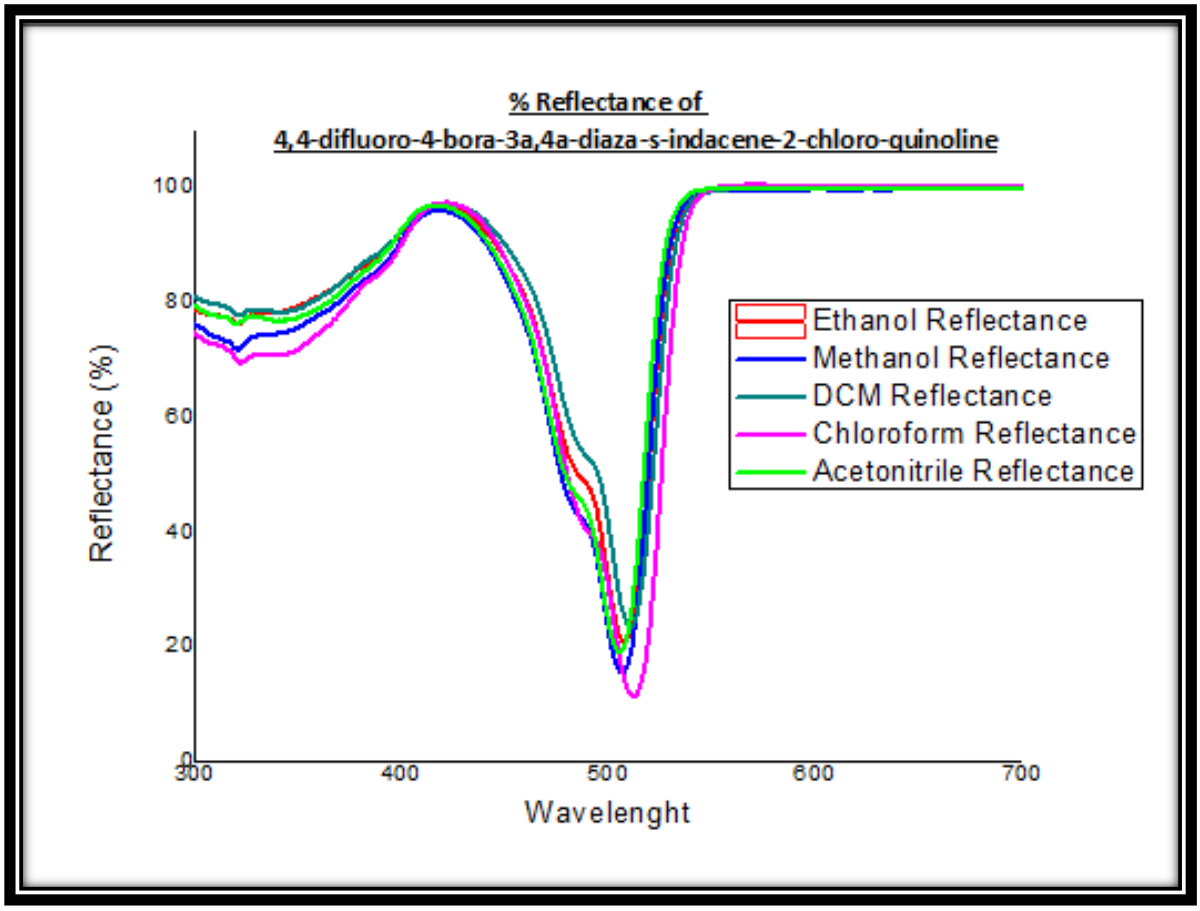

Appendix 127: Reflectance Spectra of 4,4-difluoro-4-bora-3a,4a-diaza-s-indacene-2-oxo-quinoline

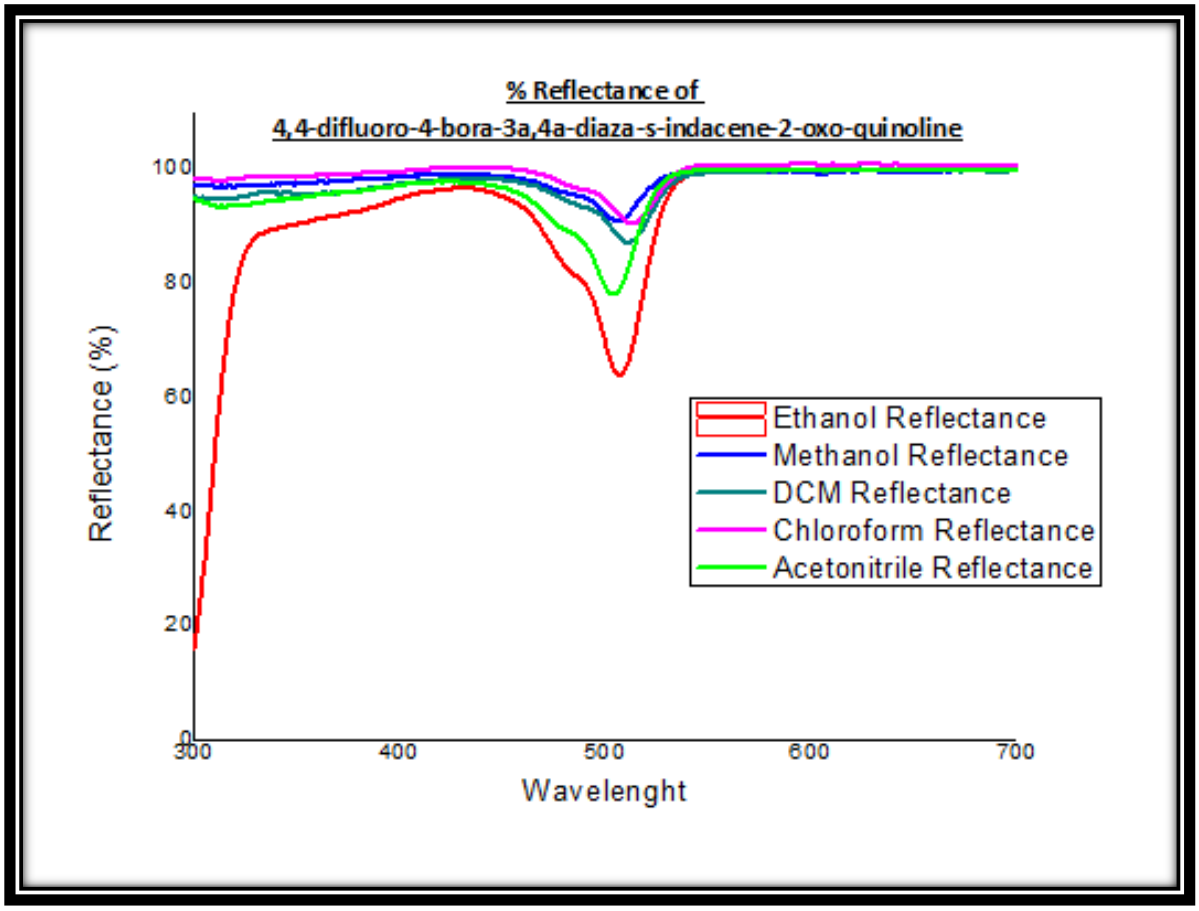

Appendix 128: Binding of Metal ions with 2

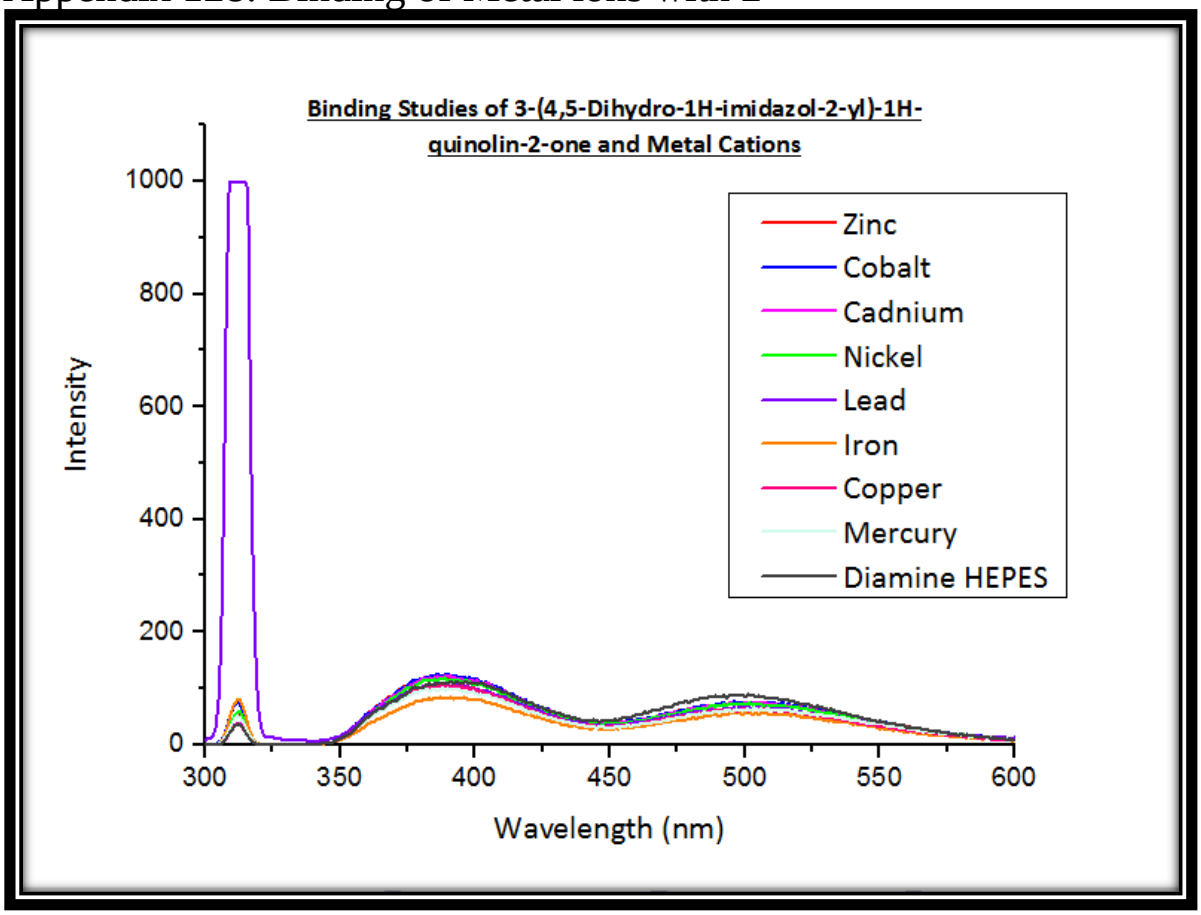

Appendix 129: 2 in HEPES vs. in ACN

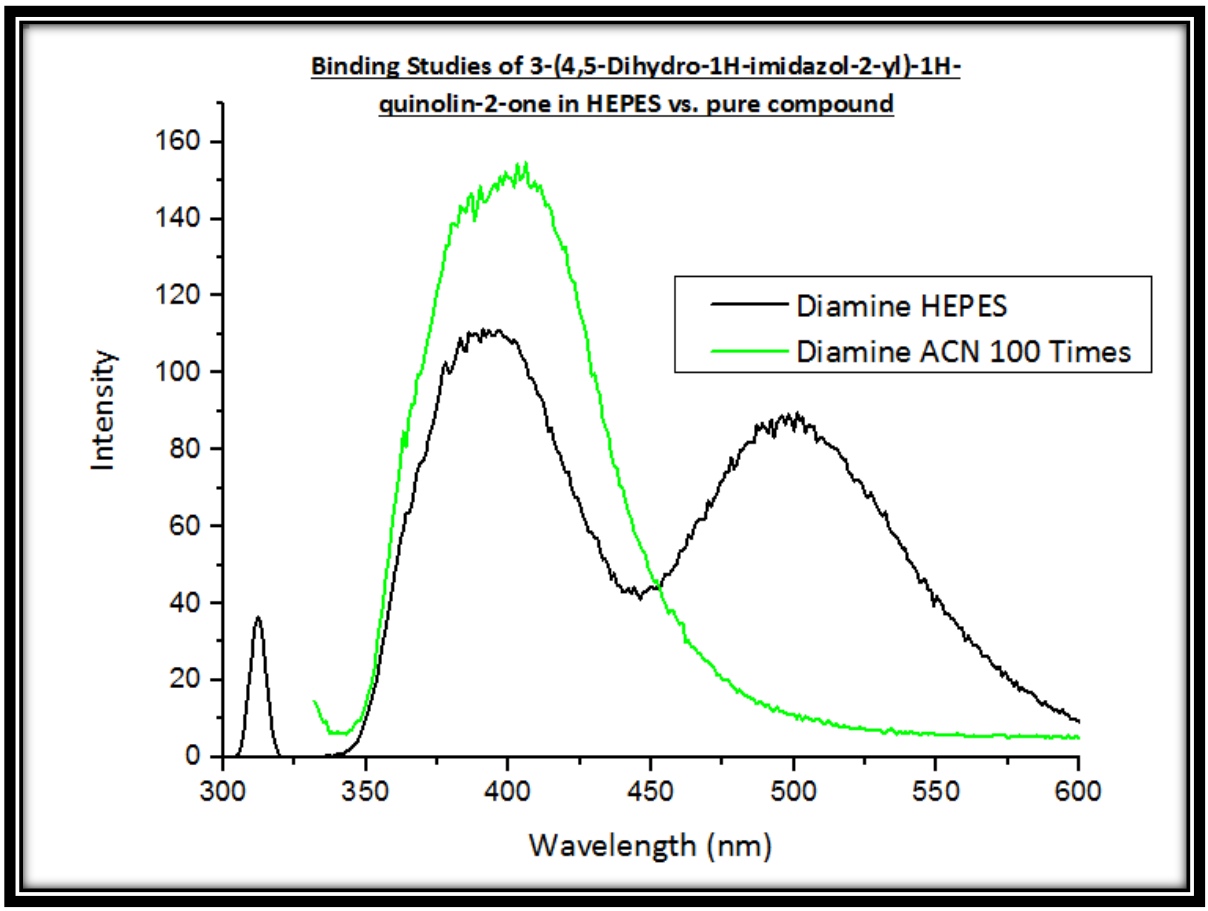

Appendix 130: 2 Binding with Zinc Ion

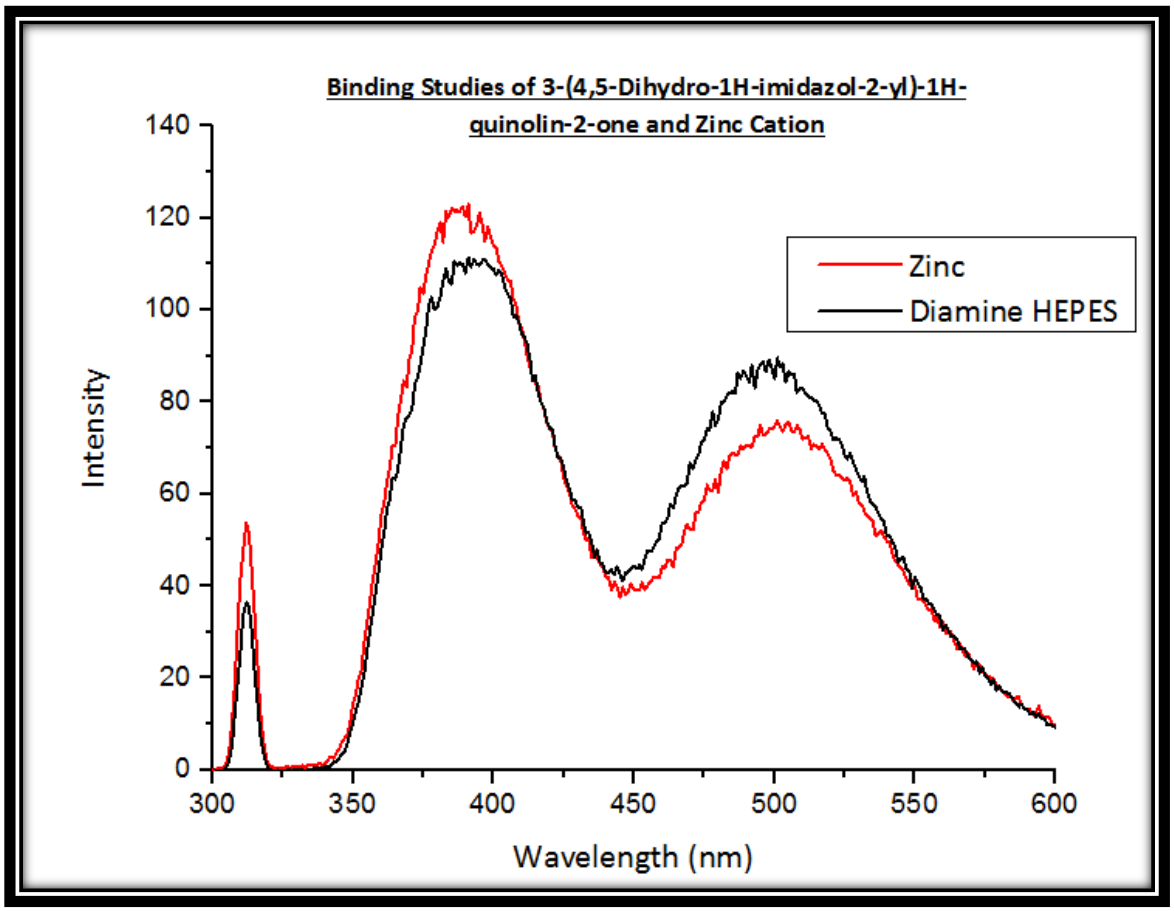

Appendix 131: 2 Binding with Cobalt Ion

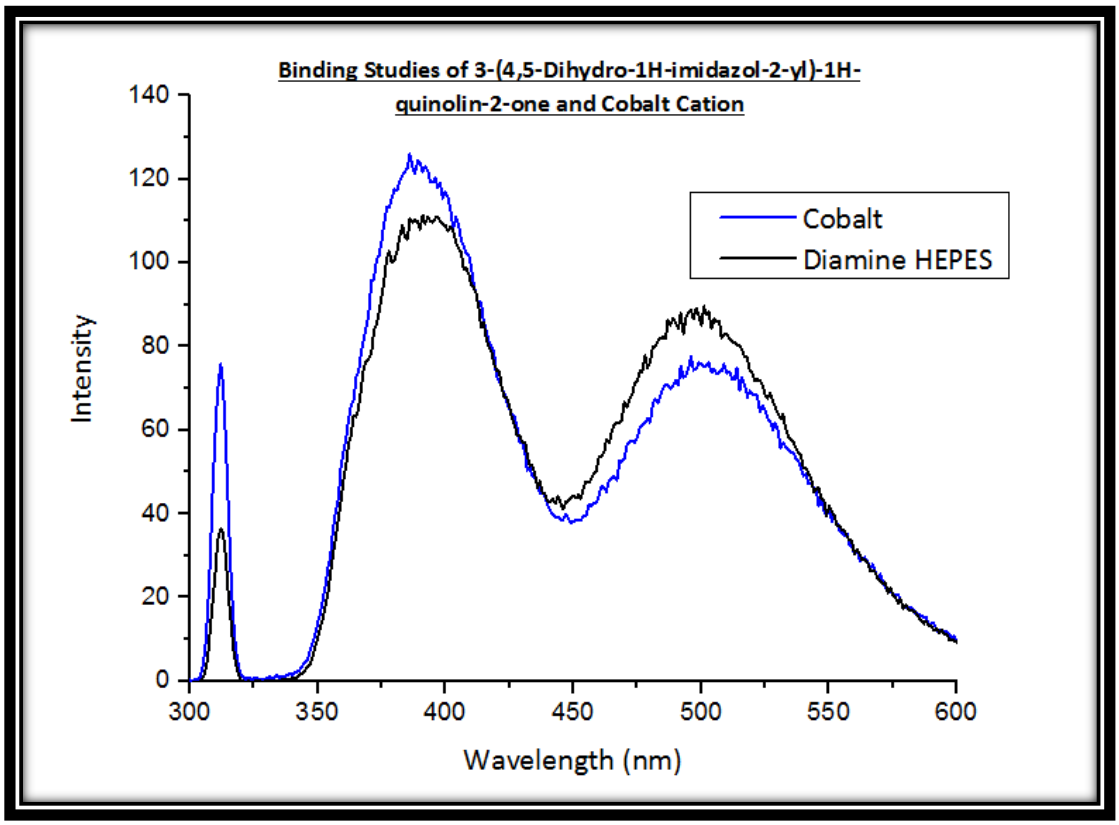

Appendix 132: 2 Binding with Cadmium Ion

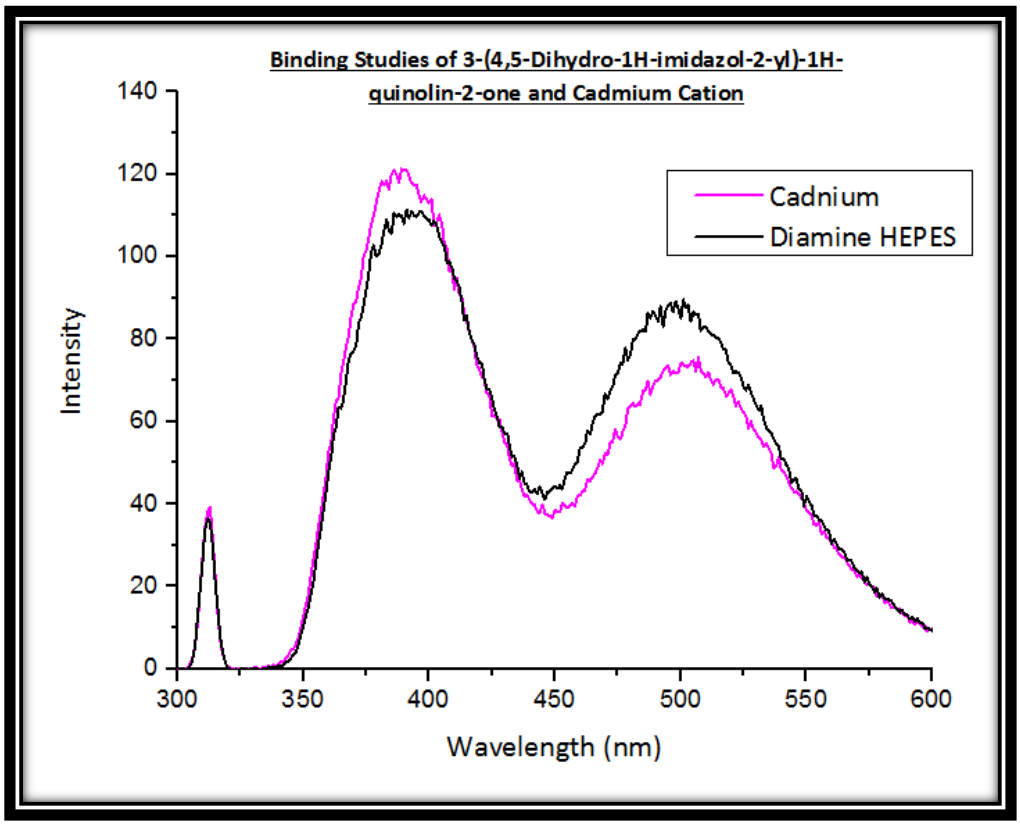

Appendix 133: 2 Binding with Nickel Ion

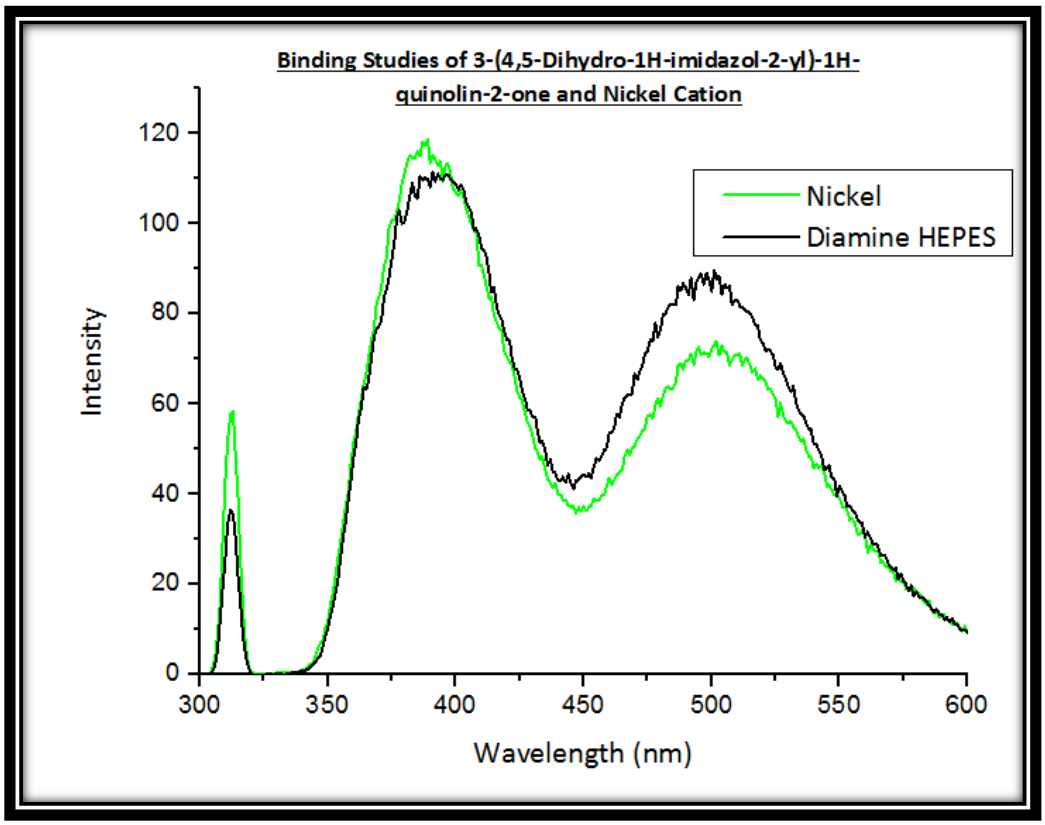

Appendix 134: 2 Binding with Lead Ion

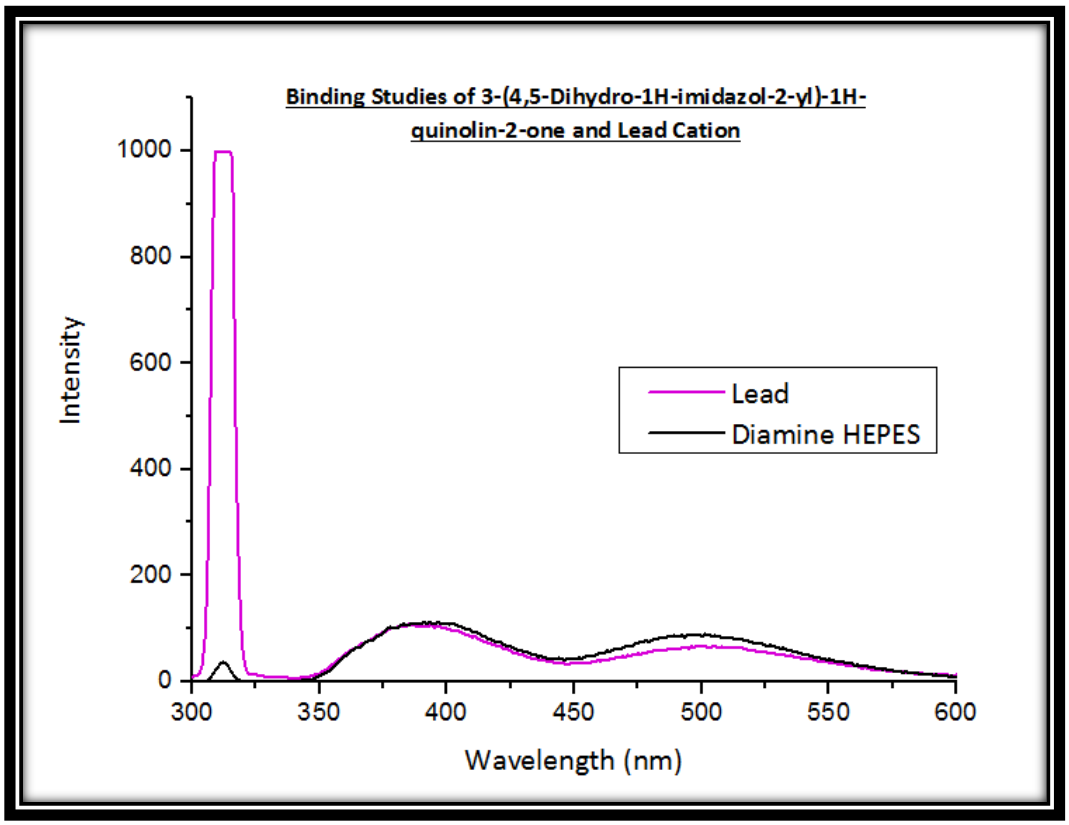

Appendix 135: 2 Binding with Iron Ion

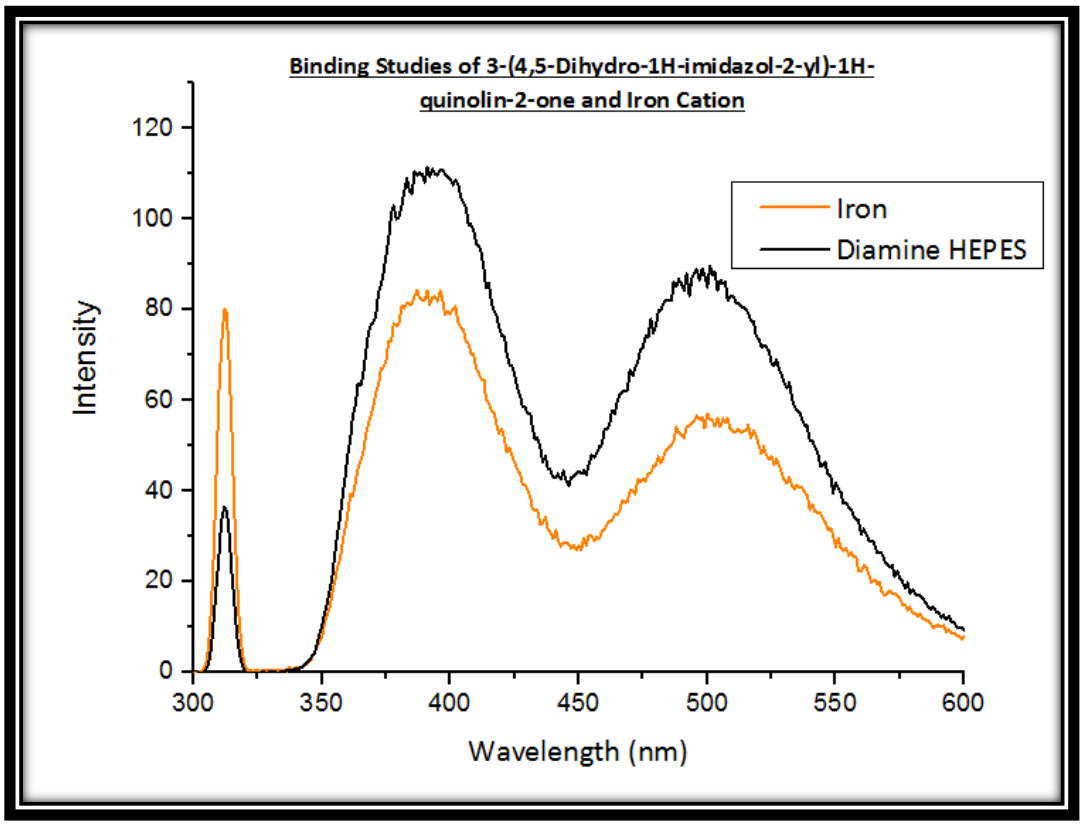

Appendix 136: 2 Binding with Copper Ion

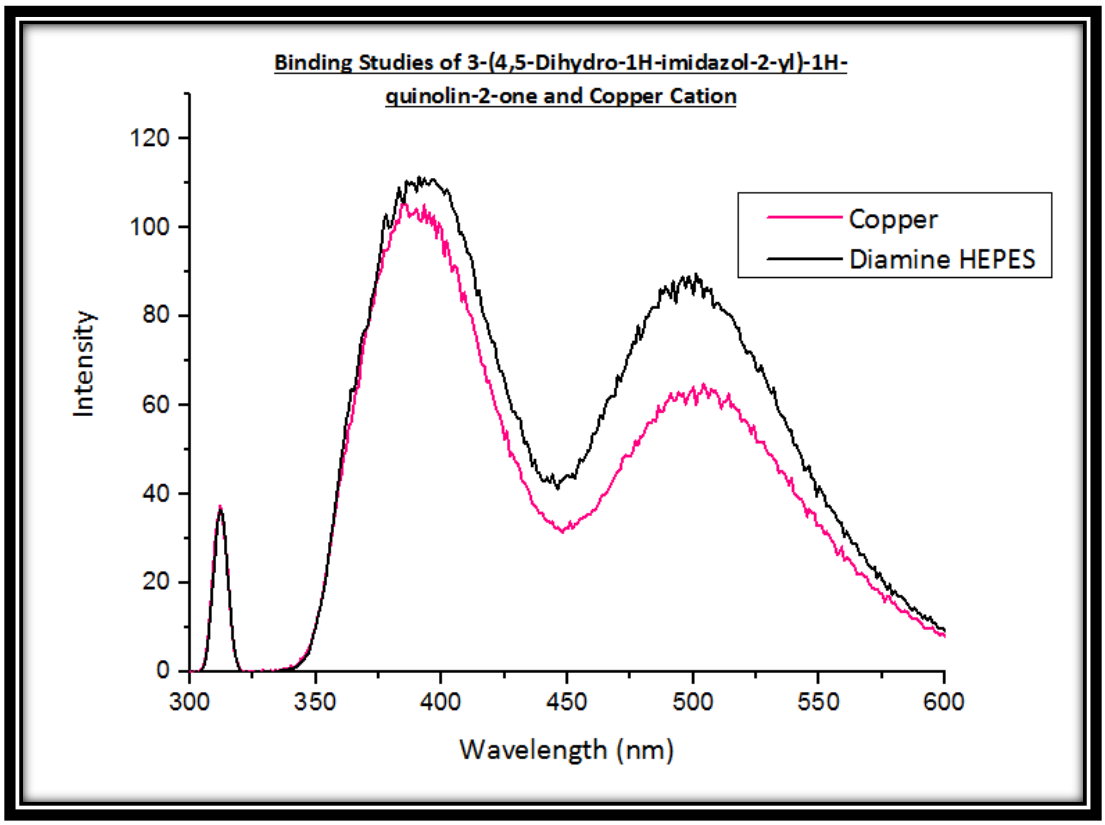

Appendix 137: 2 Binding with Mercury Ion

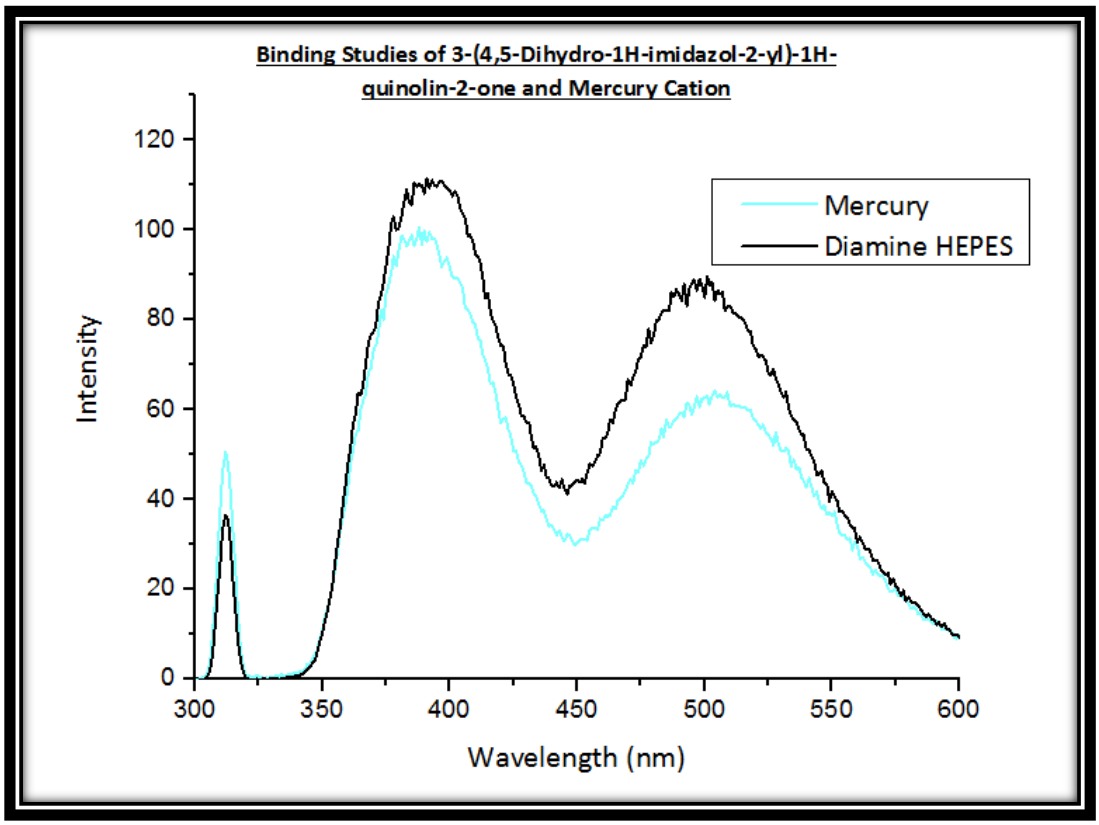

Appendix 138: Binding of Metal ions with 3

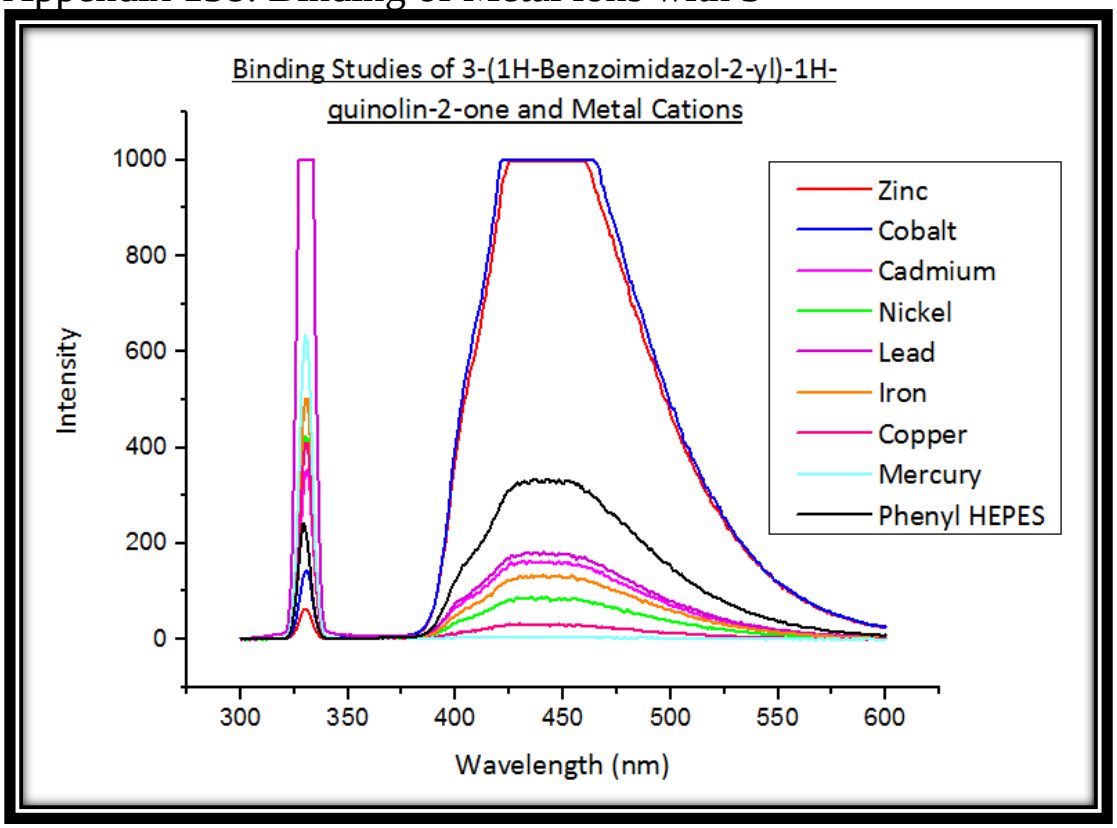

Appendix 139: 3 in HEPES vs. in ACN

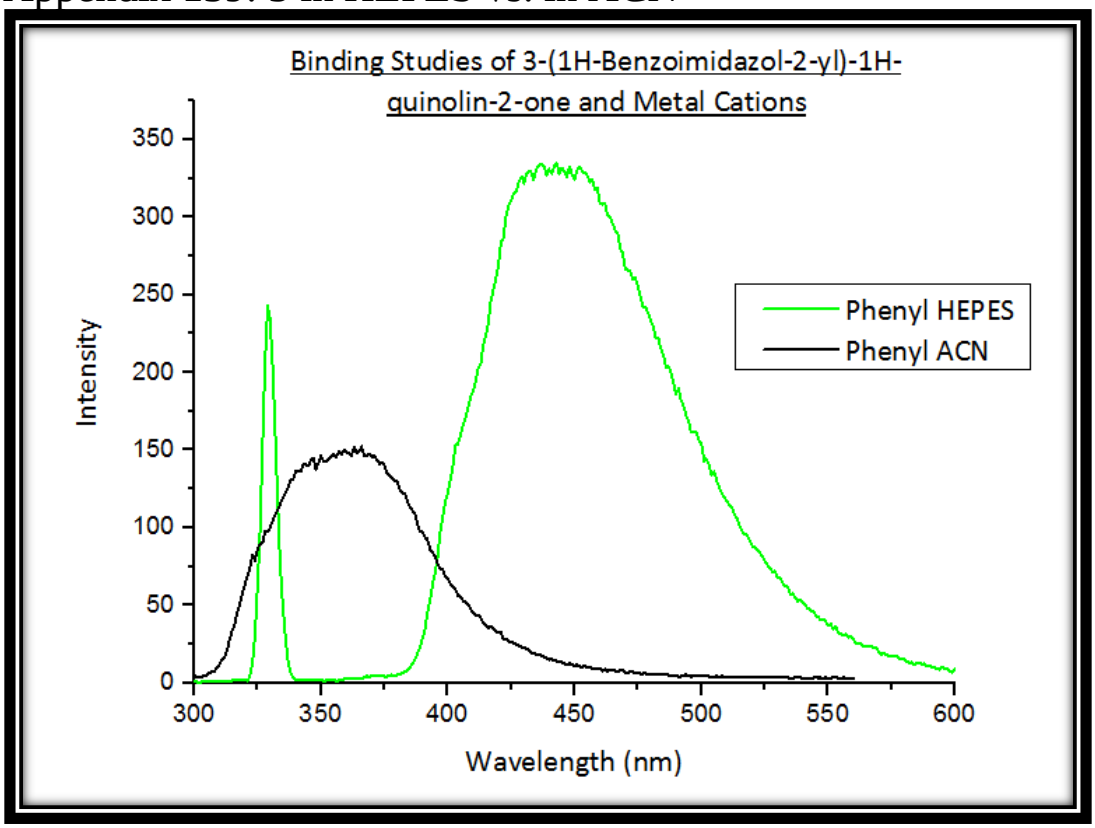

Appendix 140: 3 Binding with Zinc Ion

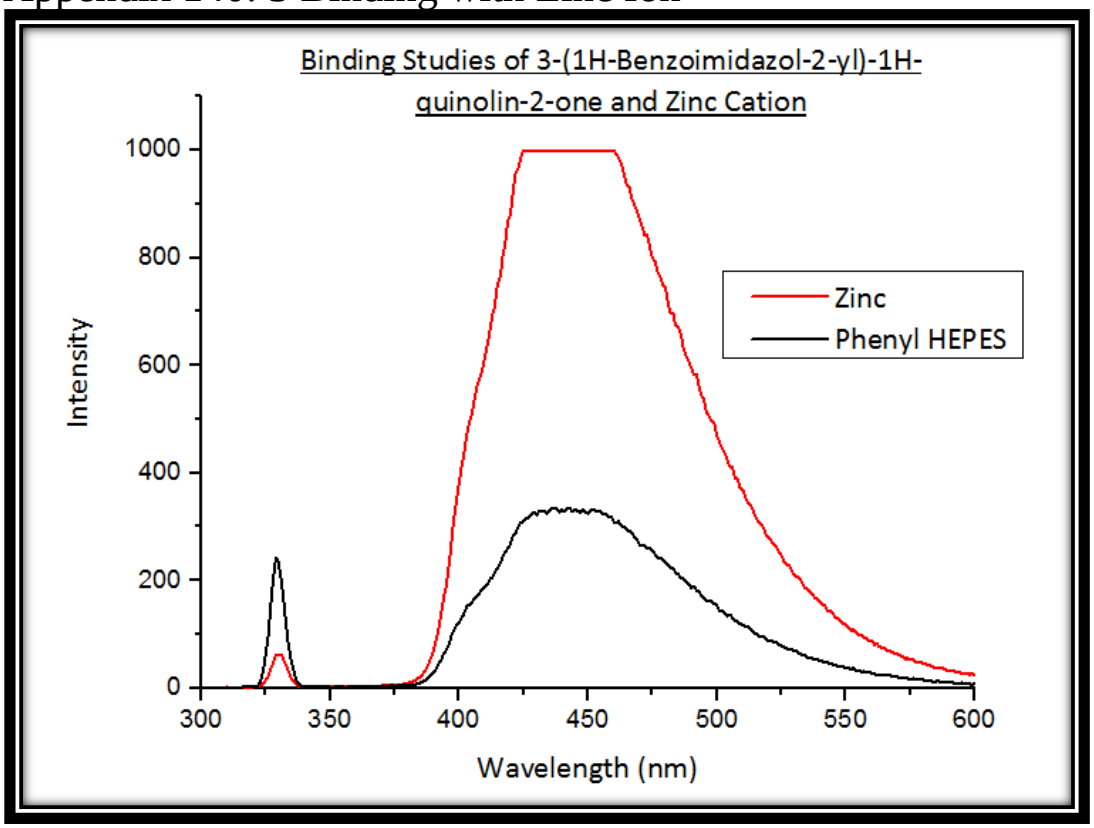

Appendix 141: 3 Binding with Cobalt Ion

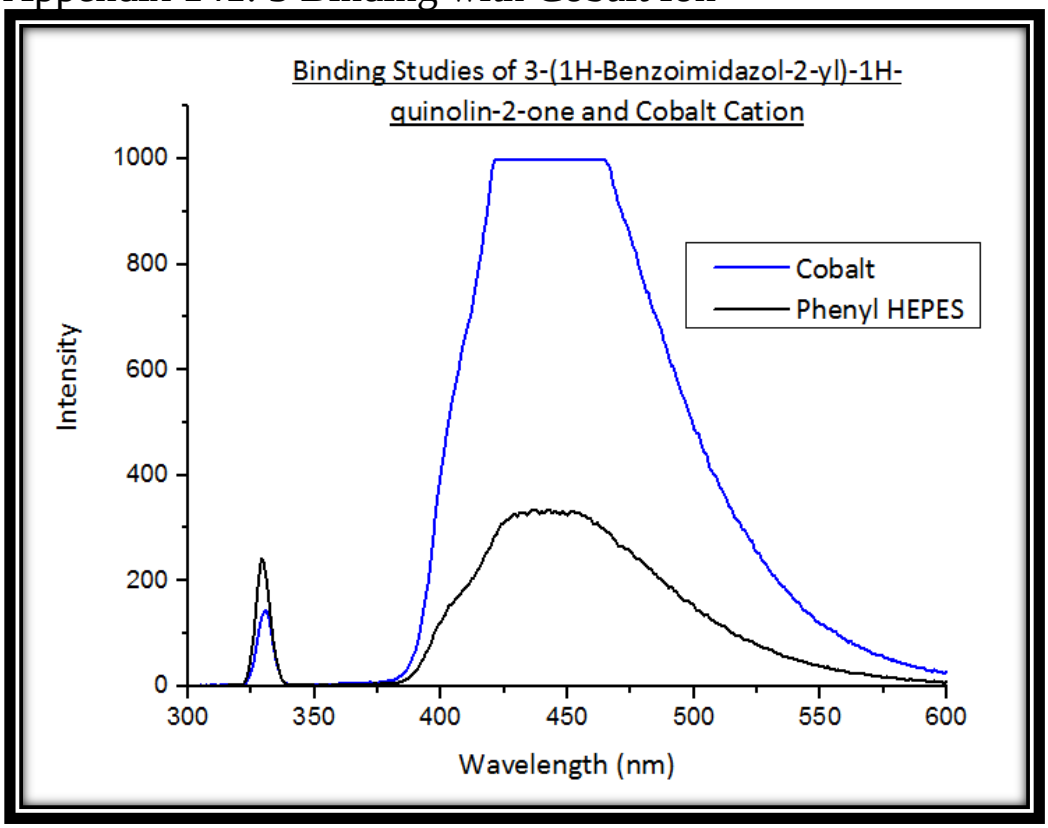

Appendix 142: 3 Binding with Cadmium Ion

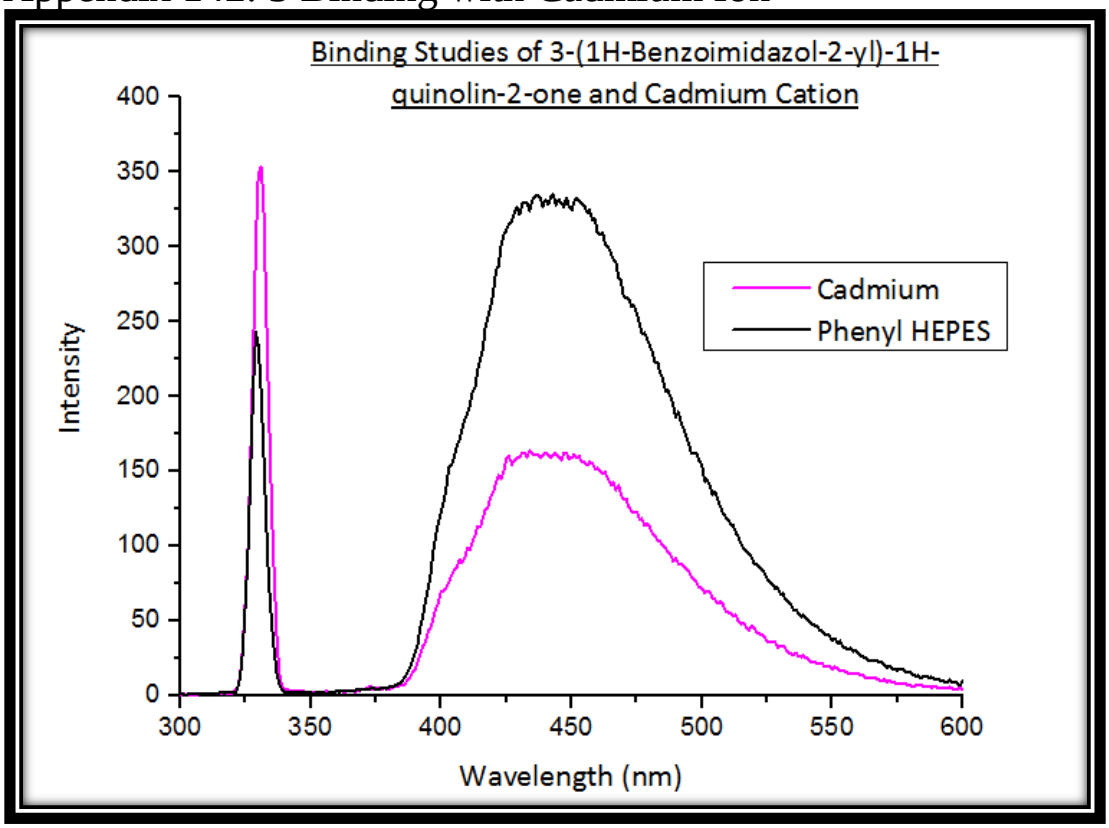

Appendix 143: 3 Binding with Nickel Ion

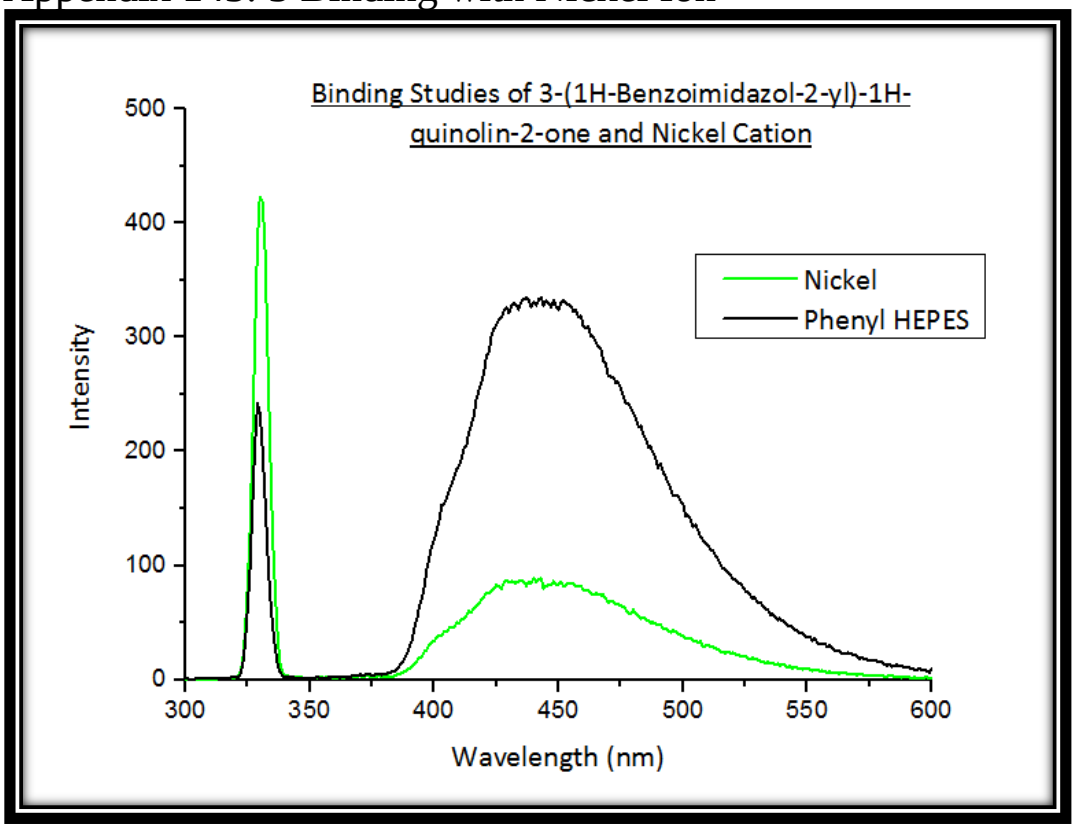

Appendix 144: 3 Binding with Lead Ion

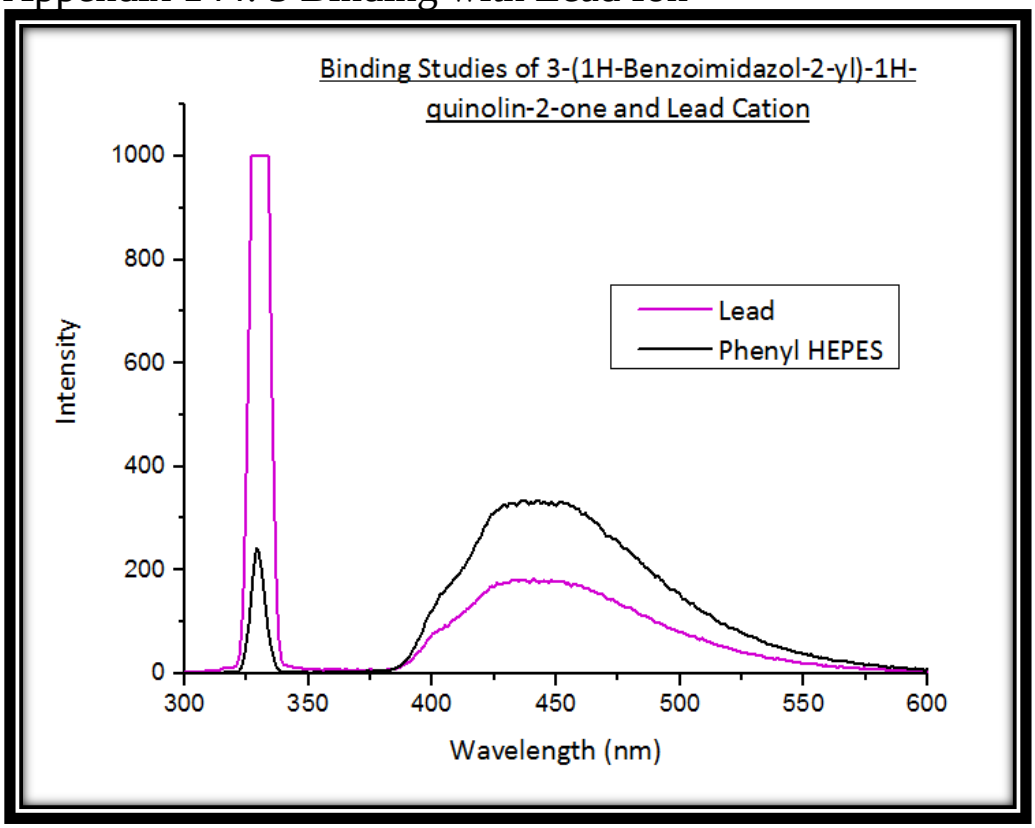

Appendix 145: 3 Binding with Iron Ion

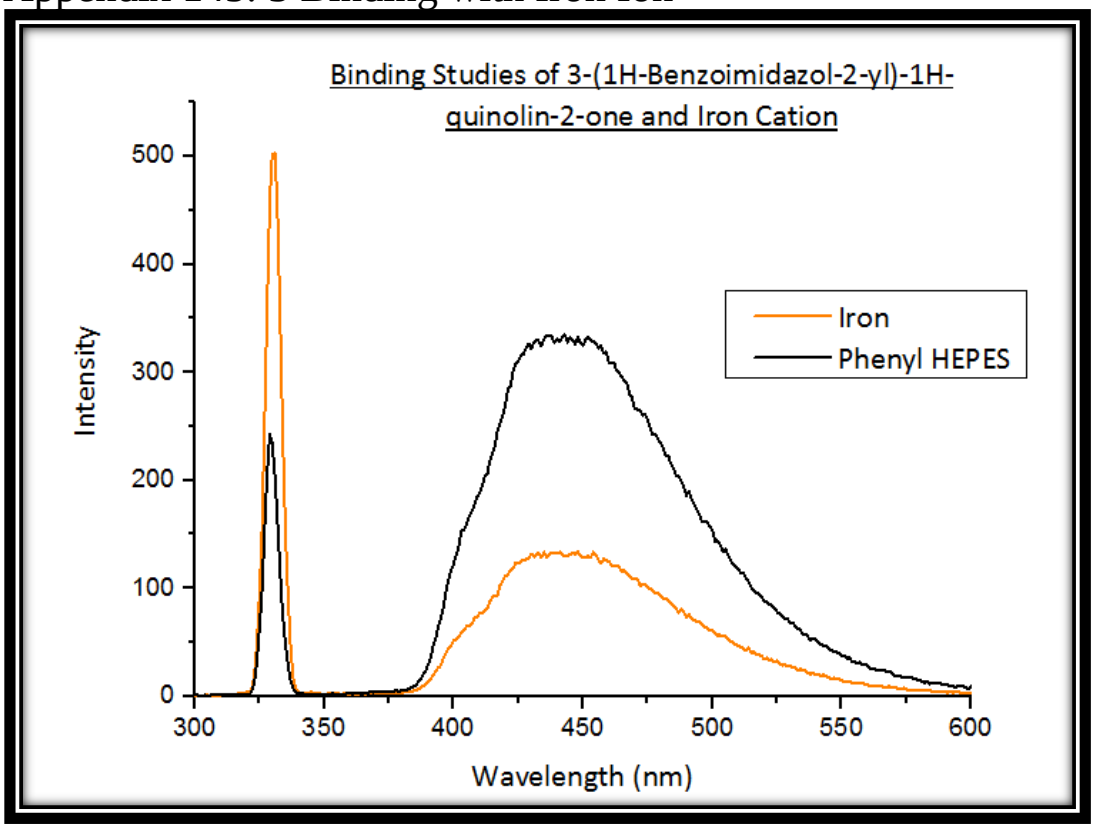

Appendix 146: 3 Binding with Copper Ion

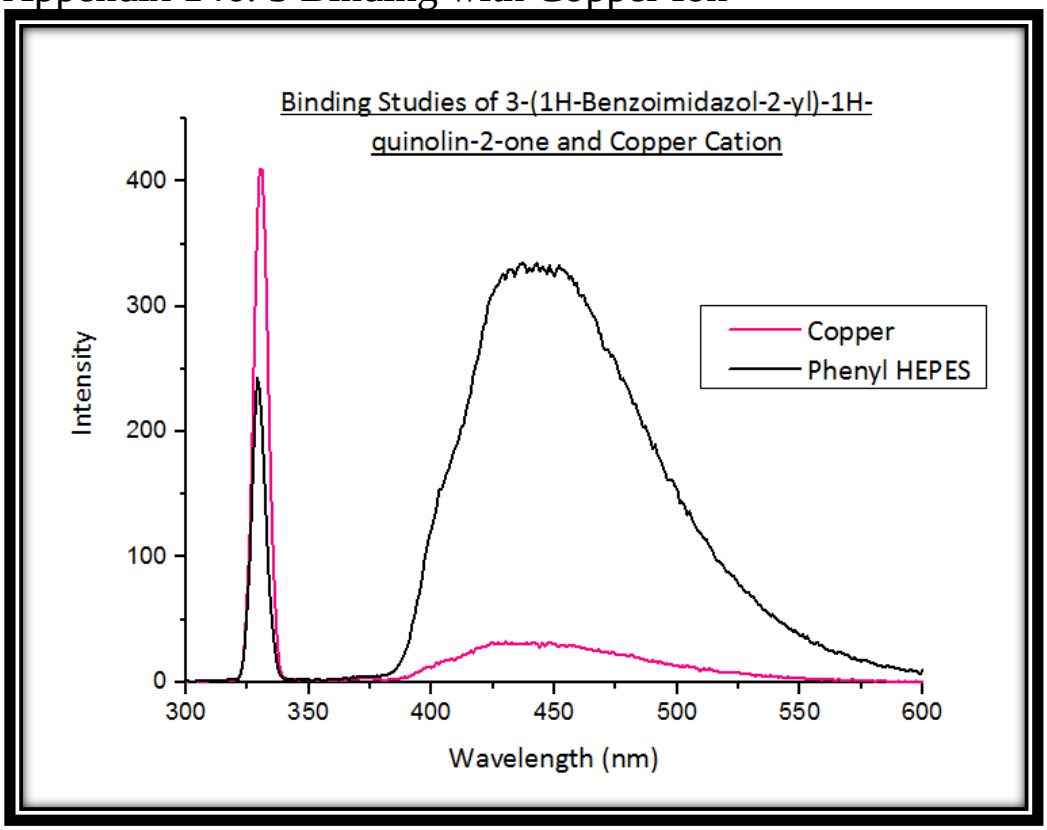

Appendix 147: 3 Binding with Mercury Ion

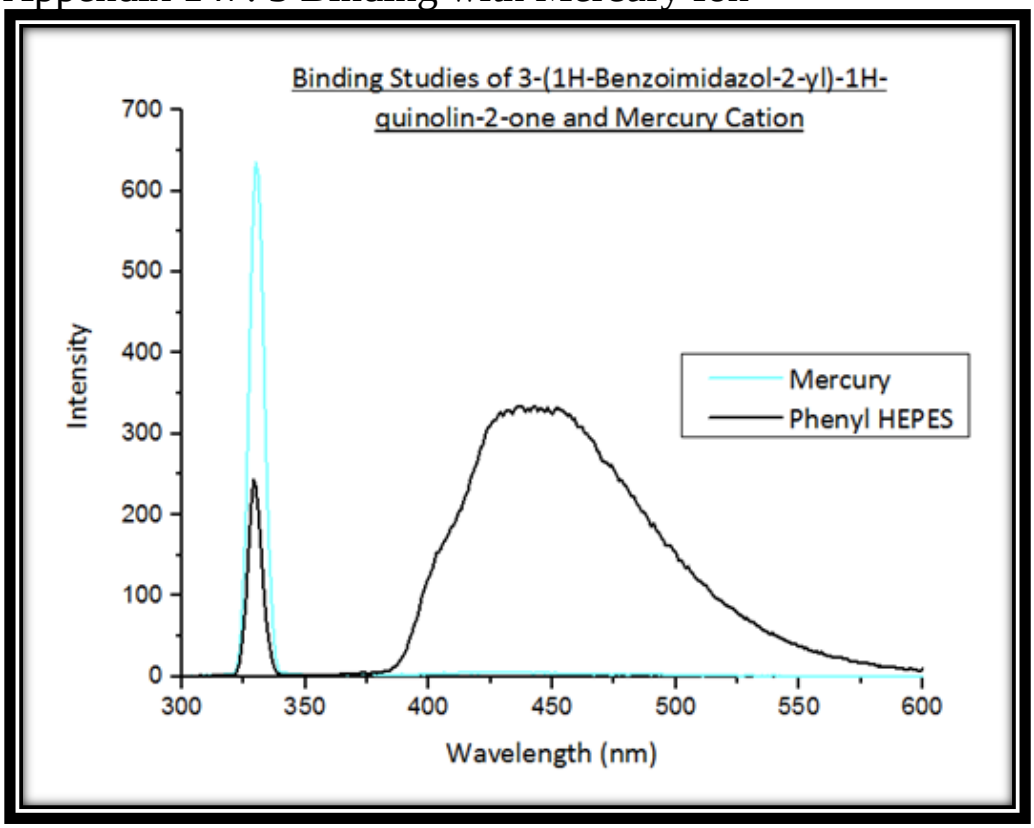

Appendix 148: Binding of Metal ions with 4

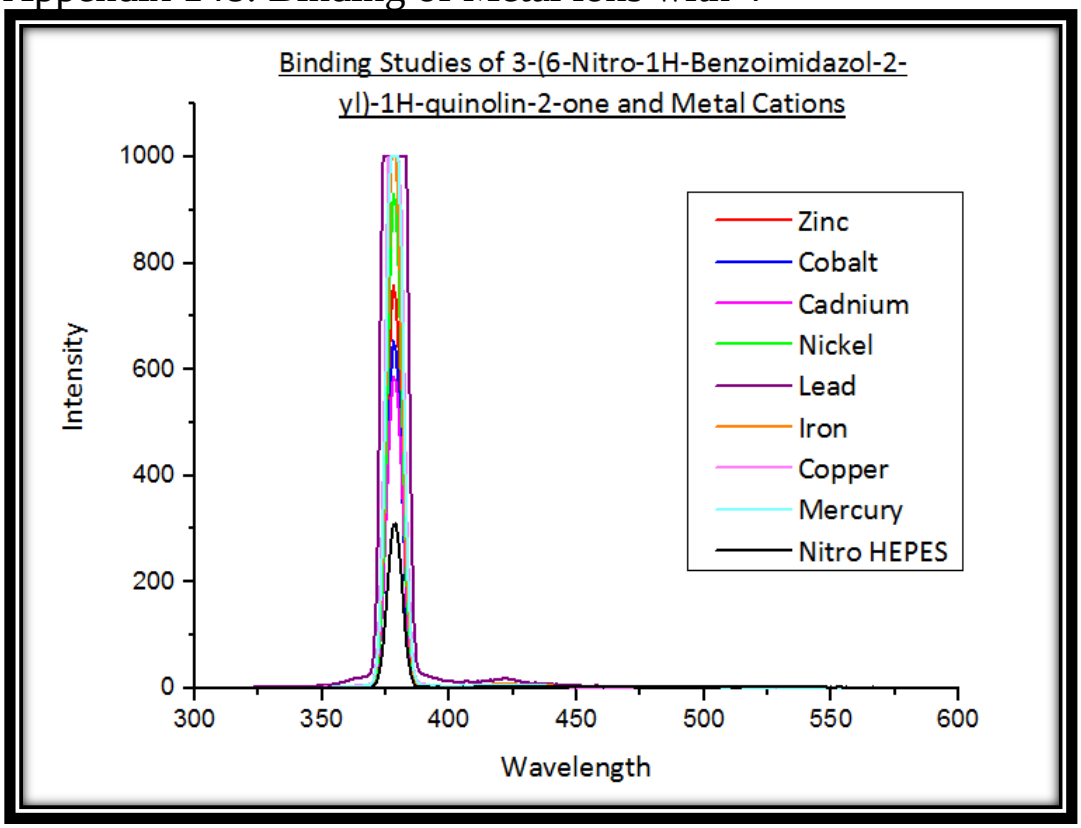

Appendix 149: 4 in HEPES vs. in ACN

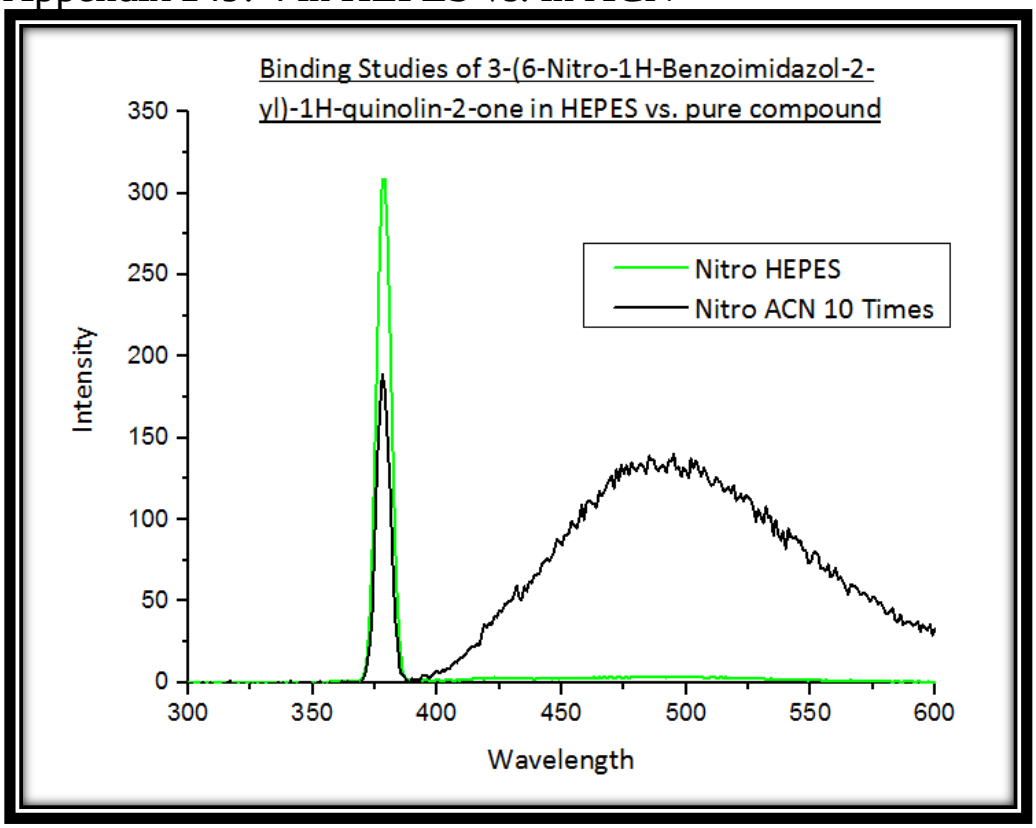

Appendix 150: 4 Binding with Zinc Ion

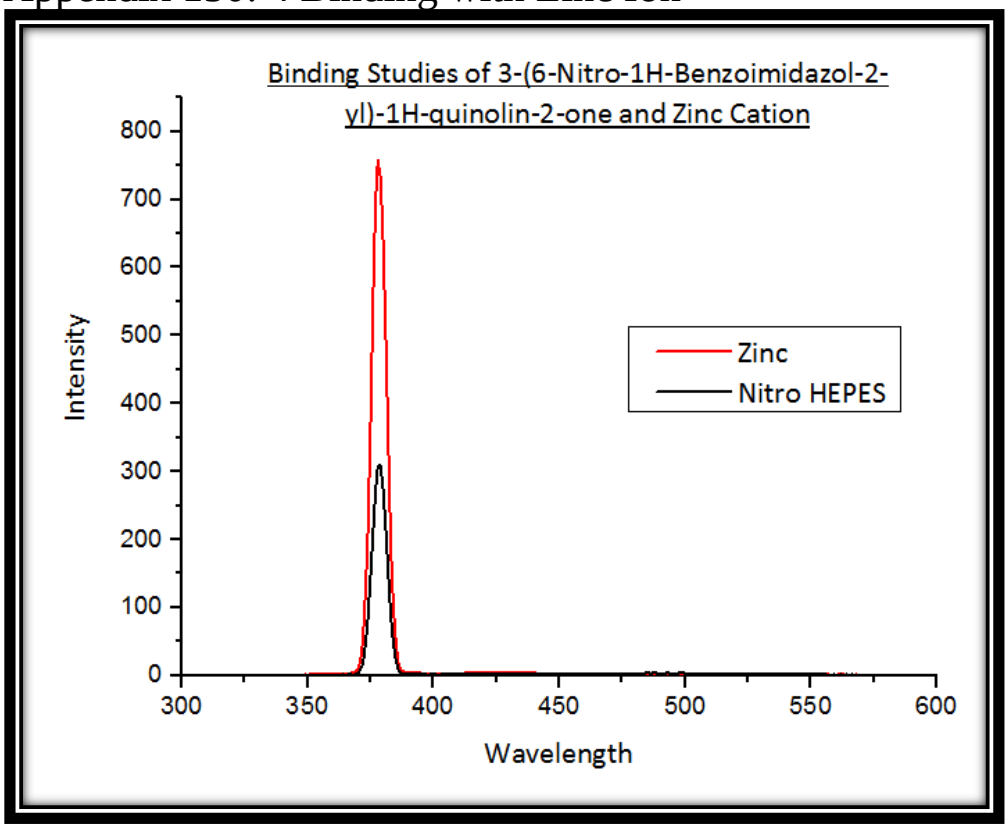

Appendix 151: 4 Binding with Cobalt Ion

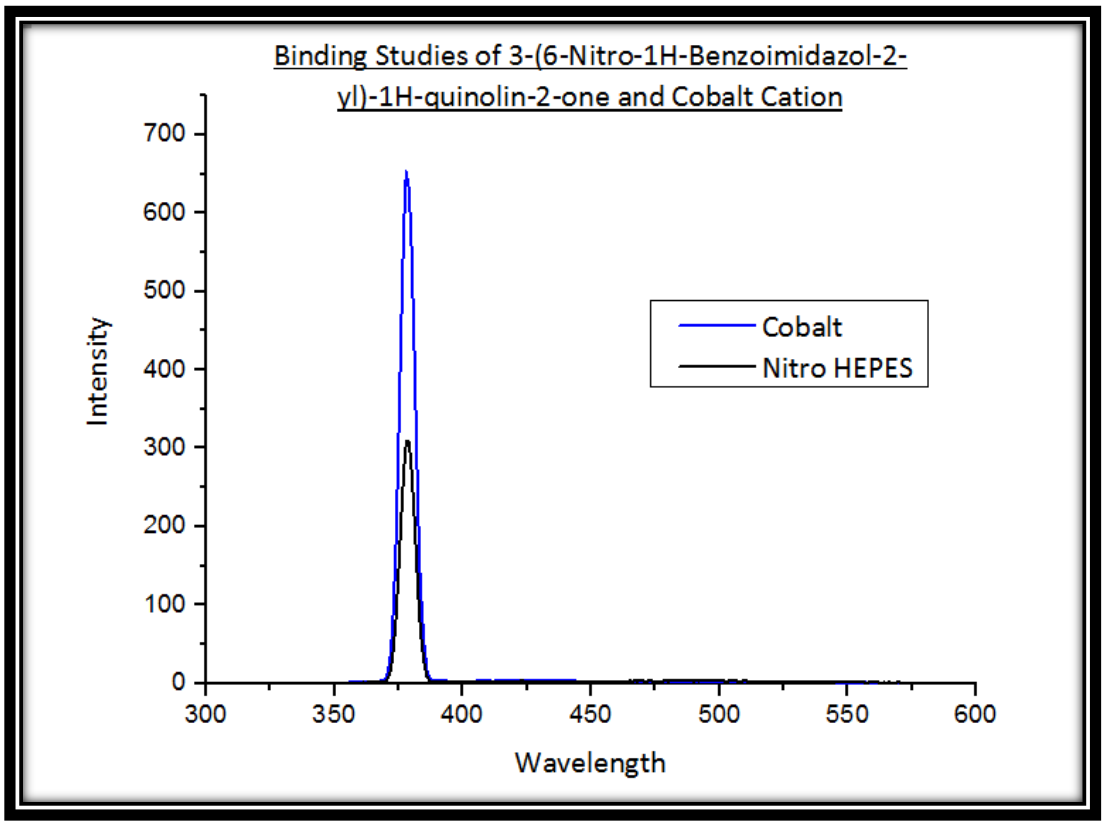

Appendix 152: 4 Binding with Cadmium Ion

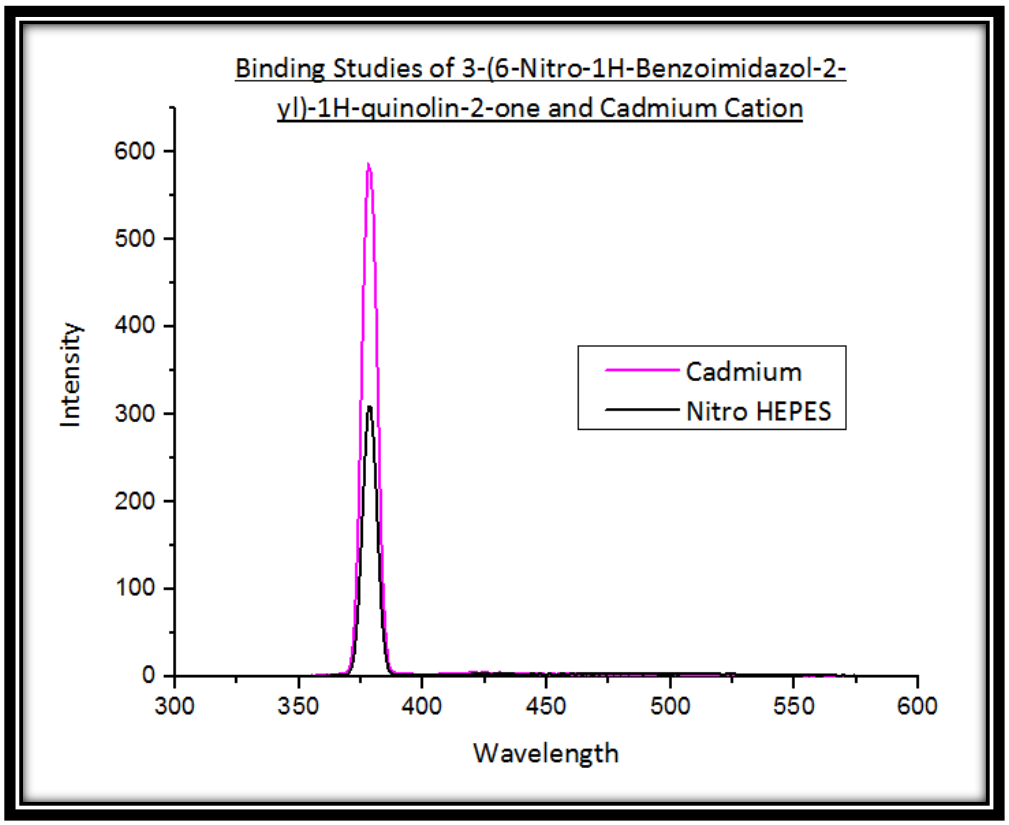

Appendix 153: 4 Binding with Nickel Ion

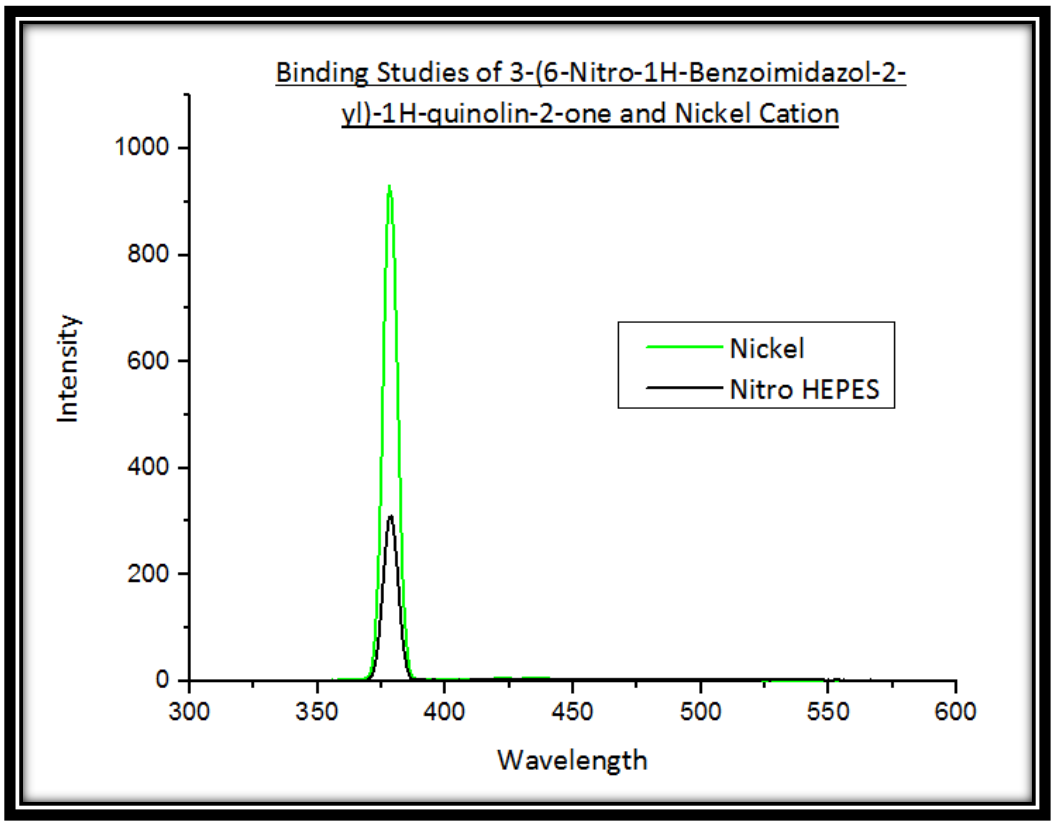

Appendix 154: 4 Binding with Lead Ion

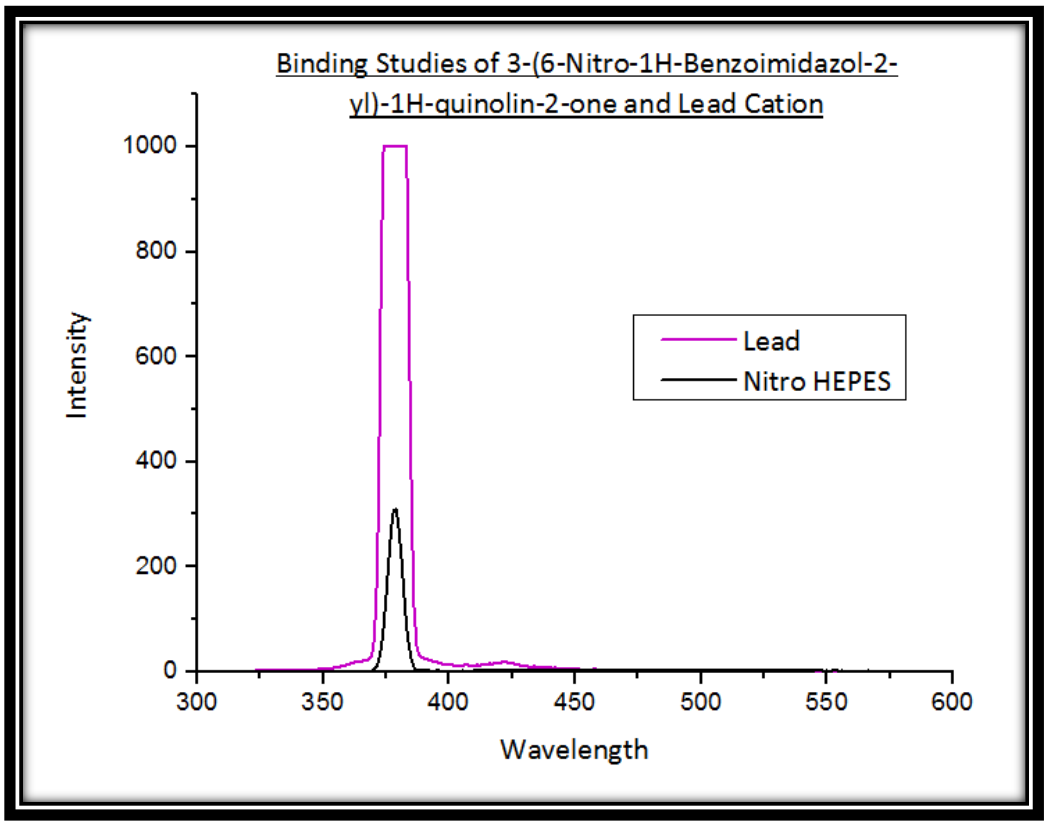

Appendix 155: 4 Binding with Iron Ion

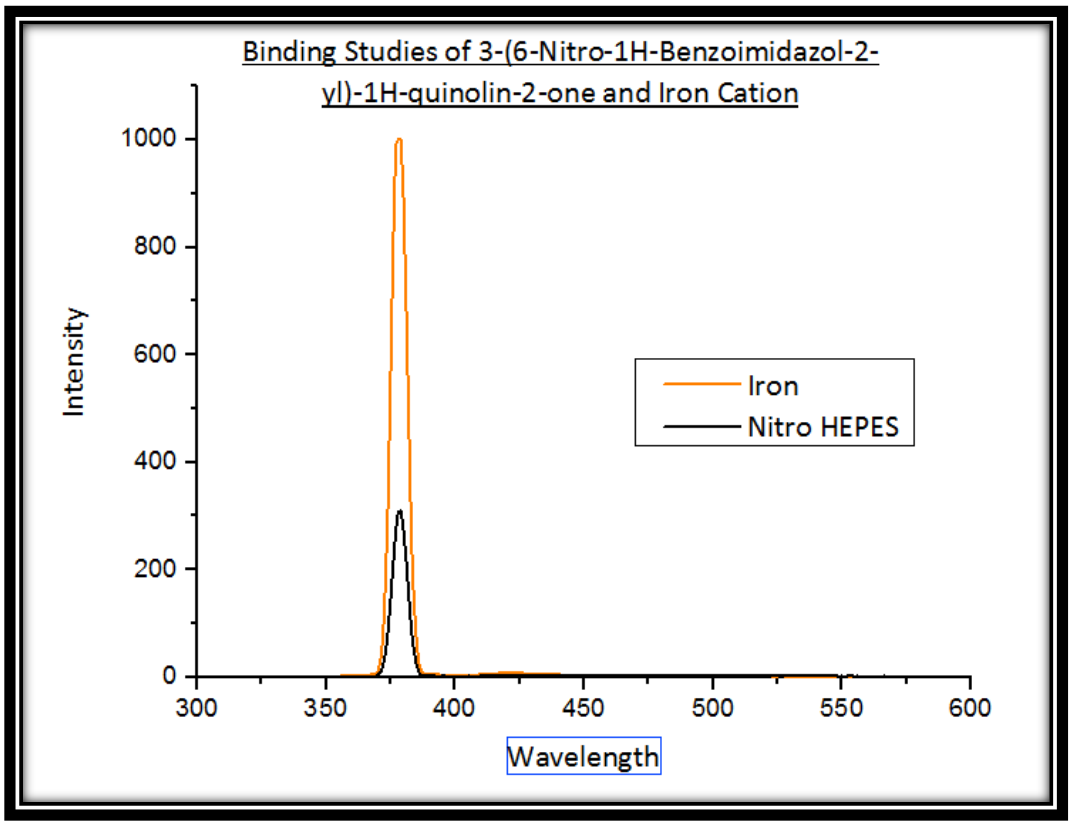

Appendix 156: 4 Binding with Copper Ion

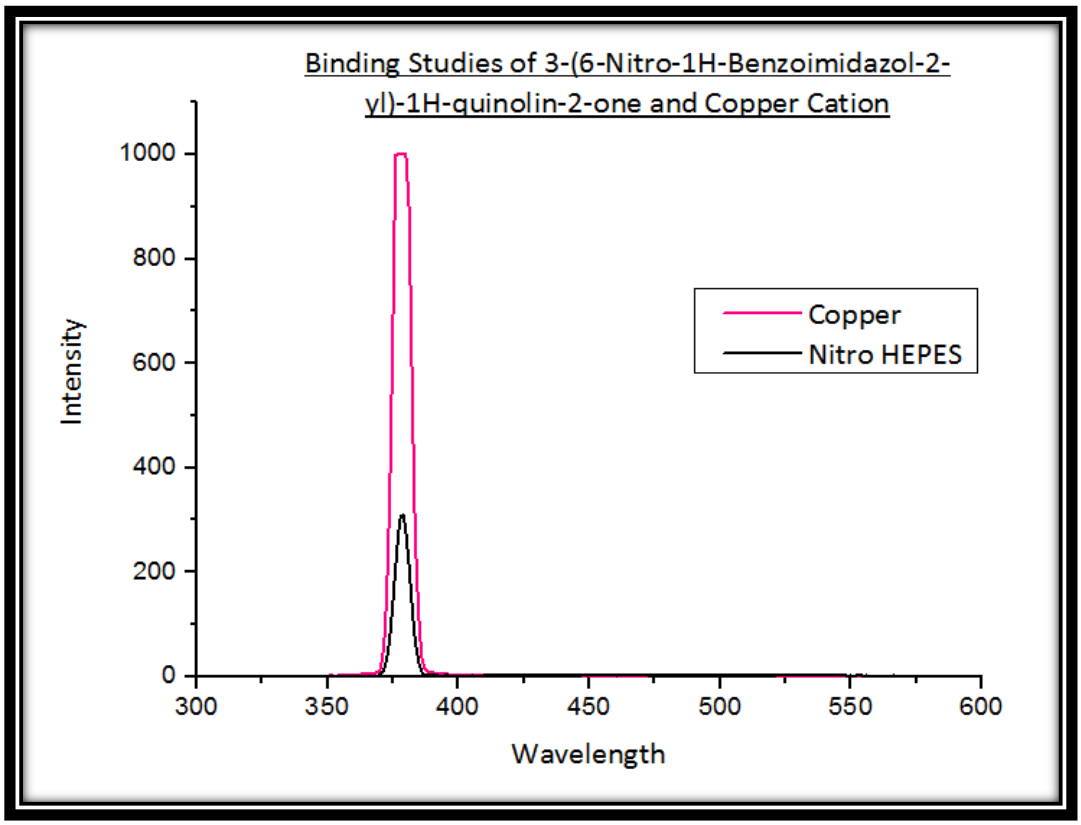

Appendix 157: 4 Binding with Mercury Ion

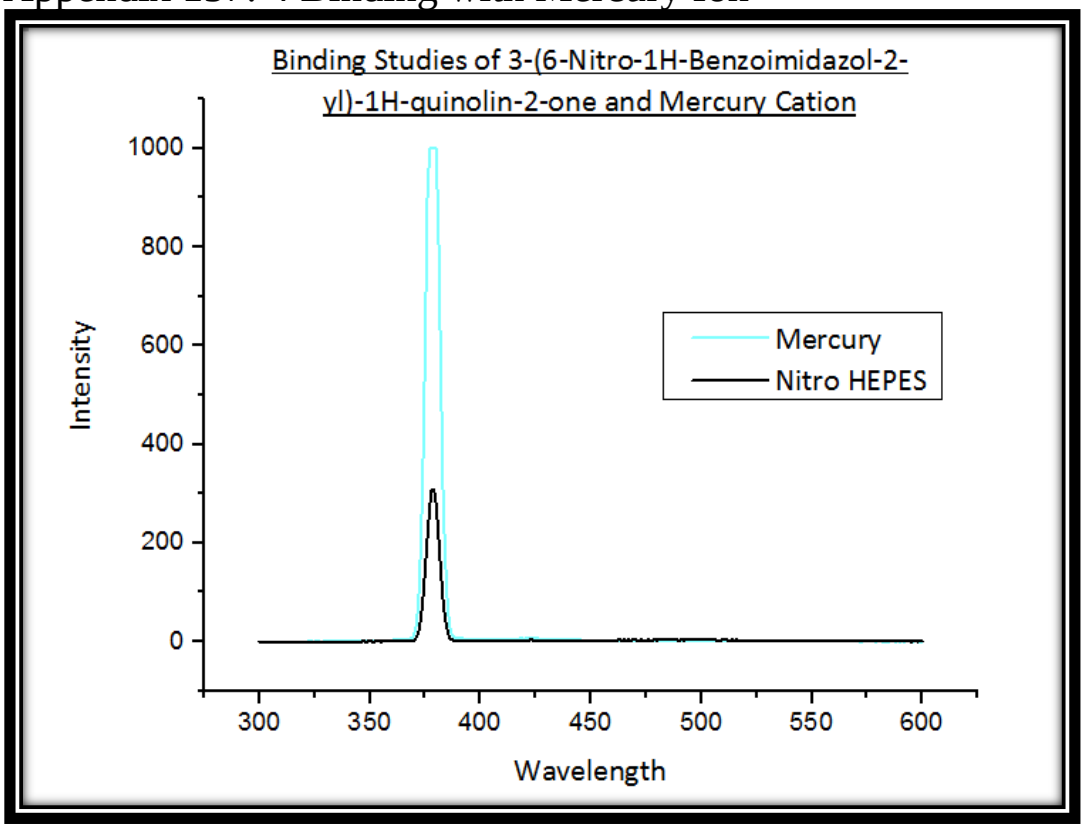

Appendix 158: Calculation of Gibbs Free Energies- Binding Affinity

$$k_{eq} = \frac{[ML]}{[M][L]}$$

Where ML is the complex, M is the metal ion and L is the ligand.

Binding affinity is calculated as the same for all metal ions with 2+ charge, as all metal ions prepared were of the same concentration.

Bind affinity

$\Delta G = -RT\ Ln\ k_{eq}$

Two moles of the ligand was used to form a hexavalent complex.

$$K_{eq} = \frac{[200 + 60]}{[200][60]} = 21667$$

The binding was done in ambient conditions - 25°C = 298K

$\Delta G = -(8.314)(298)\ Ln\ 21667$

$$\Delta G = -24726.17\ J.mol^{-1}$$

No energy is required of the reaction to occur and thus it can be said to be spontaneous.

Appendix 159: Raw Data of Molecular Docking Studies

Compound	Glide Score	Glide energy	No. of H bonds	Interacting Residues	Distance(Å)	Hydrogen bond donor	Hydrogen bond acceptor
2	-3.350	-18.051	1	Glu 25	1.90	Ligand: (H)	A: GLU 25: (O)O
3	-5.843	-41.338	1	Leu 27	1.57	Ligand: (H)	A: LEU 27: (O)O
4	-4.825	-44.056	-	-	-	-	-
3.12	-4.709	-22.539	-	-	-	-	-
5	-5.168	-46.288	-	-	-	-	-